



Selective catalytic conversion of biomass-derived furanic compounds

Design of solid catalysts and structure-performance relations

Fang, Wenting

Publication date:
2022

Document Version
Publisher's PDF, also known as Version of record

[Link back to DTU Orbit](#)

Citation (APA):
Fang, W. (2022). *Selective catalytic conversion of biomass-derived furanic compounds: Design of solid catalysts and structure-performance relations*. DTU Chemistry.

General rights

Copyright and moral rights for the publications made accessible in the public portal are retained by the authors and/or other copyright owners and it is a condition of accessing publications that users recognise and abide by the legal requirements associated with these rights.

- Users may download and print one copy of any publication from the public portal for the purpose of private study or research.
- You may not further distribute the material or use it for any profit-making activity or commercial gain
- You may freely distribute the URL identifying the publication in the public portal

If you believe that this document breaches copyright please contact us providing details, and we will remove access to the work immediately and investigate your claim.

Selective catalytic conversion of biomass-derived furanic compounds – Design of solid catalysts and structure- performance relations

PhD dissertation by
Wenting Fang 方雯婷

December 2022



Technical University of Denmark

Preface

This PhD thesis was carried out at the Centre for Catalysis and Sustainable Chemistry (CSC), Department of Chemistry at the Technical University of Denmark (DTU) under the supervision of Prof. Anders Riisager and Assoc. Prof. Sebastian Meier. The duration of the PhD study was three years and four months, from September 2019 to December 2022. The PhD project was financed by the Chinese Scholarship Council and the Department of Chemistry, DTU.

The PhD thesis focuses on the design of solid catalysts and their application in the conversion of biomass-derived furanic compounds together with establishment of structure-performance relations. Chapter 1 presents an overview of reactions with furfural - a biomass-derived furanic compound - as substrate and introduce aluminophosphate-based microporous molecular sieves. The utilized synthesis methods, characterization of catalysts and catalytic activity tests are summarized in Chapter 2 and the main outcomes of the PhD project are described in Chapters 3-7. Finally, Chapter 8 summarizes the main conclusions and perspectives of the project.

Acknowledgements

Firstly, I would like to thank the China Scholarship Council (No. 201908330324) and the Department of Chemistry, DTU, to provide the funding to support my study and life in Denmark. Also, I want to express my sincere appreciation to my main supervisor Prof. Anders Riisager for giving me the opportunity to undertake this PhD project. I am very grateful to his valuable inputs and suggestions for the research and also the strong support and encouragement. Thanks to co-supervisor Assoc. Prof. Sebastian Meier for his kind support with NMR analyses and intense discussions.

Thanks to the technicians who assisted me with characterization and analysis during the whole project, including Mariusz Kubus, Johanne Marie Nielsen, Maria Blanner Bang, Kasper Enemark-Rasmussen, and Bodil Fliis Holten. Also, I wish to thank the DTU Chemistry administration and support staff for their help in the past three years and four months, including Mette Hansen, Maria Bundgaard, Jette Berg Nestén, Monica Esterajher Søndergaard, Ishaq Khaliqdad, Philip Charlie Johansen, Regitze Børsen Hansen and Bo Sørensen.

Also thanks to the members of Prof. Riisager's group and CSC for the friendly work environment, including Ping Zhu, Mahtab Madani, Rosa Maria Padilla Paz, Deepthy Krishnan, Wenfeng Zhao, Kai Gao, Faliu Yang, Kalina Grzelak, Betsy Kurisingal Joseph, Chantal Abou Fayssal, Pablo Doménech Martínez, Sakhitha Koranchalil, Brenda Rabell Montiel, Dimitra Iltsiou, Mikkel Kock Larsen, and so on. Special thanks to Leonhard Schill for helping with XPS analysis and different other issues in the lab.

Thanks also to my work partner Sihang Liu for contributing with DFT calculations and constructive suggestions for the associated papers, and Astrid Kjær Steffensen, Jonas Egebo, Hua Chen, Shaofeng Li, and Xianbiao Fu for their contributions to this project.

I am grateful to Prof. Walter Leitner and Dr. Alexis Bordet for giving me the opportunity to complete three months' external stay in the Max Planck Institute for Chemical Energy Conversion, Mulheim, Germany. Special thanks to Yuyan Zhang and Sheng-hsiang Lin for their kind help during my stay.

I want to thank my best friends, Huirong Li and Qi Gao, and roommate, Junjie Kang, for great friendship and good memories in and out of DTU. Thanks to friends for their encouragements and happiness to me, including Hua Chen, Qian Zhao, Yuhan Luo, and Mianle Xu. Thanks also to my boyfriend Johannes Zenner for his understanding and company.

Finally, I would like to express my deepest gratitude to my beloved parents, Rongwu Fang 方荣武 and Huiqun Xu 徐惠群, and brother, Mingwei Fang 方铭伟, for their support and love.

Wenting Fang

Wenting Fang

Lyngby, December, 2022

Abstract

The depletion of nonrenewable fossil fuels and emergent environmental issues make the sustainable production of useful biofuels and chemicals from renewable biomass resources highly attractive and crucial. In line with this, the aim of this thesis was to develop efficient catalytic systems with heterogeneous catalysis to valorize biomass-derived furanic compounds into biofuels and other chemicals by acetalization, hydrogenation, reductive etherification, and aldol condensation.

Aluminum phosphates (APO-5s) and metal-modified APO-5s with suitable pore size and specific adsorption of the C=O moiety of aldehydes were developed as catalysts for furfural (FF) conversion. Weakly acidic APO-5(Al/P = 1) efficiently catalyzed FF acetalization in ethylene glycol, while more acidic APO-5(Al/P = 1.5) catalyzed catalytic transfer hydrogenation (CTH) and subsequent etherification of FF in 2-propanol (Chapter 3). Alkali earth metals (Mg, Ca, Sr, and Ba) were further introduced to tune the acidity/basicity of the acidic APO-5(Al/P = 1.5) catalyst, which additionally suppressed the subsequent etherification after CTH to improve the selectivity of CTH (Chapter 4). On the other hand, Pd nanoparticles supported on APO-5(Al/P = 1.5) selectively catalyzed reductive etherification of FF with formic acid as a hydrogen donor due to the bifunctional properties of the catalyst (Chapter 5). Moreover, the introduction of Zr into APO-5 enhanced the C=O adsorption of FF and created suitable acidic and basic sites which promoted the aldol condensation of FF with cyclohexanone (Chapter 6). Finally, KIT-6-templated mesoporous CuNiO_x exhibited excellent performance in hydrogenation of FF under moderately mild reaction conditions as a result of the co-catalysis of active sites (Cu⁺ species and CuNi alloy phases) (Chapter 7).

Overall, the thesis work introduces new approaches to obtain heterogeneous catalyst systems with tuned reactivity for valorizing biomass-derived FF into attractive biofuel-additives and commodity chemicals of industrial interest.

Resumé

Opbrug af ikke-vedvarende fossile brændstoffer samt heraf afledte miljøproblemer gør bæredygtig produktion af biobrændstoffer og kemikalier fra vedvarende biomasseressourcer yderst attraktiv og vigtig. Formålet med denne afhandling var at udvikle effektive katalytiske systemer med heterogen katalyse til at forædle biomasseafledte furanforbindelser til biobrændstoffer og andre kemikalier ved acetalisering, hydrogenering, reduktiv etherificering og aldolkondensation.

Aluminiumphosphater (APO-5'er) og metalmodificerede APO-5'er med passende porestørrelse og specifik adsorption af C=O enheden fra aldehyder blev anvendt som katalysatorer for omdannelse af furfural (FF). Svagt sur APO-5(Al/P = 1) katalyserede effektivt FF acetalisering i ethylenglycol, mens mere sur APO-5(Al/P = 1,5) katalyserede overførselshydrogenering (CTH) og efterfølgende etherificering af FF i 2- propanol (kapitel 3). Jordalkalimetaller (Mg, Ca, Sr og Ba) blev endvidere introduceret for at justere surhed/alkalinitet af sur APO-5(Al/P = 1,5), hvilket undertrykte etherificeringen efter CTH som medførte bedre selektivitet af CTH (kapitel 4). Pd-nanopartikler fordelt på APO-5(Al/P = 1,5) katalyserede selektivt reduktiv etherificering af FF med myresyre som hydrogen donor pga. katalysatorens bifunktionelle egenskaber (kapitel 5). Desuden førte introduktion af Zr i APO-5 til forbedret C=O adsorption og modificerede sure og basiske centre, som fremmede aldolkondensationen af FF med cyklohexanon (kapitel 6). Endelig udviste mesoporøs CuNiO_x fremstillet fra KIT-6-templat fremragende ydeevne ved hydrogenering af FF under moderat milde reaktionsbetingelser, som et resultat af synergi mellem aktive Cu⁺ centre og CuNi legeringsfase (kapitel 7).

Samlet set introducerer afhandlingen nye metoder til at opnå reaktivitet af heterogene katalysatorsystemer, der er tilpasset til at omdanne biomasseafledt FF selektivt til attraktive biobrændstofadditiver og vigtige kemikalier med industriel interesse.

List of abbreviations

1-HP	1-hydroxy-2-pentanone
1,2-PeD	1,2-pentanediol
1,5-PeD	1,5-pentanediol
AEM	alkaline earth metal
APO-5	aluminum phosphate
AlPO _{4-n}	aluminophosphate-based microporous molecular sieves
ATR	attenuated total reflectance
BEEF-vdW	Bayesian error estimation functional with van der Waals correlation
BET	Brunauer-Emmett-Teller
BHMF	2,5-bis(hydroxymethyl)furan
BMF	furfuryl butyl ether
CH	cyclohexanone
CH-TPD	cyclohexanone temperature-programmed desorption
CI-NEB	climbing image nudged elastic band
CO ₂ -TPD	carbon dioxide temperature-programmed desorption
CP	cyclopentanone
CTH	catalytic transfer hydrogenation
DEF	2-(diethoxymethyl)furan

DFF	2,5-diformylfuran
DFT	density functional theory
DHMF	2,5-dihydroxymethylfuran
DIPF	2-(diisopropoxymethyl)furan
DMF	2,5-dimethylfuran
DMTHF	2,5-dimethyltetrahydrofuran
DOE	Department of Energy
DRIFTS	diffuse reflectance infrared fourier transform spectroscopy
EFE	ethyl furfuryl ether
EFM	ethoxy(furan-2-yl)methanol
EG	ethylene glycol
FA	formic acid
FAC	furfuryl acetal
FAE	furfuryl alcohol ether
FAL	furfuryl alcohol
FCA	2,5-furandicarboxaldehyde
FD	2-(furan-2-yl)-1,3-dioxane
FDCA	2,5-furandicarboxylic acid
FUA	furoic acid
FF	furfural

FT-IR	Fourier transformed infrared
FF-TPD	furfural temperature-programmed desorption
GC-FID	gas chromatography flame-ionization detection
GC-MS	gas chromatography-mass spectrometry
GGA	generalized gradient approximation
H ₂ -TPD	hydrogen temperature-programmed desorption
H ₂ -TPR	hydrogen temperature-programmed reduction
HMF	5-hydroxymethylfurfural
IPF	2-(isopropoxymethyl)furan
IPL	isopropyl levulinate
LA	levulinic acid
LB	lignocellulosic biomass
MAS NMR	magic-angle spinning nuclear magnetic resonance
MF	2-methylfuran
MFA	5-methylfurfural
MPV	Meerwein–Ponndorf–Völery
MTHF	2-methyltetrahydrofuran
NH ₃ -TPD	ammonia temperature-programmed desorption
NP	nanoparticle
PAW	projector augmented wave

RPBE	revised Perdew-Burke-Ernzerhof
rpm	revolutions per minute
SAXS	small angle X-ray scattering
SEM	scanning electron microscopy
SM	substitution mechanism
TEM	transmission electron microscopy
TG	thermogravimetric
THFA	tetrahydrofurfuryl alcohol
THFU	tetrahydrofurfural
TMI	transition metal ion
VASP	Vienna Ab initio Software Package
XAES	X-ray excited Auger electron spectroscopy
XPS	X-ray photoelectron spectroscopy
XRD	X-ray diffraction
XRF	X-ray fluorescence
ZrAPO-5	Zr-doped aluminum phosphate

List of publications

The work in this PhD thesis is based on the manuscripts I, II, III, IV, and V listed below. The full manuscripts are collected in different chapters with minor modifications and the supporting information documents are provided in the Appendixes. Besides, the publications not included in this thesis are also listed.

List of publications included in the thesis

Paper I: Efficient valorization of biomass-derived furfural to fuel bio-additive over aluminum phosphate. W. Fang, A. Riisager*, *Applied Catalysis B: Environmental* **2021**, 298, 120575.

Paper II: Improved catalytic transfer hydrogenation of biomass-derived aldehydes with metal-loaded aluminum phosphate. W. Fang, A. Riisager*, *ACS Sustainable Chemistry & Engineering* **2022**, 10, 1536-1543.

Paper III: Reductive etherification of furfural *via* hydrogenolysis with Pd-modified aluminum phosphate and formic acid. W. Fang, J. Egebo, L. Schill, H. Chen, A. Riisager* *Green Chemistry*, **2022**, 24, 7346-7349.

Paper IV: On the role of Zr to facilitate the synthesis of diesel and jet fuel range intermediates from biomass-derived carbonyl compounds over aluminum phosphate. W. Fang, S. Liu, L. Schill, M. Kubus, T. Bligaard, A. Riisager*, *Applied Catalysis B: Environmental*, **2023**, 320, 121936.

Paper V: Rationalizing the structure-activity relationships in mesoporous CuNiO_x for selective furfural hydrogenation. W. Fang[†], S. Liu[†], A. K. Steffensen, L. Schill, G. Kastlunger, A. Riisager*, *ACS Catalysis* (Under review)

List of publications not included in the thesis

- I. Recent advances in heterogeneous catalytic transfer hydrogenation/hydrogenolysis for valorization of biomass-derived furanic compounds. W. Fang, A. Riisager* *Green Chemistry*, **2021**, 23, 670-688.
- II. Ultrafast charge transfer dynamics in 2D covalent organic frameworks/Re-complex hybrid photocatalyst. Q. Pan, M. Abdellah*, Y. Cao, W. Lin, Y. Liu, J. Meng, Q. Zhou, Q. Zhao, X. Yan, Z. Li, H. Cui, H. Cao, W. Fang, D. A. Tanner, M. Abdel-Hafiez, Y. Zhou*, T. Pullerits, S. E. Canton, H. Xu*, K. Zheng* *Nature Communications*, **2022**, 13, 845.

List of conference contributions

I. Efficient valorization of biomass-derived furfural to fuel bio-additive over aluminum phosphate. W. Fang, A. Riisager.

Oral presentation at Annual PhD symposium organized by the Department of Chemistry of DTU, November 2021, Copenhagen (Denmark).

II. Tuning of catalytic sites in mesoporous CuNiO₂ for furfural hydrogenation. W. Fang, S. Liu, A. K. Steffensen, L. Schill, A. Riisager.

Poster presentation at International Symposium on Green Chemistry 2022, 15-19 May, 2022, La Rochelle (France).

III. Design of aluminum phosphate catalysts for selective valorization of biomass-derived furfural. W. Fang, A. Riisager.

Oral presentation at 20th International Zeolite Conference, 2-7 July, 2022, Valencia (Spain).

IV. Tuning of catalytic sites in mesoporous CuNiO₂ for furfural hydrogenation. W. Fang, S. Liu, A. K. Steffensen, L. Schill, A. Riisager.

Poster presentation at Annual PhD symposium organized by the Department of Chemistry of DTU, November 2022, Copenhagen (Denmark).

List of Content

1 Introduction	1
1.1 Biomass-derived furanic compounds	2
1.2 The value-added reactions of furfural	4
1.2.1 Hydrogenation	5
1.2.2 Acetalization	14
1.2.3 Aldol condensation	17
1.3 Acidity and basicity of aluminophosphate	20
1.4 Scope of this thesis	22
1.5 References	24
2 Experimental	28
2.1 Chemicals	28
2.2 Catalyst preparation	29
2.2.1 The synthesis of APO-5 and metal-modified APO-5	29
2.2.2 The synthesis of mesoporous CuNiO _x	31
2.3 Catalyst characterization	32
2.4 Catalyst activity	35
2.4.1 Acetalization, reductive etherification, CTH, and aldol condensation	35
2.4.2 Hydrogenation	36
2.5 Catalyst leaching and recycling test	36
2.6 Theoretical calculations	38
2.6.1 Aldol condensation system	38
2.6.2 Hydrogenation system	39
2.7 References	40
3 Efficient valorization of biomass-derived furfural to fuel bio-additive over aluminum phosphate	42
3.1 Introduction	43
3.2 Results and discussion	45
3.2.1 Characterization of APO-5 catalysts	45
3.2.2 Catalytic performance of APO-5 catalysts	49
3.2.3 Acetalization of furfural over APO-5(1)	50

3.2.4 Reductive etherification of furfural over APO-5(1.5)	54
3.3 Summary	60
3.4 References.....	61
4 Improved catalytic transfer hydrogenation of biomass-derived aldehydes with metal-loaded aluminum phosphate	64
4.1 Introduction	65
4.2 Results and discussion	67
4.2.1 Characterization of APO-5 and AEM-loaded catalysts	67
4.2.2 Catalytic activity of APO-5 and AEM-loaded catalysts	70
4.2.3 Effect of acidity and basicity on activity of AEM-loaded catalysts	74
4.2.4 Reaction mechanism of AEM-loaded catalysts	76
4.2.5 Durability of 3Ca/APO1.5 catalyst.....	77
4.2.6 Substrate scope.....	78
4.3 Summary	79
4.4 References.....	80
5 Reductive etherification of furfural <i>via</i> hydrogenolysis with Pd-modified aluminum phosphate and formic acid.....	83
5.1 Introduction	84
5.2 Results and discussion	85
5.2.1 Characterization of Pd-loaded APO-5 catalysts	85
5.2.2 Catalytic performance of Pd-loaded APO-5 catalysts	87
5.3 Summary	92
5.4 References.....	92
6 On the role of Zr to facilitate the synthesis of diesel and jet fuel range intermediates from biomass-derived carbonyl compounds over aluminum phosphate	95
6.1 Introduction	96
6.2 Results and discussion	99
6.2.1 Structure of catalysts	99
6.2.2 Cross-aldol condensation of furfural and cyclohexanone	102
6.2.3 Catalyst recycling.....	105
6.2.4 Substrate scope.....	106

6.2.5 Self-aldol condensation of cyclohexanone	107
6.2.6 The role of Zr in the aldol condensation.....	108
6.2.7 The role of acidity/basicity in the aldol condensation	110
6.3 Summary	112
6.4 References.....	113
7 Rationalizing the structure-activity relationships in mesoporous CuNiO_x for selective furfural hydrogenation	116
7.1 Introduction	117
7.2 Results and discussion	120
7.2.1 Catalytic performance of catalysts	120
7.2.2 Composition, morphology and active phases of catalysts	122
7.2.3 Adsorption sites on catalysts	124
7.3 Summary	128
7.4 References.....	129
8 Main conclusions and perspectives	131
Appendices A – Support information for Chapter 3	133
Appendices B – Support information for Chapter 4	141
Appendices C – Support information for Chapter 5	152
Appendices D – Support information for Chapter 6.....	158
Appendices E – Support information for Chapter 7	171
Appendices F – First page of published articles.....	189

1 Introduction

The huge consumption of nonrenewable fossil energy (84% of total energy consumption)¹ and the associated environmental impact are key challenges in the modern society.^{2,3} The traditional fossil-based industry approach induces many environmental problems at all stages of processing and production; especially, it increases the CO₂ concentration in the atmosphere due to gas emissions (6 billion tons CO₂ in 1950, while 37 billion tons in 2021)⁴ (Fig. 1.1a), leading to global warming.⁵⁻⁷ Therefore, the utilization of renewable resources and the development of sustainable technologies are the key drivers of ongoing efforts in science and technology to overcome the challenges.^{8,9} Biomass, including a wide range of animal and plant materials available on a renewable or recurring basis, represents a globally available and reproducible resource that can be used as a feedstock for production of biofuels and chemicals. Biomass conversion is a promising way to overcome dependency on fossil hydrocarbons (oil, coal, and gas). The U.S. Department of Energy (DOE) believes that 10% of transportation fuels can come from biomass by 2010, and 50% by 2030. Accordingly, the idea of a “biorefinery concept”, including integration of conversion processes to produce fuels, power, heat, and value-added chemicals by targeting the utilization of all carbon atoms of the resource, was born.¹⁰ The formed CO₂ can be reused by plants through photosynthesis. Therefore, the overall process can be balanced in terms of a closed CO₂ cycle (Fig. 1.1b).

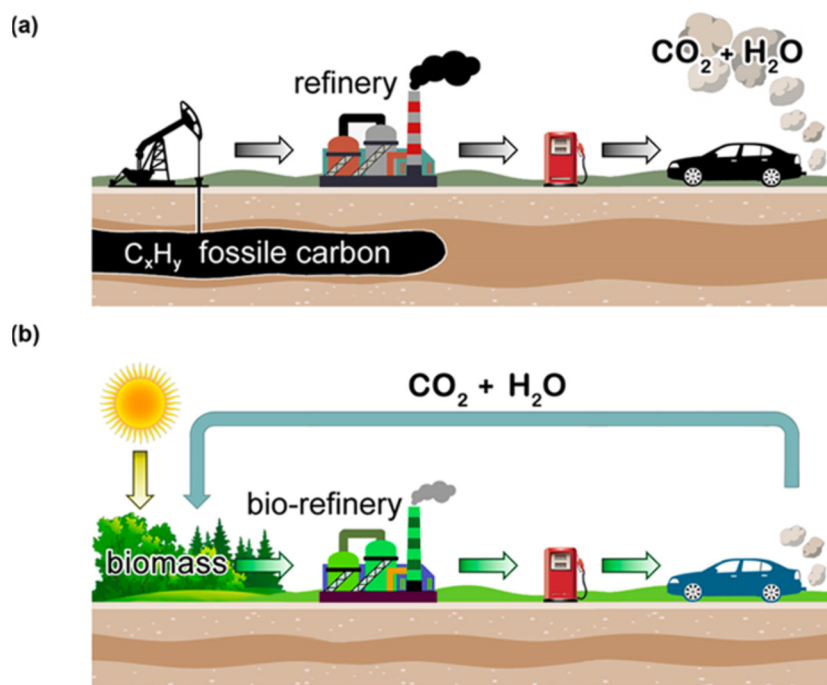
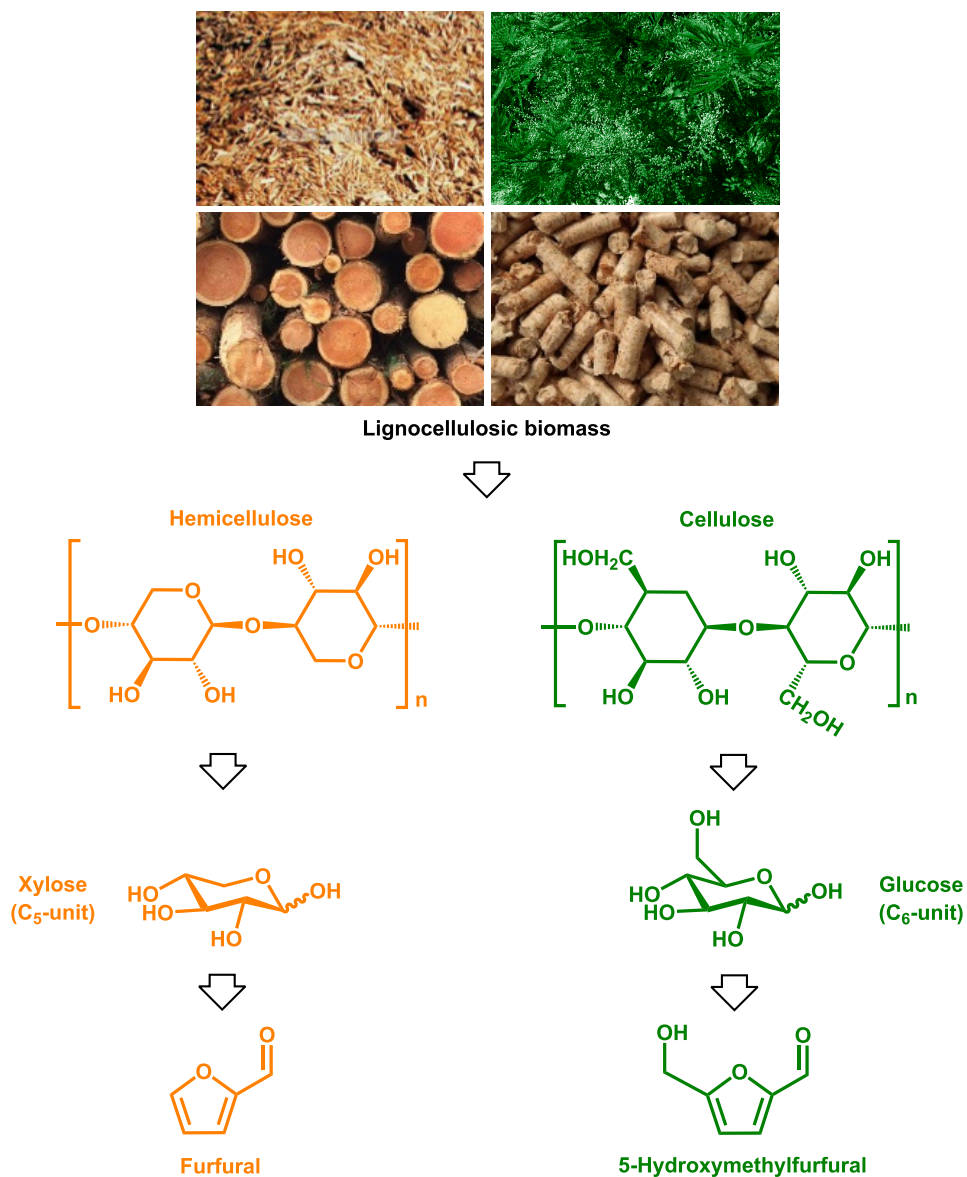


Fig. 1.1 (a) Comparison of traditional fossil-based and (b) sustainable biomass-based approaches to produce fuels and chemicals. Adapted from ref 11.

1.1 Biomass-derived furanic compounds

Lignocellulosic biomass (LB), one of the most available and abundant renewable resource in nature, is composed of cellulose (40–50 wt%), hemicellulose (25–35 wt%), and lignin (15–20 wt%)^{10,12–14} and appears to be the promising feedstock for the biorefinery.^{15–17} Cellulose is a homopolymer of glucose¹⁸ whereas hemicellulose consists of short, highly branched polymers of C₅ and C₆ polysaccharide units.^{19,20} 5-Hydroxymethylfurfural (HMF) and furfural (FF) formed by the dehydration of glucose and xylose (Scheme 1.1) are on the list of the ‘Top 10’ biomass-derived platform compounds endorsed by the U.S. DOE.^{16,21} HMF and FF stand out as bridges connecting biomass resources and the chemical industry owing to the potential of volume production methods.¹⁶

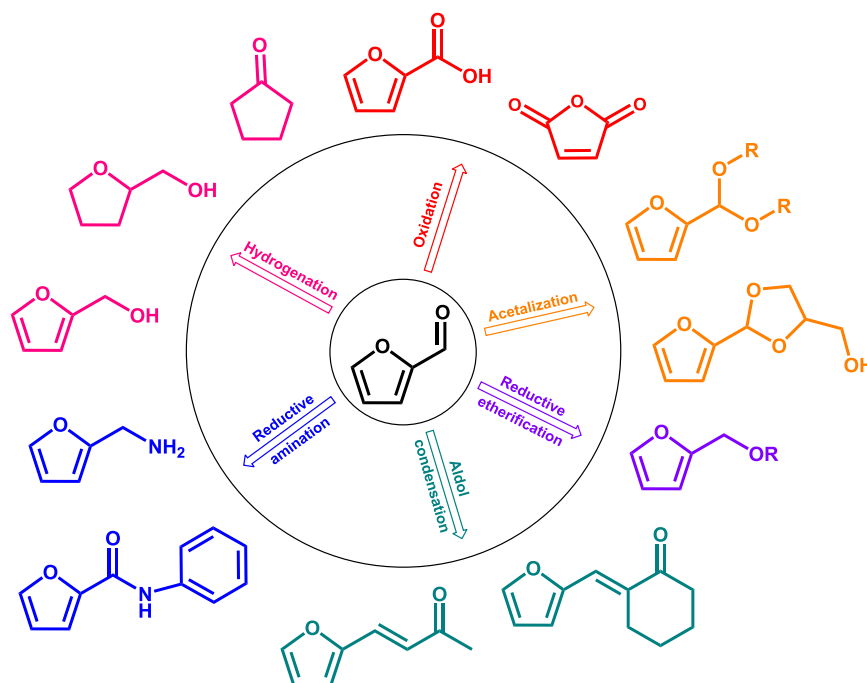


Scheme 1.1 Reaction pathway from LB to platform compounds. Adapted and redrawn from ref 10.

HMF was first reported in 1875 as an intermediate in the sulfuric acid catalyzed conversion of sugar to levulinic acid (LA).²² It is a multifunctional molecule with an aldehyde group, a hydroxyl group and a furan ring system. Therefore, HMF has been called a ‘sleeping giant’^{23,24} and used for the production of potential biofuels and value-added chemicals, such as 2,5-dihydroxymethylfuran (DHMF)²⁵, 2,5-dimethylfuran (DMF)²⁶, 2,5-dimethyltetrahydrofuran (DMTHF)²⁷,

2,5-diformylfuran (DFF)²⁸, 2,5-furandicarboxylic acid (FDCA)²⁸, LA²⁹ and linear alkanes³⁰. FF also has an aldehyde group and a furan ring, which can be converted to make various value-added chemicals and fuels.¹⁴ FF was first isolated as an ethereal oily substance in 1832, and the Quaker Oats factory at Cedar Rapids realized the commercial production of FF in 1922.³¹ The world market for FF was estimated to be 200,000–300,000 tons per year.³¹

1.2 The value-added reactions of furfural

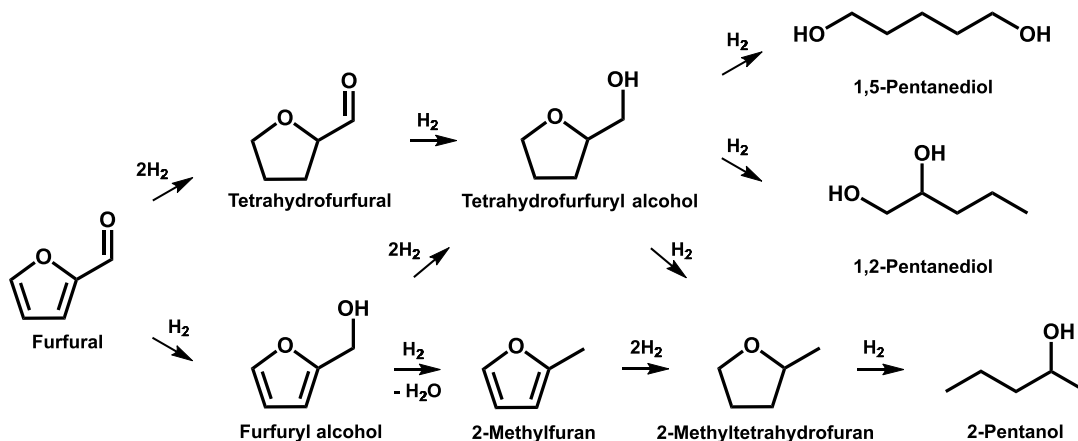


Scheme 1.2 FF as a platform compound for the production of fuels and chemicals.

The aldehyde group and the furan ring of FF can be transformed into many useful derivatives *via* various reactions (Scheme 1.2). FF can undergo hydrogenation and oxidation of the aldehyde group or both the aldehyde group and the furan ring to form furfuryl alcohol (FAL)^{32,33}, tetrahydrofurfuryl alcohol (THFA)³⁴, furoic acid (FUA)³⁵ and so on. Meanwhile, the aldehyde group of FF can be exploited alone to various derivatives by acetalization, reductive etherification, aldol condensation, reductive amination, and so on.³⁶ This thesis

focuses on hydrogenation, acetalization, and aldol condensation of FF for their widely applications in the biomass valorization, and how the adsorption modes of FF on the catalysts and acidic/basic sites affect the catalytic performance and product distribution.

1.2.1 Hydrogenation



Scheme 1.3 Roadmap for hydrogenation of FF into high value-added chemicals.

FF can be hydrogenated *via* several pathways (Scheme 1.3) as it possesses both an aldehyde group and a furan ring. However, there exists a hydrogenation order difference between the aldehyde group and the furan ring, subsequent hydrogenolysis and ring opening reaction due to the different activation energies.^{37,38} The value-added products obtained include FAL^{32,33}, 2-methylfuran (MF)³⁹, THFA³⁴, tetrahydrofurfural (THFU)⁴⁰, 2-methyltetrahydrofuran (MTHF)⁴¹, 1,5-pentanediol (1,5-PeD)⁴², 1,2-pentanediol (1,2-PeD)⁴³, and 2-pentanol⁴⁴. The downstream products are used as furan resin precursors, green solvents, fuel bio-additives, and other platform compounds.³² According to previous studies^{36,38}, adsorption modes of FF and/or acidic/basic sites are responsible for the product selectivity in FF hydrogenation. Therefore, the investigation of

the relationship between catalyst properties and its performance will further help to design efficient catalysts.

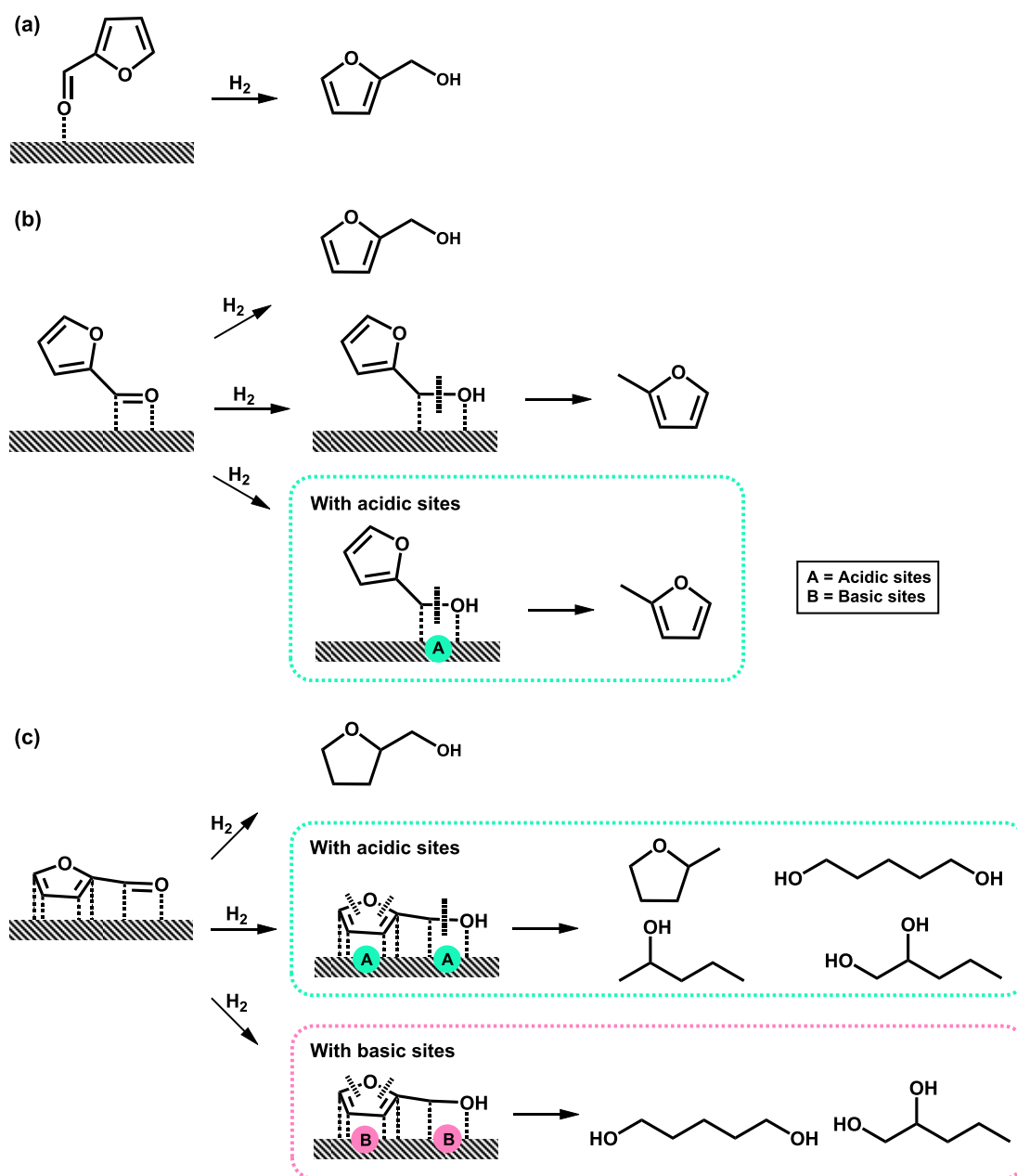
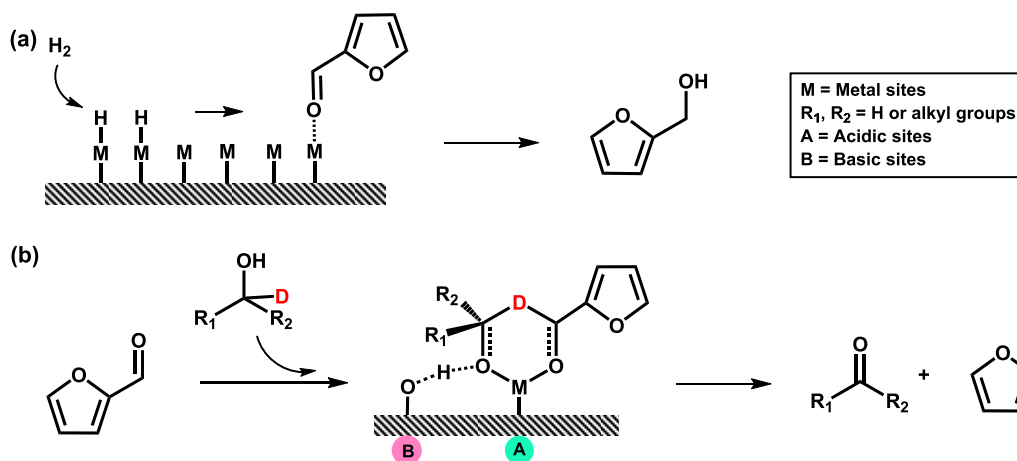


Fig.1.2 Mechanisms of FF hydrogenation by different adsorption configurations.

Density functional theory (DFT) calculations as well as spectroscopic techniques (e.g. Fourier transformed infrared (FT-IR) spectra) have previously been applied to investigate adsorption modes of FF on different metal-based catalysts. Three

different modes have been proposed. (Fig. 1.2) Cu-based catalysts have first mode. FF adsorbs preferentially *via* the lone pair of electrons on oxygen to Cu adopting a top $\eta^1(\text{O})$ -aldehyde binding mode.^{45,46} The FF molecule lies perpendicular to the catalyst surface, while the furan ring experiences net repulsion due to overlap of the 3d band of the surface Cu atoms with the furan ring.⁴⁵ Therefore, the aldehyde group would be hydrogenated by activated H attack and FAL forms (Scheme 1.4a). Based on DFT calculation Lee et al. proposed a mechanism where the Cu-based catalyst under H_2 gas firstly adsorbs FF *via* the oxygen of the aldehyde group, then the migration and addition of dissociated H atoms into FF to form FAL (Scheme 1.4a).⁴⁷ Liu et al. used *in situ* FT-IR spectroscopy to measure FF adsorbed on copper powders, which also gave the result that FF has a $\eta^1(\text{O})$ adsorption configuration of the carbonyl moiety (1666 cm^{-1}) *via* the interaction between the oxygen atom in the C=O bond and the metal atom.⁴⁸



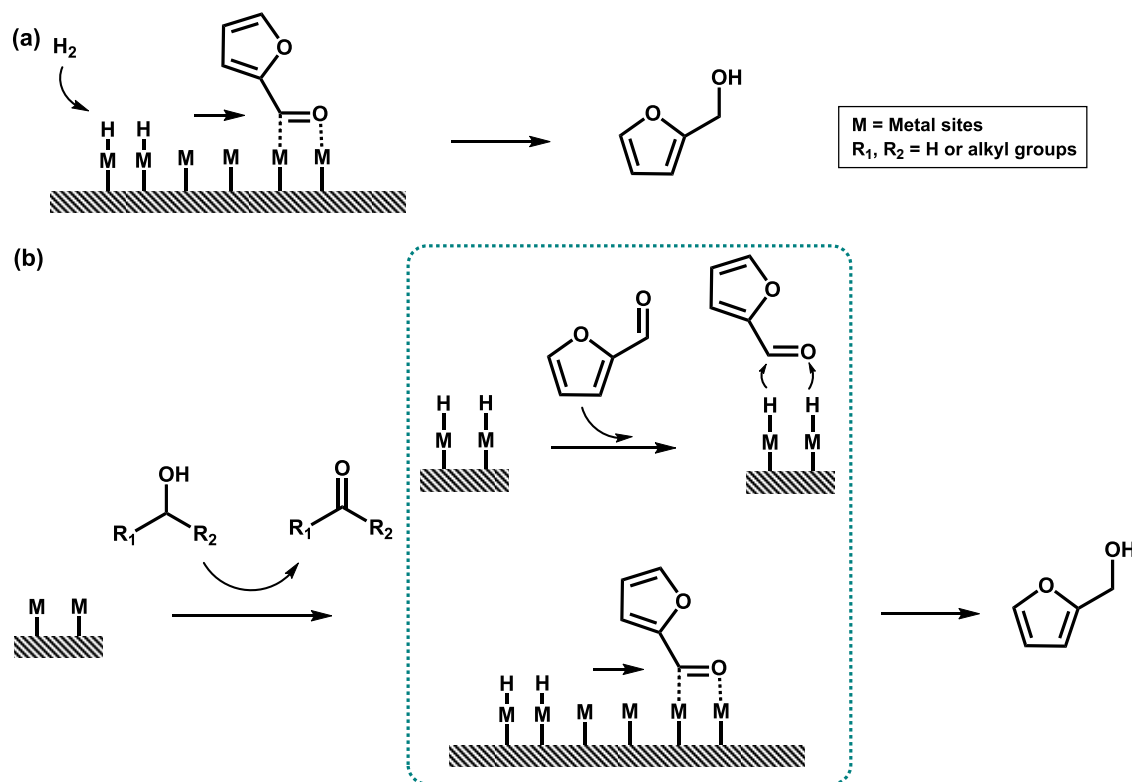
Scheme 1.4 (a) FF hydrogenation reaction on Cu-based catalyst under H_2 gas. Adapted and redrawn from ref 47. (b) Catalytic transfer hydrogenation reactions of FF *via* direct hydrogenation transfer. Adapted and redrawn from ref 49.

FF can also be hydrogenated without the use of external hydrogen gas, which can reduce complexity and cost of experimental steps and increase the safety.⁴⁹

Catalytic transfer hydrogenation (CTH) employs liquid-phase hydrogen sources, e.g. alcohols, formic acid (FA), formates and hydrosilanes.⁴⁹ In the direct transfer hydrogenation route, the hydrogen transfer occurs directly from alcohol to carbonyl group *via* a six-membered cyclic transition state, referred to as the Meerwein–Ponndorf–Velery (MPV) mechanism. Acidic and basic sites of the catalyst are dominantly responsible for the CTH reaction during the hydrogen transfer. Basic sites can adsorb a proton from the alcohol and acidic sites bond with oxygen from hydroxyl and carbonyl groups to form six-membered intermediates. Then α -H is transferred from the α -C of the alcohol to the carbonyl group of FF (Scheme 1.4b).⁴⁹ Ma et al. combined FF absorbed attenuated total reflectance (ATR)-IR, X-ray photoelectron spectroscopy (XPS), and NH_3 -IR spectra to prove that in basic zirconium carbonate Zr^{4+} species (Lewis acidic sites) can activate the C=O group and both acidic and basic sites co-catalyze the CTH.⁵⁰ A poisoning experiment was performed by adding pyridine and boric acid to block the corresponding acidic and basic centers in the CTH of FF catalyzed by Zr-containing polyphenolic biopolymer catalysts in 2-propanol. The results indicated that both acidic and basic species contributed to the catalytic performance.⁵¹

The repulsion between the furan ring and the metal surface is absent or low with Group VIII metal-based (Pd, Pt, Ni, Co, etc.) or bimetallic (i.e. CuNi, PdIr, PdCu) catalysts making flat $\eta^2(\text{C}=\text{O})$ binding modes with or without furan ring adsorption favored (Figs. 1.2b and 1.2c).⁵²⁻⁵⁵ As only the aldehyde group of FF is adsorbed by a flat $\eta^2(\text{C}=\text{O})$ configuration, the C=O bond would be hydrogenated to form FAL (Scheme 1.5a). In Co-based catalyst system both FF adsorptive experiment and DFT study revealed that the highly selective hydrogenation of FF to FAL was resulted from the favorable activation of the aldehyde group of FF.⁵⁶

Tang et al. synthesized a CuNi alloy which had a tilted adsorption mode with $\eta^2(\text{C}=\text{O})$ for FF to enable the selective conversion of FF to FAL or THFA under H_2 gas.³³ Other works also found that the addition of Ni to Cu can shift the FF adsorption from $\eta^1(\text{O})$ to $\eta^2(\text{C}=\text{O})$.^{48,57} The most stable adsorption mode of FF on a Pd (111) surface involves both the furan ring and aldehyde group lying flat onto the metal surface. The addition of Ir/Cu to Pd could promote the adsorption of C=O group of FF and weaken the adsorption of furan ring, shifting the FF adsorption configuration from flat adsorption to mostly C=O moiety adsorption, thereby facilitating the formation of FAL.^{55,58}

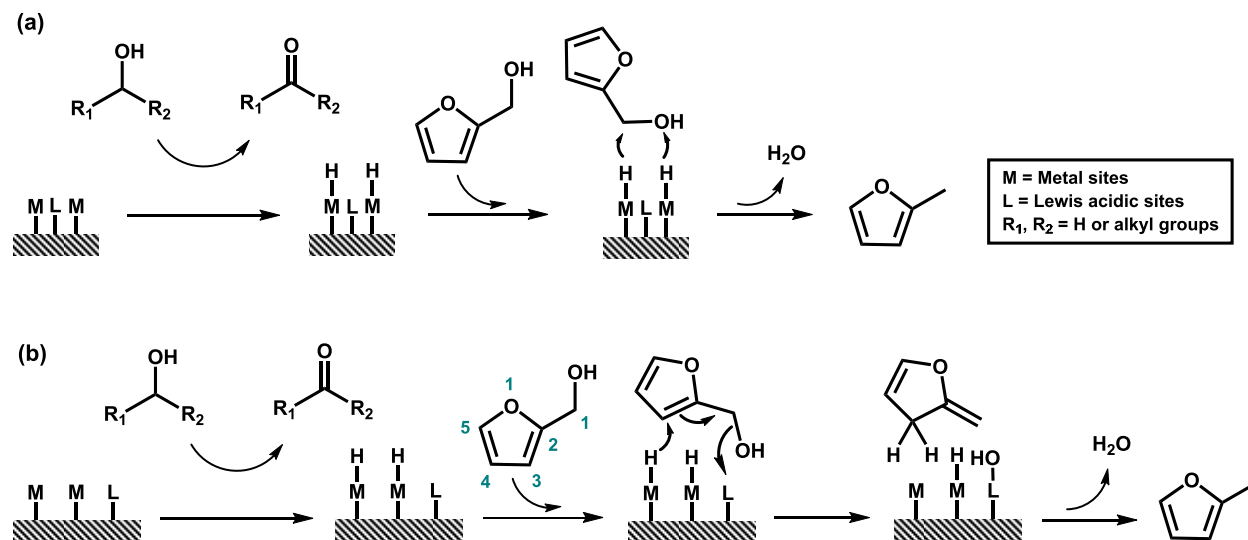


Scheme 1.5 (a) FF hydrogenation reaction on metal-based catalyst under H_2 gas. Adapted and redrawn from ref 33. (b) Catalytic transfer hydrogenation reactions of FF *via* direct metal hydride route. Adapted and redrawn from ref 49.

Some metals or certain oxidation states of metals have the ability to extract the α -H from alcohols leading to the metal hydride route (Scheme 1.5b). In this

reaction, the dehydrogenation of the alcohol firstly occurs on metal sites to form H atoms and aldehyde or ketone, followed by the addition of the adsorbed H atoms to the C=O bonds of FF or the transfer of adsorbed H atoms to the adsorbed aldehyde group of FF. All H atoms are adsorbed and activated onto the metal sites before being added to the carbonyl group of FF. Ren et al. used both experimental studies (*in situ* diffuse reflectance infrared fourier transform spectroscopy (DRIFTS) and isotope labelling mass spectrometry (MS)) and DFT calculations to reveal that Cu⁰ and Cu⁺ species co-catalyzed the CTH. Cu⁺ sites could adsorb and activate the C=O group of FF and C–O bond of 2-propanol, while Cu⁰ species promoted the transfer of H atoms between adsorbed substrates.⁵⁹

There are some metal combinations, such as PtZn, NiZn, NiMo, NiFe, which can help to weaken and break C–O bonds, promoting the formation of MF (Fig.1.2b).^{52,60-62} The addition of Zn/Mo/Fe to Pt/Ni significantly weakens the interaction of the aromatic furan ring with the Pt/Ni surface, further tilting the furan ring away from the surface and preventing its hydrogenation. Meantime, this bonding configuration also weakens the C–OH bond leading to the production of MF.^{52,60-62} However, for bifunctional catalysts with acidic sites the C–OH bond could be broken by the acidic sites after the formation of FAL to form MF (Fig.1.2b). Lan et al. introduced phosphorus into nickel (NiP) to adjust the FF adsorption mode from planar adsorption to more stable $\eta^2(\text{C=O})$ configuration in order to, together with the formation of Brønsted acidic sites by phosphorus species, promote the high production of MF.⁶³



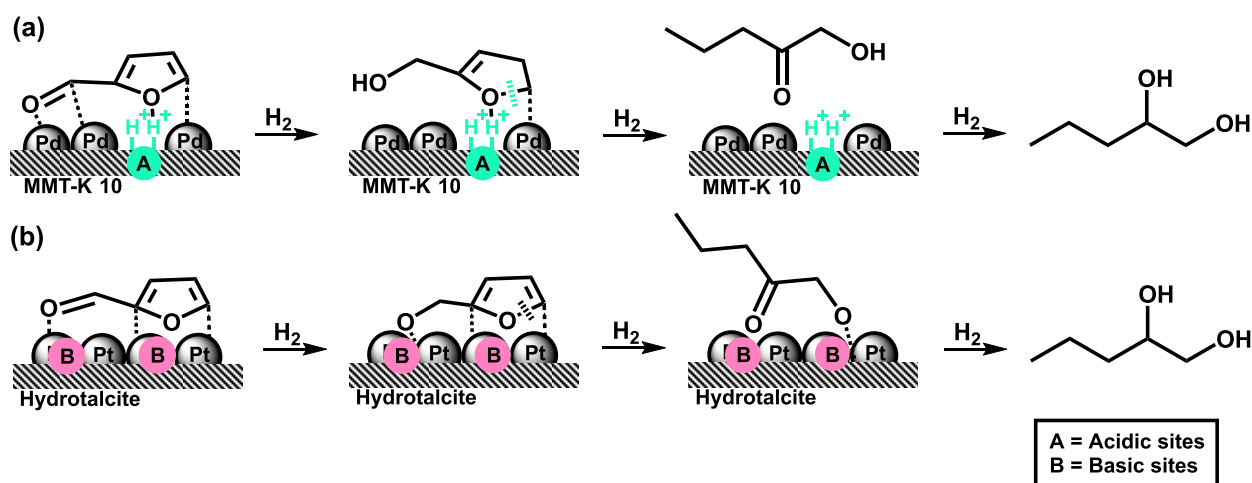
Scheme 1.6 (a) Proposed mechanism for transfer hydrogenation of FF in methanol over copper-based catalyst. Adapted and redrawn from ref 64. (b) Reaction mechanism for the hydrogenolysis of FAL over Ru/RuO_x/C catalyst using isotopic labelling. Adapted and redrawn from ref 49.

In some studies, alcohols are used as hydrogen donors to avoid the use of H₂ gas.⁴⁹ There are two main pathways for the cleavage of the C–OH bond in FAL resulting in hydrogenolysis *via* a direct route or *via* an activation of the furan ring, respectively (Scheme 1.6). In the direct pathway, hydrogen is firstly transferred from the alcohol to metal sites where after FAL is protonated by the hydrogen on the metal surface. The C–OH bond at the α-position is dissociated to produce H₂O with the assist of the Lewis acidic sites and lastly another hydrogen atom on the metal attacks the C-atom at the α-position forming MF (Scheme 1.6a). Oppositely, in the pathway with activation of the furan ring the hydrogens transferred from the alcohol to metal sites attack the C3 of the ring leading to dearomatization of the furan ring by shifting the double bond between C2 and C3 to C1 and C2. The unstable intermediate drives the cleavage of the C–OH bond when associated with a Lewis acidic site and facilitates the generation of water and the target product (Scheme 1.6b). For the FAL hydrogenolysis step with Cu-based systems, Cu⁰ species are active for the

dehydrogenation of the alcohol to form activated hydrogen, and Cu^+ species serve as acidic sites for the dissociation of the C–OH bond. FAL firstly interacts with the active H to generate H_2O with the assistance of acidic sites; then another activated H attacks the C atom at the α -position to form MF (Scheme 1.6a).⁶⁴ Gilkey et al. investigated the formation of MF from FF over Ru/RuO₂/C in 2-propanol *via* a combination of isotopic labelling experiments with mass fragmentation analysis and kinetic studies. After the production of FAL the cleavage of the C–OH bond occurred mainly by ring activation (Scheme 1.6b), which proceeds by a Lewis acid-catalyzed intermolecular hydride transfer mechanism.⁶⁵

Some metal-based catalysts can adsorb both the aldehyde group and furan ring of FF (Fig.1.2c), including Ni which exhibits both $\eta^2(\text{C}=\text{O})$ adsorption as well as furan ring adsorption. As both functional groups are prone to be hydrogenated this leads to THFA formation. In line with this, Meng et al. found that a high exposure of the Ni(111) plane promotes activated adsorption of both the furan ring and aldehyde group of FF, resulting in the production of THFA.⁶⁶ However, not only the metal but also the nature of the support affect the distribution of products. Supports which can provide C=C bond adsorption sites and basic/acidic sites have shown high efficiency in formation of pentanediols from FF (Scheme 1.7).⁶⁷ Date et al. used a metal-acid dual-site catalyst, Pd/montmorillonite clay K10 (MMT-K10), for the hydrogenation of FF to 1,2-PeD (Scheme 1.7a).⁶⁸ The presence of acidic sites (H^+) on the support plays a key role during the reaction. Based on the results of experiments and catalyst characterization, a reaction mechanism was proposed where the aldehyde group of FF was adsorbed on the Pd and firstly hydrogenated to FAL. Both Pd and the acidic sites in the support could adsorb the furan ring of FAL, leading to the

oblique adsorption on the surface of the catalyst. The activated H on the Pd surface hydrogenated the C4=C5 bond, forming a p- π conjugate consisting of the p orbital of O1 with the C2=C3 double bond. Meanwhile, the C5-O1 bond was weakened and subsequently broken to produce 1-hydroxy-2-pentanone (1-HP), which is further hydrogenated to 1,2-PeD over the Pd metal. In this reaction acidic sites catalyzed the ring opening and dehydration while metal sites catalyzed the hydrogenation.⁶⁸



Scheme 1.7 (a) Possible mechanistic pathway for 1,2-PeD formation over Pd/MMT-K10 catalyst. Adapted and redrawn from ref 68. (b) Mechanism of furfural over Pt/hydrotalcite to 1,2-PeD with FAL as an intermediate. Adapted and redrawn from ref 43.

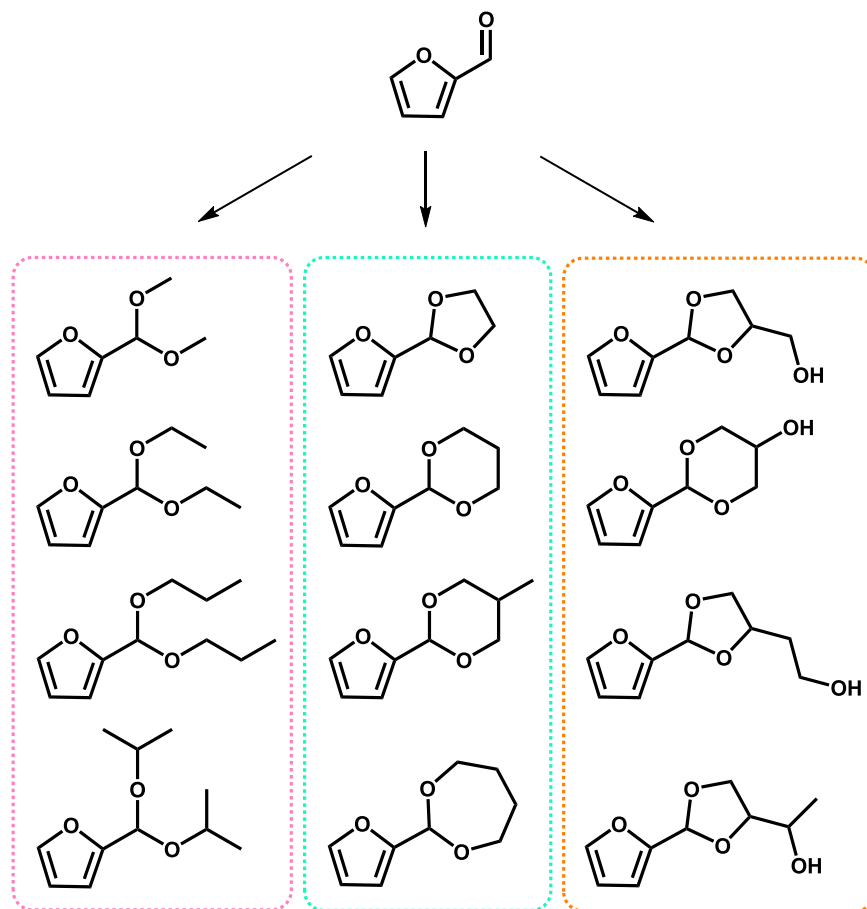
Mizugaki et al. found that a Pt/hydrotalcite catalyst with basicity could also catalyze the hydrogenation of FF to 1,2-PeD without adding any additives, and the existence of basic sites was critical to the formation of 1,2-PeD.⁴³ On this basis, the reaction path for the conversion FF to 1,2-PeD over such bifunctional Pt-based catalyst was proposed to differ from that of metal-acid catalyst (Scheme 1.7b). Firstly, H₂ was adsorbed and dissociated on the surface of Pt forming FAL, where after a basic site adjacent to Pt adsorbed the -OH group of FAL. Subsequently, the activated hydrogen at the interface between Pt and its

adjacent basic site was quickly transferred to C4=C5, hydrogenating the functionality. Simultaneously, the C5–O1 bond was weakened and broken to produce 1-HP, which was lastly converted into 1,2-PeD. The cooperative behavior of the Pt and basic sites catalyzed the ring opening and dehydration while Pt catalyzed hydrogenation.⁴³

Overall, both the selection of metal(s), support as well as hydrogen source has an impact on the product distribution during FF hydrogenation. The metal sites dominate the adsorption configuration of FF and further affect the hydrogenation of different functional groups. The acidity/basicity of the support can promote the breaking of bonds, such as the C1–OH, C2–O1, and C5–O1 bonds. The combination of acidity/basicity and hydrogen source (alcohol) facilitates the CTH. Chapter 3, 4, 5, and 7 in the thesis are based on these principles for the hydrogenation of furanic compounds.

1.2.2 Acetalization

Acetalization is an effective way to convert biomass-derived platform compounds, such as glycerol, FF, and HMF, into fuel additives.⁶⁹ The aldehyde group of FF can form acetals with different alcohols, diols, and triols, obtaining a variety of products (Scheme 1.8). In alcohol systems (e.g. methanol, ethanol, propanol, and so on), two alcohol molecules react with the aldehyde group to form furfuryl acetals (FACs). In diol systems (e.g. ethylene glycol, 1,2-propanediol, 1,3-propanediol, and so on) one diol molecule reacts with the C=O group to produce cyclic FACs. In triol systems (e.g. glycerol, butane-1,2,3-triol, butane-1,2,4-triol, and so on) two of the –OH groups react with the aldehyde group to yield cyclic FACs.

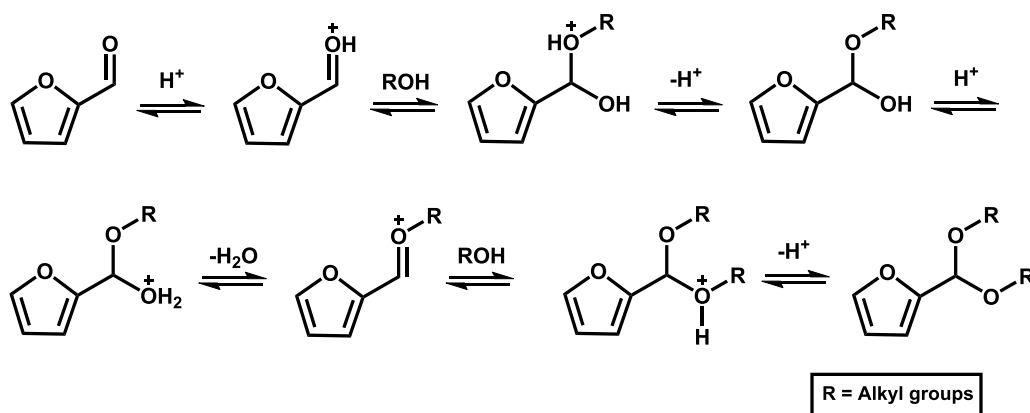


Scheme 1.8 The acetalization of FF with different alcohols, diols, and triols.

According to previous literature, the acetalization is known as an acid-catalyzed equilibrium reaction⁶⁹ with a possible reaction mechanism as shown in Scheme 1.9. The first step is the protonation of the carbonyl group of FF by the acidic site of the catalyst. Then the alcohol reacts with the protonated C=O bond to form a hemiacetal after the removal of the proton. The –OH group of the hemiacetal is further protonated and dehydrated to form an intermediate, which would react with another alcohol molecule. After deprotonation the FAC forms and the acidic site regenerates.^{70,71}

Acetalization of FF has been studied with various acid-catalyzed systems such as Brønsted acids (e.g. p-TSA⁷²), Lewis acids (e.g. ZnCl₂⁷³), solid acids (e.g.

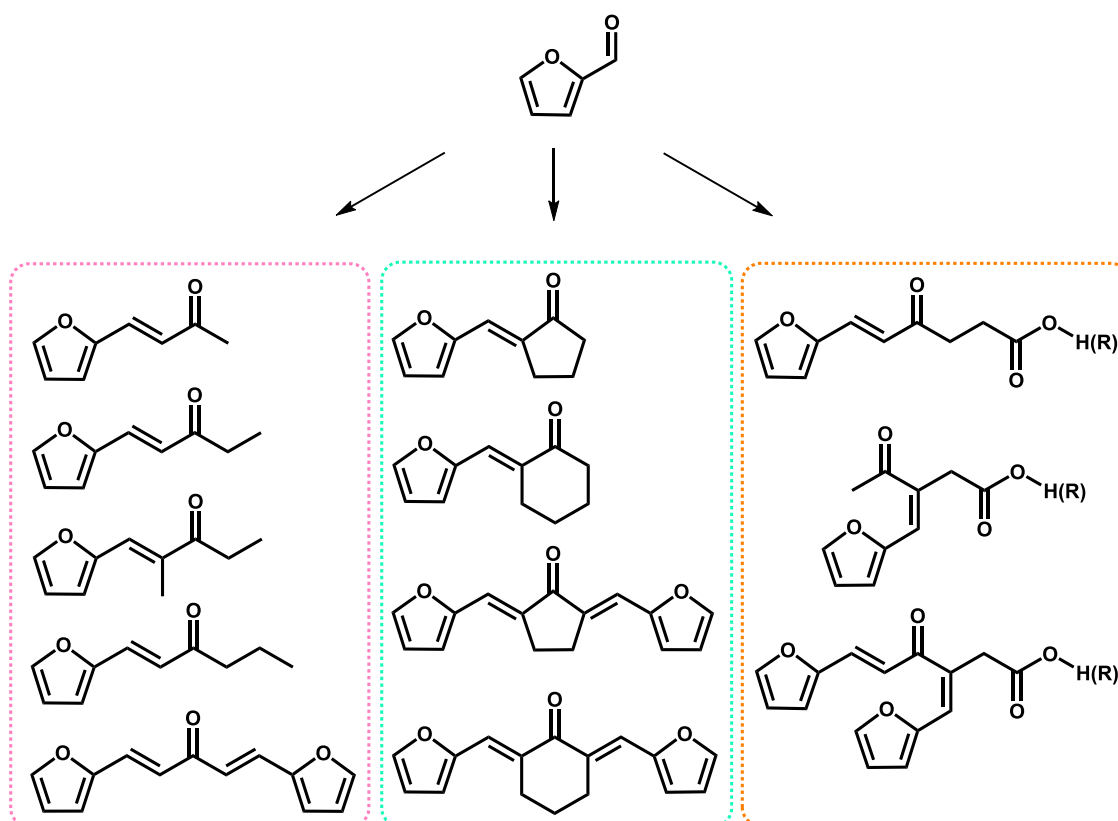
aluminosilica MCM-41⁷³, Montmorillonite K-10 clay⁷³, Zr-Mont⁷⁴, zeolites⁷⁰, heteropolyacids⁷¹). The homogeneous systems show good catalytic activities, however they are highly corrosive and their use require additional steps for neutralization and further products purification, which usually generates undesired waste. Solid acid catalysts have emerged as preferred alternatives for FF acetalization because the products are easily separable and the catalysts reusable, which often makes the process less energy demanding as well as waste-generating and thus more environmentally friendly. Importantly, solid acid catalysts also have adjustable pore size and acidity. Rubio-Caballero et al. tested the zeolites H-ZSM-5, H-USY, H-beta, H-mordenite as solid catalysts for FF acetalization in ethanol. H-USY with large-pore showed the highest catalytic performance. In this case the pore size of zeolites had a stronger influence on the reaction outcome than the amount of acid.⁷⁰ Mallesham et al. added WO_3 , MoO_3 and SO_4^{2-} to SnO_2 to modify the acidity and found that an increase in acidity promoted the FF acetalization with glycerol.⁷⁵



Scheme 1.9 Proposed mechanism of the acid-catalyzed acetalization. Adapted and redrawn from ref 70,71.

Overall, solid catalysts with suitable pore structure and acidities are beneficial for the FF acetalization. In this thesis, Chapter 3 and 5 further explore acetalization of FF.

1.2.3 Aldol condensation

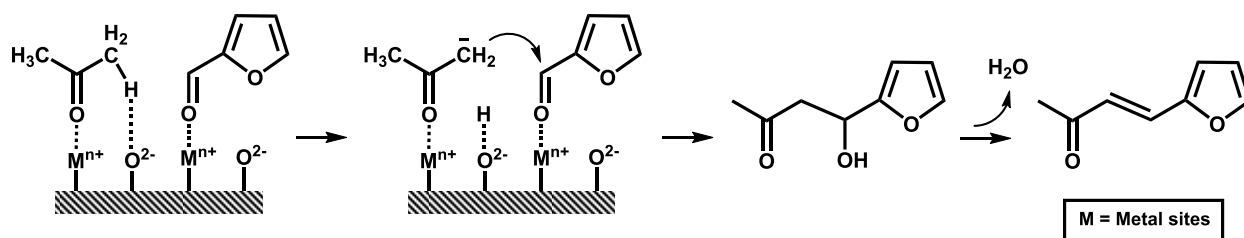


Scheme 1.10 The aldol condensation of FF with different carbonyl compounds.

Aldol condensation is an effective strategy to increase the carbon number of biomass-derived platform compounds.⁷⁶ For the FF aldol condensation various value-added products can be obtained by using different carbonyl compounds (Scheme 1.10), such as open-chain aliphatic ketones, cyclic ketones, LA(levulinate), and so on.⁷⁶ Various catalysts including base catalysts, acid catalysts and bifunctional acid-base catalysts have been used for the FF aldol

condensation. The reaction pathways for the aldol condensation are dependent on the nature of the employed catalysts.

Solid base catalysts like, e.g. Mg-Zr, Mg-Al, Mg-Fe, Zn-Al as well as other mixed oxides have been widely used in the FF aldol condensation due to their suitable basicity (preferably medium-strength basic sites).⁷⁷⁻⁷⁹ The reaction pathway towards aldol condensation of FF with acetone is asserted to contain three consecutive steps (Scheme 1.11). The abstraction of α -H from acetone forms a carbanion, then the nucleophilic addition reaction of the formed carbanion with FF gives an α,β -hydroxyl ketone intermediate, and lastly the dehydration of the α,β -hydroxyl ketone intermediate generates the aldol condensation product.⁷⁸ Basic sites promote the aldol condensation for the strong abstraction of α -H from acetone but have weak ability for the dehydration therefore resulting in high selectivity of α,β -hydroxyl ketone intermediate.^{77,80} Mixed oxide catalysts showed good performance in this reaction owing to the suitable basicities, but reusability was always poor due to the facile blockage of active sites by heavy deposits.⁸⁰

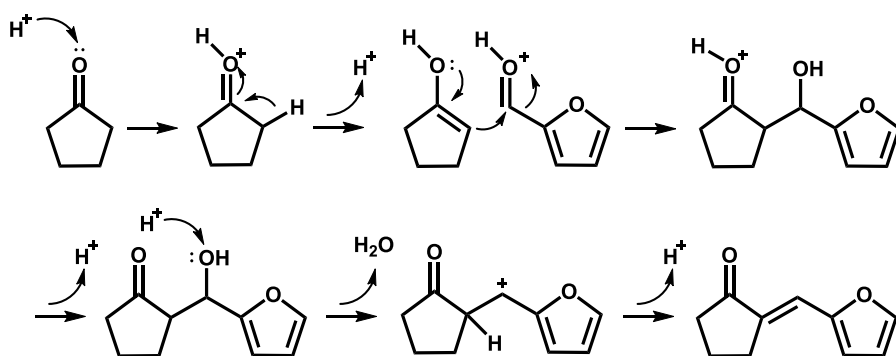


Scheme 1.11 The reaction pathway towards aldol condensation of FF with acetone over base catalyst. Adapted and redrawn from ref 78.

As solid acid catalysts, iron benzene-1,3,5-tricarboxylate and copper benzene-1,3,5-tricarboxylate with Lewis acidity, metal chlorides, ZnO, Nafion, Amberlyst-15, Amberlyst-36 and other catalysts have been applied in the FF aldol condensation.⁸¹⁻⁸³ Compared to the base catalyzed reaction, the acid catalyzed

aldol condensation follows a different mechanism because acidic sites are less active in the abstraction of the H adjacent to the carbonyl group. A proposed mechanism for the acid-catalyzed FF aldol condensation with cyclopentanone (CP) is shown in Scheme 1.12.⁸¹ CP firstly reacted with a proton (H^+) over the solid acid to generate an electron-deficient intermediate, which further activated the carbonyl group and led to the formation of an enol structure. The negatively charged carbon attacked the C atom of $C=O$ of the protonated FF to form an α,β -hydroxyl ketone intermediate, which was further dehydrated to form the aldol condensation product with the assist of H^+ (Scheme 1.12).

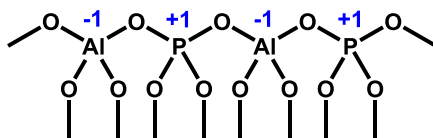
Bifunctional acid-base catalysts are also active for FF aldol condensation. From a combination of characterization results and results from control experiments, Thanh et al. reported that basic sites were the real active species to provide α,β -hydroxyl ketone intermediate, whereas the dehydration of intermediate occurred with the participation of acidic sites.⁸⁴ The synergistic catalysis of acidic and basic sites shows a positive influence on promoting aldol condensation of FF. In the thesis, Chapter 6 focuses on FF aldol condensation.



Scheme 1.12 Reaction mechanism of aldol condensation from FF and CP by acid catalyst. Adapted and redrawn from ref 81.

1.3 Acidity and basicity of aluminophosphate

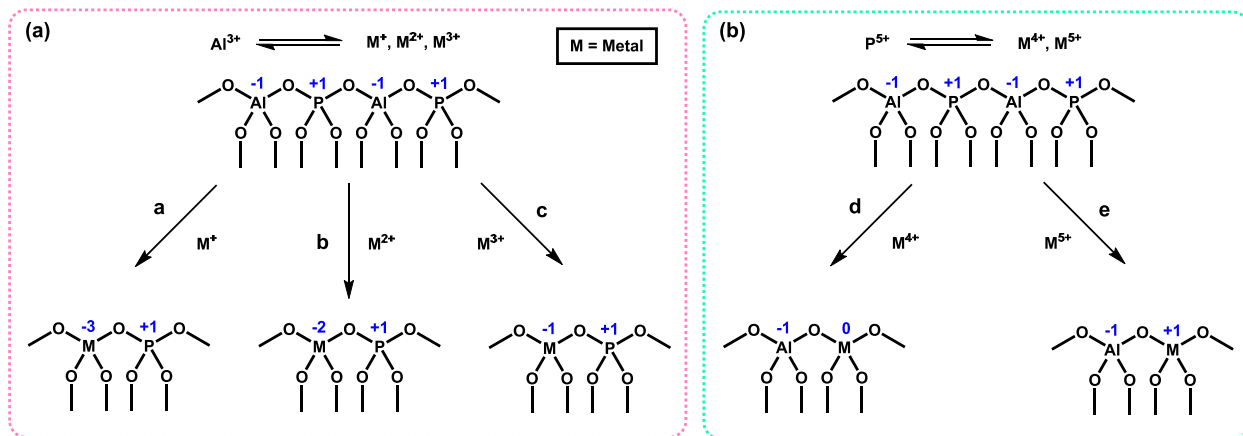
Aluminophosphate-based microporous molecular sieves ($\text{AlPO}_4\text{-}n$), where n denotes a particular structure type, are the first family of framework oxide molecular sieves synthesized without silica.⁸⁵ $\text{AlPO}_4\text{-}n$ frameworks are three-dimensional channels, and consist of tetrahedron of Al^{3+} and P^{5+} linked by oxygen atoms, resulting neutral frameworks (Scheme 1.13).^{86,87} $\text{AlPO}_4\text{-}n$ cover a wide range of various structure types, such as APO-5 (AFI), APO-11 (AEL), APO-34 (CHA), APO-31 (ATO), APO-36 (ATS), and APO-37 (FAU).⁸⁸ The APO-5, composed of 4-ring, 6-ring, and 12-ring, has widely catalytic applications. The diameter of main channels is 7.3 Å,⁸⁹ which fits the kinetic diameter of FF (5.6 Å) well.⁹⁰ Therefore, APO-5 molecular sieves were chosen as catalysts for FF conversion in this thesis.



Scheme 1.13 Assembly of a microporous aluminophosphate material. Adapted and redrawn from ref 86.

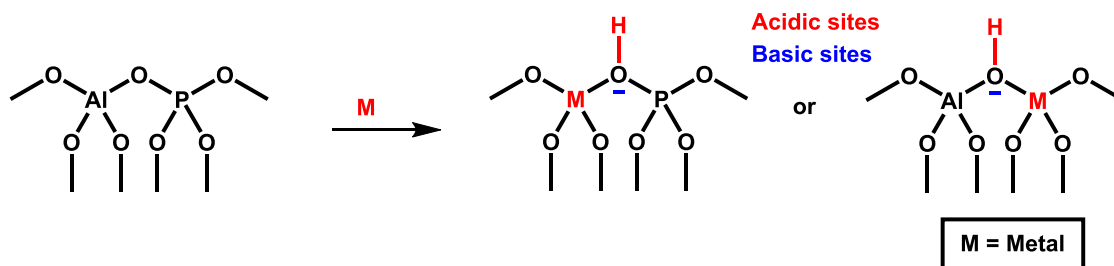
Transition metal ions (TMIs) can be introduced to create acidic and basic sites by two different methods (isomorphous substitution and impregnation) as $\text{AlPO}_4\text{-}n$ frameworks are neutral.^{91,92} Isomorphous substitution is a method that Al and/or P can be partially replaced by another metal element with similar cation radius and coordination requirements.⁸⁸ According to the valence of TMI different substitution mechanisms (SMs) can be envisaged (Scheme 1.14). An aluminum atom can be replaced with a TMI with valence +1 (A), +2 (B), and +3 (C), while P can be substituted with elements with valence from +4 (D) to +5 (E).^{86,88} However, other types not mentioned in the Scheme 1.15 are very unlikely because they

lead to either positively or too negatively charged frameworks. And it is also clear from Scheme 1.14 SM A, B, and D result in negatively charged frameworks, which needs to be balanced by protons or other ions. On the other hand, SM C and E lead to electroneutral frameworks without charge balancing ions.



Scheme 1.14 Proposed models for framework substitution, (a) Al substitution and (b) P substitution. Adapted and redrawn from ref 86,88.

Protons used to balance negatively charged frameworks and TMI act as acidic sites (Scheme 1.15).^{88,93} The framework oxygen atom adjacent to the proton should also possess a negative charge, generating basic sites (Scheme 1.15).⁹⁴⁻⁹⁶ Therefore, different TMI substitutions can be used to form various acidic and basic sites.

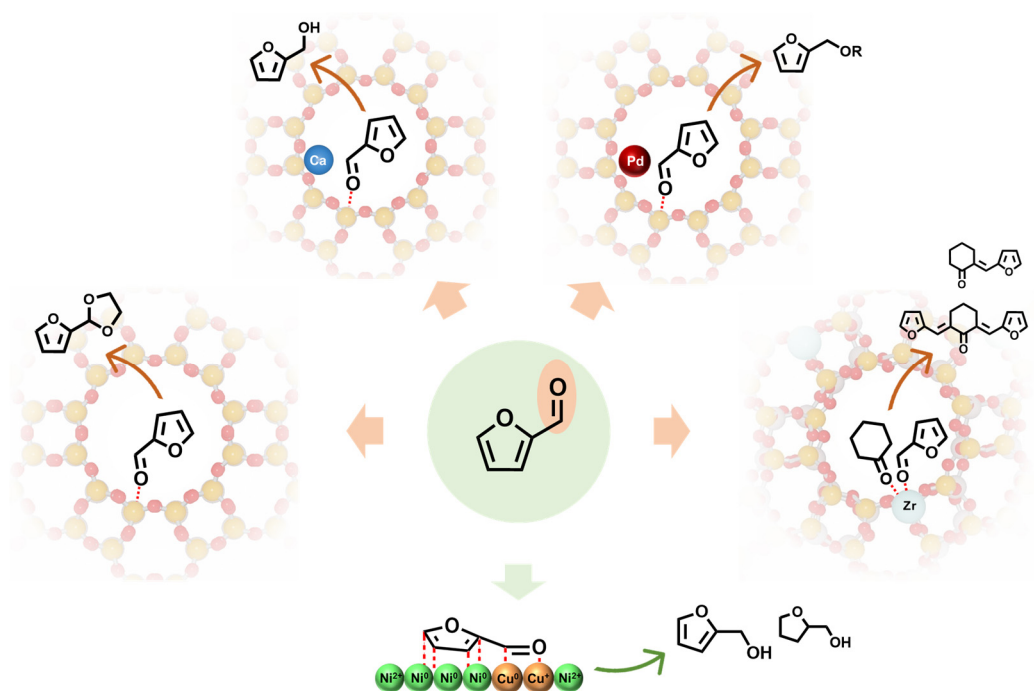


Scheme 1.15 Model explaining the way isomorphous substitution generates surface acidic and basic sites. Adapted and redrawn from ref 88,96.

As $\text{AlPO}_4\text{-}n$ have no formal ion-exchange capacity,⁸⁷ impregnation is the other way to introduce TMI. After impregnation TMIs exist as metal or metal oxide species in channels and cavities outside the framework to provide acidic and basic sites.⁹⁷

These two methods are used in this thesis to create or modify the acidity and basicity of APO-5.

1.4 Scope of this thesis



Scheme 1.16 Overview of the whole PhD project.

This thesis focuses on the efficient and selective valorization of biomass-derived FF with heterogeneous catalysis (Scheme 1.16), and demonstrates how value-added reactions can be developed to obtain more sustainable chemistry. The thesis comprises five parts describing the highly selective conversion of FF into various products with rationally designed and synthesized catalyst systems. However, all the catalytic systems are also applicable for the conversion of

analogous carbonyl compounds. The catalyst design strategies used included major and minor adjustments of acidity/basicity of catalysts by the introduction of different metals and also the oxidation states of metals by reduction at different temperatures. The five parts are summarized below:

Part I: APO-5s with different Al to P ratios were synthesized for the FF conversion. As the APO-5s showed specific adsorption of the C=O bond of FF, weakly acidic APO-5(1) catalyzed FF acetalization in ethylene glycol (EG) with 96% yield and acidic APO-5(1.5) catalyzed CTH and subsequent etherification of FF in 2-propanol with 55% yield.

Part II: Alkaline earth metals (Mg, Ca, Sr, and Ba) were introduced to tune the acidity/basicity of acidic APO-5(1.5) further suppressing the subsequent etherification after CTH. 90% FAL yield was obtained.

Part III: Furanic ether biofuels formed in high yield (99%) from FF by a novel, simple, and efficient catalytic approach using Pd nanoparticles supported on APO-5(1.5) with FA as a hydrogen donor.

Part IV: Zr-doped aluminum phosphate (ZrAPO-5) catalysts were synthesized by replacement of P with Zr in APO-5. The introduction of Zr enhanced C=O adsorption of FF and created suitable acidic and basic sites, further promoting the aldol condensation of FF with cyclohexanone (CH).

Part V: KIT-6-templated mesoporous CuNiO_x catalysts were synthesized and applied for the selective hydrogenation of FF under moderately mild reaction conditions. Cu⁺ species contributed with hydrogen activation and CuNi alloy phases were the active adsorption sites for the FF. The co-catalysis realized excellent performance with 98% FAL yield and 97% THFA yield.

1.5 References

- [1] H. Ritchie, M. Roser, P. Rosado, in *Energy*, <https://ourworldindata.org/energy>, **2022**.
- [2] J. Tollefson, *Nature* **2015**, 521, 16-17.
- [3] D. R. Gentner, S. H. Jathar, T. D. Gordon, R. Bahreini, D. A. Day, I. El Haddad, P. L. Hayes, S. M. Pieber, S. M. Platt, J. de Gouw, A. H. Goldstein, R. A. Harley, J. L. Jimenez, A. S. Prevot, A. L. Robinson, *Environ. Sci. Technol.* **2017**, 51, 1074-1093.
- [4] H. Ritchie, M. Roser, P. Rosado, in *CO₂ and Greenhouse Gas Emissions*, [https://ourworldindata.org/CO₂-emissions](https://ourworldindata.org/CO2-emissions), **2020**.
- [5] M. R. Allen, D. J. Frame, C. Huntingford, C. D. Jones, J. A. Lowe, M. Meinshausen, N. Meinshausen, *Nature* **2009**, 458, 1163-1166.
- [6] H. D. Matthews, N. P. Gillett, P. A. Stott, K. Zickfeld, *Nature* **2009**, 459, 829-832.
- [7] N. P. Gillett, V. K. Arora, K. Zickfeld, S. J. Marshall, W. J. Merryfield, *Nat. Geosci.* **2011**, 4, 83-87.
- [8] T. Li, C. Chen, A. H. Brozena, J. Y. Zhu, L. Xu, C. Driemeier, J. Dai, O. J. Rojas, A. Isogai, L. Wagberg, L. Hu, *Nature* **2021**, 590, 47-56.
- [9] A. Sharma, M. Dharwal, T. Kumari, *Mater. Today: Proc.* **2022**, 60, 788-790.
- [10] L. T. Mika, E. Csefalvay, A. Nemeth, *Chem. Rev.* **2018**, 118, 505-613.
- [11] F. A. Kuchеров, L. V. Romashov, K. I. Galkin, V. P. Ananikov, *ACS Sustain. Chem. Eng.* **2018**, 6, 8064-8092.
- [12] M. J. Climent, A. Corma, S. Iborra, *Green Chem.* **2014**, 16, 516.
- [13] S. K. Bhatia, S. S. Jagtap, A. A. Bedekar, R. K. Bhatia, A. K. Patel, D. Pant, J. Rajesh Banu, C. V. Rao, Y. G. Kim, Y. H. Yang, *Bioresour. Technol.* **2020**, 300, 122724.
- [14] J. P. Lange, E. van der Heide, J. van Buijtenen, R. Price, *ChemSusChem* **2012**, 5, 150-166.
- [15] D. M. Alonso, J. Q. Bond, J. A. Dumesic, *Green Chem.* **2010**, 12, 1493-1513.
- [16] J. J. Bozell, G. R. Petersen, *Green Chem.* **2010**, 12, 539.
- [17] P. Gallezot, *Chem. Soc. Rev.* **2012**, 41, 1538-1558.
- [18] Y.-B. Huang, Y. Fu, *Green Chem.* **2013**, 15, 1095.
- [19] X. Li, Y. Chen, J. Nielsen, *Curr. Opin. Biotechnol.* **2019**, 57, 56-65.
- [20] Y. Luo, Z. Li, X. Li, X. Liu, J. Fan, J. H. Clark, C. Hu, *Catal. Today* **2019**, 319, 14-24.
- [21] X. Li, P. Jia, T. Wang, *ACS Catal.* **2016**, 6, 7621-7640.
- [22] A. F. V. Grote, B. Tollens, *Justus Liebigs Ann. Chem.* **1875**, 175, 181-204.
- [23] X. Tong, Y. Ma, Y. Li, *Appl. Catal. A-Gen.* **2010**, 385, 1-13.
- [24] M. E. Zakrzewska, E. Bogel-Lukasik, R. Bogel-Lukasik, *Chem. Rev.* **2011**, 111, 397-417.
- [25] L. Hu, J. X. Xu, S. Y. Zhou, A. Y. He, X. Tang, L. Lin, J. M. Xu, Y. J. Zhao, *ACS Catal.* **2018**, 8, 2959-2980.
- [26] Y. Qian, L. Zhu, Y. Wang, X. Lu, *Renew. Sust. Energ. Rev.* **2015**, 41, 633-646.

- [27] Z. Gao, C. Y. Li, G. L. Fan, L. Yang, F. Li, *Appl. Catal. B-Environ.* **2018**, 226, 523-533.
- [28] T. S. Hansen, I. Sádaba, E. J. García-Suárez, A. Riisager, *Appl. Catal. A-Gen.* **2013**, 456, 44-50.
- [29] B. Girisuta, L. P. B. M. Janssen, H. J. Heeres, *Green Chem.* **2006**, 8, 701.
- [30] G. W. Huber, J. N. Chheda, C. J. Barrett, J. A. Dumesic, *Science* **2005**, 308, 1446-1450.
- [31] B. Kamm, M. Gerhardt, G. Dautzenberg, *New and Future Developments in Catalysis: Chapter 5. Catalytic Processes of Lignocellulosic Feedstock Conversion for Production of Furfural, Levulinic Acid, and Formic Acid-Based Fuel Components*, Elsevier Science, **2013**.
- [32] Y. Wang, D. Zhao, D. Rodríguez-Padrón, C. Len, *Catalysts* **2019**, 9, 796.
- [33] F. Tang, L. Wang, M. Dessie Walle, A. Mustapha, Y.-N. Liu, *J. Catal.* **2020**, 383, 172-180.
- [34] J. Wu, G. Gao, J. Li, P. Sun, X. Long, F. Li, *Appl. Catal. B-Environ.* **2017**, 203, 227-236.
- [35] C. D. Hurd, J. W. Garrett, E. N. Osborne, *J. Am. Chem. Soc.* **1933**, 55, 1082-1084.
- [36] S. Chen, R. Wojcieszak, F. Dumeignil, E. Marceau, S. Royer, *Chem. Rev.* **2018**, 118, 11023-11117.
- [37] C. Xu, E. Paone, D. Rodriguez-Padron, R. Luque, F. Mauriello, *Chem. Soc. Rev.* **2020**, 49, 4273-4306.
- [38] Y. Nakagawa, M. Tamura, K. Tomishige, *ACS Catal.* **2013**, 3, 2655-2668.
- [39] A. Tuan Hoang, V. Viet Pham, *Renew. Sust. Energ. Rev.* **2021**, 148, 111265.
- [40] R. Huang, Q. Cui, Q. Yuan, H. Wu, Y. Guan, P. Wu, *ACS Sustain. Chem. Eng.* **2018**, 6, 6957-6964.
- [41] F. Dong, Y. Zhu, G. Ding, J. Cui, X. Li, Y. Li, *ChemSusChem* **2015**, 8, 1534-1537.
- [42] S. Liu, Y. Amada, M. Tamura, Y. Nakagawa, K. Tomishige, *Catal. Sci. Technol.* **2014**, 4, 2535-2549.
- [43] T. Mizugaki, T. Yamakawa, Y. Nagatsu, Z. Maeno, T. Mitsudome, K. Jitsukawa, K. Kaneda, *ACS Sustain. Chem. Eng.* **2014**, 2, 2243-2247.
- [44] B. Seemala, R. Kumar, C. M. Cai, C. E. Wyman, P. Christopher, *React. Chem. Eng.* **2019**, 4, 261-267.
- [45] S. Sitthisa, T. Sooknoi, Y. Ma, P. B. Balbuena, D. E. Resasco, *J. Catal.* **2011**, 277, 1-13.
- [46] Y. Shi, Y. Zhu, Y. Yang, Y.-W. Li, H. Jiao, *ACS Catal.* **2015**, 5, 4020-4032.
- [47] J. Lee, J. H. Seo, C. Nguyen-Huy, E. Yang, J. G. Lee, H. Lee, E. J. Jang, J. H. Kwak, J. H. Lee, H. Lee, K. An, *Appl. Catal. B-Environ.* **2021**, 282, 119576.
- [48] M. Liu, L. Yuan, G. Fan, L. Zheng, L. Yang, F. Li, *ACS Appl. Nano Mater.* **2020**, 3, 9226-9237.
- [49] W. Fang, A. Riisager, *Green Chem.* **2021**, 23, 670-688.
- [50] M. Ma, P. Hou, J. Cao, H. Liu, X. Yan, X. Xu, H. Yue, G. Tian, S. Feng, *Green Chem.* **2019**, 21, 5969-5979.

- [51] S. H. Zhou, F. L. Dai, Z. Y. Xiang, T. Song, D. T. Liu, F. C. Lu, H. S. Qi, *Appl. Catal. B-Environ.* **2019**, 248, 31-43.
- [52] S. Sitthisa, W. An, D. E. Resasco, *J. Catal.* **2011**, 284, 90-101.
- [53] V. Vorotnikov, G. Mpourmpakis, D. G. Vlachos, *ACS Catal.* **2012**, 2, 2496-2504.
- [54] J. W. Medlin, *ACS Catal.* **2011**, 1, 1284-1297.
- [55] Y. Nakagawa, K. Takada, M. Tamura, K. Tomishige, *ACS Catal.* **2014**, 4, 2718-2726.
- [56] H. Ishikawa, M. Sheng, A. Nakata, K. Nakajima, S. Yamazoe, J. Yamasaki, S. Yamaguchi, T. Mizugaki, T. Mitsudome, *ACS Catal.* **2021**, 11, 750-757.
- [57] B. Seemala, C. M. Cai, C. E. Wyman, P. Christopher, *ACS Catal.* **2017**, 7, 4070-4082.
- [58] K. Fulajtárova, T. Soták, M. Hronec, I. Vávra, E. Dobročka, M. Omastová, *Appl. Catal. A-Gen.* **2015**, 502, 78-85.
- [59] Y. Ren, Y. Yang, L. Chen, L. Wang, Y. Shi, P. Yin, W. Wang, M. Shao, X. Zhang, M. Wei, *Appl. Catal. B-Environ.* **2022**, 314, 121515.
- [60] D. Shi, J. M. Vohs, *ACS Catal.* **2015**, 5, 2177-2183.
- [61] X. Meng, L. Wang, L. Chen, M. Xu, N. Liu, J. Zhang, Y. Yang, M. Wei, *J. Catal.* **2020**, 392, 69-79.
- [62] W. Liu, Y. Yang, L. Chen, E. Xu, J. Xu, S. Hong, X. Zhang, M. Wei, *Appl. Catal. B-Environ.* **2021**, 282, 119569.
- [63] X. Lan, R. Pestman, E. J. M. Hensen, T. Weber, *J. Catal.* **2021**, 403, 181-193.
- [64] J. Zhang, J. Z. Chen, *ACS Sustain. Chem. Eng.* **2017**, 5, 5982-5993.
- [65] M. J. Gilkey, P. Panagiotopoulou, A. V. Mironenko, G. R. Jenness, D. G. Vlachos, B. J. Xu, *ACS Catal.* **2015**, 5, 3988-3994.
- [66] X. Meng, Y. Yang, L. Chen, M. Xu, X. Zhang, M. Wei, *ACS Catal.* **2019**, 9, 4226-4235.
- [67] J. Tan, Y. Su, K. Gao, J. Cui, Y. Wang, Y. Zhao, *J. Fuel Chem. Technol.* **2021**, 49, 780-790.
- [68] N. S. Date, R. C. Chikate, H.-S. Roh, C. V. Rode, *Catal. Today* **2018**, 309, 195-201.
- [69] A. R. Trifoi, P. Ş. Agachi, T. Pap, *Renew. Sust. Energ. Rev.* **2016**, 62, 804-814.
- [70] J. M. Rubio-Caballero, S. Saravanamurugan, P. Maireles-Torres, A. Riisager, *Catal. Today* **2014**, 234, 233-236.
- [71] M. G. Teixeira, R. Natalino, M. J. da Silva, *Catal. Today* **2020**, 344, 143-149.
- [72] E. V. Gromachevskaya, F. V. Kvitkovsky, E. B. Usova, V. G. Kulnevich, *Chem. Heterocycl. Com.* **2004**, 40, 979-985.
- [73] B. L. Wegenhart, S. Liu, M. Thom, D. Stanley, M. M. Abu-Omar, *ACS Catal.* **2012**, 2, 2524-2530.
- [74] A. Patil, S. Shinde, S. Kamble, C. V. Rode, *Energ. Fuel* **2019**, 33, 7466-7472.
- [75] B. Mallesham, P. Sudarsanam, B. M. Reddy, *Catal. Sci. Technol.* **2014**, 4, 803-813.
- [76] J. He, Q. Qiang, S. Liu, K. Song, X. Zhou, J. Guo, B. Zhang, C. Li, *Fuel* **2021**, 306, 121765.

- [77] I. Sadaba, M. Ojeda, R. Mariscal, J. L. G. Fierro, M. L. Granados, *Appl. Catal. B-Environ.* **2011**, *101*, 638-648.
- [78] L. Faba, E. Diaz, S. Ordonez, *Appl. Catal. B-Environ.* **2012**, *113*, 201-211.
- [79] V. K. Díez, C. R. Apesteguía, J. I. Di Cosimo, *J. Catal.* **2006**, *240*, 235-244.
- [80] O. Kikhtyanin, D. Kadlec, R. Velvarska, D. Kubicka, *ChemCatChem* **2018**, *10*, 1464-1475.
- [81] W. Wang, X. H. Ji, H. G. Ge, Z. Z. Li, G. H. Tian, X. Z. Shao, Q. Zhang, *RSC Adv.* **2017**, *7*, 16901-16907.
- [82] O. Kikhtyanin, D. Kubička, J. Čejka, *Catal. Today* **2015**, *243*, 158-162.
- [83] H. Li, Z. Xu, P. Yan, Z. C. Zhang, *Green Chem.* **2017**, *19*, 1751-1756.
- [84] D. Nguyen Thanh, O. Kikhtyanin, R. Ramos, M. Kothari, P. Ulbrich, T. Munshi, D. Kubička, *Catal. Today* **2016**, *277*, 97-107.
- [85] Stephen T. Wilson, Brent M. Lok, Celeste A. Messina, Thomas R. Cannan, E. M. Flanigen, *J. Am. Chem. Soc.* **1982**, *104*, 1146-1147.
- [86] Bert M. Weckhuysen, R. Ramachandra Rao, Johan A. Martens, R. A. Schoonheydt, *Eur. J. Inorg. Chem.* **1999**, 565-577.
- [87] S. Prasad, I. Balakrishnan, *Catal. Letters* **1991**, *11*, 105-110.
- [88] M. Hartmann, L. Kevan, *Res. Chem. Intermed.* **2002**, *28*, 625-695.
- [89] P. Demontis, J. G. González, G. B. Suffritti, A. Tilocca, *J. Am. Chem. Soc.* **2001**, *123*.
- [90] J. Jae, G. A. Tompsett, A. J. Foster, K. D. Hammond, S. M. Auerbach, R. F. Lobo, G. W. Huber, *J. Catal.* **2011**, *279*, 257-268.
- [91] B. Feng, J. Li, X. Zhu, Q. Guo, W. Zhang, G. Wen, Z. Zhang, L. Gu, Z. Yang, Q. Zhang, B. Shen, *Catal. Today* **2016**, *263*, 91-97.
- [92] B. P. G. Lischke, U. Lohse, E. Schreier, R. Fricke, *Appl. Catal. A-Gen.* **1908**, 166.
- [93] L. Márchese, J. Chen, J. M. Thomas, *J. Phys. Chem.* **1994**, *98*, 13350-13356.
- [94] M. Huang, S. Kaliaguine, A. Auroux, *Stud. Surf. Sci. Catal.* **1995**, *97*, 311-318.
- [95] R. A. Schoonheydt, P. Geerlings, E. A. Pidko, R. A. van Santen, *J. Mater. Chem.* **2012**, *22*, 18705.
- [96] D. B. Akolekar, M. Huang, S. Kaliaguine, *Zeolites* **1994**, *14*, 519-522.
- [97] T. T. H. Dang, H.-L. Zubowa, U. Bentrup, M. Richter, A. Martin, *Micropor. Mesopor. Mat.* **2009**, *123*, 209-220.

2 Experimental

2.1 Chemicals

Phosphoric acid 85% (H_3PO_4 , $\geq 99.8\%$), aluminum isopropoxide ($\text{Al}(\text{O-}i\text{-Pr})_3$, $\geq 98\%$), triethylamine (Et_3N , $\geq 99\%$), furfural (FF, 99%), furfuryl alcohol (FAL, 98%), methanol ($\geq 99.9\%$), ethanol ($\geq 99.8\%$), 1-propanol ($\geq 99.9\%$), 2-propanol ($\geq 99.5\%$), 1-butanol ($\geq 99.4\%$), 2-butanol (99.5%), 2-methyl-1-propanol (99.5%), 1-pentanol ($\geq 99\%$), 1-hexanol ($\geq 99\%$), 1-octanol ($\geq 99\%$), formic acid (HCOOH , FA, 99%), acetone ($\geq 99.5\%$), 3-pentanone ($\geq 99\%$), 4-heptanone (98%), 5-nonanone (98%), cyclopentanone (CP, $\geq 99\%$), cyclohexanone (CH, $\geq 99.0\%$), cycloheptanone (CHP, 99%), toluene ($\geq 99.9\%$), tetrahydrofuran (THF, $\geq 99.9\%$), 1,4-dioxane (99.8%), ethylene glycol (EG, 99.8%), 1,2-propanediol ($\geq 99.5\%$), 1,3-propanediol (98%), glycerol (99.5%), 1,4-butanediol (99%), 1,5-pentanediol ($\geq 97\%$), 1,6-hexanediol (97%), 5-hydroxymethylfurfural (HMF, $\geq 99\%$), 5-methylfurfural (MFA, 99%), 2,5-furandicarboxaldehyde (FCA, 97%), benzaldehyde ($\geq 99\%$), *m*-tolualdehyde (97%), *p*-tolualdehyde (97%), *o*-tolualdehyde (97%), magnesium nitrate hexahydrate ($\text{Mg}(\text{NO}_3)_2 \cdot 6\text{H}_2\text{O}$, 99%), calcium nitrate tetrahydrate ($\text{Ca}(\text{NO}_3)_2 \cdot 4\text{H}_2\text{O}$, 99%), strontium nitrate ($\text{Sr}(\text{NO}_3)_2$, $\geq 99\%$), barium nitrate ($\text{Ba}(\text{NO}_3)_2$, $\geq 99\%$), calcium oxide (CaO , 99.9%), palladium nitrate dihydrate ($\text{Pd}(\text{NO}_3)_2 \cdot 2\text{H}_2\text{O}$, 99%), palladium chloride (PdCl_2 , 99%), zirconium acetate solution in dilute acetic acid (15.0-17.0 wt.% Zr), polyethylene-polypropyleneglycol (Pluronic P123), hydrochloric acid (HCl , 37 wt.%), tetraethyl orthosilicate (TEOS, 99%), nickel nitrate hexahydrate ($\text{Ni}(\text{NO}_3)_2 \cdot 6\text{H}_2\text{O}$, $\geq 98.5\%$), copper(II) nitrate trihydrate ($\text{Cu}(\text{NO}_3)_2 \cdot 3\text{H}_2\text{O}$, $\geq 99\%$), acetophenone (99%), crotonaldehyde ($\geq 99.0\%$), cinnamaldehyde ($\geq 95\%$), 4-(furan-2-yl)but-3-en-2-one (98%), 2,3-benzofuran (99%), 1,3-diphenyl-2-propenone ($\geq 98.0\%$), dimethyl

sulfoxide (DMSO, $\geq 99.9\%$), methanol- d_4 (MeOD, $\geq 99.8\%$), and decane ($\geq 99\%$) were purchased from Sigma-Aldrich. 2-Propanol-OD ($>98\%$) was purchased from Apollo Scientific Ltd. Sodium hydroxide ($\geq 98.5\%$) was obtained from VWR. All reagents were used without further purification.

2.2 Catalyst preparation

2.2.1 The synthesis of APO-5 and metal-modified APO-5

APO-5

The APO-5 catalysts were prepared as described elsewhere¹ using a gel composition of $1 \sim 1.5\text{Al}_2\text{O}_3:1\text{P}_2\text{O}_5:1\text{Et}_3\text{N}:45\text{H}_2\text{O}$. $\text{Al}(\text{O-}i\text{-Pr})_3$ (14.30 g~21.45 g, 0.07 mol~0.105 mol) was added to 23 mL distilled water and the mixture vigorously stirred for 0.5 h. Then a solution of 85% H_3PO_4 (8.07 g, 0.07 mol) in 5 mL distilled water was added dropwise and the resulting solution stirred for 2 h. Subsequently, Et_3N (4.9 mL) was added slowly followed by stirring for another 1 h where after the solution was transferred to an autoclave, which was tightly closed and kept at 175°C under autogenous pressure for 48 h. After reaction, the autoclave was cooled to room temperature and the obtained product washed with distilled water several times, oven dried at 110°C for 12 h and finally calcined at 550°C for 7 h.

APO-5 with $\text{Al/P} = 1, 1.25$, and 1.5 were denominated as APO-5(1), APO-5(1.25) and APO-5(1.5), respectively. APO-5(1.5) without calcination was denominated as UC/APO-5(1.5)

AEM-loaded APO-5

Alkali earth metal (AEM)-loaded APO-5 ($\text{Al/P} = 1.5$, crystallized at 180°C for 72 h) catalysts were prepared by wet-impregnation using appropriate amounts of

various AEM nitrate salts dissolved in deionized water. The mixture of the AEM nitrate solution and APO-5(1.5) was kept in a close system at room temperature for 12 h, where after the catalyst was dried at 110°C for 12 h followed by calcination at 550°C for 7 h.² The AEM-loaded APO-5(1.5) catalysts were denominated as xM/APO1.5 (x = wt.% metal loading, metal M = Mg, Ca, Sr or Ba).

Pd-loaded APO-5

Palladium-loaded APO-5 (Al/P = 1.5, crystallized at 180°C for 73 h) catalysts were prepared by wet-impregnation using appropriate amounts of Pd(NO₃)₂·2H₂O dissolved in deionized water. The mixture of the Pd solution and APO-5 was kept in a close system at room temperature for 12 h, whereafter the catalyst was dried at 110°C for 12 h followed by calcination at 400°C for 2 h under a flow of formier gas 10% H₂/N₂ (50 mL/min). The Pd-loaded APO-5 catalysts were denominated as Pd-x (x = wt.% Pd metal).

ZrAPO-5

The ZrAPO-5 catalysts were prepared as described elsewhere^{1,3} using a gel composition of nZrO₂:1Al₂O₃:1P₂O₅:1Et₃N:45H₂O (n = 0~0.1). Al(O-i-Pr)₃ (14.30 g, 0.07 mol) was added to 23 mL distilled water and the mixture vigorously stirred (1000 rpm) for 0.5 h. Then a solution of 85% H₃PO₄ (8.07 g, 0.07 mol) in 5 mL distilled water was added dropwise and the resulting solution stirred for 1 h. Subsequently, designated amount of zirconium acetate solution (2.00~7.98 g, 3.5~14 mmol) and Et₃N (4.9 mL) were added slowly one by one with intermediate stirring (600 rpm) for 1 h, where after the solution was transferred to an autoclave which was tightly closed and kept at 180°C under autogenous pressure and static condition for 48 h. After crystallization, the autoclave was

cooled to room temperature and the obtained product washed with distilled water several times, oven dried at 110°C for 12 h and finally calcined at 550°C for 7 h. ZrAPO-5 with $\text{Zr}/\text{Al} = n$ was denominated as ZrAPO(n). For example, ZrAPO-5 with $\text{Zr}/\text{Al} = 0.20$ (the ratio of the synthesis gel) was denominated as ZrAPO(0.20).

2.2.2 The synthesis of mesoporous CuNiO_x

KIT-6 template

KIT-6 was synthesized by a well-known cooperative assembly process.⁴ 13.5 g of P123 was dissolved in 487 mL deionized water and 22 mL HCl. Then the solution was placed on an oil bath at 35°C and 16.7 mL 1-butanol was added. After 1 hour of stirring 29.0 g TEOS was added. The mixture was stirred at 35°C for 24 h and then performed at 60°C under static condition for another 24 h. After that the product was filtrated, washed with water and ethanol, dried at 80°C and then calcined at 550°C for 6 h (7 h ramp).

Mesoporous CuNiO_x

Mesoporous CuNiO_x was prepared *via* nanocasting method using KIT-6 as a template.^{5,6} Aqueous solutions of either 4M $\text{Cu}(\text{NO}_3)_2 \cdot 3\text{H}_2\text{O}$, $\text{Ni}(\text{NO}_3)_2 \cdot 6\text{H}_2\text{O}$ or mixed $\text{Cu}(\text{NO}_3)_2 \cdot 3\text{H}_2\text{O}$ - $\text{Ni}(\text{NO}_3)_2 \cdot 6\text{H}_2\text{O}$ (6 mL) were added dropwise to a mixture of 1.0 g KIT-6 in toluene (10 mL), where after the mixture was heated at 65°C under stirring to remove the solvent. After evaporation, the precipitate was dried at 60°C overnight and ground into a fine powder followed by calcination at 300°C for 5 h under static air. The KIT-6 template was then removed by four consecutive treatments with fresh 2M NaOH (10 mL) at 90°C for 2 h, and the mesoporous CuNiO_x collected and dried at 60°C overnight. The obtained

mesoporous CuNiO_x are denoted as $\text{CuNiO}_x(a/b)$, where a and b represent the relative mole ratio of Cu and Ni.

The as-synthesized CuNiO_x was finally reduced in a flow of 10% H_2/N_2 (50 mL/min) at 120°C, 150°C, 250°C, and 350°C for 1 h. The reduced catalysts are denoted as $\text{CuNiO}_x(a/b)-c$, where c represents the reduction temperature.

2.3 Catalyst characterization

Powder X-ray diffraction (XRD) was carried out on a Huber G670 diffractometer with Cu-K α radiation ($\lambda = 0.154056$ nm) with 2θ ranging from 3-100°. Small angle X-ray scattering (SAXS) was measured for 2θ angles 0.01-7.5° on a XEUS 3.0 X-ray Scattering instrument with CuK α radiation ($\lambda = 0.154189$ nm).

Brunauer-Emmett-Teller (BET) surface area and porosity analysis were analyzed by N_2 physisorption performed at -196°C by a Micromeritics ASAP 2020 instrument. The samples (0.1 g) were degassed at 250°C for 4 h before the measurement.

X-ray fluorescence (XRF) spectra were performed on a PANalytical epsilon3-XL instrument. Samples were prepared by fusing them into disks using a Claisse LeNeo fluxer oven before measurement.

Ammonia and carbon dioxide temperature-programmed desorption (NH_3 -TPD and CO_2 -TPD) were conducted on a Micromeritics AutoChem II 2920 apparatus. Initially, the samples (0.1 g) were exposed to He gas flow (25 mL/min) and heated up to 600°C (10°C/min ramp rate) for 1 h followed by cooling to 100°C. Then NH_3/CO_2 adsorption were carried out by purging with NH_3/CO_2 -He gas mixture (1% NH_3/He ; 5% CO_2/He) for 1 h, where after physically adsorbed gas was removed by purging with He gas for 1 h. Desorption of NH_3/CO_2 was eventually

conducted in the temperature range 100/50 to 600°C with a heating ramp of 10°C/min and the amount of liberated gas quantified by a thermal conductivity detector and calibration curves.

H₂-Temperature-programmed reduction (H₂-TPR) was measured on a Micromeritics AutoChem II 2920 machine. For Pd-loaded APO-5s, before measurement metallic Pd was oxidized in flowing air to allow reduction to metallic Pd by hydrogen. The sample (0.1 g) was firstly calcined under an air flow (25 mL/min) with a heating ramp of 10°C/min to 400°C, then holded at 400°C for 5 h. After cooling to 50°C the gas switched to 5% H₂ in Ar (50 mL/min) then followed by a temperature ramp to 600°C at 10°C/min.

FF and CH temperature-programmed desorption (FF-TPD and CH-TPD) were conducted on a Micromeritics AutoChem II 2920 apparatus. The catalysts with FF/CH were prepared by the following method before the measurements: Catalyst (100 mg), FF (192 mg, 2 mmol) or CH (196 mg, 2 mmol) and methanol (1 mL) were mixed and shaken vigorously for 5 min followed by oven drying at 50°C for 2 h to remove the methanol. Then the samples were transferred for the TPD analysis. Desorption of FF/CH was eventually conducted in the temperature range 50-600°C with a heating ramp of 10°C/min.

H₂-Temperature-programmed desorption (H₂-TPD) was recorded on a Micromeritics AutoChem II 2920 instrument. For CuNiO_x catalysts, before measurement catalysts (0.05 g) were pretreated under He flow (50 mL/min) at 300°C for 1 h after heating (10°C/min). After cooling to 50°C the catalysts were treated under a flow of 5% H₂ in Ar (50 mL/min) while heated to 600°C (10°C/min).

FT-IR spectra of fresh, used and adsorptive catalysts were performed on a NICOLET iS50 (Thermo) spectrometer equipped with an iS50 ATR attachment. The preparation of the adsorptive catalysts with FF and other additives were done as the following method: Catalyst (50 mg), substrate (0.5 mmol), additive (50 mg) and methanol (1 mL) were mixed and shaken vigorously for 5 min followed by oven drying at 80°C for 2 h to remove the methanol.

Scanning electron microscopy (SEM) images were recorded on an AFEG 250 Analytical ESEM at 5 kV.

Transmission electron microscopy (TEM) images of samples were conducted on a Tecnai T20 G2 microscope operated at an acceleration voltage of 200 kV. TEM samples were prepared by ultrasonically dispersing samples in ethanol for 5 min, and two drops of the solution were deposited onto a carbon-coated copper grid.

Thermogravimetric (TG) analysis of samples was evaluated under air flow (30 mL/min) from 25-800°C on a Mettler Toledo thermal analyzer with 10°C/min heating rate.

^{27}Al and ^{31}P magic-angle spinning nuclear magnetic resonance (MAS NMR) spectra were performed on a Bruker AVANCE III HD spectrometer operating at a magnetic field of 14.05 T equipped with a 4 mm CP/MAS BBFO probe.

XPS and X-ray excited Auger electron spectroscopy (XAES) of samples were evaluated ex-situ with a Thermo Scientific system at room temperature using AlK α radiation (1484.6 eV) and a spot size of 400 μm . A flood gun was used to reduce sample charging effects and the obtained spectra were then corrected by setting the C1s binding energy to 284.8 eV. Data processing was done using the Advantage 4.87 software. Signals were corrected using a "Smart" background.

2.4 Catalyst activity

2.4.1 Acetalization, reductive etherification, CTH, and aldol condensation

The acetalization, reductive etherification, CTH, and aldol condensation of FF (Chapter 3, 4, 5, and 6) were conducted in 15 mL ACE pressure tubes in an oil bath with a magnetic stirrer. A mixture of FF, catalyst, and solvent was added to the tube and then the tube placed in an oil bath with stir (600 rpm) and a designated reaction temperature. After a specified reaction time, the tube was cooled to room temperature. For the acetalization, reductive etherification, and CTH of FF the catalyst was filtered and liquid samples of the reaction mixture were analyzed. For the aldol condensation of FF the reaction mixture diluted with acetone to 10 mL in a volumetric flask followed by analysis. The reaction solutions after FF acetalization and reductive etherification were analyzed using DMSO as an internal standard by ^1H NMR (Bruker 400 MHz spectrometer, room temperature, MeOD). The reaction solutions after CTH and aldol condensation were analyzed using decane as an internal standard with gas chromatography-mass spectrometry (GC-MS) (Agilent 6850-5975C) with GC flame-ionization detection (GC-FID) (Agilent 6890N), both equipped with an HP-5MS capillary column (30.0 m \times 250 μm \times 0.25 μm). A mixture of H_2 with a flow rate of 30 mL/min and N_2 with a flow rate of 25 mL/min was used as a carrier gas. The sample injection volume was 1 μL . The injection port temperature was 270°C. The oven was temperature programmed to start at 40°C for 1 min, ramp with 10°C/min to 200°C, ramp with 5°C/min to 270°C, and then hold at this temperature for 5 min. The temperature of flame ionization detector was 270°C. The calibration of all substrates and products was quantified based on the response factor method proposed by Scanlon and Willis.⁷ The cross-aldol condensation products consisted of two possible geometrical isomers of C_{11} (*cis*

and *trans*) and three of C₁₆ (double *cis*, *cis-trans*, and double *trans*) (Fig. S6.1). And self-aldol condensation products consisted of two possible stereoisomers of C₁₂ and three of C₁₈ (Fig. S6.2). All isomers were quantified together when calculating the selectivity and yield.

Acetalization, reductive etherification, CTH, and aldol condensation of other aldehydes were also performed according to the above procedures.

2.4.2 Hydrogenation

The FF hydrogenation reactions (Chapter 7) were conducted in 15 mL stainless-steel high-pressure reactors positioned in an aluminum heating block with controlled magnetic stirring (600 rpm). A mixture of FF (96 mg, 1 mmol), catalyst (20 mg) and 2-propanol (5 mL) was added to the reactor, which was then flushed with N₂ three times and pressurized to 30 bar before placed in the (pre-heated) aluminum heating block at a designated reaction temperature. After a specified reaction time, the reactor was cooled to room temperature and a liquid sample of the reaction mixture filtered, collected, and analyzed by ¹H NMR (Bruker 400 MHz spectrometer, room temperature, MeOD) using DMSO as an internal standard for quantification of FF and the products FAL and THFA.

2.5 Catalyst leaching and recycling test

The reusability of APO-5(1) (Chapter 3) was examined for the acetalization of FF at 150°C after 2 h reactions. After initial reaction, the catalyst was collected *via* centrifugation, washed with acetone and methanol twice (2 × 10 mL), respectively, followed by drying at 80°C for 2 h before being used in the next reaction run. The reusability of APO-5(1.5) was evaluated for the reductive etherification of FF at 140°C in 24 h reactions. Since APO-5(1.5) showed deactivation after applying the

same washing protocol used for APO-5(1), the catalyst was calcined in air at 550°C for 1 h after the third run before being used in the next run.

The 3Ca/APO1.5 catalyst (Chapter 4) was tested for both leaching and reusability after separate reactions performed for 6 h at 140°C. For the leaching test, the reaction mixture was rapidly cooled to room temperature after reaction, the catalyst removed by filtration and the solution reheated to 140°C and reacted for another 42 h. For the reusability test, the catalyst was collected *via* centrifugation (12,000 rpm) after reaction, washed twice with 2-propanol and acetone (2×10 mL), followed by drying at 80°C for 2 h before being used in a next reaction run. The collected reaction mixtures were analyzed as described above. After forth run, the catalyst was calcined under 550°C for 3 h.

Leaching and catalyst recyclability was examined for the Pd-2 catalyst (Chapter 5) after separate reactions performed for 4 h at 140°C. For the leaching test, the reaction mixture was rapidly cooled to room temperature, the catalyst removed by filtration, and the solution then reheated to 140°C for another 20 h. For the reusability test, the catalyst was collected *via* filtration after the reaction, and then directly used in a next reaction run. The collected reaction mixtures were analyzed as described above.

The reusability of ZrAPO(0.20) (Chapter 6) was examined for the cross-aldol condensation of FF and CH in the neat reaction system at 120°C after 1 h reaction. After initial reaction, the catalyst was collected *via* centrifugation (12,000 rpm, 5 min), washed with methanol and acetone twice (2×10 mL), respectively, followed by drying at 80°C for 2 h before being reused. After three reaction runs, the catalyst was collected *via* centrifugation (12,000 rpm, 5 min), dried and calcined at 550°C for 4 h before being used in the next reaction run.

The reusability of ZrAPO(0.20) in the analogous reaction system with toluene was examined at 120°C after 4 h reaction. After reaction, the catalyst was collected and washed by using the aforementioned method, and after the first two reaction runs the catalyst was also calcined.

Catalyst reusability was examined for the hydrogenation of FF with CuNiO_x(1/1)-150 (Chapter 7) at 120°C after 0.5 h reaction. After initial reaction, the catalyst was collected *via* filtration and directly used for the next reaction run.

2.6 Theoretical calculations

2.6.1 Aldol condensation system

The bulk structure of APO-5 was adapted from the Material Project.⁸ Considering the relative size of the catalyst pores and the FF and CH molecules, the primitive unit structure of $1 \times 1 \times 1$ APO-5 was applied as the model. Note that in the unit cell of APO-5, all Al or P atoms have identical chemical environments. To simulate the ZrAPO-5 catalysts in the experiments, one Zr atom was replaced with one P atom to form the Zr-doped APO-5 model and the structure was fully relaxed before adding adsorbates, ca. 0.08 Zr/Al molar ratio was used per unit cell in the model. The model of APO-5 was restructured a bit after Zr substitution due to the different chemical coordination of P and Zr atoms.

DFT calculations were carried out using Vienna Ab initio Software Package (VASP).⁹ The calculations employed the generalized gradient approximation (GGA)¹⁰ in the form of the Bayesian error estimation functional with van der Waals correlation (BEEF-vdW)¹¹, which was reported to exhibit good description for the interaction between adsorbates and surfaces.^{12,13} Moreover, Goncalves et al. recently benchmarked the accuracy of DFT functionals in zeolite catalysis

and showed that BEEF-vdW displays good accuracy in quantifying adsorption strength of organic species in zeolites at GGA level.¹⁴

The projector augmented wave (PAW) method¹⁵ was applied to describe the interaction between the atomic cores and valence electrons. The geometries of both zeolites and adsorbates in the calculations were relaxed until the force on every atom was less than 0.02 eV/Å with a cutoff energy of 500 eV. Considering the bulk structure of the zeolite, a k-points set of $3 \times 3 \times 3$ was applied in all calculations after the convergence test. The adsorption energy ΔE of CH or FF was calculated as below:

$$\Delta E = E_{total} - E_{zeolite} - E_{CH/FF}$$

Where E_{total} is the calculated total energy of adsorption system, $E_{zeolite}$ is the calculated energy of the zeolite structure without adsorbates and $E_{CH/FF}$ is the calculated energy of the CH or FF molecules.

2.6.2 Hydrogenation system

DFT calculations were performed with the VASP.⁹ Core electrons were treated using projector augmented wave potentials.¹⁰ The Revised Perdew-Burke-Ernzerhof (RPBE) exchange-correlation functional¹⁶ with Grimme's D3¹⁷ was applied to describe the dispersion correction to adsorption energies of FF molecules on different surfaces.

A dense Monkhorst-Pack¹⁸ k-point mesh of $12 \times 12 \times 12$ was used to obtain lattice constants of Cu, Ni, CuNi alloys and Cu₂O (Figs. S7.1 and S7.2), while a k-point mesh of $3 \times 3 \times 1$ was used to sample the reciprocal first Brillouin zone for p(2 × 2) surface (111) slabs and a 15 Å vacuum spacing at z direction to avoid periodic interactions. The lattice constant of Cu₂O was determined as 4.27 Å, in

excellent agreement with experimental results for cuprite structure.¹⁹ An energy cutoff of 400 eV was set to construct the plane waves. Self-consistent iteration was converged up to 1×10^{-6} eV. A force threshold of 0.02 eV/Å was used in geometry optimizations. The reaction barriers for H₂ dissociation were calculated *via* the climbing image nudged elastic band (CI-NEB) method,²⁰ with a convergence criterion of 0.05 eV/Å on each atom and 6-8 images extrapolated linearly between initial (H₂) and final states (two adsorbed H).

The adsorption energy ΔE of a generic adsorbate A was calculated as below (Eq. 1), where E_A^* is the energy of adsorbed A, E_{slab} is the energy of the clean surface i.e., Cu(111), Ni(111), Cu₃Ni(111), Cu₂Ni₂(111), Cu₁Ni₃(111) and Cu₂O(111), and E_A is the energy of A in its reference state (gas phase for H₂ and FF).

$$\Delta E = E_A^* - E_{\text{slab}} - E_A \quad (1)$$

Similarly, the activation energy E_a for H₂ surface dissociation was obtained as below (Eq. 2), where $E_{\text{TS}}(\text{H-H})$ and $E_{\text{IS}}(\text{H}_2(\text{g}))$ are energies of transition state and initial state respectively.

$$E_a = E_{\text{TS}}(\text{H-H}) - E_{\text{IS}}(\text{H}_2(\text{g})) \quad (2)$$

2.7 References

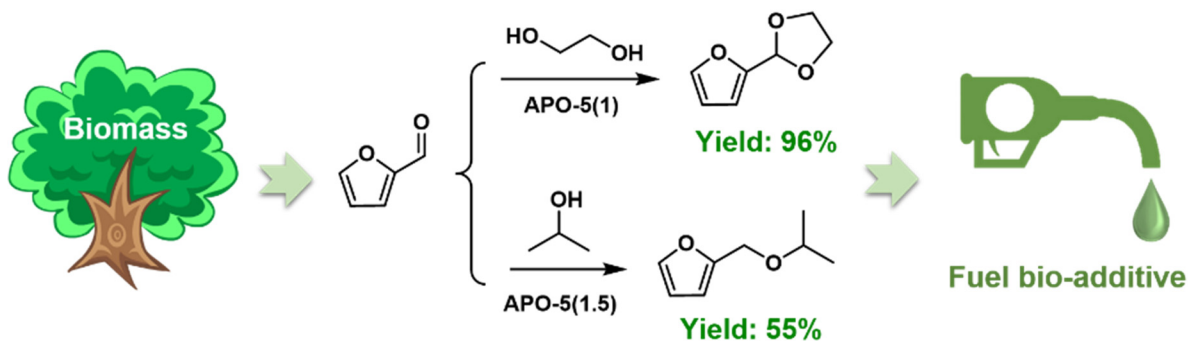
- [1] S.P. Elangovan, V. Krishnasamy, V. Murugesan, *Catal. Letters* **1996**, 36, 271-277.
- [2] W. Fang, H. Hu, P. Dong, Z. Ma, Y. He, L. Wang, Y. Zhang, *Appl. Catal. A-Gen.* **2018**, 565, 146-151.
- [3] W. Fang, A. Riisager, *Appl. Catal. B: Environ.* **2021**, 298, 120575.
- [4] X. H. Deng, K. Chen, H. Tuysuz, *Chem. Mater.* **2017**, 29, 40-52.
- [5] C. Nguyen-Huy, H. Lee, J. Lee, J. H. Kwak, K. An, *Appl. Catal. A-Gen.* **2019**, 571, 118-126.
- [6] J. Lee, J. H. Seo, C. Nguyen-Huy, E. Yang, J. G. Lee, H. Lee, E. J. Jang, J. H. Kwak, J. H. Lee, H. Lee, K. An, *Appl. Catal., B* **2021**, 282, 119576.
- [7] J. T. Scanlon, D. E. Willis, *J. Chromatogr. Sci.* **1985**, 23, 333-340.

-
- [8] A. Jain, S. P. Ong, G. Hautier, W. Chen, W. D. Richards, S. Dacek, S. Cholia, D. Gunter, D. Skinner, G. Ceder, K. A. Persson, *Apl Mater.* **2013**, 1.
 - [9] G. Kresse, J. Furthmüller, *Phys. Rev. B* **1996**, 54, 11169-11186.
 - [10] J. P. Perdew, K. Burke, M. Ernzerhof, *Phys. Rev. Lett.* **1996**, 77, 3865-3868.
 - [11] J. Wellendorff, K. T. Lundgaard, A. Møgelhøj, V. Petzold, D. D. Landis, J. K. Nørskov, T. Bligaard, K. W. Jacobsen, *Phys. Rev. B* **2012**, 85.
 - [12] A. J. Medford, J. Wellendorff, A. Vojvodic, F. Studt, F. Abild-Pedersen, K. W. Jacobsen, T. Bligaard, J. K. Nørskov, *Science* **2014**, 345, 197-200.
 - [13] J. Wellendorff, T. L. Silbaugh, D. Garcia-Pintos, J. K. Nørskov, T. Bligaard, F. Studt, C. T. Campbell, *Surf. Sci.* **2015**, 640, 36-44.
 - [14] T. J. Goncalves, P. N. Plessow, F. Studt, *ChemCatChem* **2019**, 11, 4368-4376.
 - [15] G. Kresse, D. Joubert, *Phys. Rev. B* **1999**, 59, 1758-1775.
 - [16] B. Hammer, L. B. Hansen, J. K. Nørskov, *Phys. Rev. B* **1999**, 59, 7413-7421.
 - [17] S. Grimme, J. Antony, S. Ehrlich, H. Krieg, *J. Chem. Phys.* **2010**, 132, 154104.
 - [18] H. J. Monkhorst, J. D. Pack, *Phys. Rev. B* **1976**, 13, 5188-5192.
 - [19] A. Werner, H. D. Hochheimer, *Phys. Rev. B* **1982**, 25, 5929-5934.
 - [20] G. Henkelman, B. P. Uberuaga, H. Jo´nsson, *J. Chem. Phys.* **2000**, 113, 9901-9904.

3 Efficient valorization of biomass-derived furfural to fuel bio-additive over aluminum phosphate

W. Fang, A. Riisager*, *Applied Catalysis B: Environmental* **2021**, 298, 120575.

Reproduced from (W. Fang, A. Riisager*, *Applied Catalysis B: Environmental* **2021**, 298, 120575.). Copyright [2021] Elsevier. In this chapter, the manuscript was directly used with a minor modification.



APO-5 with different Al/P ratios were synthesized and evaluated as efficient heterogeneous catalysts for the valorization of FF to FACs and furfuryl alcohol ethers (FAEs). Weakly acidic APO-5 with Al/P = 1 (APO-5(1)) exhibited excellent catalytic performance with 96% FAC yield in ethylene glycol, and analysis of the acetalization reaction supported that adsorptive and acidic catalyst sites co-catalyzed the reaction. In addition, the catalyst was stable and reusable though with some deactivation after five recycles. Oppositely, more acidic APO-5 with Al/P = 1.5 (APO-5(1.5)) catalyzed the one-pot synthesis of FAE with 55% yield in 2-propanol with unchanged performance in three successive reactions after intermediate calcination. The reaction pathway for the direct hydrogenolysis of acetal into ether by CTH and etherification was found to be promoted by the co-solvent 1,4-dioxane, possibly by hydrogen bonding. Overall, the study demonstrate a simple approach to design APO-5 catalyst systems allowing very efficient and highly selective valorization of FF to attractive fuel bio-additives.

3.1 Introduction

The world's energy demand has been covered predominantly by nonrenewable carbon-based fossil fuels in the last century, which are gradually becoming exhausted. This has led to severe environmental problems such as global warming, and uncertainty about future supply safety. Accordingly, great efforts have been undertaken to develop potential substitutes to fossil fuels. Biofuels, which are obtained from biomass, are renewable and environmental friendly alternatives to fossil fuels.¹ Biofuels can either be used directly or mixed in fossil fuels as bio-additives to improve the cetane number, density, cloud point, flash point or other fuel properties.²⁻⁴

FF has been emphasized as one of the top value-added chemicals derived from biomass and can be widely used to produce different other chemicals.⁵ Especially bio-additives derived from FF by acetalization (FACs) and reductive etherification (FAEs) have attracted attention due to their potential as blending high-octane gasoline components.⁶⁻¹⁰ Formation of cyclic FACs from FF and diols can be obtained using various heterogeneous acid catalysts, where the pore structure and nature of the acidic sites can be important.^{11,12} Hence, ZSM-5 zeolite converted 35% of FF with 100% selectivity to FAC in 1,2-propanediol,¹³ whereas sulfated-SnO₂ allowed to obtain a total yield of 82% of 1,3-dioxolane and 1,3-dioxane isomers in glycerol.¹⁴ Moreover, Zr-Montmorillonite catalyzed the conversion of FF in different C₂-C₆ diols to the corresponding cyclic FACs with yields above 75%, and particularly the products with EG and 1,5-PeD were shown to exhibit high miscible in commercial diesel obtaining improved density, cloud point and flash point.¹⁵ Similarly, FAEs are typically synthesized from acid-catalyzed direct etherification of FAL,^{8,16,17} and ethyl furfuryl ether (EFE) has been noted for its excellent property to curb soot emissions and shows superior anti-knocking properties compared to the reference Euro 95 gasoline.^{18,19} Recently, Sn-beta and Zr-TUD-1 zeotype catalysts were applied for one-pot formation of furfuryl butyl ether (BMF) from FF allowing to obtain 58% BMF yield with 95% FF conversion and 25% BMF yield with 87% FF conversion, respectively.^{20,21}

In this work, APO-5 catalysts with different Al/P ratios were synthesized by hydrothermal method, characterized by multiple techniques and applied for acetalization and reductive etherification of FF. Weakly acidic APO-5(1) showed excellent catalytic performance and high stability for FF acetalization with EG. The active sites of the catalyst were investigated, and the reaction evaluated with

respect to substrate and solvent scope. More acidic APO-5(1.5) exhibited high activity for the one-pot synthesis of FAE from FF in 2-propanol, and isotopic tracing study provided insight to the reaction pathway. The reusability of the spent catalysts was examined by catalytic as well as characterization studies.

3.2 Results and discussion

3.2.1 Characterization of APO-5 catalysts

The XRD patterns (Fig. 3.1a) of the APO-5 catalysts matched well with the AFI structure.^{22,23} APO-5(1) exhibited the best crystallinity among the three samples, while a very broad and weak peak occurred for APO-5(1.25) and APO-5(1.5) in the 2θ range of 15-30°. The Al source ($\text{Al}(\text{O-}i\text{-Pr})_3$) was calcined at the same conditions as the catalysts and analyzed by XRD (Fig. S3.1). The broad and weak peak found matched with the peak of the calcined Al source, indicating that some amorphous extra-framework Al species was formed when the Al concentration was increased.²⁴

The N_2 adsorption-desorption isotherms of the APO-5 catalysts are shown in Fig. 3.1b. APO-5(1) displayed type I isotherms indicative of a microporous structure in consistence with previous data.²⁵ In contrast, APO-5(1.25) and APO-5(1.5) exhibited type IV isotherms typical of mesoporous materials with H3 type hysteresis loops in the region $0.7 < P/P_0 < 0.95$. The BET surface area of APO-5(1.5) (236 m^2/g) was close to that of APO-5(1) (197 m^2/g), but the mesopore volume of the former (0.51 cm^3/g) was nearly six times larger than the latter (0.09 cm^3/g) (Table 3.1). The pore size distribution analysis showed mesopores in APO-5(1.25) of 24 nm, while APO-5(1.5) had mesopores of both 16 and 22 nm, which may be formed by the accumulation of amorphous Al species.²⁶ In addition, the mesopore volume of APO-5(1.5) before calcination (UC/APO-5(1.5)) was

much larger than that of APO-5(1) (Table 3.1, entry 1 and Table S3.1, entry 1), indicating that the mesoporosity mostly originated from aggregation of Al species and only partly from the organic template.²⁶

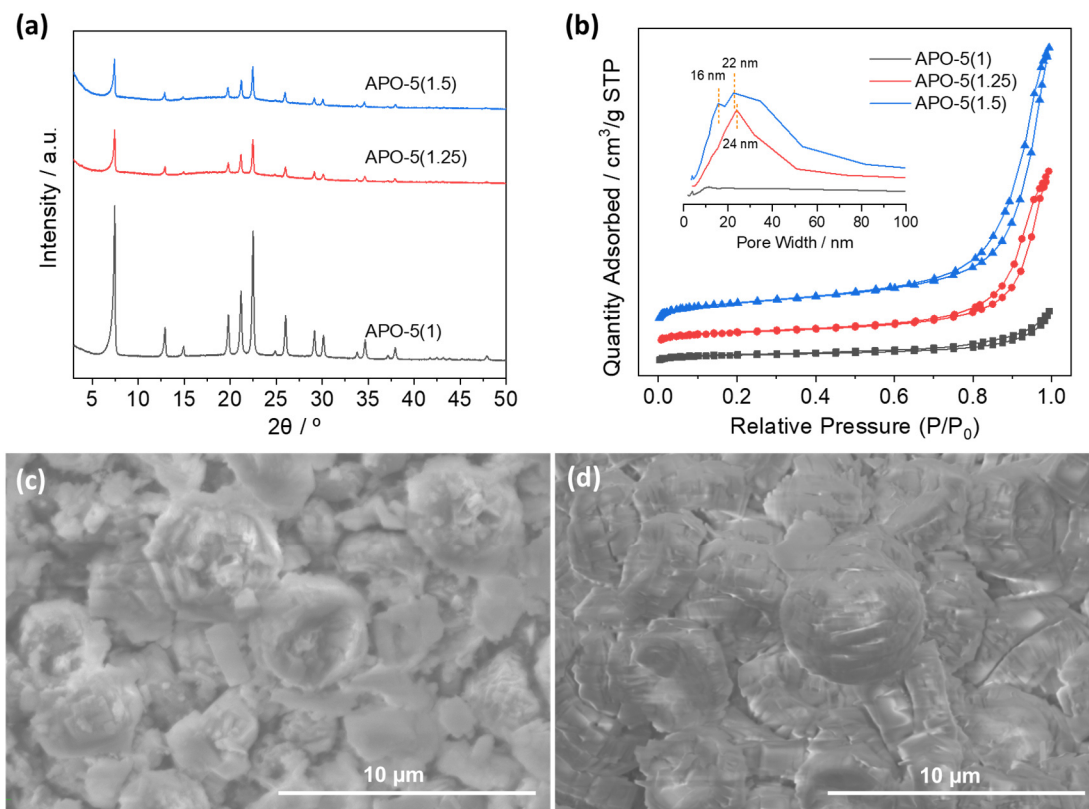


Fig. 3.1 (a) XRD patterns and (b) N_2 adsorption-desorption isotherms (inset: BJH mesopore size distribution) of APO-5 catalysts. (c) SEM image of APO-5(1) and (d) SEM image of APO-5(1.5).

Table 3.1 Textural properties of the APO-5 catalysts

Sample	Al/P molar ratio ^a	S_{BET} (m^2/g) ^b	V_{micro} (cm^3/g) ^c	V_{meso} (cm^3/g) ^d	Acidity (mmol/g) ^e
APO-5(1)	0.95	197	0.07	0.09	0.0012
APO-5(1.25)	1.19	177	0.04	0.32	0.29
APO-5(1.5)	1.43	236	0.04	0.51	0.40

^a Determined by XRF. ^b Calculated by the BET method. ^c Estimated by the t-plot method. ^d Calculated by subtraction of the micropore volume from the total pore volume. ^e Determined by NH_3 -TPD.

From the SEM images of APO-5(1) and APO-5(1.5) (Figs. 3.1c and 3.1d), the particle sizes were found to be 4-5 μm which is normal sizes for APO-5 crystallites.^{27,28} APO-5(1) had a hexagon prism-like shape, while the particles appeared as spherical plates in APO-5(1.5). This change in morphology may be a result of different pH of the gels during synthesis.^{28,29} The cracks observed in the particles of APO-5(1.5) may contribute to the meso- and macroporosity obtained from the N_2 adsorption-desorption isotherms (Table 3.1).

To investigate the coordination environment of phosphorus and aluminum in the APO-5 samples, solid-state MAS NMR spectroscopy was performed. The ^{31}P MAS NMR spectra (Fig. 3.2a) revealed a characteristic broad asymmetric signal at -26 ppm with a shoulder at around -20 ppm associated to $\text{P}(\text{OAl})_4$, as also found in previous reports.^{30,31} The signal at -26 ppm is assigned to fully crystallized $\text{P}(\text{OAl})_4$, while the signal at -20 ppm corresponds to a semicrystalline phase which continuously evolve to the fully crystalline phase.^{30,32} Higher Al concentration in the APO-5s led to a larger peak intensity at -20 ppm, suggesting that APO-5(1) had the most stable structure. The ^{27}Al MAS NMR spectra of the catalysts (Fig. 3.2b) showed a signal at 41 ppm characteristic of tetrahedrally coordinated Al linked to four phosphorus atoms *via* bridging oxygen atoms ($\text{Al}(\text{OP})_4$).³³ Moreover, a signal at 10 ppm could according to literature be assigned to unreacted Al or pentacoordinated Al with four Al atoms and one water molecule ($\text{P}(\text{OAl})_4(\text{H}_2\text{O})$).³⁴⁻³⁶ However, FT-IR spectra of the samples (Fig. 3.2c) did not indicate water in the structure and XRD showed presence of amorphous Al, thus suggesting the signal belonging instead to extra-framework Al species. In the FT-IR spectra of APO-5, the strong band at around 1100 cm^{-1} is characteristic of an asymmetric P-O-Al stretching vibration,²² and the red shift of the band observed with higher Al/P ratio may be due to small structural

differences caused by the increased amount of Al. The bands at 704 and 665 cm^{-1} are assigned to the symmetric stretching and bending mode vibrations of P-O-Al, respectively. The bands at 634 and 561 cm^{-1} are assigned to double-ring vibration modes, while the band located at 458 cm^{-1} can be assigned to the internal T-O bending mode vibration.^{22,37,38}

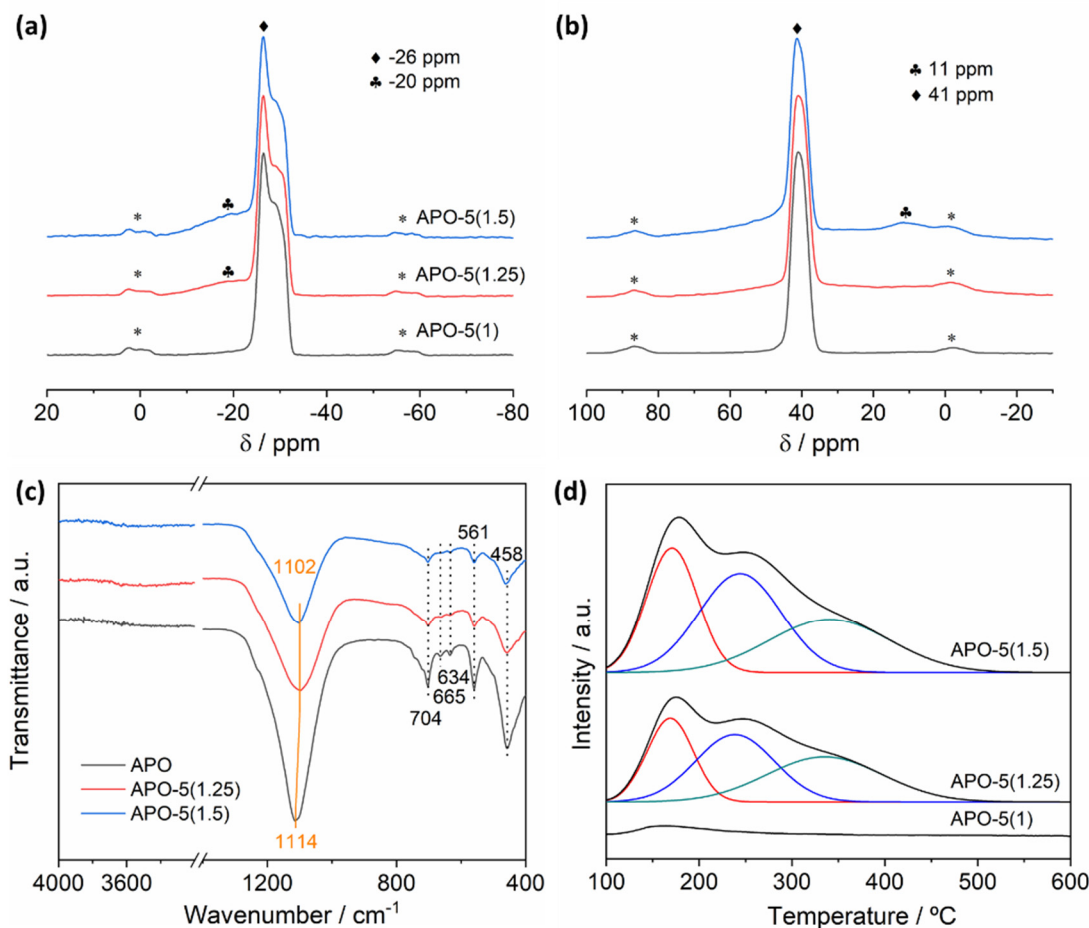


Fig. 3.2 (a) ^{31}P MAS NMR and (b) ^{27}Al MAS NMR spectra (* corresponds to spinning bands), (c) FT-IR spectra and (d) NH_3 -TPD profiles of APO-5 catalysts.

NH_3 -TPD profiles of the APO-5 samples are shown in Fig. 3.2d. APO-5(1) had only a small peak at 164°C, indicating a low amount of weak acidic sites consistent with the assumption that APO-5 is neutral. In contrast, APO-5(1.25) and APO-5(1.5) had three major peaks at 170, 240 and 340°C correspondingly

assigned to weak, medium and strong acidic sites. The acidity of the catalysts increased with the Al concentration (Table 3.1), which in combination with the XRD and ^{27}Al MAS NMR results inferred that the acidity was likely ascribed to extra-framework Al species.

3.2.2 Catalytic performance of APO-5 catalysts

The APO-5 catalysts were initially screened for the catalytic conversion of FF in 2-propanol and the results are shown in Table 3.2. Interestingly, the APO-5 catalysts with diverse acidity showed different product selectivity. Obviously, APO-5(1) gave high acetalization selectivity towards 2-(diisopropoxymethyl)furan (DIPF) despite the reaction was completed in a solvent with high hydrogen-donor ability. In contrast, APO-5(1.5) exhibited a strong preference for hydrogen-transfer hydrogenation to FAL and the subsequent etherification to 2-(isopropoxymethyl)furan (IPF), providing the possibility of one-pot formation of FAEs with higher temperature where etherification is promoted.³⁹ Therefore, APO-5(1) and APO-5(1.5) were selected for further optimization of acetalization and reductive etherification of FF in different solvents, respectively.

Table 3.2 Catalytic performance of APO-5 catalysts for FF conversion.^a

Catalyst	Conv. (%) ^b	Product Selec. (%) ^b			
		FAL	DIPF	IPF	IPL
APO-5(1)	19.8	16.9	66.8	12.0	0.6
APO-5(1.25)	29.1	58.1	37.5	3.3	0.2
APO-5(1.5)	47.3	69.5	18.6	8.1	1.0

^a Reaction conditions: FF (96 mg, 1 mmol), catalyst (50 mg), 2-propanol (5 mL), 100°C, 48 h. ^b Conversion and yield were quantified using GC. FAL: furfuryl alcohol; DIPF: 2-(diisopropoxymethyl)furan; IPF: 2-(isopropoxymethyl)furan; IPL: isopropyl levulinate.

3.2.3 Acetalization of furfural over APO-5(1)

3.2.3.1 Time course study

The acetalization of FF to 2-(furan-2-yl)-1,3-dioxane (FD) in EG/1,4-dioxane mixture using APO-5(1) was investigated as a representative reaction to demonstrate cyclic FAC formation (Fig. 3.3). An excellent performance of the catalyst with FD selectivity >98% throughout the reaction led to 97% FF conversion and 96% FD yield after 24 h. Moreover, both the FF conversion and FD yield remained very constant after 16 h of reaction (Fig. 3.3), indicating that FD remained stable under the condition.

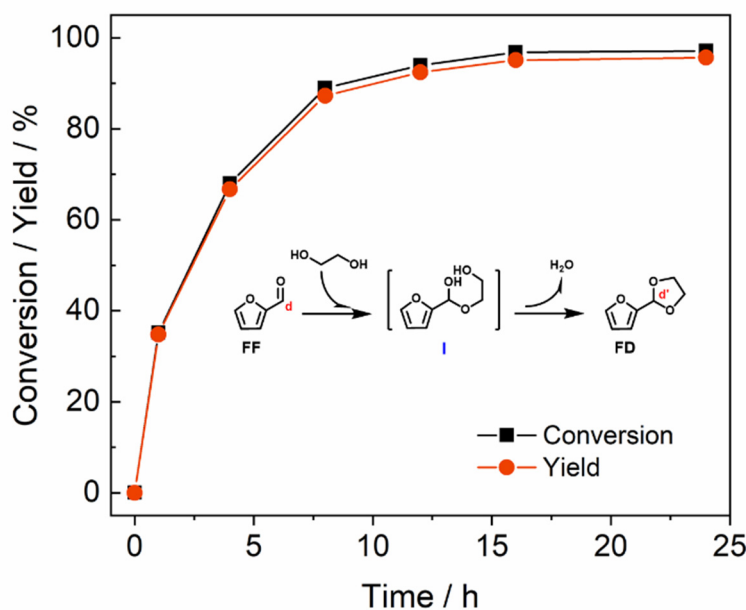


Fig. 3.3 FF conversion and FD yield at various reaction times during acetalization using APO-5(1). Reaction conditions: FF (96 mg, 1 mmol), APO-5(1) (100 mg), EG (2 mL), 1,4-dioxane (3 mL), 150°C.

To corroborate if furan-2-yl(hydroxymethoxy)methanol (I) was formed as an intermediate during the reaction, the product mixtures were analyzed by ex-situ ^1H NMR (Fig. S3.3). The aldehydic proton (d) of FF gradually disappeared while the acetalic proton (d') in FD appeared without indication of a hemiacetal

intermediate being formed, thus implying that the formation of FD by water removal from (I) was most likely very fast. Notably, when the reaction was performed in neat EG instead of EG/1,4-dioxane mixture both the FF conversion and the FD selectivity were lowered significantly and 2,2'-((furan-2-ylmethylene)bis(oxy))bis(ethan-1-ol) formed (Table S3.3, entry 2), confirming that 1,4-dioxane improved both catalyst activity and selectivity.

3.2.3.2 Active site study

Acetalization is reported to be acid-catalyzed reaction in the literature.^{1,40} Nevertheless, APO-5(1) having only few acidic sites (0.0012 mmol/g) showed excellent catalytic performance in the acetalization of FF. Hence, in order to determine the role of acidity and basicity for the catalytic system pyridine, benzoic acid, and 2,6-lutidine were separately introduced into the reaction as poisoning additives for acidic, basic, and Brønsted acidic sites, respectively.⁴¹ (Fig. 3.4a). In the presence of benzoic acid, the conversion of FF and yield of FD were almost unaffected while the addition of pyridine drastically reduced both FF conversion and FD yield, suggesting that the active centers of acetalization were acidic sites. Furthermore, when Brønsted acidic sites were selectively poisoned by 2,6-lutidine the catalytic activity was suppressed even more than with pyridine, showing that Brønsted acidic sites were the main active centers which is also in line with previous studies.¹³ FT-IR spectra of APO-5(1) with adsorbed FF with or without poison additives were further recorded (Fig. 3.4b). Comparison of the C=O stretching bands of FF and FF adsorbed on APO-5(1) revealed a red shift from 1668 to 1663 cm^{-1} , indicating that the C=O group of FF adsorbed strongly on APO-5(1),^{42,43} which may further lead to excellent activity of APO-5(1). Notably, an additional red shift of the band occurred after pyridine or 2,6-lutidine addition (1659 cm^{-1}), which combined with the results of the

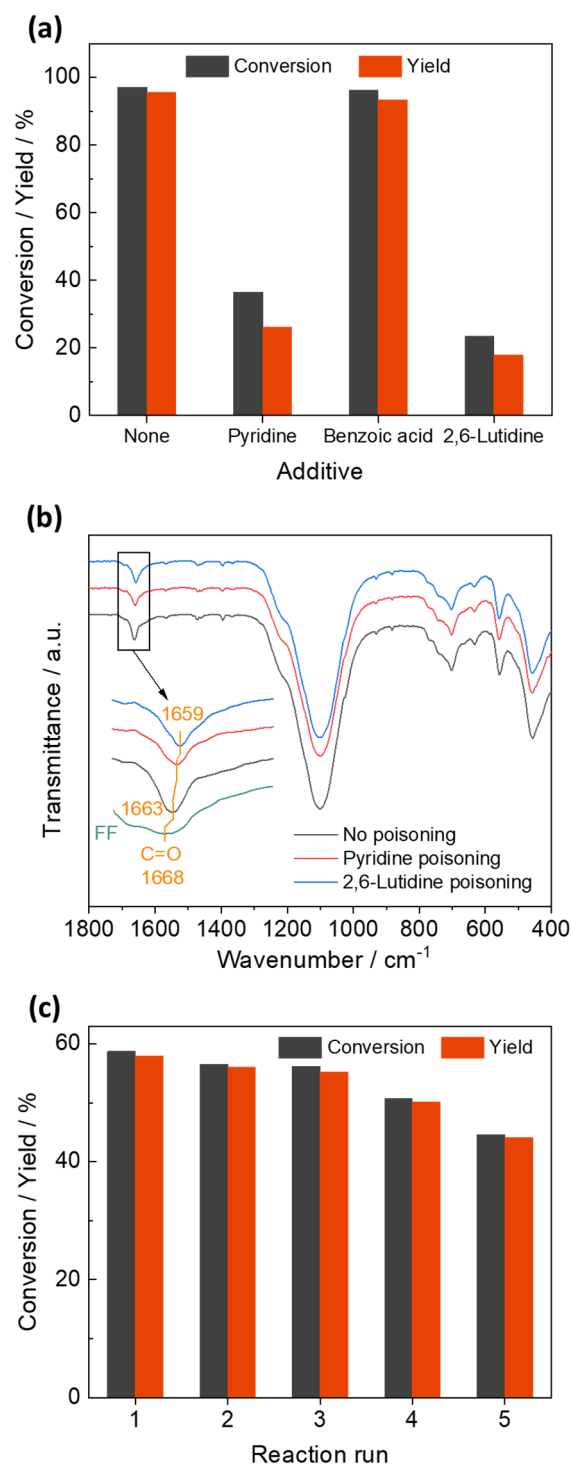


Fig. 3.4 (a) Acetalization of FF to FD with APO-5(1) with/without poisoning additives. Reaction conditions: FF (96 mg, 1 mmol), APO-5(1) (100 mg), additive (100 mg), EG (2 mL), 1,4-dioxane (3 mL), 150°C, 24 h. (b) FT-IR spectra of FF, APO-5(1) with pre-adsorbed FF with/without poisoning additives. (c) Reusability of APO-5(1) in the conversion of FF to FD. Reaction conditions: FF (96 mg, 1 mmol), APO-5(1) (100 mg), EG (2 mL), 1,4-dioxane (3 mL), 150°C, 2 h.

poisoning reactions inferred that the adsorption sites of FF were not the acidic sites. Thus, the acidic sites and the FF adsorptive sites probably together catalyzed the acetalization of FF in the system.

3.2.3.3 Catalyst recycling study

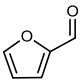
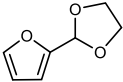
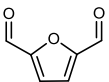
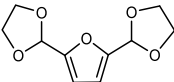
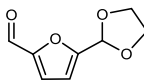
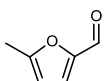
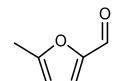
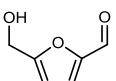
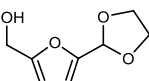
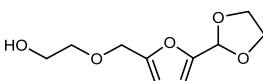
The recyclability of the APO-5(1) catalyst was studied for the acetalization of FF to FD after reaction at 150°C for 2 h (Fig. 3.4c). During five consecutive reaction cycles, the FD yield reduced from 57.9 to 44.1% whereas a high constant FD selectivity of 98-99% was maintained, clearly indicating that only slight part of the active centers were clogged. N₂ physisorption analysis of the spent catalyst revealed significant reductions of surface area and microporous volume compared to the fresh catalyst (Table 3.1, entry 1 and Table S3.1, entry 2), implying that micropores were blocked. Therefore, most of the active sites were not in the micropores. In line with this, TG analysis of the recovered catalyst (Fig. S3.5) gave new peaks at 297 and 450°C ascribed to adsorbed organic species (9.3 wt.%), which were likely responsible for the deactivation of the catalyst. Also new bands formed in the FT-IR spectra (Fig. S3.6) around 2900 and 1400 cm⁻¹ (C-H stretching and bending vibrations of CH₃ and CH₂) demonstrated remnant of organic species (bands at 1220 and 870 cm⁻¹ attributed to adsorption of 1,4-dioxane⁴⁴).

3.2.3.4 Substrate and solvent scope study

As the APO-5(1) catalyst exhibited remarkable activity in the acetalization of FF to FD in EG, the study was expanded to acetalization of other furanic carbonyl compounds like 2,5-furandicarboxaldehyde (FCA), 5-methylfurfural (MFA) and HMF (Table 3.3). All substrates were efficiently converted to the corresponding acetals, but FCA with two carbonyl groups required probably longer reaction

time to reach high yield (Table 3.3, entry 2), and the hydroxyl group of HMF etherified with EG and formed side product (Table 3.3, entry 4). Cyclic acetalization of FF in alternative C₃-C₆ diols was also evaluated (Table S3.3). The APO-5(1) catalyst revealed also here high activity in especially 1,2-propanediol and 1,3-propanediol giving around 90% yields of the corresponding cyclic acetals, whereas the total yield of acetal isomers in glycerol was above 70% which is similar to previous work.¹¹ However, with increasing diol chain length the yield of FAC and the conversion of FF became lower likely because the pore size of the catalyst limited the acetalization reaction of the larger sized diols.

Table 3.3 Acetalization of various aldehydes with APO-5(1) catalyst.^a

Entry	Substrate	Conv. (%) ^b		Yield (%) ^b		Yield (%) ^b
1		97.2		95.7	-	-
2		90.1		83.8		4.7
3		95.7		93.4	-	-
4		98.0		88.4		3.9

^a Reaction conditions: Substrate (1 mmol), APO-5(1) (100 mg), EG (2 mL), 1,4-dioxane (3 mL), 150°C, 24 h. ^b Conversion and yield were quantified using ¹H NMR.

3.2.4 Reductive etherification of furfural over APO-5(1.5)

3.2.4.1 Time course study

In order to investigate the reductive etherification of FF in 2-propanol a time course was completed at 120°C for 70 h (Fig. 3.5a). During the reaction, FF was

gradually converted (>95% after 50 h) into a mixture of mainly FAL by hydrogenation, IPF by consecutive etherification of FAL and isopropyl levulinate (IPL) by continuous hydrolysis of IPF, respectively. Additionally, a minor amount of the acetal intermediate DIPF formed in the beginning of the reaction, but was gradually converted along with the consumption of FF either by reversible hydrolysis of the formed DIPF (pathway **a**)⁴⁵⁻⁴⁷ or by direct hydrogenolysis of DIPF as previously indicated possible in the literatures (pathway **b**).^{9,48}

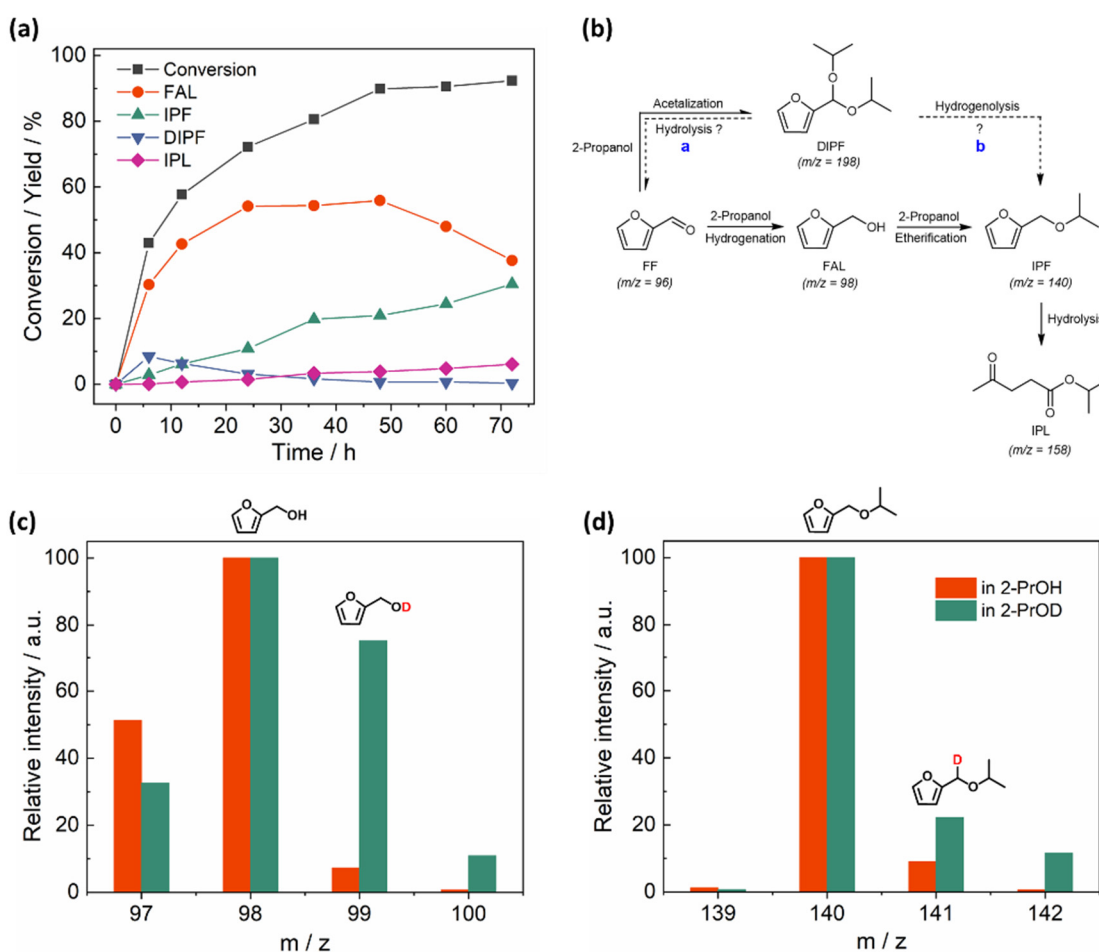
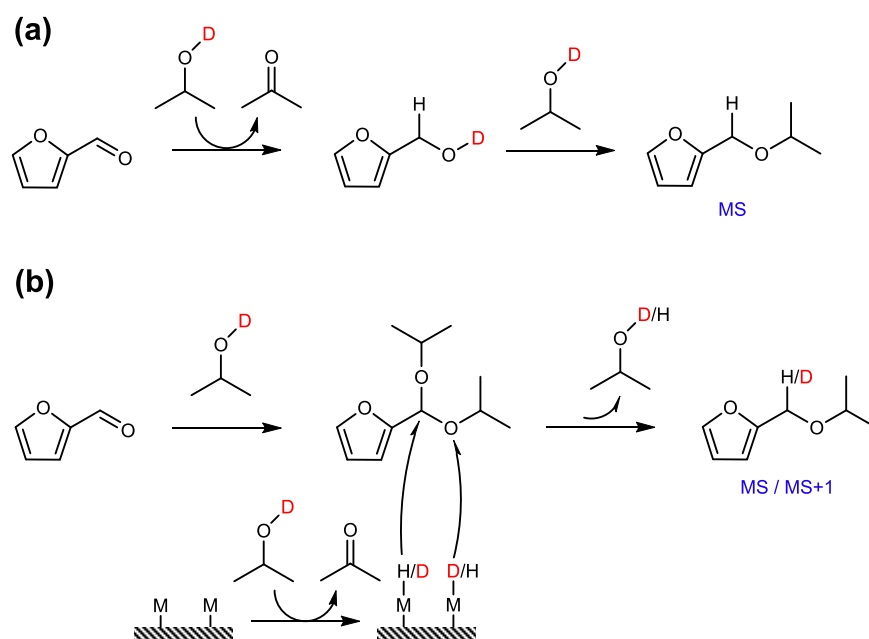


Fig. 3.5 (a) Time course of the reductive etherification of FF over APO-5(1.5). Reaction conditions: FF (96 mg, 1 mmol), APO-5(1.5) (100 mg), 2-propanol (5 mL), 120°C. (b) Possible pathways for the reductive etherification of FF. (c) and (d) Results from GC-MS analysis of reaction products FAL and IPF after the reductive etherification of FF over APO-5(1.5). Reaction conditions: FF (96 mg, 1 mmol), APO-5(1.5) (100 mg), 2-propanol/2-propanol-OD (5 mL), 140°C, 24 h.

In Scheme 3.1, two possible mechanisms for the formation of IPF (from DIPF) *via* pathways **a** and **b** are proposed. To investigate if both reaction pathways occurred with APO-5(1.5), isotopic tracing experiments in deuterated 2-propanol, $\text{CH}_3\text{CH}(\text{OD})\text{CH}_3$ (2-PrOD), followed by GC-MS analysis were performed (Figs. 3.5c and 3.5d). With unlabeled 2-propanol (2-PrOH) as solvent, the MS fragments of the FAL and IPF products provided the parent ions m/z 97, 98 and 99 and m/z 140, 141 and 142, respectively, in relative ratios which was the same as obtained in a reference reaction without catalyst (as expected). However, using 2-PrOD as solvent, the ratio (34.4%) of FAL with the ion m/z 99 was much higher than that of the reference reaction (4.6%). This indicated replacement of a hydrogen atom in the molecule with deuterium, thus supporting an intermolecular hydrogen-transfer mechanism from 2-propanol to FF.⁴¹ For the IPF product, the intensity of the ion m/z 140 was also reduced, but to a lower extent, while the intensities of the ions m/z 141 and 142 were increased correspondingly. This indicated that IPF formation also partly occurred by hydrogenolysis *via* pathway **b**.⁴⁸



Scheme 3.1 Two possible mechanisms for the formation of IPF from FF.

3.2.4.2 Co-solvent and hydrogen donor study

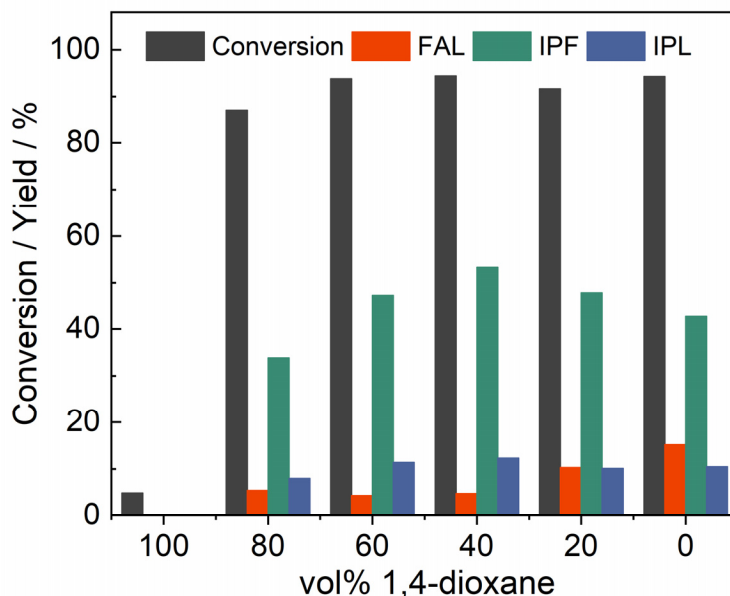


Fig. 3.6 The effect of 1,4-dioxane as co-solvent in the reductive etherification of FF over APO-5(1.5) in 2-propanol. Reaction conditions: FF (96 mg, 1 mmol), APO-5(1.5) (100 mg), solvent (5 mL), 140°C, 24 h.

Previous work has suggested 1,4-dioxane to be a beneficial co-solvent for etherification,⁴⁹ and its influence was therefore also investigated here using various added amounts in 2-propanol (Fig. 3.6). In neat 1,4-dioxane (100 vol.%) only 5% of FF was converted and FAL, IPF and IPL products were not formed because 1,4-dioxane cannot transfer hydrogen to FF. With 40 vol.% 1,4-dioxane added the FF conversion and IPF yield were significantly enhanced providing an apparent optimal mixture for CTH and successive etherification. However, with lower amounts of added 1,4-dioxane the IPF yield decreased and the FAL yield increased, while the FF conversion and IPL yield remained almost constant. To confirm that 1,4-dioxane facilitated the etherification, FAL was used as substrate in 2-propanol alone and in 40 vol.% 1,4-dioxane mixture. The results (Table S3.4, entries 1 and 2) revealed a higher IPF yield (12%) in the mixed solvent than in 2-propanol alone, showing that the co-solvent indeed facilitated the etherification

consistent with earlier observations for other etherification reactions.⁴⁹ Notably, the presence of minor amount of water significantly inhibited the catalyst and the conversion of FF and production of IPF (Table S3.4, entries 3 and 4). Since 1,4-dioxane is prone to form hydrogen bonds with water,^{50,51} it may infer that hydrogen bond formation between 1,4-dioxane and water prevented the catalyst inhibition and thereby facilitated the reaction.

The effect of the hydrogen donor on the reductive etherification of FF catalyzed by APO-5(1.5) was also investigated (Fig. S3.7). When primary alcohols (ethanol, 1-propanol, 1-butanol and isobutanol) were used as solvent and hydrogen donor, FF conversion and FAL selectivity were markedly lower than when using secondary alcohols (2-propanol and 2-butanol), confirming that secondary alcohols have a higher tendency to release hydrogen than primary alcohols.⁵² In the 2-butanol system, both the FF conversion and FAE selectivity were lower than in 2-propanol while the FAL selectivity was higher, suggesting that steric hindrance of the solvent affected both the hydrogen transfer and the etherification.

3.2.4.3 Catalyst recycling study

Finally, the reusability of the APO-5(1.5) catalyst was investigated for the reductive etherification of FF (Fig. 3.7). After the initial reaction run and successive washing (acetone and methanol) and drying of the catalyst the performance altered in the next reaction run with lower FF conversion and IPF yield. Characterization of the reused catalyst by TG and N₂ physisorption analysis (Fig. S3.8 and Table S3.1, entry 3) revealed an increased weight loss (9.1 wt.%) as well as a drastically decreased surface area and pore volume compared to the fresh catalyst. Similarly, the FT-IR spectrum (Fig. S3.9) showed

bands at around 2950 and 1400 cm^{-1} (C-H stretching and bending vibrations of CH_3 and CH_2), 1628 cm^{-1} (C=C stretching vibrations) and 869 cm^{-1} which may be assigned to adsorbed 1,4-dioxane.⁴⁴ Combined this corroborated that the catalyst deactivation originated from adsorbed organic species blocking the pores and lowering the accessibility of the substrates to the catalytically active sites like found for the APO-5(1) catalyst in the acetalization of FF to FD (see above). Intermediate calcination (550°C, 1 h) of the catalyst, allowed removing the adsorbed species and restore the original catalyst performance in three consecutive reaction runs. And the adsorbed species on the part of active sites may result in the different products distribution of run 2 by slowing down the reaction. Importantly, the XRD pattern of the reused catalyst after five recycles was identical to the fresh catalyst (Fig. S3.10), clearly suggesting that the catalyst structure remained stable upon the thermal treatment and that the catalyst system was highly durable.

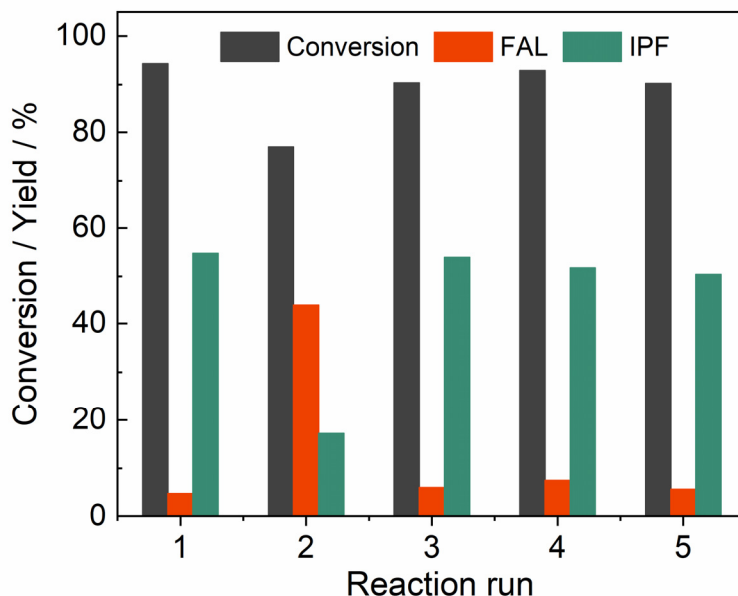


Fig. 3.7 Reusability of APO-5(1.5) in the reductive etherification of FF to IPF. Reaction conditions: FF (96 mg, 1 mmol), APO-5(1.5) (100 mg), 2-propanol (3 mL), 1,4-dioxane (2 mL), 140°C, 24 h.

3.3 Summary

Hydrothermally synthesized APO-5s ($\text{Al/P} = 1, 1.25 \text{ and } 1.5$) were applied as catalysts in the acetalization and reductive etherification of FF. The materials had lower crystallinity with higher Al content but larger surface area, pore volume and acidity, and these characteristics facilitated high catalyst selectivity in the valorization of FF into FACs and FAEs, respectively. Hence, APO-5(1) provided an excellent yield of 96% of the cyclic acetal FD in EG/1,4-dioxane, and a low degree of catalyst deactivation after five recycles correlated to pore blocking by adsorbed organic species. Similarly, high catalytic activity was shown with alternative furanic carbonyl compounds and longer chained diols. Furthermore, poisoning experiments suggested that Brønsted acidic sites of the catalyst dominated the acetalization performance, whereas pre-adsorption experiments with FF supported that adsorptive and acidic sites co-catalyzed the reaction. On the other hand, APO-5(1.5) provided good performance in the reductive etherification of FF in 2-propanol yielding 55% of IPF. The pathway for direct hydrogenolysis of acetal by hydrogen transfer by 2-propanol as a hydrogen donor was investigated, and the addition of 1,4-dioxane was shown to improve the etherification, possibly due to hydrogen bond formation between 1,4-dioxane and the formed water. The APO-5(1.5) catalyst deactivated more severely than APO-5(1) after reuse, but intermediate calcination completely regained the initial catalyst performance and left the catalyst structure intact.

The work demonstrates a simple approach to design heterogeneous APO-5 catalyst systems for the efficient and highly selective valorization of biomass-derived FF to attractive fuel bio-additives. Future work should focus on product separation and evaluate the potential for industrial implementation.

3.4 References

- [1] A. R. Trifoi, P. Ş. Agachi, T. Pap, *Renew. Sust. Energ. Rev.* **2016**, 62, 804-814.
- [2] O. M. Ali, R. Mamat, C. K. M. Faizal, *J. Renew. Sustain. Energy* **2013**, 5.
- [3] C. J. A. Mota, C. X. A. da Silva, N. Rosenbach, J. Costa, F. da Silva, *Energ. Fuel.* **2010**, 24, 2733-2736.
- [4] A. Cornejo, I. Barrio, M. Campoy, J. Lázaro, B. Navarrete, *Renew. Sust. Energ. Rev.* **2017**, 79, 1400-1413.
- [5] R. Mariscal, P. Maireles-Torres, M. Ojeda, I. Sádaba, M. López Granados, *Energ. Environ. Sci.* **2016**, 9, 1144-1189.
- [6] B. L. Wegenhart, S. Liu, M. Thom, D. Stanley, M. M. Abu-Omar, *ACS Catal.* **2012**, 2, 2524-2530.
- [7] K. S. Arias, A. Garcia-Ortiz, M. J. Climent, A. Corma, S. Iborra, *ACS Sustain. Chem. Eng.* **2018**, 6, 4239-4245.
- [8] D. R. Chaffey, T. E. Davies, S. H. Taylor, A. E. Graham, *ACS Sustain. Chem. Eng.* **2018**, 6, 4996-5002.
- [9] V. E. Tarabanko, M. Y. Chernyak, I. L. Simakova, K. L. Kaigorodov, Y. N. Bezborodov, N. F. Orlovskaya, *Russ. J. Appl. Chem.* **2016**, 88, 1778-1782.
- [10] J. P. Lange, E. van der Heide, J. van Buijtenen, R. Price, *ChemSusChem* **2012**, 5, 150-166.
- [11] E. V. Gromachevskaya, F. V. Kvitkovsky, E. B. Usova, V. G. Kulnevich, *Chem. Heterocycl. Com.* **2004**, 40, 979-985.
- [12] S. P. Gavriiova, T. G. Serkina, L. A. Badovskaya, *Chem. Heterocycl. Com.* **1993**, 29, 268-270.
- [13] Hartati, D. Prasetyoko, M. Santoso, *Indones. J. Chem.* **2016**, 16, 289-296.
- [14] B. Malleshham, P. Sudarsanam, B. M. Reddy, *Catal. Sci. Technol.* **2014**, 4, 803-813.
- [15] A. Patil, S. Shinde, S. Kamble, C. V. Rode, *Energ. Fuel.* **2019**, 33, 7466-7472.
- [16] T. A. Natsir, T. Hara, N. Ichikuni, S. Shimazu, *ACS Appl. Energy Mater.* **2018**, 1, 2460-2463.
- [17] M. Paniagua, J. A. Melero, J. Iglesias, G. Morales, B. Hernandez, C. Lopez-Aguado, *Appl. Catal. A-Gen.* **2017**, 537, 74-82.
- [18] M. Tian, R. L. McCormick, J. Luecke, E. de Jong, J. C. van der Waal, G. P. M. van Klink, M. D. Boot, *Fuel* **2017**, 202, 414-425.
- [19] C. R. Patil, C. V. Rode, *ChemistrySelect* **2018**, 3, 12504-12511.
- [20] M. M. Antunes, S. Lima, P. Neves, A. L. Magalhaes, E. Fazio, A. Fernandes, F. Neri, C. M. Silva, S. M. Rocha, M. F. R. Eiro, M. Pillinger, A. Urakawa, A. A. Valente, *J. Catal.* **2015**, 329, 522-537.
- [21] M. M. Antunes, S. Lima, P. Neves, A. L. Magalhaes, E. Fazio, F. Neri, M. T. Pereira, A. F. Silva, C. M. Silva, S. M. Rocha, M. Pillinger, A. Urakawa, A. A. Valente, *Appl. Catal. B-Environ.* **2016**, 182, 485-503.
- [22] T. Munõz, A. M. Prakash, L. Kevan, K. J. Balkus, *J. Phys. Chem. B* **1998**, 102, 1379-1386.

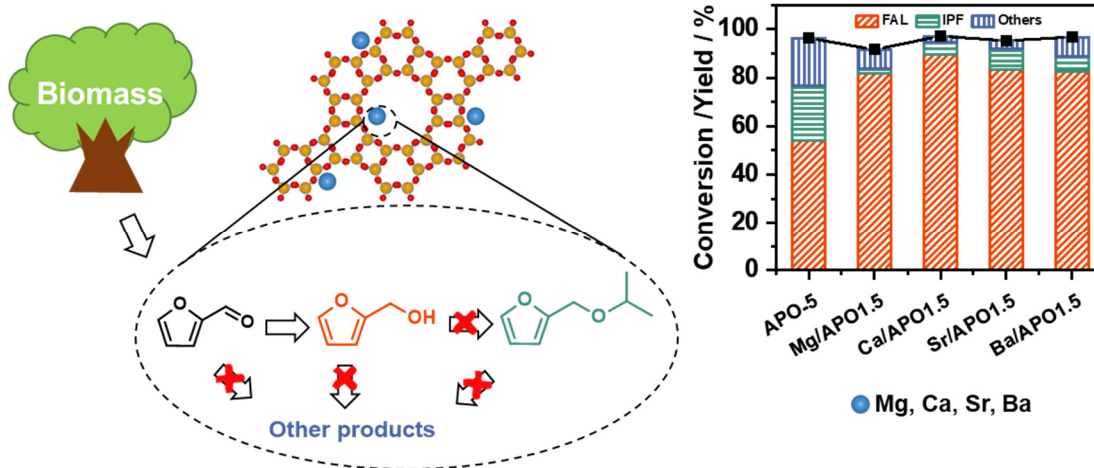
- [23] L. Zhou, T. Lu, J. Xu, M. Chen, C. Zhang, C. Chen, X. Yang, J. Xu, *Micropor. Mesopor. Mat.* **2012**, *161*, 76-83.
- [24] S. D. Ponja, I. P. Parkin, C. J. Carmalt, *RSC Adv.* **2016**, *6*, 102956-102960.
- [25] X. Zhao, X. Zhang, Z. Hao, X. Gao, Z. Liu, *J. Porous Mat.* **2017**, *25*, 1007-1016.
- [26] M. Wang, Z. Wang, S. Liu, R. Gao, K. Cheng, L. Zhang, G. Zhang, X. Min, J. Kang, Q. Zhang, Y. Wang, *J. Catal.* **2021**, *394*, 181-192.
- [27] T. Kodaira, K. Miyazawa, T. Ikeda, Y. Kiyozumi, *Micropor. Mesopor. Mat.* **1999**, *29*, 329-337.
- [28] S. H. Jhung, Y. K. Hwang, J.-S. Chang, S.-E. Park, *Micropor. Mesopor. Mat.* **2004**, *67*, 151-157.
- [29] S. H. Jhung, J. S. Chang, Y. K. Hwang, S. E. Park, *J. Mater. Chem.* **2004**, *14*, 280-285.
- [30] B. Chen, C. W. Kirby, Y. Huang, *J. Phys. Chem. C* **2009**, *113*, 15868-15876.
- [31] C. A. Fyfe, K. C. Wong-Moon, Y. Huang, *Zeolites* **1996**, *16*, 50-55.
- [32] N. Sheng, Y. Y. Chu, S. H. Xing, Q. Wang, X. F. Yi, Z. C. Feng, X. J. Meng, X. L. Liu, F. Deng, F. S. Xiao, *J. Am. Chem. Soc.* **2016**, *138*, 6171-6176.
- [33] L. S. de Saldarriaga, C. Saldarriaga, M. E. Davis, *J. Am. Chem. Soc.* **1987**, *109*, 2686-2691.
- [34] Z. Yan, B. Chen, Y. Huang, *Solid State Nucl. Mag.* **2009**, *35*, 49-60.
- [35] A. Sayari, I. Moudrakovski, J. S. Reddy, C. I. Ratcliffe, J. A. Ripmeester, K. F. Preston, *Chem. Mater.* **1996**, *8*, 2080-2088.
- [36] L. Gomez-Hortigueela, C. Marquez-Alvarez, F. Cora, F. Lopez-Arbeloa, J. Perez-Pariente, *Chem. Mater.* **2008**, *20*, 987-995.
- [37] S. Endud, N. Roslan, Z. Ramli, H. O. Lintang, *Adv. Mat. Res.* **2015**, *1109*, 360-364.
- [38] M. Zaarour, O. Perez, P. Boullay, J. Martens, B. Mihailova, K. Karaghiosoff, L. Palatinus, S. Mintova, *CrystEngComm* **2017**, *19*, 5100-5105.
- [39] X.-L. Li, K. Zhang, S.-Y. Chen, C. Li, F. Li, H.-J. Xu, Y. Fu, *Green Chem.* **2018**, *20*, 1095-1105.
- [40] M. R. Nanda, Y. Zhang, Z. Yuan, W. Qin, H. S. Ghaziaskar, C. Xu, *Renew. Sust. Energ. Rev.* **2016**, *56*, 1022-1031.
- [41] S. H. Zhou, F. L. Dai, Z. Y. Xiang, T. Song, D. T. Liu, F. C. Lu, H. S. Qi, *Appl. Catal. B-Environ.* **2019**, *248*, 31-43.
- [42] Y. Yang, L. Chen, Y. Chen, W. Liu, H. Feng, B. Wang, X. Zhang, M. Wei, *Green Chem.* **2019**, *21*, 5352-5362.
- [43] M. Ma, P. Hou, J. Cao, H. Liu, X. Yan, X. Xu, H. Yue, G. Tian, S. Feng, *Green Chem.* **2019**, *21*, 5969-5979.
- [44] F. E. Malherbe, H. J. Bernstein, *J. Am. Chem. Soc.* **1952**, *74*, 4408-4410.
- [45] M. Balakrishnan, E. R. Sacia, A. T. Bell, *Green Chem.* **2012**, *14*, 1626-1634.
- [46] H. Nguyen, N. Xiao, S. Daniels, N. Marcella, J. Timoshenko, A. Frenkel, D. G. Vlachos, *ACS Catal.* **2017**, *7*, 7363-7370.
- [47] E. R. Sacia, M. Balakrishnan, A. T. Bell, *J. Catal.* **2014**, *313*, 70-79.
- [48] Y. Wang, Q. Cui, Y. Guan, P. Wu, *Green Chem.* **2018**, *20*, 2110-2117.

- [49] K. Klepáčová, D. Mravec, A. Kaszonyi, M. Bajus, *Appl. Catal. A-Gen.* **2007**, 328, 1-13.
- [50] K. Mizuno, S. Imafuji, T. Fujiwara, T. Ohta, Y. Tamiya, *J. Phys. Chem. B* **2003**, 107, 3972-3978.
- [51] P. Borowski, W. Gac, P. Pulay, K. Woliński, *New J. Chem.* **2016**, 40, 7663-7670.
- [52] D. Scholz, C. Aellig, I. Hermans, *ChemSusChem* **2014**, 7, 268-275.

4 Improved catalytic transfer hydrogenation of biomass-derived aldehydes with metal-loaded aluminum phosphate

W. Fang, A. Riisager*, *ACS Sustainable Chemistry & Engineering* **2022**, 10, 1536-1543.

Reprinted with permission from [W. Fang, A. Riisager*, *ACS Sustainable Chemistry & Engineering* **2022**, 10, 1536-1543.]. Copyright [2022] American Chemical Society. In this chapter, the manuscript was directly used with a minor modification.



CTH is a benign and effective process for the conversion of biomass-derived platforms into fuels and chemicals. Here, APO-5 and AEM loaded APO-5s were synthesized by impregnation and applied in the CTH of FF into FAL. The introduction of AEM created weak and medium basic sites instead of weak acidic and strong basic sites in the pristine APO-5, allowing co-catalysis of the AEM oxide species (basic sites) and the APO-5 (acidic sites) to facilitate hydrogenation instead of etherification and acetalization. For 3 wt.% Ca/APO1.5 this tuning of acidity and basicity improved the FAL yield significantly from 54 to 90% (140°C, 48 h), and the catalyst remained stable as well as reusable for at least four consecutive reactions with only slight deactivation. Notably, 3 wt.% Ca/APO1.5 catalyst also showed high catalytic activity for CTH of other bio-derived aldehydes, thus demonstrating its versatile use for valorization of platforms generated during biomass refining.

4.1 Introduction

The steady increase of the world's population and associated demand for energy will gradually result in a future exhausting of traditional fossil resources, i.e. coal, oil and natural gas. Accordingly, the development of renewable energy from consistent alternative resources like biomass has attracted significant attention.¹⁻³ FF is a LB-derived platform molecule, which can be used directly as an energy source or indirectly *via* its conversion into value-added chemicals.⁴ The FF molecule is prone for many chemical transformations at both its aldehyde group and its furan ring, such as hydrogenation, oxidation, acetalization, acylation, aldol condensation, reductive amination.⁵ FAL, one of the most common hydrogenation products, has been widely used in the manufacture of lubricants, resins, lysine, and vitamins.⁶⁻⁸ Conventionally, hydrogen gas is used as an external hydrogen source for hydrogenation of FF to FAL.^{9,10} However, in

the last decades liquid-phase CTH of FF to FAL using different alcohols as hydrogen donors has been investigated as an attractive green alternative.⁷ CTH provides a more benign protocol by avoiding the use of hydrogen gas, thereby rendering the complexity and cost of experimental procedures.¹¹

Previous studies with solid catalysts have confirmed that CTH is both acid and base catalyzed^{12,13} and competing side reactions also catalyzed by acidity or basicity, such as acetalization, etherification and aldol condensation,¹⁴⁻¹⁷ are usually associated when using an alcohol as the hydrogen donor. Zeolites with pore structures and adjustable acidity and basicity have been applied in the CTH reaction.⁷ For example, CTH of FF in ethanol with zeolite β catalyst loaded with zirconium (Zr- β) afforded a FAL selectivity of 81.7% at 49.2% conversion at 140°C with acetalization and aldol condensation reducing the FAL selectivity.¹⁶ Gao et al. also used Zr-substituted β (Zr-Al- β) as catalyst in the CTH of FF in 2-propanol and obtained 32.7% FF conversion at 120°C with a selectivity of 90.2% of IPF formed by the etherification of FAL. However, after modification of the Zr-Al- β catalyst with alkali-metal ions (Li^+ , Na^+ or K^+) by a post-synthetic reflux method, the etherification was significantly suppressed and Na^+ -Zr-Al- β afforded 97.7% FAL selectivity with 99.6% FF conversion at the same reaction conditions.¹⁸ In other work, Wei et al. found that the introduction of basic BaO could inhibit the etherification reaction.¹⁹ Thus, introduction of alkali metal or AEM ions into solid catalysts seems a very promising approach for improving the product selectivity of the CTH reaction of FF into FAL in alcohols.

Recently, we introduced an APO-5 catalyst (Al/P ratio = 1.5) that, depending on the reaction conditions, facilitated highly efficient CTH of FF in 2-propanol to FAL or IPF with moderate to good product selectivity.²⁰ In this work, acidity and basicity of the APO-5 catalyst have been tuned by simple impregnation with

different concentrations of AEMs (Mg, Ca, Sr or Ba) to make catalysts with improved selectivity towards FAL. Twelve catalysts were synthesized and their acidity, basicity, and other physiochemical properties characterized by NH_3 -TPD, CO_2 -TPD, N_2 physisorption, XRD, XRF, FT-IR spectroscopy and SEM, to establish relationship between reaction selectivity and acidity/basicity. Furthermore, a plausible reaction mechanism for the CTH of FF into FAL over AEM-loaded APO-5 was proposed, and durability of the best performing catalyst examined by leaching and recycling tests.

4.2 Results and discussion

4.2.1 Characterization of APO-5 and AEM-loaded catalysts

The XRD patterns of APO-5 and AEM-loaded catalysts with 1-5 wt.% AEM matched well with the AFI structure (Fig. S4.1) and all materials had almost the same unit cell volumes (Table S4.1), implying that the APO-5 framework was well retained after the introduction of the AEMs by impregnation on the surface of catalysts.^{21,22} Notably, no XRD patterns of AEM oxides were found indicating that the oxides were highly dispersed on the surface of APO-5 or amorphous.^{23,24} SEM images of the catalysts before and after AEM loading revealed similar morphology (Figs. S4.2 and S4.3), and EDS analysis confirmed the AEMs to be homogeneously distributed on the external surface of the catalysts (Fig. S4.4).

In the FT-IR spectra both APO-5 and the AEM-loaded catalysts (Fig. S4.5) had a strong band at around 1106 cm^{-1} characteristic of an asymmetric P-O-Al stretching vibration,^{21,25} and bands at 704 and 663 cm^{-1} assignable to the symmetric stretching and bending mode vibrations of P-O-Al, respectively. Additionally, the bands at 632 and 559 cm^{-1} were assigned to double-ring vibration modes, while the band located at 460 cm^{-1} could be assigned to the

internal T-O bending mode vibration.^{21,25,26} Importantly, there were no formation of new band and no shift in all of these characteristic bands after the introduction of AEM into the APO-5,²⁶ indicating that the AEMs were indeed outside the framework, in line with the XRD results.

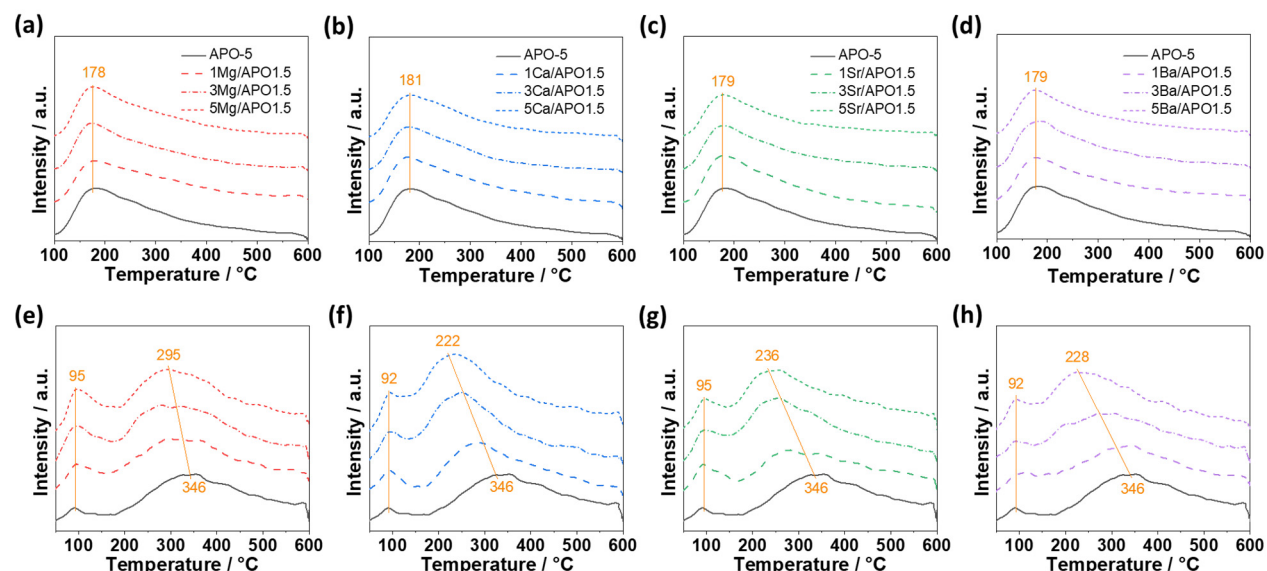


Fig. 4.1 (a)-(d) NH_3 -TPD and (e)-(h) CO_2 -TPD profiles of APO-5 and AEM-loaded APO-5 catalysts.

N_2 physisorption measurements on the catalysts showed all typical IV isotherms with H3 type hysteresis loops in the region $0.75 < P/P_0 < 0.95$ (Fig. S4.6) indicating mesoporous structures.²⁷ At $P/P_0 < 0.05$ the volume of adsorbed N_2 was slightly increased showing the limited existence of microporous structure,²⁸ confirming that all the catalysts had hierarchical porous systems. After the introduction of the AEMs, the volumes of adsorbed N_2 in the low P/P_0 region of the resulting catalysts were slightly changed and the hysteresis loops became smaller, suggesting that the AEM phases were mostly located in the mesopores. The BET surface and mesopore volumes of the catalysts (Table 4.1) were significantly reduced after AEM loading with an apparent correlation with both the size and the content of the AEM oxides, as expected.

Table 4.1 Physiochemical properties of APO-5 and AEM-loaded APO-5 catalysts.

Sample	AEM content (wt.%) ^a	S_{total} (m ² /g) ^b	V_{micro} (cm ³ /g) ^c	V_{meso} (cm ³ /g) ^d	Acidity (μmol/g) ^e	Basicity (μmol/g) ^f
APO-5	-	211	0.04	0.38	302	97
1Mg/APO1.5	0.6	108	0.01	0.28	298	92
3Mg/APO1.5	3.4	101	0.01	0.26	270	128
5Mg/APO1.5	4.6	98	0.01	0.25	255	138
1Ca/APO1.5	0.8	117	0.02	0.29	280	90
3Ca/APO1.5	2.9	106	0.01	0.29	248	106
5Ca/APO1.5	4.7	71	0.01	0.23	240	153
1Sr/APO1.5	1.0	107	0.02	0.27	277	95
3Sr/APO1.5	3.0	108	0.02	0.26	246	119
5Sr/APO1.5	5.4	102	0.02	0.25	239	134
1Ba/APO1.5	1.1	103	0.02	0.25	271	102
3Ba/APO1.5	3.1	108	0.02	0.24	254	103
5Ba/APO1.5	4.8	108	0.02	0.24	245	120

^a Determined by XRF. ^b Calculated by the BET method. ^c Estimated by the t-plot method. ^d Calculated by subtraction of the micropore volume from the total pore volume. ^e Determined by NH₃-TPD. ^f Determined by CO₂-TPD.

Fig. 4.1 shows the NH₃-TPD and CO₂-TPD profiles measured of APO-5 and the AEM-loaded APO-5 catalysts and the corresponding acidities and basicities are compiled in Table 4.1. As shown in Fig. 4.1a-d (NH₃-TPD), all catalysts seemed to have only weak acidic sites with a similar desorption temperature about 179°C, implying that the acidic site strength of the catalysts was the same. However, the number of acidic sites (i.e. acidity) decreased after AEM modification and with higher AEM loading as also previously reported,²⁸⁻³⁰ suggesting interaction between the AEM oxides and the acidic sites.^{31,32} In all the AEM-loaded catalysts, the Mg/APO1.5 catalysts had the highest amounts of acidic sites.

The basicity of the catalysts was analyzed by CO₂-TPD (Fig. 4.1e-h).³³ All the catalysts appeared to have two desorption peaks corresponding to weak (below 100°C) and medium/strong (above 200°C) basic sites,³⁴ respectively, and both the relative amounts of the different sites as well as the total site density changed upon AEM-loading as also found before in previous studies.^{24,35} Notably, the desorption temperature for the medium/strong basic sites decreased with higher AEM content indicative of lower basic strength. However, deconvolution of the CO₂-TPD profiles of the APO-5 and 5wt.% AEM-loaded catalysts (Fig. S4.7) into medium (230-300°C) and strong (around 415°C) basic sites, revealed that a combined change of these sites actually resulted in the apparent overall lower desorption temperature. In addition, the density of the medium basic sites increased with higher AEM loading while the density of the strong basic sites decreased, indicating that the latter sites were removed by AEM species and other medium and weakly basic sites created by the formed AEM oxides. Previous work on Mg-impregnated zeolites have assigned weak basicity to bicarbonates formed with surface OH groups, and medium basicity to bidentate carbonates desorbed from Mg²⁺-O²⁻ pairs.³⁴ The calcination temperature (550°C) used in this work facilitated the formation of medium strength Mg²⁺-O²⁻ pairs,³⁶ and accordingly the medium basicity increased with the enhancement of Mg content. The basicity variations observed for the other used AEMs may originate from similar properties.

4.2.2 Catalytic activity of APO-5 and AEM-loaded catalysts

The catalytic activity of APO-5 and the prepared AEM-loaded catalysts were measured for CTH of FF (Table 4.2). All of the AEM-loaded catalysts yielded lower FF conversion and lower selectivity towards IPF and IPL, but higher FAL and DIPF selectivity, than APO-5, indicating that the AEMs improved the formation

of FAL by reducing the consumption rate of FF. In more detail, Mg provided the highest FAL selectivity but lowest FF conversion, while Ca had the highest FF conversion but intermediate FAL selectivity, further revealing that the impact of the four AEMs was different.

Table 4.2 The conversion of FF using 2-propanol as H-donor over APO-5 catalysts.^a

Catalyst	Conv. (%) ^b	Product Selec. (%) ^b				Carbon balance (%)
		FAL	DIPF	IPF	IPL	
APO-5	91.5	59.3	0.8	22.9	3.4	86.4
1Mg/APO1.5	81.8	85.5	8.5	5.0	0.2	99.2
1Ca/APO1.5	90.7	83.1	2.6	10.2	0.8	96.7
1Sr/APO1.5	85.5	82.3	3.8	9.8	0.8	96.7
1Ba/APO1.5	87.0	80.6	4.6	9.5	0.9	95.6

^a Reaction conditions: FF (96 mg, 1 mmol), catalyst (50 mg), 2-propanol (5 mL), 140°C, 24 h. ^b Conversion and yield were quantified using GC. FAL: furfuryl alcohol, DIPF: 2-(diisopropoxymethyl)furan, IPF: 2-(isopropoxymethyl)furan, IPL: isopropyl levulinate.

The effect of AEM content (1-5 wt.%) was further investigated (Fig. 4.2). The FF conversion and IPF selectivity were reduced with higher metal contents, while the DIPF selectivity was increased. In contrast, the FAL selectivity apparently reached a maximum with intermediate metal loading of 3 wt.% (except for Mg/APO1.5), corroborating that the metal content strongly affected the reaction. Notably, among the series of 3 wt.% AEM-loaded catalysts, the FAL selectivity reached above 90% for 3Ca/APO1.5 and 3Ba/APO1.5, implying that the metal inventory likely played an important role on reaction progression due to different acidic/basic properties.

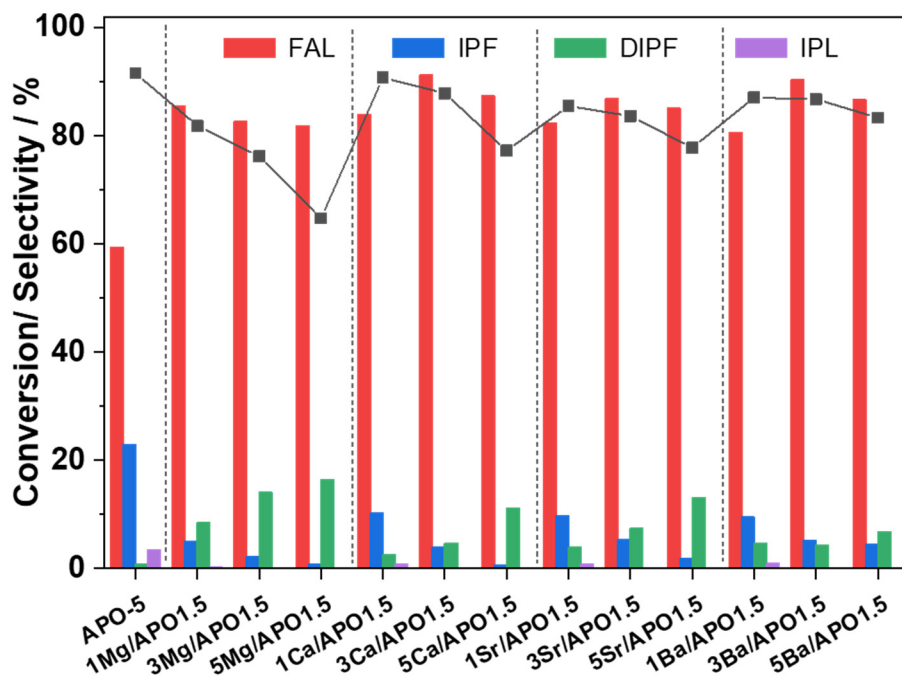


Fig. 4.2 The influence of metal amounts on the CTH of FF over AEM-loaded APO-5 catalysts. Reaction conditions: FF (96 mg, 1 mmol), catalyst (50 mg), 2-propanol (5 mL), 140°C, 24 h.

Time course studies were then performed with the best-performing catalysts, i.e. 1Mg/APO1.5, 3Ca/APO1.5, 3Sr/APO1.5 and 3Ba/APO1.5, to get more insight into product formation during the CTH reactions (Fig. 4.3). During reaction, FF gradually converted into a mixture of FAL (main product) by hydrogenation, IPF by consecutive etherification of FAL and IPL by continuous hydrolysis of IPF, respectively. Additionally, the acetal intermediate DIPF formed initially in the reaction but concurrently transformed (along with the consumption of FF) *via* reversible hydrolysis of the formed DIPF (Fig. 4.3a).^{17,37,38} After 48 h of reaction, the FF conversions of the APO-5 and AEM-loaded catalysts were almost identical (Fig. 4.3b), whereas the IPF yield in the former catalyst was much higher than the latter catalysts, leading to the lowest FAL yield (Fig. 4.3c). Acetalization of FF was reversible for all catalysts, but DIPF hydrolysis was relatively slow under the reaction conditions making DIPF a side product (Fig. 4.3d). Similarly, the hydrolysis of IPF to form IPL was negligible (Fig. 4.3e). Thus, among the studied

catalysts 3Ca/APO1.5 exhibited the best performance yielding 89.7% FAL and 97.2% FF conversion with low IPF and DIPF yield, and to further improve FAL selectivity both acetalization and etherification needed to be inhibited.

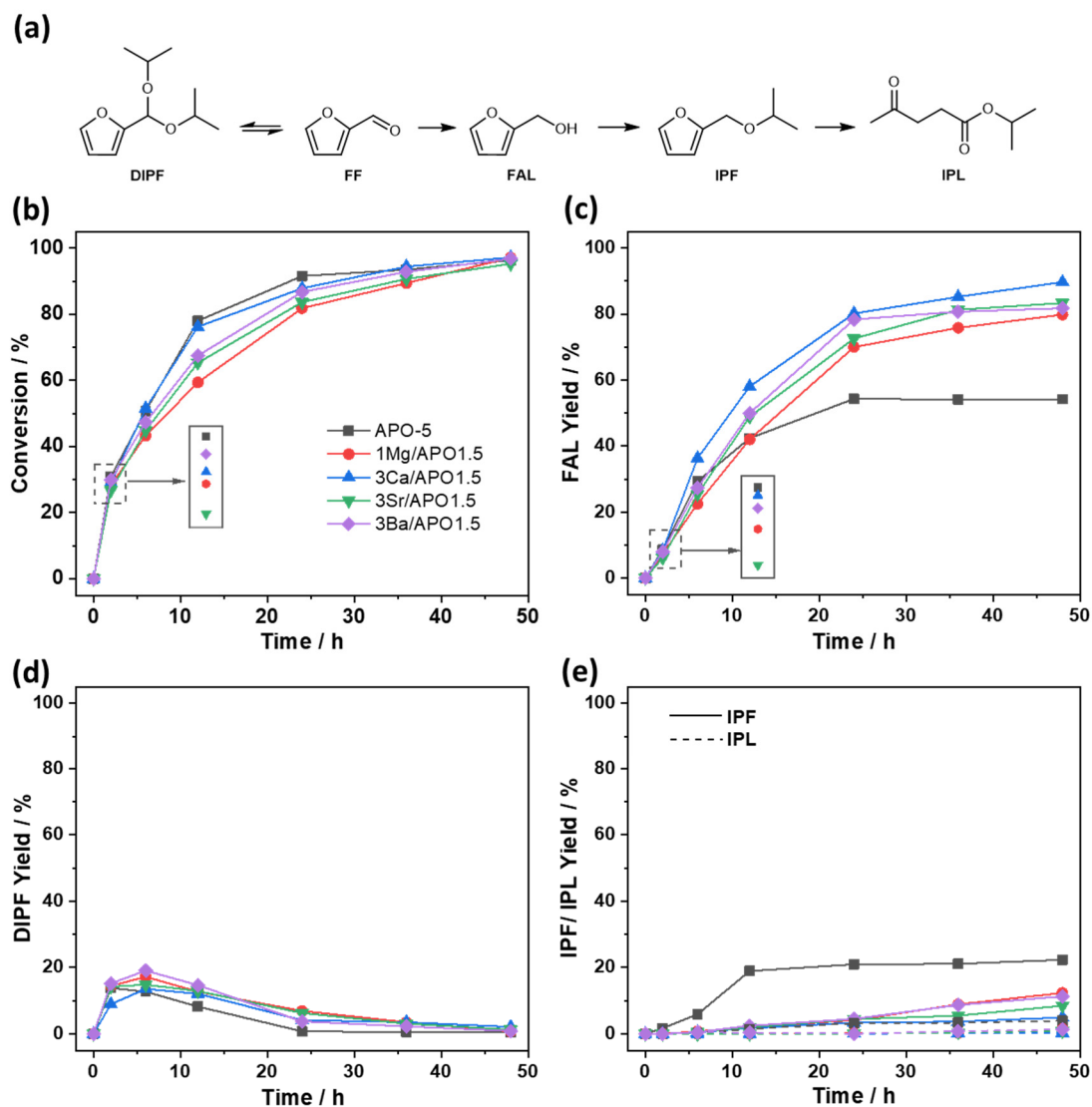


Fig.4.3 (a) Reaction pathway for the conversion of FF in 2-propanol. (b) Conversions, (c) FAL yields, (d) DIPF yields, and (e) IPF/IPL yields of APO-5 and AEM-loaded APO-5 catalysts for the CTH of FF in 2-propanol. Reaction conditions: FF (96 mg, 1 mmol), catalyst (50 mg), 2-propanol (5 mL), 140°C.

4.2.3 Effect of acidity and basicity on activity of AEM-loaded catalysts

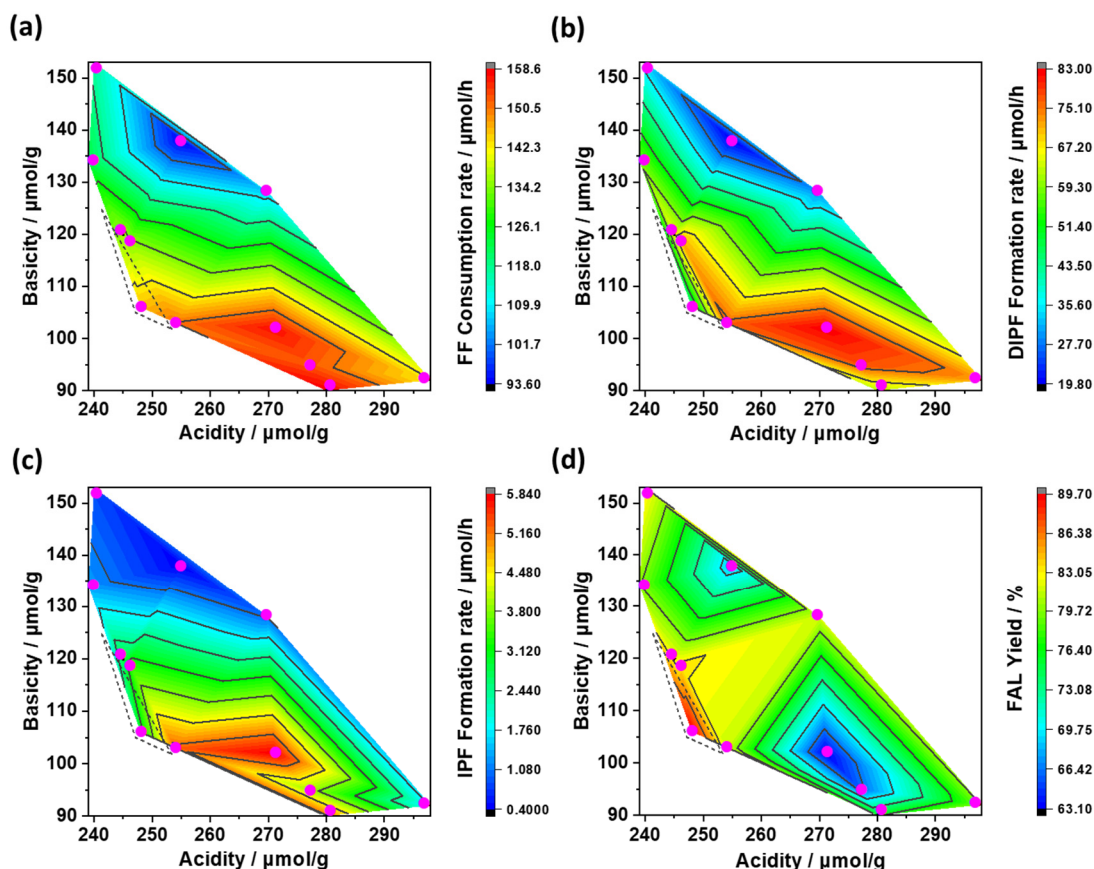


Fig. 4.4 Correlations between a combination of acidity and basicity as well as (a) FF consumption rate, (b) DIPF formation rate, (c) IPF formation rate, and (d) FAL yield for CTH of FF with different AEM-loaded APO-5 catalysts. Reaction conditions: (a) and (b) FF (96 mg, 1 mmol), catalyst (50 mg), 2-propanol (5 mL), 140°C, 2 h; (c) FAL (98 mg, 1 mmol), catalyst (50 mg), 2-propanol (5 mL), 140°C, 6 h; (d) FF (96 mg, 1 mmol), catalyst (50 mg), 2-propanol (5 mL), 140°C, 48 h.

FT-IR spectra of APO-5 and the AEM-loaded catalysts were recorded with pre-adsorbed FF to verify the interaction of FF with the catalysts (Fig. S4.8a). All the samples had an identical C=O stretching band of FF, which was slightly red shifted from 1668 to 1663 cm^{-1} suggesting that the C=O group of FF adsorbed strongly on the catalysts^{12,13,39} and likely promoted the effective conversion of FF. The adsorption capacity of FAL on the catalysts were also monitored (Fig. S4.8b) as continuous etherification is less likely to occur if FAL is easily detached from

the active sites after formation. The bending vibration of O-H (731 cm^{-1}) and stretching vibration of C-OH (1009 cm^{-1}) of FAL were identifiable,¹² but occurred at similar wavelengths for all the catalysts. This indicated that the detachment of FAL from the catalysts after formation would also be similar, and accordingly acidity and basicity may instead have key impacts on the product distribution observed (*vide supra*).

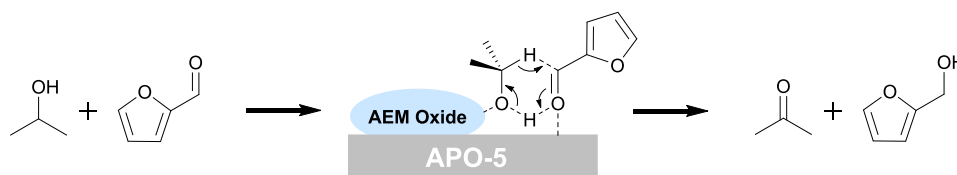
The correlations between the density of acidic and basic sites of the different AEM-loaded APO-5 catalysts with FF consumption rates as well as FAL, DIPF and IPF formation rates, respectively, are shown in Fig. S4.9. For the catalysts having the same AEM loadings, the FF consumption rate and FAL formation rate had a positive dependence on the acidity while the dependence was negative on the basicity, indicating that both acidity and basicity catalyzed hydrogenation.^{40,41} Reference reactions using pyridine or benzoic acid as poisoning additives also supported that both acidity and basicity catalyzed the CTH reaction (Fig. S4.10). IPF formation by etherification (using FAL as substrate) and DIPF formation by acetalization also had positive correlations with acidity and negative correlations with basicity over the same AEM-loaded catalysts.^{17,37,42} Overall, this suggests that suitable combinations of acidity and basicity may be possible to facilitate to obtain high hydrogenation selectivity but low acetalization and etherification selectivity.

Figs. 4.4a-c visualize the correlation between a combination of acidity and basicity and FF consumption rates as well as DIPF and IPF formation rates for the different AEM-loaded APO-5 catalysts. The contour plots show that catalysts with relatively high acidity and low basicity were prone to fast FF consumption and fast DIPF formation, while intermediate acidity and basicity facilitated IPF formation. In order to improve the FAL yield of the reaction, high FF consumption

rate and both low DIPF and IPF formation rates were desired and catalyst acidity around 245-254 $\mu\text{mol/g}$ and basicity around 103-120 $\mu\text{mol/g}$ (areas shown in dotted triangles on Figs. 4.4a-c) meet these requirements best. In line with this, the AEM-loaded catalysts having such acidic and basic properties achieved the high FAL yields (>83%), when reaction time was prolonged to 48 h (Fig. 4.4d). An excellent FAL yield of 89.6% was even reached for the 3Ca/APO1.5 catalyst, thus clearly demonstrating how rational catalyst optimization and tuning can improve the performance for CTH of FF to FAL.

4.2.4 Reaction mechanism of AEM-loaded catalysts

Based on the obtained results and previous reports,⁴³ a plausible mechanism for the CTH of FF with the AEM-loaded APO-5 catalysts are proposed involving hydrogen transfer *via* a six-membered cyclic intermediate (Scheme 4.1). The electron-rich oxygen in the hydroxyl group of 2-propanol firstly interact with the AEM oxide species (basic sites) to attenuate the O-H bond.^{44,45} Meanwhile, the O atoms of the carbonyl groups of the FF also interact with the APO-5 (acidic sites) to form six-membered intermediates allowing hydrogen transfer directly from 2-propanol to FF. The proposed mechanism infer that the basic and acidic sites should be adjacent to form the six-membered ring effectively, and in order to validate this assumption the reaction was examined with a mixture of CaO (3 wt.%) and APO-5 catalyst (97 wt.%). Both FF conversion and FAL yield decreased dramatically here (from 97.2 to 58.3% and 89.7 to 27.1%, respectively) (Table S4.2), implying adjacent acidic and basic sites indeed promoted with reaction significantly (i.e. formation of six-membered intermediates).



Scheme 4.1 Proposed mechanism for CTH of FF to FAL with 2-propanol over AEM-loaded APO-5 catalysts.

4.2.5 Durability of 3Ca/APO1.5 catalyst

Leaching and recycling tests were further carried out with the best-performing 3Ca/APO1.5 catalyst to assess its durability. The catalyst initially provided a FF conversion of 51.5% and a FAL selectivity of 70.5% (FAL yield 36.3%) at 140°C after 6 h of reaction (Fig. 4.5a). After removing the catalyst and continuing the reaction for additionally 42 h, the FAL yield remained essentially unchanged suggesting that no catalytically active species had leached into the solution. However, upon catalyst recycling, the FF conversion gradually decreased from 51.2 to 39.9% and FAL selectivity reduced slightly from 70.5 to 64.5% after four consecutive reactions (Fig. 4.5b).

TG analysis of the recovered catalyst after the fourth reaction showed that the catalyst had 5.7 wt.% carbon residues deposited, and porosity analysis suggested that the deposit was mainly located in the mesopores of the catalyst where CaO also was located (Figs. S4.12-13, Table S4.3). In combination, this resulted in the slight deactivation observed. The recovered catalyst from the fourth reaction was calcined and attempted used for a fifth reaction. However, the activity was here even worse due to changed acidity and basicity and the loss of Ca after the reuse and calcination (Fig. S4.14, Table S4.3), strongly supporting the opinion that catalysts with specified acidity and basicity promote the conversion of FF and the formation of FAL.

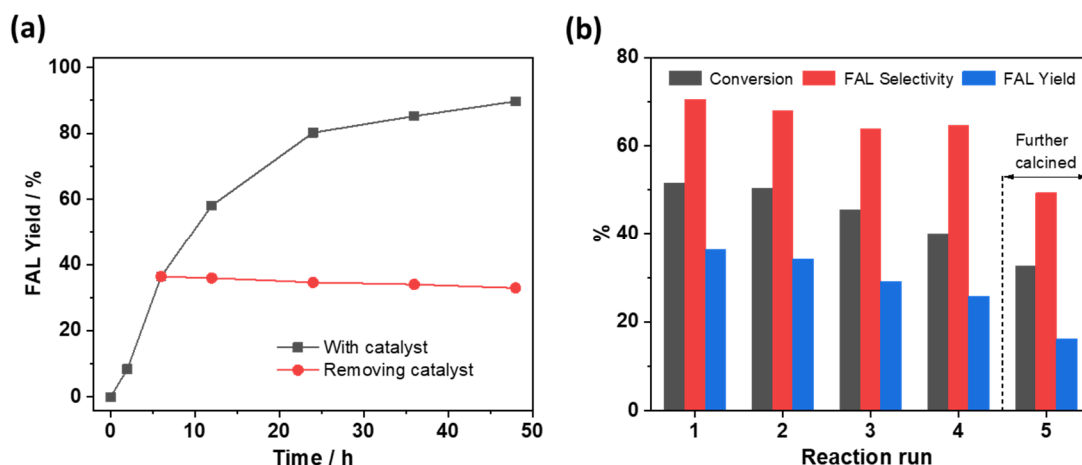
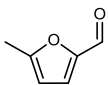
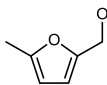
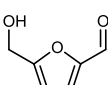
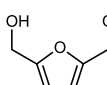
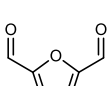
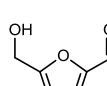
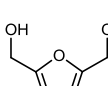
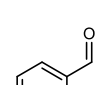
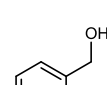
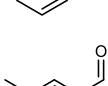
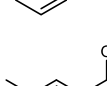
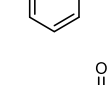
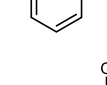


Fig. 4.5 (a) Leaching study of 3Ca/APO1.5 catalyst. Reaction conditions: FF (96 mg, 1 mmol), 3Ca/APO1.5 (50 mg), 2-propanol (5 mL), 140°C. (b) Recycling study of 3Ca/APO1.5. Reaction conditions: FF (96 mg, 1 mmol), 3Ca/APO1.5 (50 mg), 2-propanol (5 mL), 140°C, 6 h.

4.2.6 Substrate scope

Table 4.3 CTH of various carbonyl molecules with 3Ca/APO1.5 catalyst.^a

Entry	Substrate	Product	Conv. (%) ^b	Yield (%) ^b	Product	Yield (%) ^b
1			93.2	90.6		
2			81.8	76.4		
3			94.4	48.1		46.3
4			91.9	91.0		
5			90.5	90.0		
6			91.8	91.0		

^a Reaction conditions: substrate (1 mmol), catalyst (50 mg), 2-propanol (5 mL), 140°C, 48 h. ^b Conversion and yield were quantified using ¹H NMR.

Finally, the 3Ca/APO1.5 catalyst was applied for CTH with a selection of alternative bio-derived furanic and aromatic aldehydes under identical reaction conditions as used with FF (Table 4.3). The compounds were converted with very high selectivity (97-99%) to the corresponding alcohols providing yields above 90%, except HMF which reacted slower and gave slightly lower selectivity (93.3%) to 2,5-bis(hydroxymethyl)furan (BHMF). Similarly, FCA formed HMF as intermediate product under the applied reactions conditions corroborating that HMF was less reactive and thus requiring longer reaction time to reach full conversion to BHMF. Also, the aromatic aldehydes benzaldehyde, *m*-tolualdehyde and *p*-tolualdehyde gave very good yields of the corresponding alcohols (above 90%), suggesting that the high catalytic activity of 3Ca/APO1.5 in CTH was universal for aldehyde molecules in general.

4.3 Summary

APO-5 catalysts with 1-5 wt.% of different AEMs (Mg, Ca, Sr, and Ba) have been synthesized by wet-impregnation to promote catalytic performance in CTH of FF to FAL. Characterization of the catalysts after calcination showed that the AEM-loaded catalysts mainly contained well-dispersed AEM oxides in the mesopore channels of APO-5, and that density of acidic and basic sites were altered after the introduction of the AEM resulting in catalysts with overall adjusted acidity and basicity. During CTH of FF competitive hydrogenation, acetalization and etherification reactions were prudently controlled by acidity and basicity of the catalysts, and tuning of acidity and basicity combinations allowed obtaining high selectivity of hydrogenation significantly promoting the FAL selectivity. Thus, APO-5 catalysts with acidity (248-254 $\mu\text{mol/g}$) and basicity (103-120 $\mu\text{mol/g}$) proved favorable for obtaining high FAL yield, which was exemplified by 3Ca/APO1.5 providing a 90% FAL yield with 97% FF conversion at 140°C after

48 h of reaction. The 3Ca/APO1.5 catalyst also showed high stability and reusability for four successive CTH reactions with only slightly deactivation and high catalytic activity in CTH of other aldehyde compounds. This work offers a simple strategy to promote the catalytic performance in CTH reaction by rational tuning the acidity and basicity.

4.4 References

- [1] M. Besson, P. Gallezot, C. Pinel, *Chem. Rev.* **2014**, *114*, 1827-1870.
- [2] A. Corma, S. Iborra, A. Velty, *Chem. Rev.* **2007**, *107*, 2411-2502.
- [3] C. Z. Li, X. C. Zhao, A. Q. Wang, G. W. Huber, T. Zhang, *Chem. Rev.* **2015**, *115*, 11559-11624.
- [4] X. Li, P. Jia, T. Wang, *ACS Catal.* **2016**, *6*, 7621-7640.
- [5] H. E. Hoydonckx, W. M. Van Rhijn, W. Van Rhijn, D. E. De Vos, P. A. Jacobs, in *Ullmann's encyclopedia of industrial chemistry*, Vol. 16, Wiley, **2000**, pp. 285-313.
- [6] A. Mandalika, L. Qin, T. K. Sato, T. Runge, *Green Chem.* **2014**, *16*, 2480-2489.
- [7] W. Fang, A. Riisager, *Green Chem.* **2021**, *23*, 670-688.
- [8] J. Long, W. Zhao, H. Li, S. Yang, in *Biomass, Biofuels, Biochemicals*, Elsevier, **2020**, pp. 299-322.
- [9] S. Sitthisa, T. Sooknoi, Y. Ma, P. B. Balbuena, D. E. Resasco, *J. Catal.* **2011**, *277*, 1-13.
- [10] S. Sitthisa, W. An, D. E. Resasco, *J. Catal.* **2011**, *284*, 90-101.
- [11] S. Zhou, G. Chen, X. Feng, M. Wang, T. Song, D. Liu, F. Lu, H. Qi, *Green Chem.* **2018**, *20*, 3593-3603.
- [12] M. Ma, P. Hou, J. Cao, H. Liu, X. Yan, X. Xu, H. Yue, G. Tian, S. Feng, *Green Chem.* **2019**, *21*, 5969-5979.
- [13] Y. Yang, L. Chen, Y. Chen, W. Liu, H. Feng, B. Wang, X. Zhang, M. Wei, *Green Chem.* **2019**, *21*, 5352-5362.
- [14] S. H. Zhou, F. T. Dai, Y. A. Chen, C. Dang, C. Z. Zhang, D. T. Liu, H. S. Qi, *Green Chem.* **2019**, *21*, 1421-1431.
- [15] N. S. Biradar, A. M. Hengne, S. S. Sakate, R. K. Swami, C. V. Rode, *Catal. Letters* **2016**, *146*, 1611-1619.
- [16] G. Li, W. Q. Jiao, Z. Sun, Y. Zhao, Z. P. Shi, Y. Yan, L. Feng, Y. H. Zhang, Y. Tang, *ACS Sustain. Chem. Eng.* **2018**, *6*, 4316-4320.
- [17] M. Balakrishnan, E. R. Sacia, A. T. Bell, *Green Chem.* **2012**, *14*, 1626-1634.
- [18] L. Gao, G. Li, Z. Sheng, Y. Tang, Y. Zhang, *J. Catal.* **2020**, *389*, 623-630.
- [19] J. Wei, X. Cao, T. Wang, H. Liu, X. Tang, X. Zeng, Y. Sun, T. Lei, S. Liu, L. Lin, *Catal. Sci. Technol.* **2018**, *8*, 4474-4484.
- [20] W. Fang, A. Riisager, *Appl. Catal. B-Environ.* **2021**, *298*, 120575.

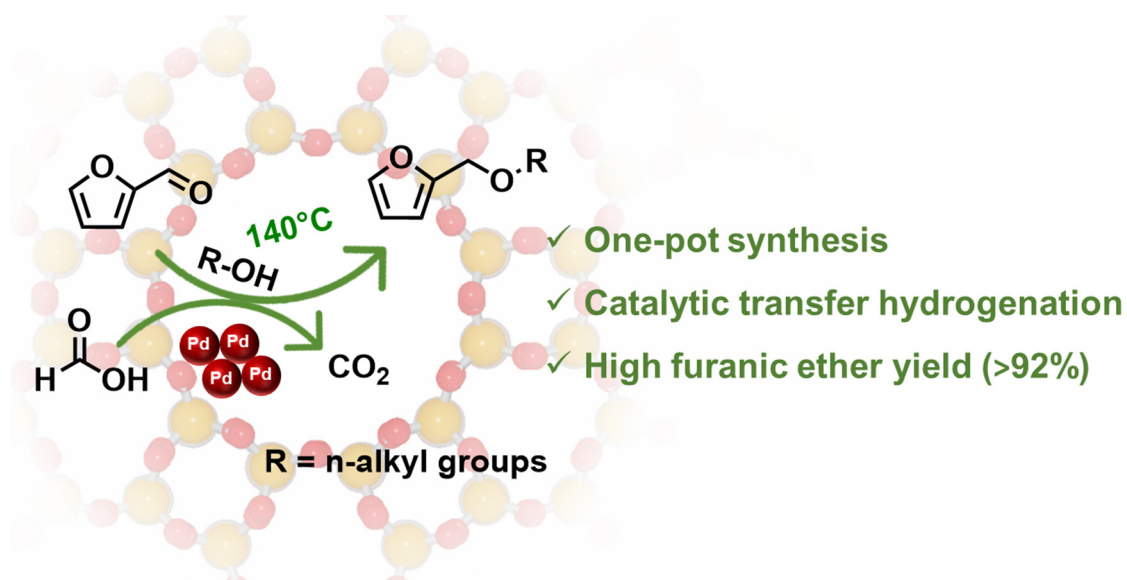
- [21] T. Munõz, A. M. Prakash, L. Kevan, K. J. Balkus, *J. Phys. Chem. B* **1998**, *102*, 1379-1386.
- [22] L. Zhou, T. Lu, J. Xu, M. Chen, C. Zhang, C. Chen, X. Yang, J. Xu, *Micropor. Mesopor. Mat.* **2012**, *161*, 76-83.
- [23] D. Mao, W. Yang, J. Xia, B. Zhang, Q. Song, Q. Chen, *J. Catal.* **2005**, *230*, 140-149.
- [24] I. Graça, D. Iruretagoyena, D. Chadwick, *Appl. Catal. B-Environ.* **2017**, *206*, 434-443.
- [25] M. Zaarour, O. Perez, P. Boullay, J. Martens, B. Mihailova, K. Karaghiosoff, L. Palatinus, S. Mintova, *CrystEngComm* **2017**, *19*, 5100-5105.
- [26] S. Endud, N. Roslan, Z. Ramli, H. O. Lintang, *Adv. Mat. Res.* **2015**, *1109*, 360-364.
- [27] M. Wang, Z. Wang, S. Liu, R. Gao, K. Cheng, L. Zhang, G. Zhang, X. Min, J. Kang, Q. Zhang, Y. Wang, *J. Catal.* **2021**, *394*, 181-192.
- [28] X. Long, Q. Zhang, Z.-T. Liu, P. Qi, J. Lu, Z.-W. Liu, *Appl. Catal. B-Environ.* **2013**, *134-135*, 381-388.
- [29] B. Mitra, D. Kunzru, *Catal. Letters* **2011**, *141*, 1569-1579.
- [30] Z. Zhao, W. Qiao, X. Wang, G. Wang, Z. Li, L. Cheng, *Micropor. Mesopor. Mat.* **2006**, *94*, 105-112.
- [31] P. Lersch, F. Bandermann, *Appl. Catal.* **1991**, *75*, 133-152.
- [32] C. Chen, Q. Zhang, Z. Meng, C. Li, H. Shan, *Appl. Petrochem. Res.* **2015**, *5*, 277-284.
- [33] M. Laspéras, H. Cambon, D. Brunel, I. Rodriguez, P. Geneste, *Microporous Materials* **1993**, *1*, 343-351.
- [34] J. I. D. Cosimo, V. K. Díez, M. X. Iglesia, E. , C. R. Apesteguía, *J. Catal.* **1998**, *178*, 499-510.
- [35] H. Y. Kim, H. M. Lee, J.-N. Park, *J. Phys. Chem. C* **2010**, *114*, 7128-7131.
- [36] J. I. Di Cosimo, V. K. Díez, C. Ferretti, C. R. Apesteguía, *Catalysis* **2014**, *26*, 1-28.
- [37] H. Nguyen, N. Xiao, S. Daniels, N. Marcella, J. Timoshenko, A. Frenkel, D. G. Vlachos, *ACS Catal.* **2017**, *7*, 7363-7370.
- [38] E. R. Sacia, M. Balakrishnan, A. T. Bell, *J. Catal.* **2014**, *313*, 70-79.
- [39] X. Meng, Y. Yang, L. Chen, M. Xu, X. Zhang, M. Wei, *ACS Catal.* **2019**, *9*, 4226-4235.
- [40] J. He, L. Schill, S. Yang, A. Riisager, *ACS Sustain. Chem. Eng.* **2018**, *6*, 17220-17229.
- [41] J. He, M. R. Nielsen, T. W. Hansen, S. Yang, A. Riisager, *Catal. Sci. Technol.* **2019**, *9*, 1289-1300.
- [42] A. R. Trifoi, P. Ş. Agachi, T. Pap, *Renew. Sust. Energ. Rev.* **2016**, *62*, 804-814.
- [43] Y. Sha, Z. Xiao, H. Zhou, K. Yang, Y. Song, N. Li, R. He, K. Zhi, Q. Liu, *Green Chem.* **2017**, *19*, 4829-4837.
- [44] S. H. Zhou, F. L. Dai, Z. Y. Xiang, T. Song, D. T. Liu, F. C. Lu, H. S. Qi, *Appl. Catal. B-Environ.* **2019**, *248*, 31-43.

- [45] Z. Gao, C. Y. Li, G. L. Fan, L. Yang, F. Li, *Appl. Catal. B-Environ.* **2018**, 226, 523-533.

5 Reductive etherification of furfural *via* hydrogenolysis with Pd-modified aluminum phosphate and formic acid

W. Fang, J. Egebo, L. Schill, H. Chen, A. Riisager* *Green Chemistry*, **2022**, 24, 7346-7349.

Reproduced from (W. Fang, J. Egebo, L. Schill, H. Chen, A. Riisager*, *Green Chemistry*, **2022**, 24, 7346-7349). Copyright [2022] Royal Society of Chemistry. In this chapter, the manuscript was directly used with a minor modification.



Practical and versatile one-pot syntheses of alkyl furanic ethers is achieved in 92-99% yield from FF with Pd nanoparticles (NPs) supported on APO-5 as catalysts in various primary alcohols (C₂-C₆) using FA as a hydrogen donor. The reductive etherification of FF occurs *via* acetalization and subsequent hydrogenolysis.

5.1 Introduction

The exploitation of renewable biomass to produce carbon-containing fuels and chemicals is established as an important approach to avoid the overuse of non-renewable fossil resources.^{1,2} FF is an attractive platform compound accessible from LB and it finds wide use as a feedstock for other numerous chemicals, especially biofuels.^{3,4} Such biofuels can either be used directly or mixed in fossil fuels as bio-additives to improve the fuel properties,⁵ and in particular furanic ethers have become very promising blending components in high-octane gasoline.^{4,6,7} Two different strategies prevail for the synthesis of furanic ethers from FF with heterogeneous catalysis; a two-step process with FF hydrogenation to FAL followed by etherification or a one-pot process relying on direct reductive etherification of FF, respectively. Due to a simpler mode of operation, the latter approach is often preferred even though it requires a bifunctional hydrogenation/acid catalyst system. Examples of such systems includes Pd/C used for the reductive etherification of FF in ethanol with pressurized hydrogen gas, where the formation of acidic PdH species allowed obtaining moderate yield (81%) of furanic ether.⁸ Likewise, Pd-I/Al₂O₃ yielded 76% of furanic ether in 2-propanol with hydrogen gas because the combination of iodine species on the Pd NPs with dissociated hydrogen generated “in situ” Brønsted acidic sites.⁹ Notably, in both systems the use of hydrogen gas also formed hydrogenation products, which led to the moderate selectivity of ether.^{8,9}

CTH with alcohols, FA or formate salts as hydrogen donors¹⁰ offers an attractive alternative to the use of pressurized hydrogen gas for reductive etherification of FF in terms of both cost and safety. Recently, Zr/Si mixed oxide and Sn-Beta catalysts were shown to give 95% and 58% yield of furanic ether from FF with 2-butanol as a hydrogen donor,^{11,12} while mixed Zr-Mont/ZrO(OH)₂ catalyst gave 67% and 69% furanic ether yields with 2-propanol and 2-butanol as hydrogen donors, respectively.¹³ Noticeably, all catalytic systems failed to offer good yields of furanic ethers of FF in primary alcohols such as, e.g. ethanol and *n*-propanol, which possesses limited hydrogen transfer capability.¹⁴ However, the use of FA (also obtainable from biomass)¹⁵ as a hydrogen source instead of alcohols can circumvent this drawback as FA can decompose catalytically into H₂ and CO₂ over metal-based catalysts, especially Pd-based catalysts.¹⁶⁻¹⁸ According to our previous work, APO-5 has specific adsorption of aldehydes, which may promote reductive etherification.^{19,20} Thus in this work are bifunctional Pd-loaded APO-5 catalysts introduced as highly efficient and selective heterogeneous catalysts for the reductive etherification of FF to form alkyl furfuryl ethers with FA in primary alcohols, including ethanol and 1-propanol.

5.2 Results and discussion

5.2.1 Characterization of Pd-loaded APO-5 catalysts

Pd-loaded APO-5 catalysts with different metal content (Pd-1: 1.72 wt.% Pd; Pd-2: 2.45 wt.% Pd) were synthesized by wet impregnation and characterized. The XRD patterns of the Pd catalysts (Fig. 5.1a) matched well with the AFI-type structure of APO-5²¹ and confirmed that the structure was retained after metal introduction. Furthermore, the intensity of the peak corresponding to the Pd

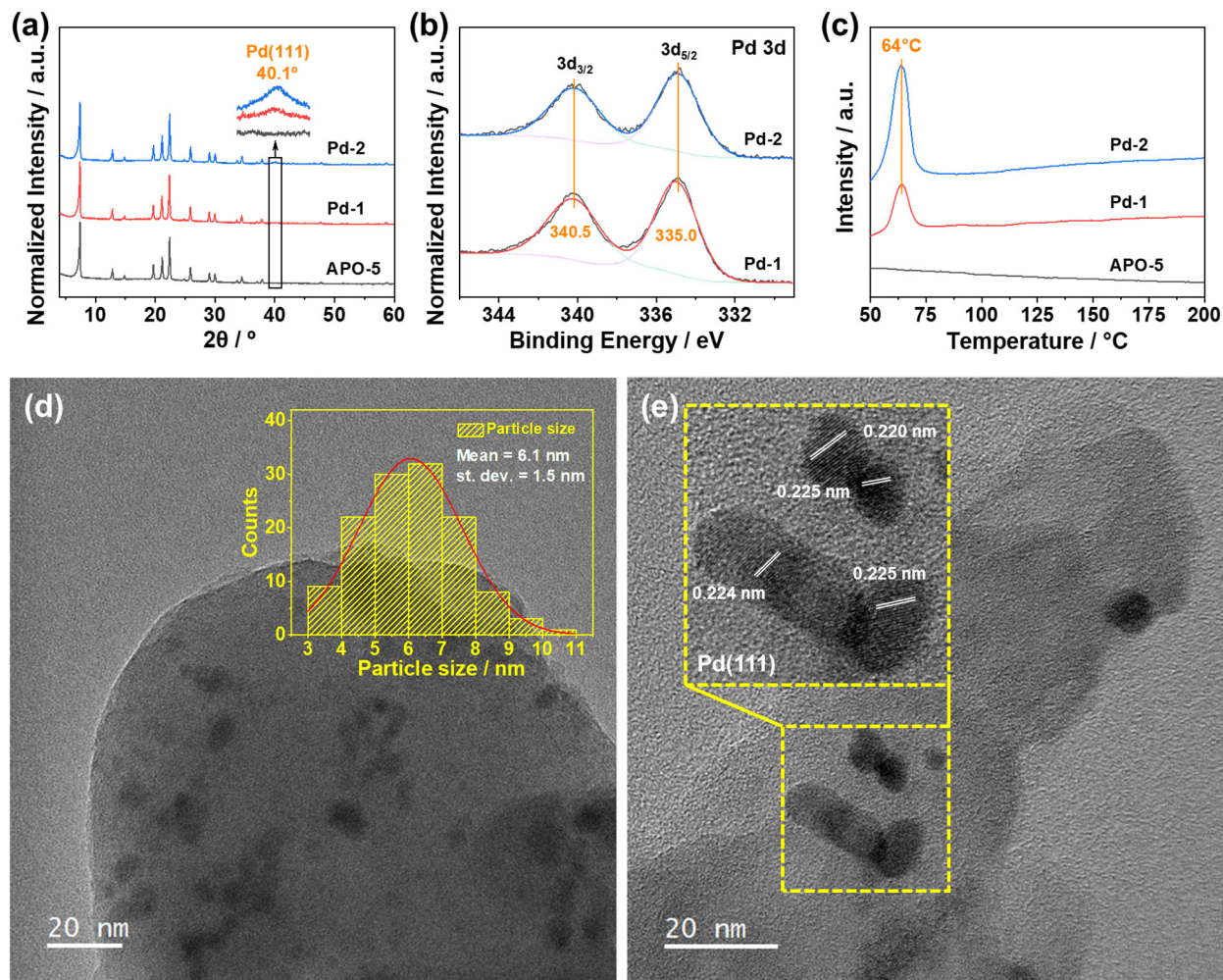


Fig. 5.1 (a) XRD patterns of APO-5, Pd-1 and Pd-2. (b) XPS spectra of Pd-1 and Pd-2; (c) H₂-TPR profiles of APO-5, Pd-1 and Pd-2. (d) and (e) TEM images of Pd-2 (inset: particle size distribution).

(111) facet (40.1°)²²⁻²⁴ was higher for Pd-2 than for Pd-1 as also expected based on their relative metal content. Porosity analysis by N₂ physisorption (Fig. S5.1 and Table S5.1) revealed that the Pd catalysts had larger mesopores (31-46 nm) than the APO-5 support (15 nm), which was attributed to an expansion of the mesopores by agglomerated Pd NPs.²⁵ This expansion also resulted in altered hysteresis loops and reduced surface areas of the Pd catalysts. SEM images further confirmed the morphologies of APO-5 and Pd-2 to be identical (5-6 μm spherical barrel shaped, Fig. S5.2), and EDS analysis of Pd-2 (Fig. S5.3)

suggested a homogeneous distribution of Pd (the overlapping signals of C K α_1 and Pd M ζ are considered artificial).

The Pd NP size distribution in Pd-2 was determined by TEM to 3-10 nm with an average particle size of 6.1 nm (Fig. 5.1d and 5.1e), and distances between adjacent Pd (111) lattice planes were 0.22-0.23 nm in accordance with literature.^{22,26} The binding energies of Pd-1 and Pd-2 was measured by XPS (Fig. 5.1b) to be identical corresponding to 3d_{5/2} (335.0 eV) and 3d_{3/2} (340.5 eV) of metallic Pd,^{9,27} and both catalysts also yielded a main peak at 64°C in H₂-TPR (Fig. 5.1c) related to the adsorption of hydrogen at the Pd (111) surface.²⁸ For Pd-2 this peak was more intense than for Pd-1 due to the higher metal content. Both catalysts possessed also weak, medium, and strong acidic/basic sites as shown by NH₃-TPD and CO₂-TPD, respectively (Figs. S5.4a and S5.4b; Tables S5.2 and S5.3). Notably, the introduction of Pd decreased the total acidity compared to the pristine support, which may be attributed to covering of the acidic sites by the Pd NPs.²⁹⁻³¹ In contrast, the total basicity remained essentially unchanged with only a small shift of strong basic sites. Hence, overall the Pd-loaded APO-5 catalysts had well-distributed Pd NPs with exposed (111) facets as well as acidic and basic surface sites.

5.2.2 Catalytic performance of Pd-loaded APO-5 catalysts

The reaction of FF in mixed FA-ethanol solvent were examined with APO-5 and the Pd-loaded catalysts (140°C, 4 h; Fig. 5.2a). With APO-5 formed 2-(diethoxymethyl)furan (DEF) exclusively (19% conversion, >99% DEF selectivity) indicating that APO-5 had a preferred acidity for the acetalization of FF.¹⁹ In contrast, Pd-loaded APO-5 catalysts formed almost exclusively EFE *via* the reductive etherification of FF, thus implying the importance of the Pd NPs for the

reactivity. The most active catalyst was Pd-2 (60% conversion, 99% EFE selectivity) with the highest metal content. Furthermore, both the leaching and recycling tests (Fig. S5.5) suggest the good stability and reusability of Pd-2.

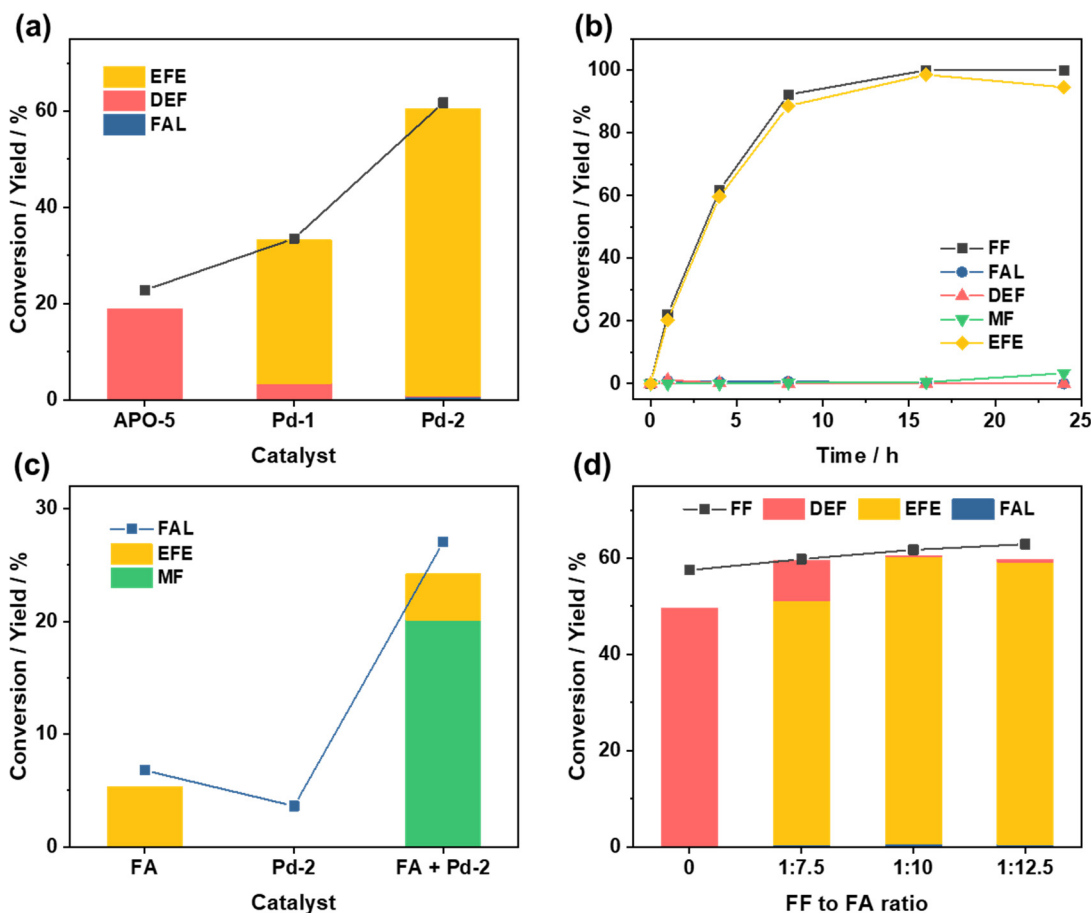
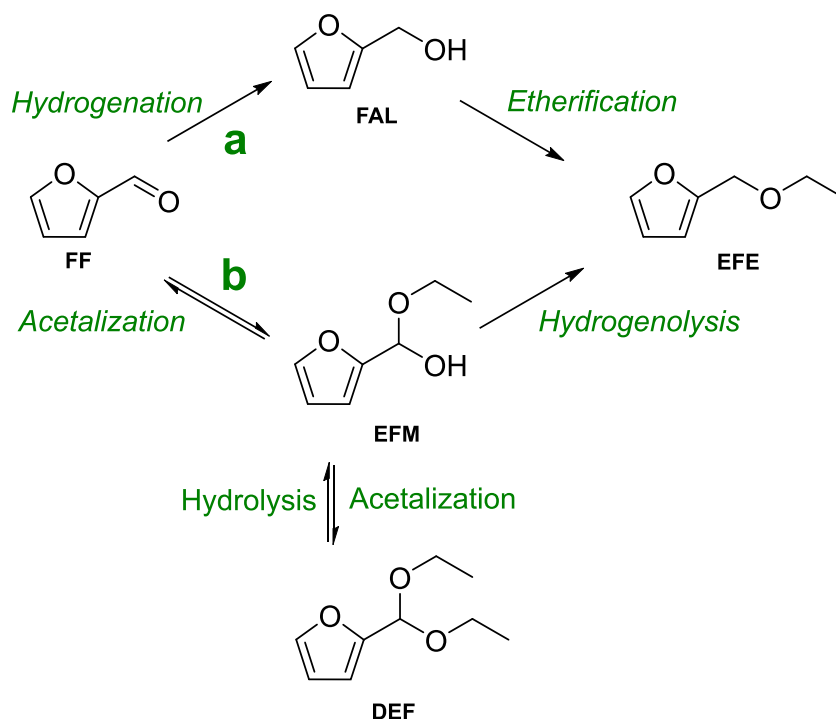


Fig. 5.2 Catalytic performance of Pd-loaded APO-5 catalysts. (a) Reductive etherification of FF with APO-5, Pd-1 and Pd-2. Reaction conditions: FF (96 mg, 1 mmol), catalyst (50 mg), FA (0.38 mL, 10 mmol), ethanol (4.62 mL), 140°C, 4 h. (b) Time course study for the reductive etherification of FF with Pd-2. Reaction conditions: FF (96 mg, 1 mmol), Pd-2 (50 mg), FA (0.38 mL, 10 mmol), ethanol (4.62 mL), 140°C. (c) Etherification of FAL with only FA or Pd-2 or a combination of FA and Pd-2. Reaction conditions: FAL (98 mg, 1 mmol), Pd-2 (50 mg), FA (0.38 mL, 10 mmol), ethanol and FA (5 mL), 140°C, 4 h. (d) Reductive etherification of FF with Pd-2 using different FF to FA ratios. Reaction conditions: FF (96 mg, 1 mmol), Pd-2 (50 mg), ethanol and FA (5 mL), 140°C, 4 h. FA: formic acid, FAL: furfuryl alcohol, FF: furfural, DEF: 2-(diethoxymethyl)furan, EFE: ethyl furfuryl ether, MF: 2-methylfuran.

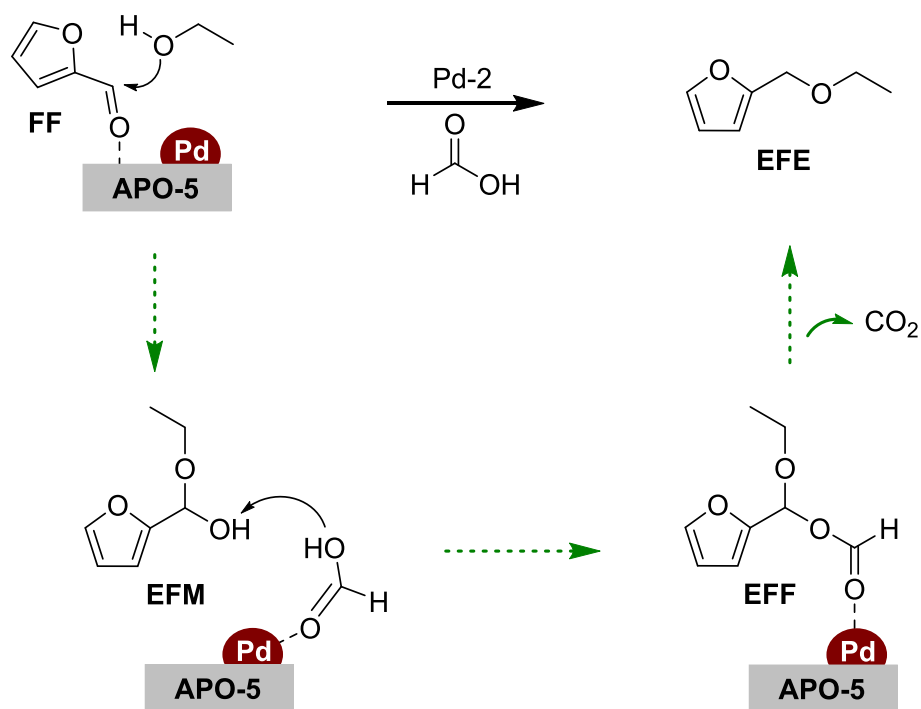
According to literature, there are two possible pathways for the reductive etherification of FF to furanic ethers (Scheme 5.1); Pathway **a** involving the formation of FAL by FF hydrogenation followed by acid-catalyzed etherification,^{11-13,32} and pathway **b** involving FF acetalization to ethoxy(furan-2-yl)methanol (EFM) followed by hydrogenolysis.^{8,9,33,34} To corroborate the pathway in the reaction with Pd-2, a time course was first completed (140°C, 24 h; Fig. 5.2b and Fig. S5.6). Here, full FF conversion was reached after 16 h with an excellent 99% EFE yield with minor amounts of FAL, DEF and MF being formed, suggesting that etherification and/or hydrogenolysis were fast reactions.



Scheme 5.1 Possible pathways for the reductive etherification of furfural to furanic ethers.^{8,9,11-13,31-33}

To examine if the reductive etherification occurred *via* pathway **a**, FAL conversion was investigated under the same reaction conditions where both FA and Pd-2, in principle, could catalyze the acid-catalyzed etherification.^{35,36} However, FAL

conversion was low using FA alone, Pd-2 alone or a combination of FA and Pd-2 with only minor or no formation of EFE (Fig. 5.2c). In contrast, hydrogenolysis product MF formed in the combined FA/Pd-2 system, suggesting that FA was a hydrogen donor for the hydrogenolysis and also provided the possibility for the reductive etherification to proceed by pathway **b**. Furthermore, only acetalization of FF to DEF occurred without the presence of FA (Fig. 5.2d) also demonstrating that FA was the source of hydrogen, and a suitable excess of FA improved both FF conversion and EFE formation resulting in >99% product selectivity.

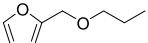
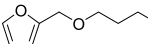
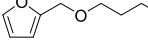
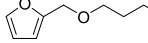
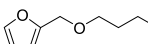
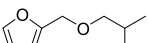
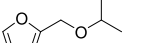
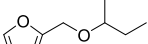


Scheme 5.2 Proposed reaction pathway for the reductive etherification of FF with FA and Pd-2.

Based on the investigations a reaction sequence can be proposed (Scheme 5.2), where FF and ethanol initially formed the EFM^{9,37} which esterified with FA to generate ethoxy(furan-2-yl)methyl formate (EFF) followed by subsequent decarboxylation leading to the release of CO₂ and formation of EFE.^{18,38} The acetalization was likely catalyzed by APO-5 as also reported in our previous

work^{19,20} and when reaction was done without Pd (Table S5.4). In line with this, a red shift of the C=O stretching band of FF (1668 to 1662 cm⁻¹) was found after adsorption of FF on Pd-2 (Fig. S5.7), indicative of strong adsorption of the aldehyde group^{39,40} further promoting the acetalization. On the other hand, the hydrogenolysis of EFM with FA was probably catalyzed by the Pd NPs,^{18,41} though both reactions were tightly connected and occurred very fast without detection of the intermediates.

Table 5.1 Catalytic performance of Pd-2 with FA in the reductive etherification of FF.^a

Entry	Alcohol	Product	Yield (%) ^b
1	1-propanol		96
2	1-butanol		95
3	1-pentanol		96
4	1-hexanol		92
5	1-octanol		19
6	2-methyl-1-propanol		91
7	2-propanol		80
8	2-butanol		50

^a Reaction conditions: FF (96 mg, 1 mmol), Pd-2 (50 mg), FA (0.38 mL, 10 mmol), alcohol (4.62 mL), 140°C, 24 h. ^b Quantified using ¹H NMR.

The reductive etherification of FF was also performed with the FA/Pd-2 system in alternative alcohols (Table 5.1; Fig. S5.8) under identical conditions as used for ethanol (i.e. 140°C, 24 h). For primary C₃-C₆ alcohols the corresponding furanic ether product yields were also excellent (>90%; entries 1-4 and 6), while 1-octanol resulted in significantly lower yield (19%; entry 5) which may be attributed to the much larger molecule size hampering diffusion and reactivity

in the pores of APO-5. Similarly, secondary C₃-C₄ alcohols gave moderate yields (50-80%; entries 7 and 8) probably due to steric hindrance with respect to the active sites. Importantly, these results also demonstrate that the alcohols were not the hydrogen donors during the reaction.

5.3 Summary

The work introduces an efficient, novel and practical approach to convert FF into furanic ethers using a catalyst system comprising Pd-loaded APO-5 with FA as a hydrogen donor. The reductive etherification of FF occurs *via* a reaction pathway involving initial acetalization and subsequent hydrogenolysis co-catalyzed by the APO-5 support and Pd NPs, thus avoiding the use of auxiliary pressurized hydrogen gas. A variety of furanic ethers were obtained with yields above 92% with Pd-2 catalyst in different primary alcohol solvents (C₂-C₆) demonstrating the general versatility of the approach. Hence, overall the work provides a very simple method to valorize FF into biofuels using a combination of Pd NPs, a suitable support (APO-5) and a hydrogen source like FA, which potentially could be recycled.

5.4 References

- [1] H. Li, Z. Fang, R. L. Smith, S. Yang, *Prog. Energ. Combust.* **2016**, 55, 98-194.
- [2] H. Li, A. Riisager, S. Saravanamurugan, A. Pandey, R. S. Sangwan, S. Yang, R. Luque, *ACS Catal.* **2017**, 8, 148-187.
- [3] T. A. Natsir, S. Shimazu, *Fuel Process. Technol.* **2020**, 200.
- [4] J. P. Lange, E. van der Heide, J. van Buijtenen, R. Price, *ChemSusChem* **2012**, 5, 150-166.
- [5] O. M. Ali, R. Mamat, C. K. M. Faizal, *J. Renew. Sustain. Energ.* **2013**, 5.
- [6] V. E. Tarabanko, M. Y. Chernyak, I. L. Simakova, K. L. Kaigorodov, Y. N. Bezborodov, N. F. Orlovskaya, *Russ. J. Appl. Chem.* **2016**, 88, 1778-1782.
- [7] R. Mariscal, P. Maireles-Torres, M. Ojeda, I. Sádaba, M. López Granados, *Energ. Environ. Sci.* **2016**, 9, 1144-1189.
- [8] Y. Wang, Q. Cui, Y. Guan, P. Wu, *Green Chem.* **2018**, 20, 2110-2117.

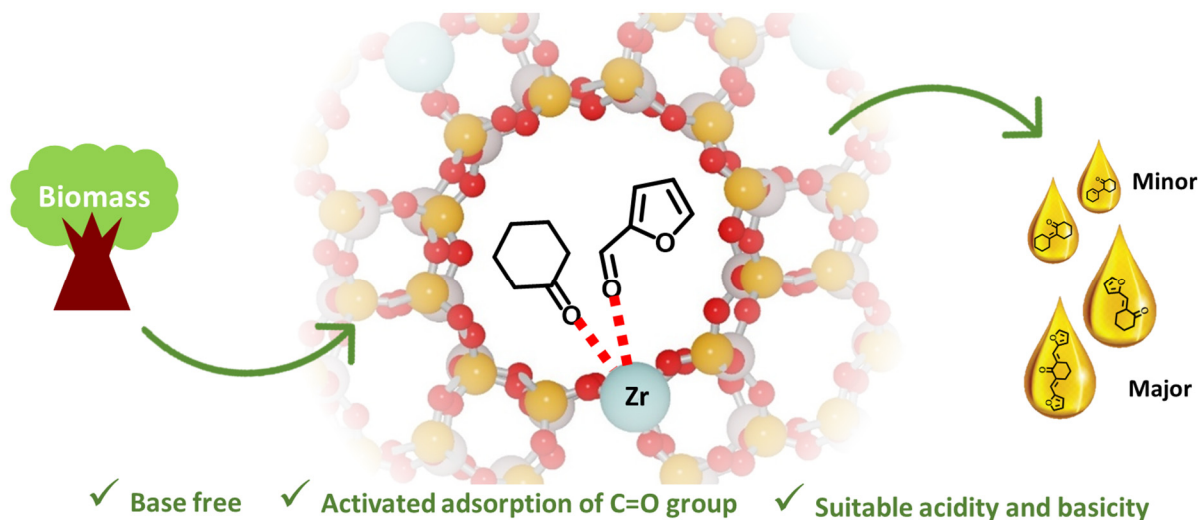
- [9] D. Wu, W. Y. Hernández, S. Zhang, E. I. Vovk, X. Zhou, Y. Yang, A. Y. Khodakov, V. V. Ordonsky, *ACS Catal.* **2019**, 9, 2940-2948.
- [10] W. Fang, A. Riisager, *Green Chem.* **2021**, 23, 670-688.
- [11] F. Zaccheria, F. Bossola, N. Scotti, C. Evangelisti, V. Dal Santo, N. Ravasio, *Catal. Sci. Technol.* **2020**, 10, 7502-7511.
- [12] M. M. Antunes, S. Lima, P. Neves, A. L. Magalhaes, E. Fazio, A. Fernandes, F. Neri, C. M. Silva, S. M. Rocha, M. F. R. Eiro, M. Pillinger, A. Urakawa, A. A. Valente, *J. Catal.* **2015**, 329, 522-537.
- [13] S. Shinde, C. Rode, *ChemSusChem* **2017**, 10, 4090-4101.
- [14] J. C. van der Waal, P. J. Kunkeler, K. Tan, H. van Bekkum, *J. Catal.* **1998**, 173, 74-83.
- [15] F. Shen, R. L. Smith Jr, J. Li, H. Guo, X. Zhang, X. Qi, *Green Chem.* **2021**, 23, 1536-1561.
- [16] M. J. Gilkey, B. Xu, *ACS Catal.* **2016**, 6, 1420-1436.
- [17] B. W. J. Chen, M. Mavrikakis, *ACS Catal.* **2020**, 10, 10812-10825.
- [18] T. Thananattathanachon, T. B. Rauchfuss, *Angew. Chem. Int. Ed.* **2010**, 49, 6616-6618.
- [19] W. Fang, A. Riisager, *Appl. Catal. B-Environ.* **2021**, 298, 120575.
- [20] W. Fang, A. Riisager, *ACS Sustain. Chem. Eng.* **2022**, 10, 1536-1543.
- [21] T. Munõz, A. M. Prakash, L. Kevan, K. J. Balkus, *J. Phys. Chem. B* **1998**, 102, 1379-1386.
- [22] S. Bhogeswararao, D. Srinivas, *J. Catal.* **2015**, 327, 65-77.
- [23] W. Zheng, S. You, Y. Yao, L. Jin, Y. Liu, *Appl. Catal. B-Environ.* **2021**, 298, 120593.
- [24] H. Chen, Y. Dai, X. Jia, H. Yu, Y. Yang, *Green Chem.* **2016**, 18, 3048-3056.
- [25] J. Zhu, Z. Kónya, V. F. Puentes, I. Kiricsi, C. X. Miao, J. W. Ager, A. P. Alivisatos, G. A. Somorjai, *Langmuir* **2003**, 19, 4396-4401.
- [26] D. Zhang, C. Jin, H. Tian, Y. Xiong, H. Zhang, P. Qiao, J. Fan, Z. Zhang, Z. Y. Li, J. Li, *Nanoscale* **2017**, 9, 6327-6333.
- [27] Y. Chai, S. Liu, Z.-J. Zhao, J. Gong, W. Dai, G. Wu, N. Guan, L. Li, *ACS Catal.* **2018**, 8, 8578-8589.
- [28] H. Conrad, G. Ertl, E. E. Latta, *Surf. Sci.* **1974**, 41, 435-446.
- [29] J. L. V. Antonio de Lucas, Paula Sánchez, Fernando Dorado, and María Jesús Ramos, *Ind. Eng. Chem. Res.* **2004**, 43, 8217-8225.
- [30] A. K. Aboul-Gheit, A. E. Awadallah, S. El-Kossy, A.-L. H. Mahmoud, *J. Nat. Gas Chem.* **2008**, 17, 337-343.
- [31] L. Wang, F. Wang, J. Wang, *Catal. Commun.* **2015**, 65, 41-45.
- [32] M. M. Antunes, S. Lima, P. Neves, A. L. Magalhaes, E. Fazio, F. Neri, M. T. Pereira, A. F. Silva, C. M. Silva, S. M. Rocha, M. Pillinger, A. Urakawa, A. A. Valente, *Appl. Catal. B: Environ.* **2016**, 182, 485-503.
- [33] R. Pizzi, R. J. van Putten, H. Brust, S. Perathoner, G. Centi, J. C. van der Waal, *Catalysts* **2015**, 5, 2244-2257.

- [34] Y. S. Long, Y. Wang, H. H. Wu, T. Xue, P. Wu, Y. J. Guan, *RSC Adv.* **2019**, 9, 25345-25350.
- [35] H. Nguyen, N. Xiao, S. Daniels, N. Marcella, J. Timoshenko, A. Frenkel, D. G. Vlachos, *ACS Catal.* **2017**, 7, 7363-7370.
- [36] Z. Wang, Q. Chen, *Green Chem.* **2016**, 18, 5884-5889.
- [37] M. Lautens, S. Ma, A. Yee, *Tetrahedron Lett.* **1995**, 36, 4235-4236.
- [38] S. De, S. Dutta, B. Saha, *ChemSusChem* **2012**, 5, 1826-1833.
- [39] M. Ma, P. Hou, J. Cao, H. Liu, X. Yan, X. Xu, H. Yue, G. Tian, S. Feng, *Green Chem.* **2019**, 21, 5969-5979.
- [40] Y. Yang, L. Chen, Y. Chen, W. Liu, H. Feng, B. Wang, X. Zhang, M. Wei, *Green Chem.* **2019**, 21, 5352-5362.
- [41] J. Mitra, X. Zhou, T. Rauchfuss, *Green Chem.* **2015**, 17, 307-313.

6 On the role of Zr to facilitate the synthesis of diesel and jet fuel range intermediates from biomass-derived carbonyl compounds over aluminum phosphate

W. Fang, S. Liu, L. Schill, M. Kubus, T. Bligaard, A. Riisager*, *Applied Catalysis B: Environmental*, **2023**, 320, 121936.

Reproduced from (W. Fang, S. Liu, L. Schill, M. Kubus, T. Bligaard, A. Riisager*, *Applied Catalysis B: Environmental*, **2023**, 320, 121936.). Copyright [2023] Elsevier. In this chapter, the manuscript was directly used with a minor modification.

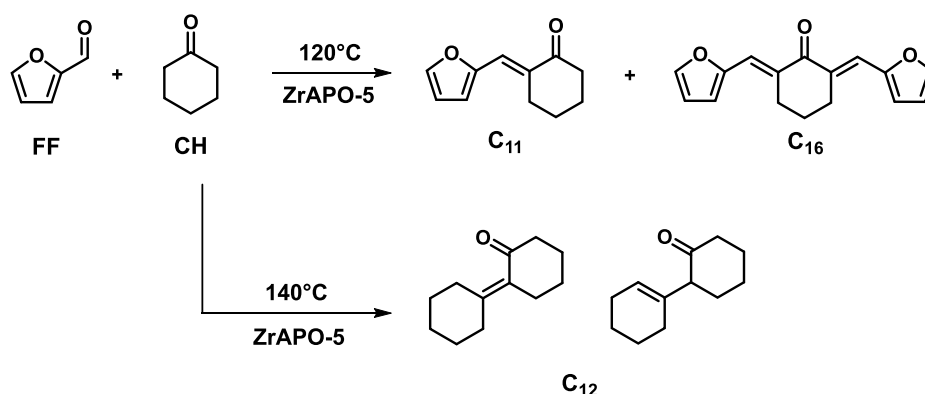


Heterogeneous zeolite/zeotype catalysts are attractive for converting renewable biomass-derived chemicals into transportation fuels by aldol condensation reactions, which provide a simple strategy to improve carbon numbers. Herein, ZrAPO-5 were applied for efficient syntheses of diesel and jet fuel range C₁₁, C₁₂ and C₁₆ intermediates from biomass-derived FF and CH. Incorporation of Zr in the APO-5 framework facilitated the adsorption of the C=O groups of FF and CH and created more and stronger acidic and basic sites, which co-catalyzed the aldol condensation and facilitated the product yields. ZrAPO-5 (Zr/Al = 0.20) yielded up to 79.3% single aldol condensation product C₁₁ or 80.7% double aldol condensation product C₁₆ in the cross-aldol condensation of FF and CH under appropriate reaction conditions, and also realized 83.3% C₁₂ yield in the self-aldol condensation of CH. In addition, the catalytic system displayed good to excellent yields of other value-added chemicals in aldol condensations of alternative carbonyl compounds.

6.1 Introduction

Catalytic conversion of renewable biomass to chemicals and potential fuels is a highly relevant topic for dealing with global challenges such as environmental preservation and the future energy demand.¹ Especially the synthesis of diesel and jet fuel range hydrocarbons from lignocellulose-derived platform compounds has drawn tremendous attention,^{2,3} and one of the frequently adopted strategies to increase carbon numbers of biomass-derivatives for producing jet fuel (C₉₋₁₄) and diesel (C₁₂₋₂₀) is the aldol condensation of carbonyl compounds.⁴ The reaction may occur between two ketones, two aldehydes or an aldehyde and a ketone.

FF and CH are platform chemicals with carbonyl groups which may be derived from xylose and aromatic ethers^{5,6} though CH synthesized from the biomass-derived compounds is not widely used. The cross-aldol condensation between FF and CH can generate (*E*)-2-(furan-2-ylmethylene)cyclohexan-1-one (labelled C₁₁) and (2*E*,6*E*)-2,6-bis(furan-2-ylmethylene)cyclohexan-1-one (labelled C₁₆).⁷ The self-aldol condensation of CH forms two stereoisomers, [1,1'-bi(cyclohexylidene)]-2-one and [1,1'-bi(cyclohexan)]-1'-en-2-one (together labelled C₁₂) (Scheme 1). All of the C₁₁, C₁₂ and C₁₆ compounds are fuel precursors with high volumetric energy density and high pour point.^{7,8}



Scheme 6.1 Strategy for the synthesis of C₁₁, C₁₂ and C₁₆ fuel precursors with FF and CH, which can be derived from biomass.

In order to generate C-C bonds with carbonyl compounds, bases are typically exploited for the abstraction of α -protons to form the enolate intermediate required for the bond formation.⁹ Accordingly, homogeneous basic catalysts (e.g., NaOH and Ca(OH)₂)¹⁰⁻¹² and heterogeneous basic catalysts (e.g., earth alkali oxides, MgZr or MgAl mixed oxides and hydrotalcite)¹³⁻¹⁶ have been widely used for the aldol condensation between FF and ketones. Although homogeneous basic catalysts show excellent activity and high selectivity for the desired products, several drawbacks remain during the synthesis, such as

catalyst/product separation and equipment corrosion.⁹ Heterogeneous basic catalysts could circumvent these issues and are thus preferred, however, they are easily deactivated in the presence of furoic acid which can form as byproduct by base-catalyzed Cannizzaro reaction of FF.^{7,17,18} Moreover, retro-aldolization is also prone to take place in systems with strong base,⁴ whereas medium-strength base is an effective active site for the aldol condensation.^{14,19} Notably, acidic sites are found most active for the consecutive dehydration of the aldol product to form C=C bonds.²⁰

Zeolite catalysts with unique shape selectivity as well as tuneable acidity and basicity have been introduced for FF aldol condensation.²¹ For example, Kikhtyanin et al. applied zeolites with different framework structures (MFI, BEA, FAU and MOR) for the aldol condensation of FF with acetone at 100°C, however, FF conversions were low (<50%) in all reactions.²² Sn-doped MFI and Beta yielded much better performance in the same reaction at 160°C with the smaller-pore Sn-MFI selectively producing C₈ (61% yield) and the larger-pore Sn-Beta generating both C₈ (40% yield) and C₁₃ (11% yield) with high reaction rate.²³ Hence, these studies suggest that metal-doped zeolites may offer both suitable acidity for aldol condensation and appropriate pore size for unique shape selectivity. Amorphous aluminophosphates have also been used in the aldol condensation,²⁴ but their potential application as metal-doped zeolite/zeotype catalysts remains elusive for such condensation and the relationship between zeotype structure and performance is poorly understood.

In this study, large-pore (7.3 Å) ZrAPO-5s with different Zr loadings have been successfully synthesized using a simple hydrothermal method and applied for the cross-aldol condensation of FF (5.6 Å)²⁵ and CH (5.7 Å)²⁵ and self-aldol condensation of CH. High C₁₁ yield (79.3%) and C₁₆ yield (80.7%) were obtained

for the cross-aldol condensation of FF and CH at 120°C, whereas 83.3% C₁₂ yield resulted from the self-aldol condensation of CH at 140°C. A combination of structural and spectroscopic characterization together with elemental analysis demonstrated the successful replacement of P by Zr atoms in the framework sites, providing suitable acidity and basicity to promote the aldol condensations. Adsorption experiments and DFT calculations unveiled that the introduction of Zr also activated the adsorption of C=O bonds of the substrates. Additionally, the best performing catalyst, i.e. ZrAPO(0.20), was demonstrated to be selective for the conversion of other aldehydes and ketones.

6.2 Results and discussion

6.2.1 Structure of catalysts

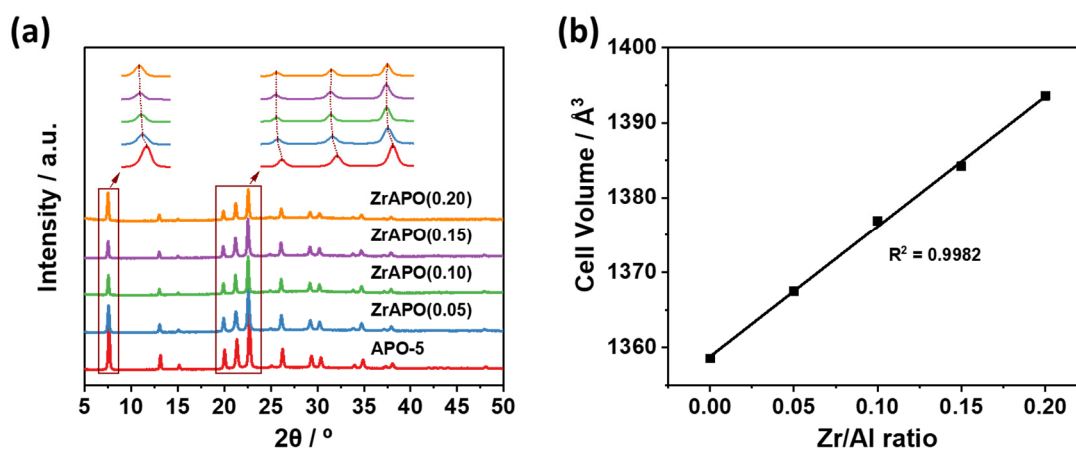


Fig. 6.1 (a) XRD patterns of APO-5 and ZrAPO-5 catalysts, and (b) the relationship between Zr/Al ratio and cell volume in the catalysts.

XRD patterns of the synthesized APO-5 and ZrAPO-5s (Fig. 6.1a) confirmed that all materials possessed a well-crystalline AFI structure without impurities such as, ZrO₂.²⁶⁻²⁸ For the ZrAPO-5s were all distinctive peaks slightly shifted (several high intensity peaks shown in zoom), and when the peaks were used to calculate the unit cell volumes a positive relationship with Zr/Al ratios were found (Table

S6.1 and Fig. 6.1b). The larger atom radius of Zr (0.59 Å) compared to that of Al (0.39 Å) and P (0.17 Å) expanded the unit cell volumes,²⁹ as also seen by comparing the calculated optimized structures of APO-5 with or without Zr doping (Figs. S6.3 and S6.4). Furthermore, nitrogen physisorption confirmed both APO-5 and ZrAPO-5s to be microporous with type I isotherms (Fig. S6.5), and the microporous volume was reduced while the mesoporous volume was enhanced with increased Zr loading. This also resulted in variations of surface area (Table 6.1), and indicated that some intercrystalline pores may have formed at high Zr loading ($n > 0.15$).

Table 6.1 Physicochemical properties of the APO-5 and ZrAPO-5s catalysts.

Sample	Zr/Al ratio ^a	Zr/P ratio ^a	Al/P ratio ^a	S _{total} (m ² /g) ^b	V _{micro} (cm ³ /g) ^b	V _{meso} (cm ³ /g) ^b	Acidity (mmol/g) ^c	Basicity (mmol/g) ^d
APO-5	-	-	0.95	197	0.07	0.11	0.0012	0.04
ZrAPO(0.05)	0.04	0.04	0.93	184	0.06	0.13	0.24	0.17
ZrAPO(0.10)	0.07	0.08	1.10	223	0.07	0.15	0.31	0.21
ZrAPO(0.15)	0.13	0.16	1.17	224	0.05	0.21	0.42	0.28
ZrAPO(0.20)	0.16	0.21	1.36	203	0.03	0.29	0.52	0.34

^a Determined by XRF. ^b N₂ physisorption. ^c Determined by NH₃-TPD. ^d Determined by CO₂-TPD.

SEM results showed that the morphology of the materials changed from hexagon prism-like shape with 3-4 µm particle size (APO-5) to around 18 µm spherical agglomerates made of rodlike shape particle for ZrAPO(0.05) (Fig. 6.2a-c), which was likely caused by differences in pH of the gel³⁰ during synthesis induced by the varied zirconium acetate concentrations. EDX mapping further suggested the homogenous distribution of elements in the ZrAPO-5 samples (Fig. 6.2d-h).

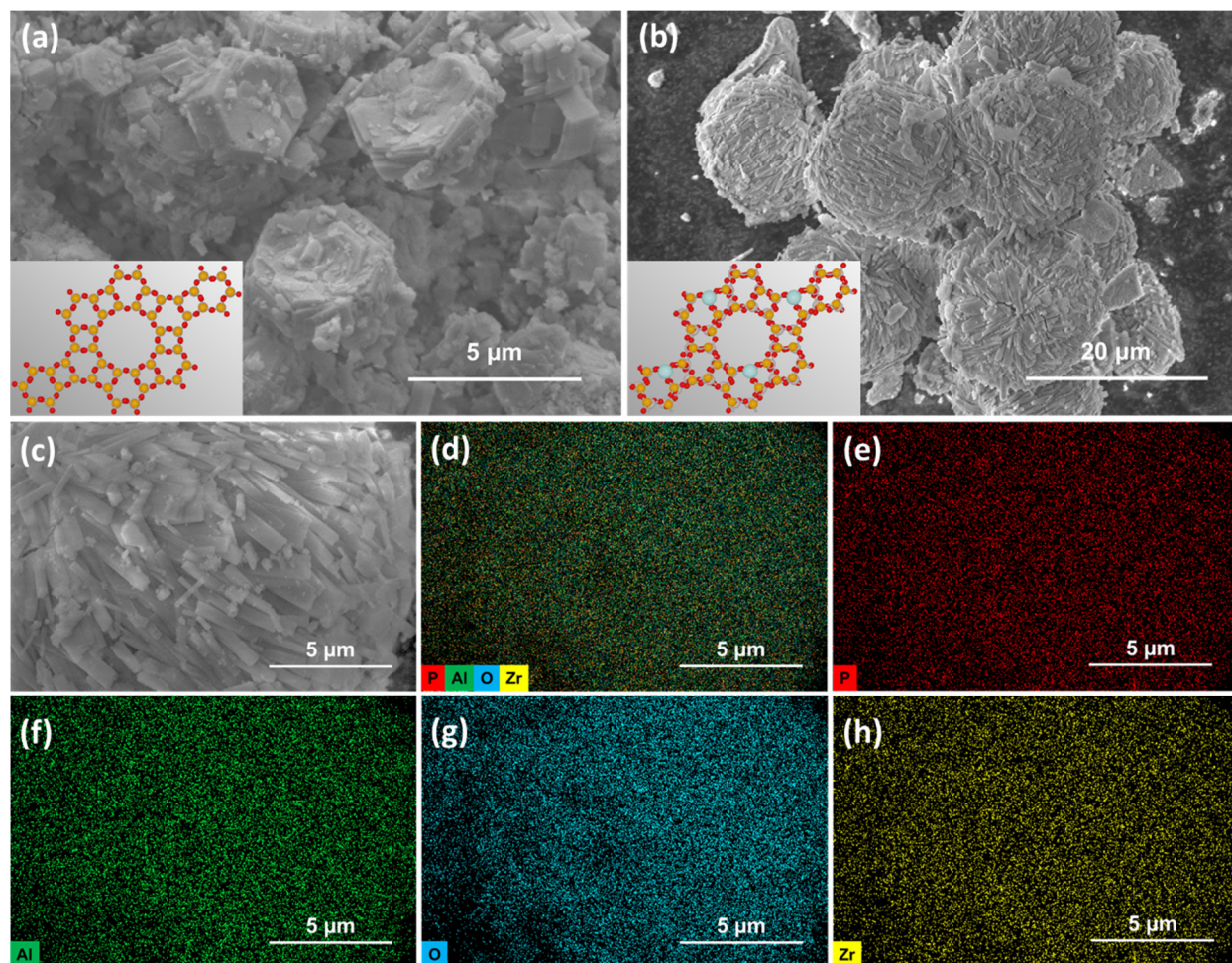


Fig. 6.2 SEM images of (a) APO-5, (b) and (c) ZrAPO(0.05) (inset: Computational models; P atom: yellow; Al atom: gray; O atom: red; Zr atom: light blue). (d)-(h) EDX mapping analysis on ZrAPO(0.05).

Characterization by XPS, FT-IR, solid-state MAS NMR, and XRF were used to understand the state of Zr in the ZrAPO-5s. The reference ZrO_2 revealed by XPS (Fig. 6.3a) two distinct peaks at 181.0 and 183.4 eV assigned to $\text{Zr } 3d_{5/2}$ and $\text{Zr } 3d_{3/2}$, respectively. For the ZrAPO-5s, these peaks were shifted to higher binding energy (182.5 and 184.9 eV) implying the incorporation of tetrahedrally coordinated Zr atoms into the framework.^{31,32} Additionally, in FT-IR spectra of the catalysts a shift of the Al-O-P band from 1108 cm^{-1} (APO-5) to 1074 cm^{-1} (ZrAPO(0.20)) (Fig. 6.3b) indicated the replacement of Al or P for Zr.³³

Furthermore, a new peak at around 3668 cm^{-1} assigned to terminal P-OH groups³⁴⁻³⁶ appeared after the incorporation of Zr, which was also in line with results obtained by ^{27}Al and ^{31}P solid-state MAS NMR spectroscopy (Fig. S6.6), where a broad peak belonging to P-OH defect groups^{34,37} was formed after the introduction of Zr with a positive area relationship to the metal content. Moreover, the Al/P molar ratio increased with increasing Zr loading (Table 6.1) indicating loss of P atoms during the substitution probably due to the replacement of P by Zr atoms in framework sites. This result is consistent with previous findings that P can be substituted by elements with valence from +4 to +5, while aluminium atoms can be replaced with atoms of valence +1 to +3.³⁸ To sum up, Zr atoms were successfully substituted in the framework of the ZrAPO-5 catalysts presumable by replacing P atoms resulting in the formation of terminal P-OH groups (Scheme S6.1).

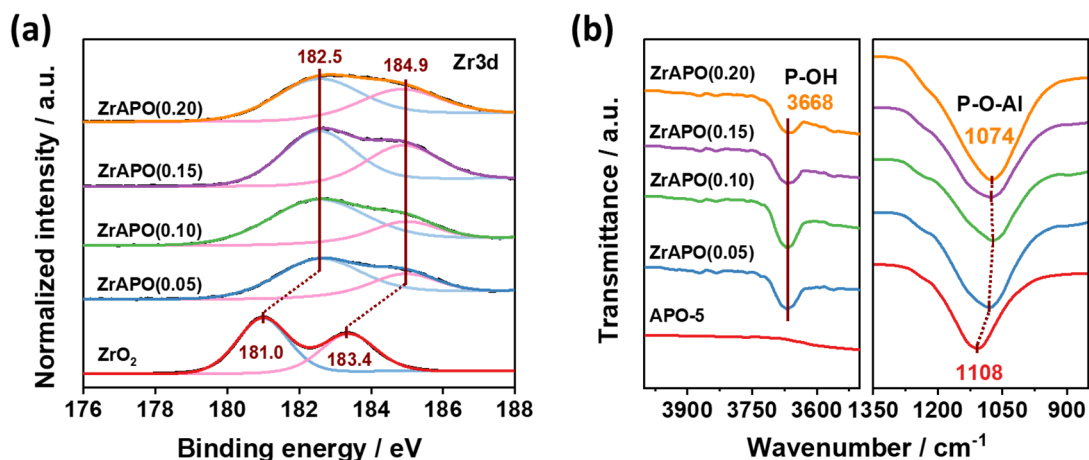


Fig. 6.3 (a) Zr 3d XPS spectra of ZrO₂ and ZrAPO-5 catalysts. (b) FT-IR spectra of APO-5 and ZrAPO-5 catalysts.

6.2.2 Cross-aldol condensation of furfural and cyclohexanone

Both APO-5 and ZrAPO-5s were catalytically active in the cross-aldol condensation of FF with CH (Fig. 6.4a) towards two main products; a first adduct

(C₁₁) and a second adduct (C₁₆) obtained from the consecutive reaction of C₁₁ and FF (Scheme 6.1). No intermediate C₁₁ or C₁₆ alcohols were observed, indicating fast dehydration of these alcohols to α,β -unsaturated ketone products. Compared to APO-5 the ZrAPO-5s exhibited better catalytic performance resulting in both higher FF conversions and C₁₁/C₁₆ selectivities, and ZrAPO(0.20) displayed the highest catalytic activity which was probably related to its suitable acidity and basicity (*vide infra*).³⁹⁻⁴¹ Moreover, increased CH concentrations promoted the aldol condensation between FF and CH, while the aldol condensation of FF and C₁₁ was suppressed leading to high C₁₁ selectivity and low C₁₆ selectivity (Fig. 6.4b). Thus, an optimal CH:FF ratio of 1:10 in ZrAPO(0.20) catalyst resulted in 79.3% C₁₁ yield and 16.4% C₁₆ yield with 99.2% FF conversion after 3 h of reaction. Notably, with FF:CH ratios lower than 1:2 a yellow solid product formed during reaction, which might be precipitated C₁₁ and C₁₆ as also reported in similar studies.^{7,42} The formation of these solid products stopped the interaction between catalyst and substrates further disrupting the reaction.

The effect of solvents was further explored in the cross-aldol condensation reaction with the ZrAPO(0.20) catalyst. As shown in Fig. 6.4c, all the reactions with solvents led to lower FF conversion possibly due to the lower substrate concentrations obtained after dilution. Especially, water resulted in significant lower product selectivity as well as large carbon loss compared to the neat reaction system, which might be due to poor FF/product solubility⁴² or side reactions such as, polymerization and decomposition.⁴³ Noticeably, the use of 1,4-dioxane and toluene solvent increased the C₁₆ selectivity and the lower CH concentration facilitated the consecutive condensation between FF and C₁₁ giving rise to 80.7% C₁₆ yield in toluene.

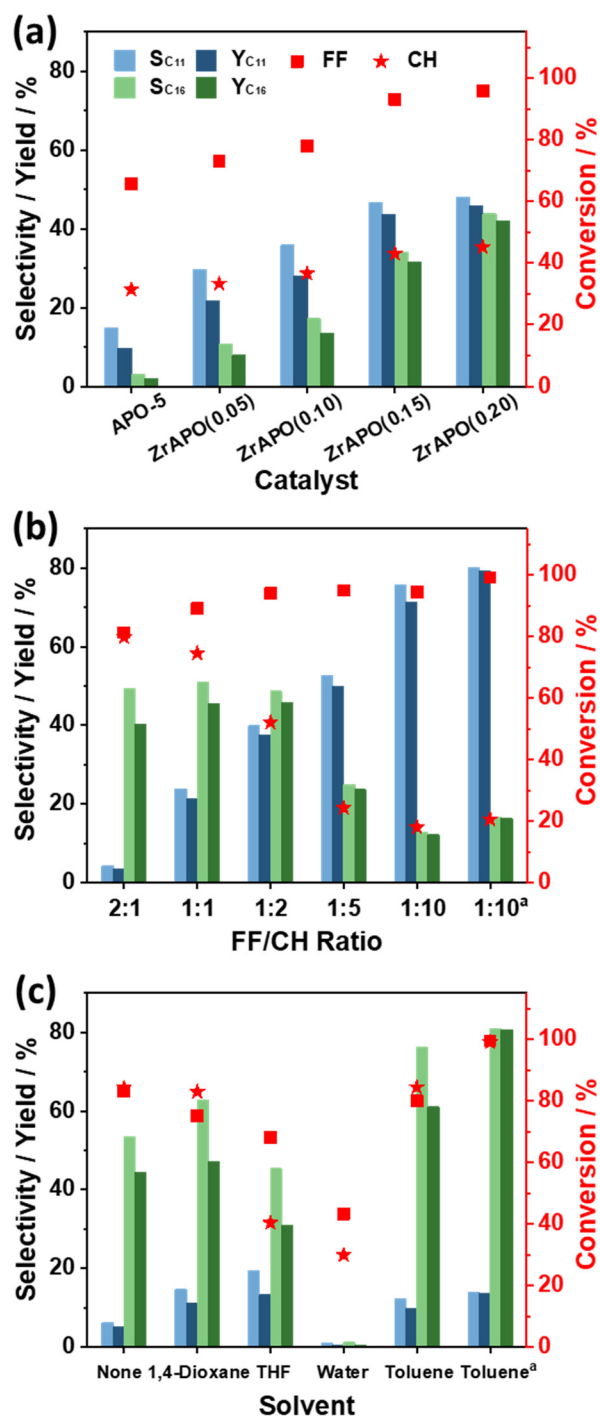


Fig. 6.4 Catalytic results from cross-aldol condensation of FF and CH using (a) different catalysts (reaction conditions: FF (166 μ L, 2 mmol), catalyst (50 mg), CH (515 μ L, 5 mmol), 120°C, 2 h), (b) different FF to CH ratios with ZrAPO(0.20) catalyst (reaction conditions: FF (166 μ L, 2 mmol), ZrAPO(0.20) (50 mg), CH (1-20 mmol), 120°C, 2 h or ^a3 h), and (c) different solvents with ZrAPO(0.20) catalyst (reaction conditions: FF (166 μ L, 2 mmol), ZrAPO(0.20) (50 mg), CH (103 μ L, 1 mmol), solvent (1 mL) 120°C, 4 h or ^a12 h).

6.2.3 Catalyst recycling

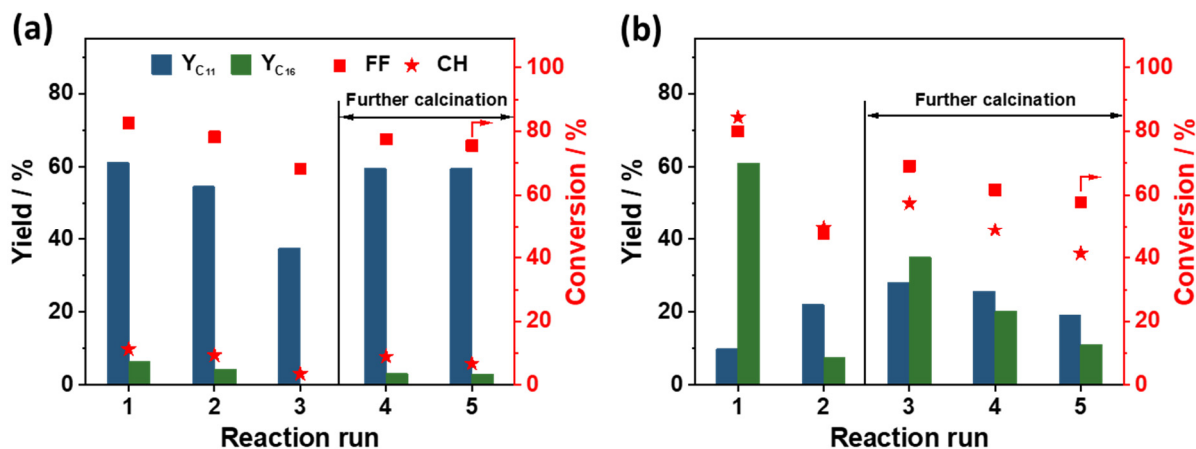


Fig. 6.5 Recyclability of ZrAPO(0.20) catalyst in the cross-aldol condensation reaction of FF with CH (reaction conditions: (a) FF (166 μ L, 2 mmol), ZrAPO(0.20) (50 mg), CH (2060 μ L, 20 mmol), 120°C, 1 h; (b) FF (166 μ L, 2 mmol), ZrAPO(0.20) (50 mg), CH (103 μ L, 1 mmol), toluene (1 mL), 120°C, 4 h).

In recycling experiments, the ZrAPO(0.20) catalyst exhibited deactivation in the neat reaction system after the first three reaction runs with only intermediate acetone/methanol washing, resulting in a decline in yield of C_{11} from 61.2 to 37.4% (Fig. 6.5a). However, the original catalytic performance restored completely in successive catalytic runs after calcination. Oppositely, severe catalyst deactivation prevailed in the toluene system after washing as well as further calcination resulting in significantly decreased C_{16} yield, while more C_{11} product apparently formed (Fig. 6.5b). TG analysis of the used ZrAPO(0.20) catalyst in the two reaction systems showed a mass loss (6.8 and 15.2 wt.%, respectively) with broad peaks around 326°C and 497°C (Fig. S6.7). Moreover, the FT-IR spectrum of the used catalyst revealed bands around 1621 cm^{-1} (C=C stretching vibration) as well as 2940 and 1461 cm^{-1} (C-H vibrations) (Fig. S6.8) along with reduced surface area and pore volume (Table S6.2). In both systems, the catalyst framework structure also remained the same after several

calcinations as shown by XRD analysis (Fig. S6.9). Combined these results suggest that adsorption of organic species on active catalyst sites partly induced deactivation and pore blocking in both systems, which could be removed by calcination (550°C). For the toluene system, additional formation of polymerization products of FF might account for more severe deactivation.

6.2.4 Substrate scope

The ZrAPO(0.20) catalyst also showed very promising catalytic performance for cross-aldol condensation of other carbonyl compounds besides FF and CH (Fig. 6.6; see Table S6.3 for reaction conditions). For example, 77.6% yield of **1** was obtained by the condensation of MFA and CH, which was similar to the C₁₁ yield obtained with FF and CH, and 93.4% yield of **2** obtained from reaction of FCA with CH at high CH concentration. Also aromatic aldehydes such as, *m*-tolualdehyde, *p*-tolualdehyde, and *o*-tolualdehyde gave good yields (>70%) with CH of the corresponding products **3**, **4**, **5**, and **6** after extended reaction time (24 h). The yield of **7** obtained with the alternative cyclic ketone CP and FF was also similar to the C₁₁ yield with FF and CH, while the corresponding yield of **8** with cycloheptanone was lower probably due to the larger ring size of cycloheptanone limited the reaction.¹⁴ Open-chain aliphatic ketones provided lower yields than cyclic ketones despite prolonged reaction time as also reported in other studies,⁴⁴ and with FF and acetone the **9** was preferentially formed with the pore size of ZrAPO(0.20) in agreement with a previous study using Sn-Beta catalyst.²³ The lower product yields of **10**, **11** and **12** (33-63%) obtained with 3-pentanone, 4-heptanone and 5-nonanone, respectively, was probably a result of the larger steric effects caused by the methyl, ethyl and propyl group in the α -carbon position⁴ as well as lower reactivity of the α -carbon atom in the longer carbon chain.⁴⁵

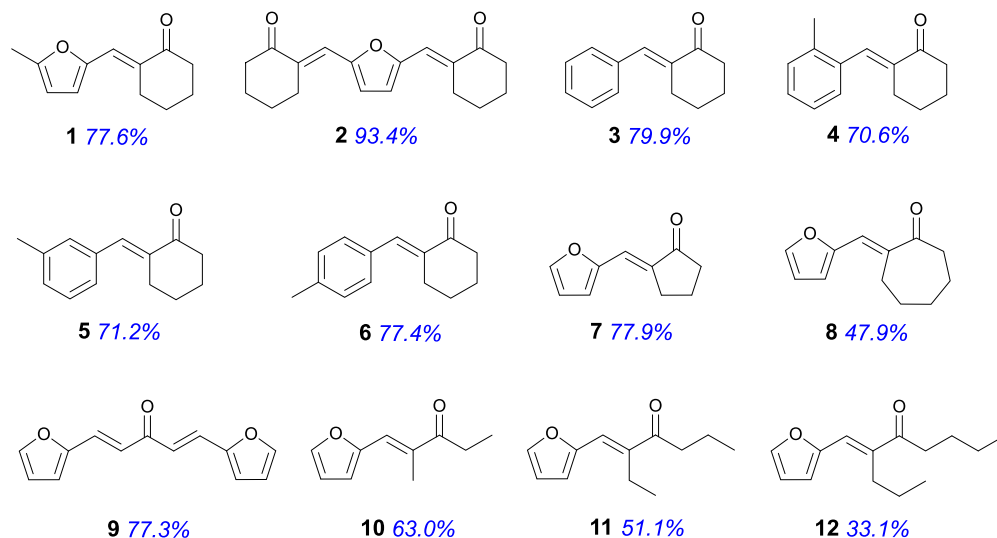


Fig. 6.6 Products formed by cross-aldol condensation of various carbonyl compounds using ZrAPO(0.20) catalyst (see Table S6.3 for reaction conditions).

6.2.5 Self-aldol condensation of cyclohexanone

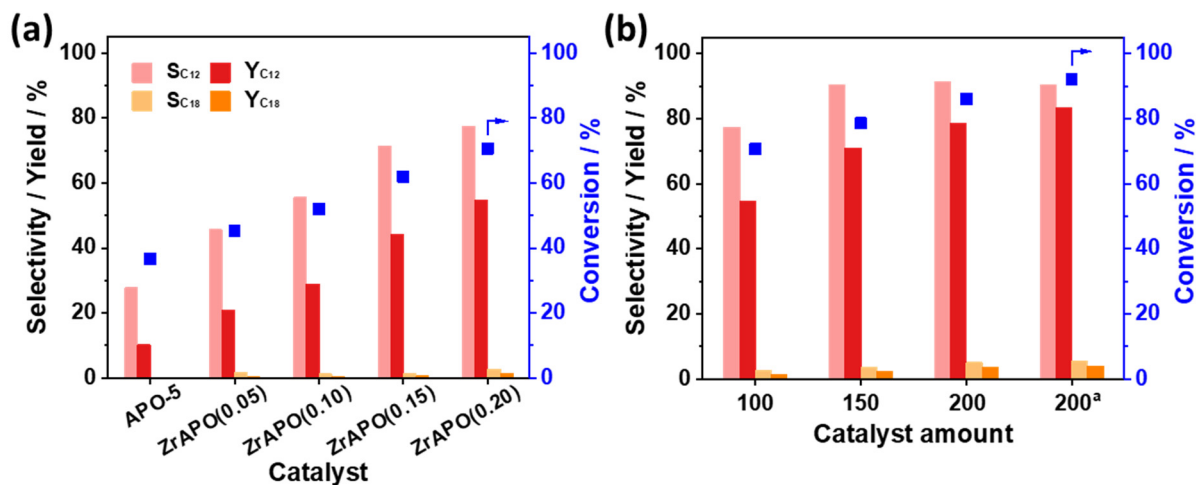


Fig. 6.7 Catalytic results from CH self-condensation with (a) different catalysts (reaction conditions: CH (515 μ L, 5 mmol), catalyst (100 mg), 140°C, 48 h) and (b) different amounts of ZrAPO(0.20) catalyst (reaction conditions: CH (103 μ L, 5 mmol), 140°C, 48 h or ^a72 h).

The APO-5 and ZrAPO-5s catalysts were also applied for the self-condensation of CH at 140°C with larger amount of catalyst than used for the cross-condensation of FF and CH (Fig. 6.7). Two products formed in the systems; a first adduct (C₁₂, Scheme 6.1) and a minor amount of a second adduct (C₁₈)

obtained from the consecutive reaction of C_{12} and CH. As for the cross-aldol condensation of FF and CH, all the ZrAPO-5s catalysts exhibited better catalytic performance than APO-5 and also here ZrAPO(0.20) provided the best catalyst performance, which after reaction optimization (increased catalyst amount and longer reaction time) resulted in a C_{12} yield of 83.3% with a 92.2% CH conversion.

6.2.6 The role of Zr in the aldol condensation

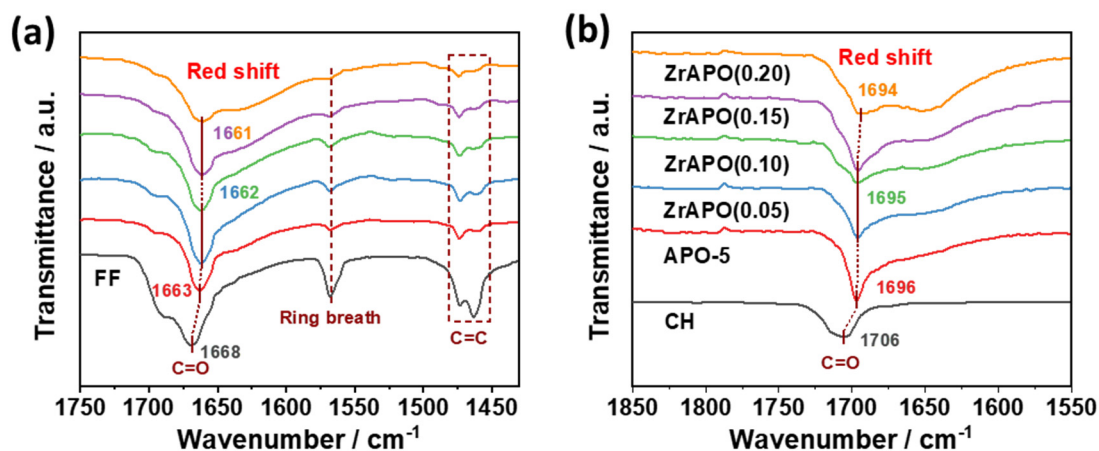


Fig. 6.8 FT-IR spectra of APO-5 and ZrAPO-5s catalysts with pre-adsorbed (a) FF and (b) CH.

FT-IR spectra of the APO-5 and ZrAPO-5s catalysts with pre-adsorbed FF or CH were recorded to get insight into the origin of the different catalytic performances. Surface adsorbed FF had a strong intensity of the $\nu(C=O)$ stretching band, while the furan ring breath and $\nu(C=C)$ stretching bands were much less intense (Fig. 6.8a), suggesting that the carbonyl group was the main adsorptive functional group of FF.^{46,47} Moreover, an obvious red-shift of the $\nu(C=O)$ band from 1668 to 1663 cm^{-1} on APO-5 and to 1661 cm^{-1} on ZrAPO(0.20) was observed for the surface adsorbed FF, implying that the C=O group of FF was activated by the adsorption.^{46,48} For the CH adsorption a red-shift of $\nu(C=O)$ also suggested that CH interacted with the catalysts with the C=O functional group (Fig. 6.8b),⁴⁹ thus

confirming that adsorption of the C=O group of both FF and CH on the catalysts promoted the aldol condensation.

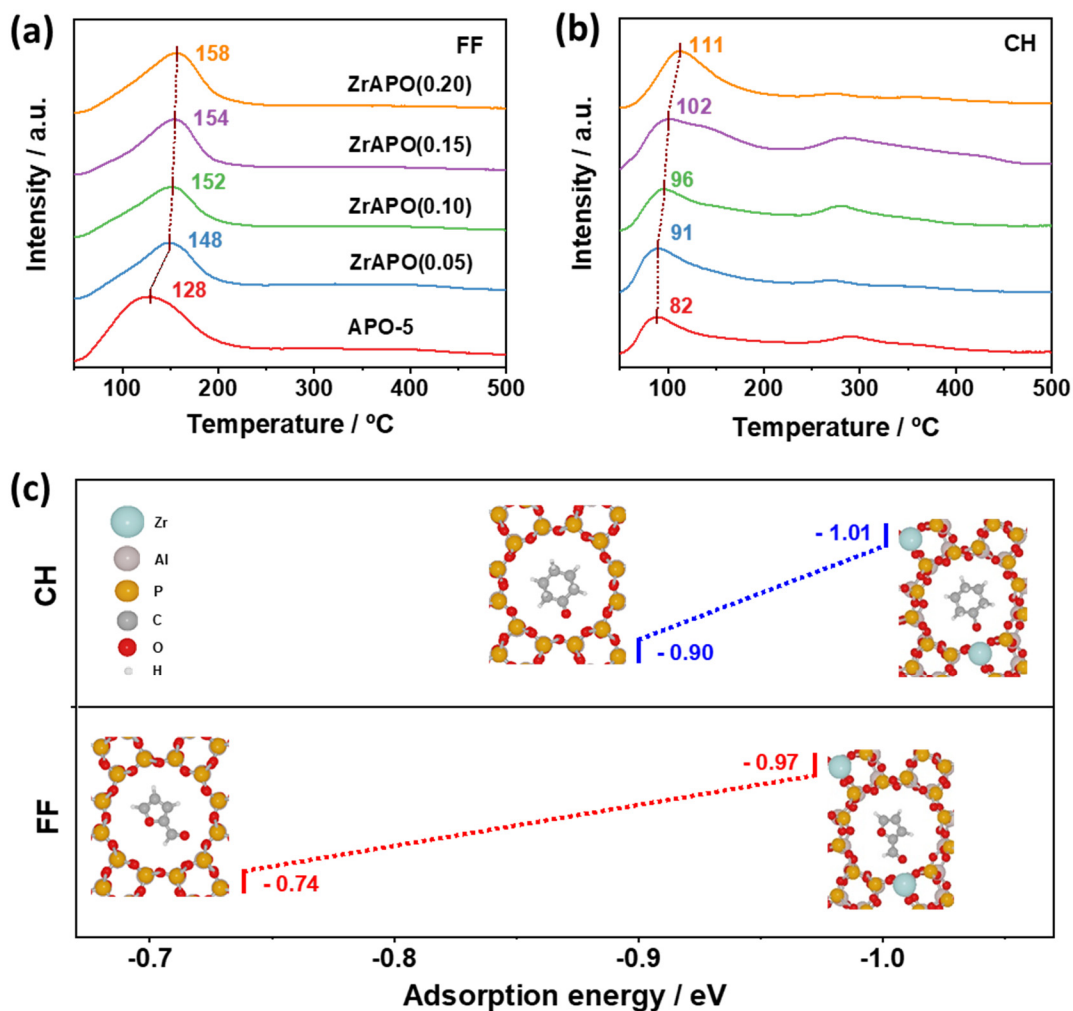


Fig. 6.9 TPD profiles of APO-5 and ZrAPO-5 catalysts with (a) FF and (b) CH. (c) The calculated adsorption energies (eV) of FF and CH on APO-5 (left) and ZrAPO-5 (right) models. Color codes of the different atoms are inserted in the upper panel.

TPD experiments and DFT calculations were additionally carried out to evaluate the difference in adsorption strength of FF and CH on the APO-5 and ZrAPO-5s catalysts. FF-TPD and CH-TPD profiles (Figs. 6.9a and 6.9b) showed that the ZrAPO-5s had higher desorption temperature of both FF and CH than APO-5, suggesting that the presence of Zr facilitated the adsorption of FF and CH on the

catalysts.⁵⁰ Meanwhile, the optimized FF and CH adsorption configurations and adsorption energies calculated for APO-5 and ZrAPO-5 with FF and CH in the large 12-membered rings are depicted in Fig. 6.9c. For APO-5, both CH and FF had only relatively weak adsorptive interaction with the surface. In contrast, the molecules interacted stronger with the surface of ZrAPO-5 with activated adsorption *via* the terminal O atom in C=O group resulting in larger adsorption strengths. Notably, FF displayed a twice as large adsorption energy enhancement (0.23 eV) compared to CH (0.11 eV) after Zr doping, implying that the Zr incorporation preferentially promoted adsorption of FF and thus cross-aldol condensation reaction of FF and CH rather than self-aldol condensation of CH, as also observed experimentally in Fig. 6.4a.

6.2.7 The role of acidity/basicity in the aldol condensation

Previous studies have shown that aldol condensations can be base- or acid-base co-catalyzed.³⁹⁻⁴¹ Herein, the FF consumption rate and C₁₁ and C₁₆ formation rates had positive relationships with both acidity and basicity of catalysts (Fig. 6.10a). Poisoning reactions with pyridine and benzoic acid led to decreased yield of both C₁₁ and C₁₆ products, implying that the cross-aldol condensation of FF and CH was catalyzed both by acid and base with ZrAPO(0.20) catalyst (Fig. 6.10b).

NH₃-TPD (Fig. 6.10c) revealed that APO-5 possessed only a low amount of weak acidic sites (small peak at 164°C; Table S6.4) consistent with the assumption that APO-5 is neutral. In contrast, the ZrAPO-5 catalysts displayed much higher acid density and acid strength (larger peaks at 220-250°C and 320-380°C; Table S6.4), possibly due to terminal P-OH and bridged hydroxyl groups, i.e., Zr-OH-Al.^{35,36} Likewise, CO₂-TPD results (Fig. 6.10d, Table S6.5) confirmed that the

basicity and strength of the basic catalyst sites also increased, which might origin from the negatively charged lattice oxygen atoms (Zr-O-Al) after Zr incorporation.^{51,52} Hence, the superior aldol condensation performance facilitated by the Zr incorporation was possibly due to the enhanced adsorption strength of substrates, and a combination of basic sites promoting α -proton abstraction of CH to form a carbanion intermediate followed by reaction with the carbonyl group of the adsorbed FF,¹³ and the presence of acidic sites promoting the subsequent dehydration to form the products (Scheme 6.2).⁴

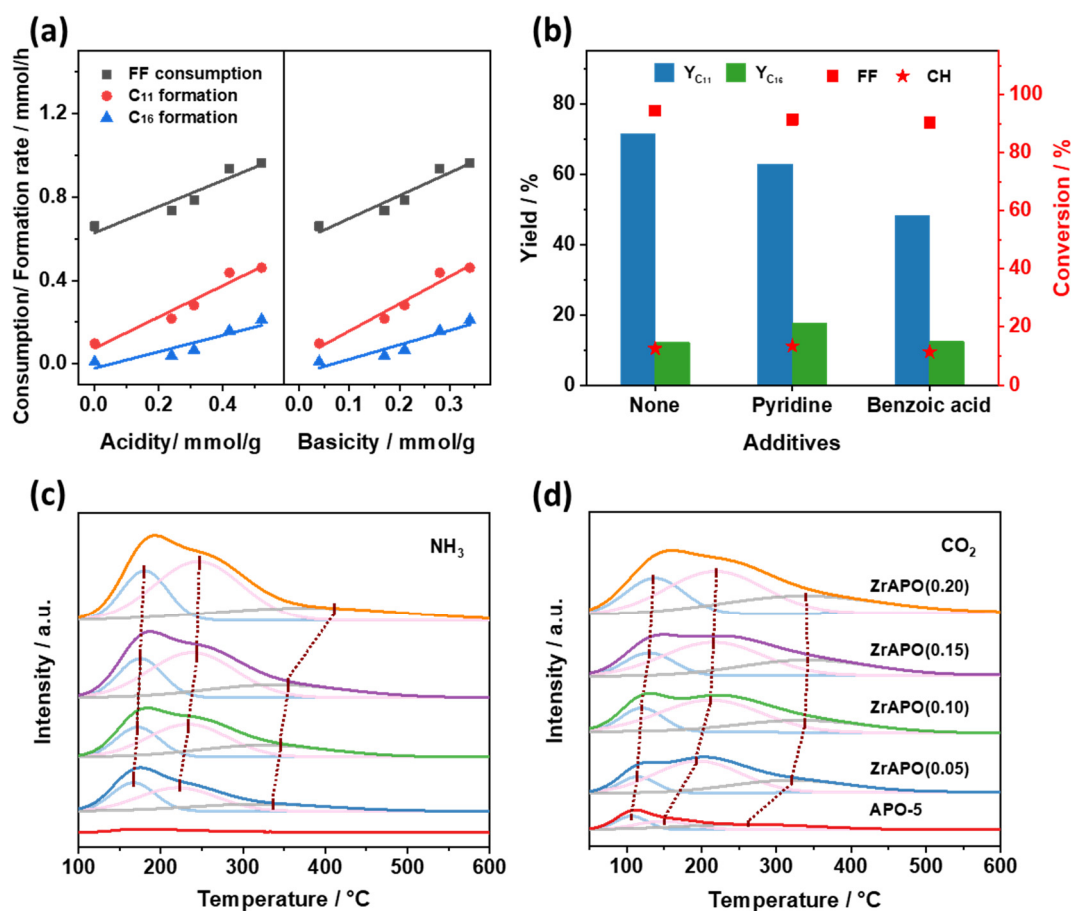
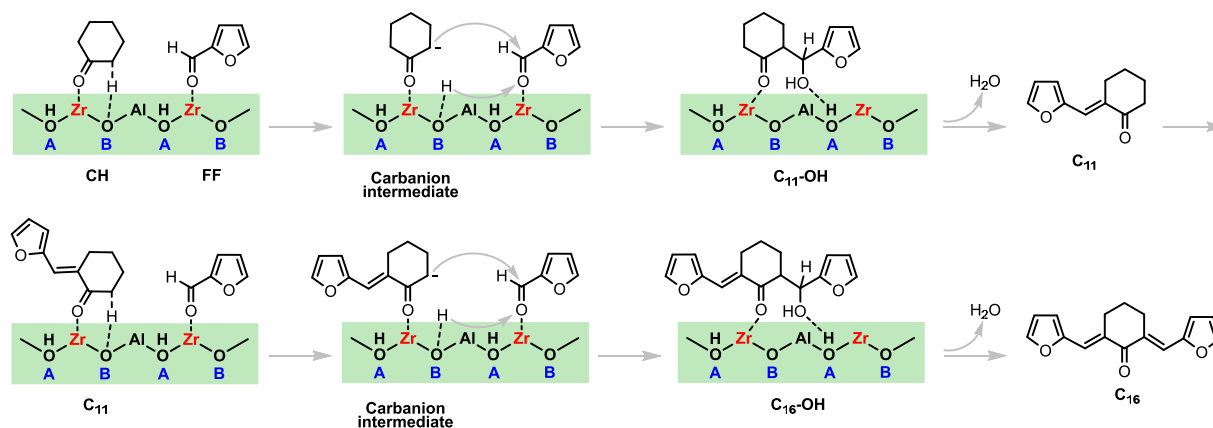


Fig. 6.10 (a) The correlation between acidity/basicity and FF consumption rate/product formation rate. (b) Poisoning reaction of cross-aldol condensation of FF and CH with ZrAPO(0.20) catalyst (reaction conditions: FF (192 mg, 2 mmol), ZrAPO(0.20) (50 mg), additive (100 mg), CH (2060 μ L, 20 mmol), 120°C, 2 h). (c) NH₃-TPD and (d) CO₂-TPD profiles of APO-5 and ZrAPO-5 catalysts.



Scheme 6.2 Possible reaction pathways for the cross-aldol condensation of FF with CH with ZrAPO(0.20) catalyst.

6.3 Summary

In this work, ZrAPO-5s with Zr substitution of P in the zeolite framework have been shown to promote the aldol condensation of FF and CH. The best catalyst ZrAPO(0.20) yielded up to 79.3% C₁₁ and 80.7% C₁₆ in the cross-aldol condensation of FF and CH and sustained high activity for five consecutive reactions run with intermediate calcination. Furthermore, ZrAPO(0.20) proved generally applicable for the cross-aldol condensation of other ketones and aldehydes as well as for the self-aldol condensation of CH, where 83.3% C₁₂ yield with 92.2% CH conversion was realized.

Structure-performance relationship between Zr-doping and the promoted reactivity was further established: 1) Both adsorption experiments and DFT calculations demonstrated that the introduction of Zr enhanced the adsorption strength of FF and CH *via* the carbonyl group interacting with Zr, further facilitating the aldol condensation reactions, and 2) the correlation between reaction rate and acidity/basicity and poisoning reaction proved that increased acidity and basicity by Zr substitution in the framework of APO-5 co-catalyzed the aldol condensation, facilitating the good yield of C₁₁, C₁₂ and C₁₆.

In perspective, this work introduces efficient routes for the synthesis of diesel and jet fuel range intermediates C₁₁, C₁₂ and C₁₆ from FF and CH *via* metal-doped zeotype catalysis, which presents efficient avenues to convert biomass-derived feedstocks.

6.4 References

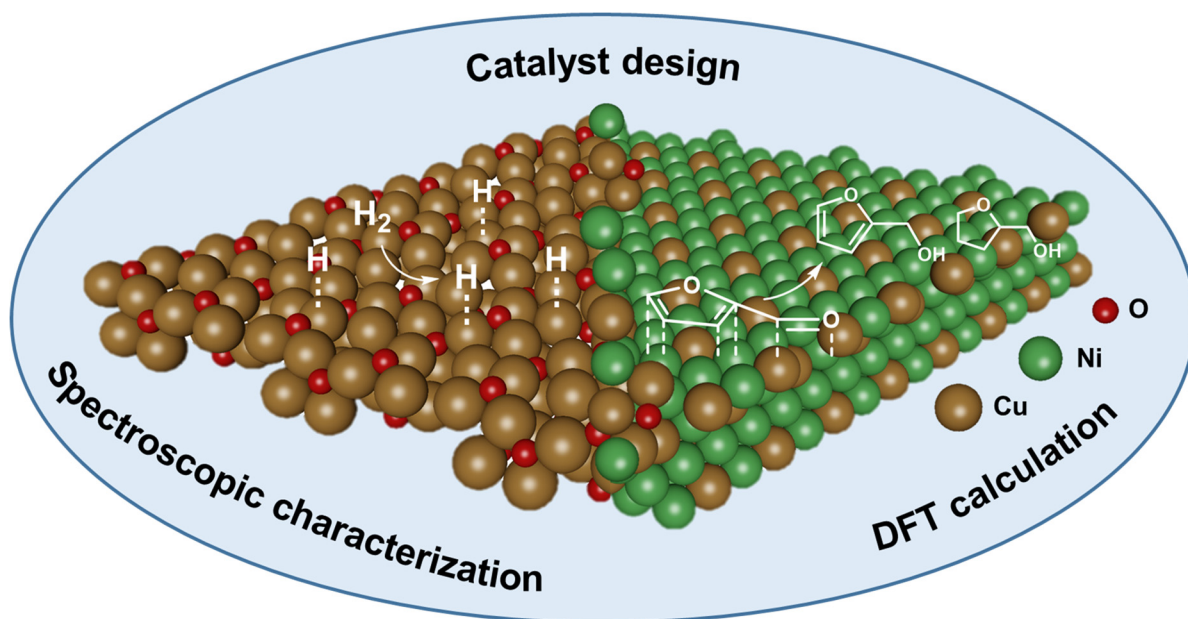
- [1] D. M. Alonso, J. Q. Bond, J. A. Dumesic, *Green Chem.* **2010**, *12*, 1493-1513.
- [2] J. Q. Bond, A. A. Upadhye, H. Olcay, G. A. Tompsett, J. Jae, R. Xing, D. M. Alonso, D. Wang, T. Y. Zhang, R. Kumar, A. Foster, S. M. Sen, C. T. Maravelias, R. Malina, S. R. H. Barrett, R. Lobo, C. E. Wyman, J. A. Dumesic, G. W. Huber, *Energ. Environ. Sci.* **2014**, *7*, 1500-1523.
- [3] Y. Jing, Y. Guo, Q. Xia, X. Liu, Y. Wang, *Chem* **2019**, *5*, 2520-2546.
- [4] H. Li, A. Riisager, S. Saravanamurugan, A. Pandey, R. S. Sangwan, S. Yang, R. Luque, *ACS Catal.* **2017**, *8*, 148-187.
- [5] Q. Meng, M. Hou, H. Liu, J. Song, B. Han, *Nat. Commun.* **2017**, *8*, 14190.
- [6] C. Xie, J. Song, B. Zhou, J. Hu, Z. Zhang, P. Zhang, Z. Jiang, B. Han, *ACS Sustain. Chem. Eng.* **2016**, *4*, 6231-6236.
- [7] O. Kikhtyanin, D. Kadlec, R. Velvarska, D. Kubicka, *ChemCatChem* **2018**, *10*, 1464-1475.
- [8] J. Yang, N. Li, G. Li, W. Wang, A. Wang, X. Wang, Y. Cong, T. Zhang, *Chem. Commun.* **2014**, *50*, 2572-2574.
- [9] R. E. O'Neill, L. Vanoye, C. De Bellefon, F. Aiouache, *Appl. Catal. B-Environ.* **2014**, *144*, 46-56.
- [10] N. Fakhfakh, P. Cognet, M. Cabassud, Y. Lucchese, M. D. de Los Ríos, *Chem. Eng. Process.* **2008**, *47*, 349-362.
- [11] R. M. West, Z. Y. Liu, M. Peter, C. A. Gartner, J. A. Dumesic, *J. Mol. Catal. A-Chem.* **2008**, *296*, 18-27.
- [12] M. Hronec, K. Fulajtárova, T. Liptaj, M. Štolcová, N. Prónayová, T. Soták, *Biomass Bioenerg.* **2014**, *63*, 291-299.
- [13] L. Faba, E. Diaz, S. Ordonez, *Appl. Catal. B-Environ.* **2012**, *113*, 201-211.
- [14] J. Cueto, L. Faba, E. Díaz, S. Ordóñez, *Appl. Catal. B-Environ.* **2017**, *201*, 221-231.
- [15] A. Tampierr, C. Russo, R. Marotta, M. Constanti, S. Contreras, F. Medina, *Appl. Catal. B-Environ.* **2021**, *282*, 119599.
- [16] D. Liang, G. Li, Y. Liu, J. Wu, X. Zhang, *Catal. Commun.* **2016**, *81*, 33-36.
- [17] O. Kikhtyanin, E. Lesnik, D. Kubička, *Appl. Catal. A-Gen.* **2016**, *525*, 215-225.
- [18] J. L. Xu, N. Li, X. F. Yang, G. Y. Li, A. Q. Wang, Y. Cong, X. D. Wang, T. Zhang, *ACS Catal.* **2017**, *7*, 5880-5886.
- [19] X. Kong, X. J. Wei, L. P. Li, Z. Fang, H. W. Lei, *Catal. Commun.* **2021**, *149*, 106207.

- [20] D. Nguyen Thanh, O. Kikhtyanin, R. Ramos, M. Kothari, P. Ulbrich, T. Munshi, D. Kubička, *Catal. Today* **2016**, 277, 97-107.
- [21] J. D. Lewis, S. Van de Vyver, Y. Roman-Leshkov, *Angew. Chem. Int. Ed.* **2015**, 127, 9973-9976.
- [22] O. Kikhtyanin, V. Kelbichova, D. Vitvarova, M. Kubu, D. Kubicka, *Catal. Today* **2014**, 227, 154-162.
- [23] M. Su, W. Li, T. Zhang, H. Xin, S. Li, W. Fan, L. Mac, *Catal. Sci. Technol.* **2017**, 7, 3555-3561.
- [24] A. Hamza, N. Nagaraju, *Chinese J. Catal.* **2015**, 36, 209-215.
- [25] J. Jae, G. A. Tompsett, A. J. Foster, K. D. Hammond, S. M. Auerbach, R. F. Lobo, G. W. Huber, *J. Catal.* **2011**, 279, 257-268.
- [26] B. Zibrowius, E. Löffler, M. Hunger, *Zeolites* **1992**, 12, 167-174.
- [27] M. K. Dongare, D. P. Sabde, R. A. Shaikh, K. R. Kamble, S. G. Hegde, *Catal. Today* **1999**, 49, 267-276.
- [28] V. L. Sushkevich, I. I. Ivanova, S. Tolborg, E. Taarning, *J. Catal.* **2014**, 316, 121-129.
- [29] R. Shannon, *Acta Crystallogr. A* **1976**, 32, 751-767.
- [30] S. H. Jhung, Y. K. Hwang, J.-S. Chang, S.-E. Park, *Micropor. Mesopor. Mat.* **2004**, 67, 151-157.
- [31] H. P. Winoto, Z. A. Fikri, J.-M. Ha, Y.-K. Park, H. Lee, D. J. Suh, J. Jae, *Appl. Catal. B-Environ.* **2019**, 241, 588-597.
- [32] B. Tang, W. Dai, X. Sun, G. Wu, N. Guan, M. Hunger, L. Li, *Green Chem.* **2015**, 17, 1744-1755.
- [33] D. Liu, B. Zhang, X. Liu, J. Li, *Catal. Sci. Technol.* **2015**, 5, 3394-3402.
- [34] P. A. Barrett, G. Sankar, C. R. A. Catlow, J. M. Thomas, *J. Phys. Chem.* **1996**, 100, 8977-8985.
- [35] G. Lischke, B. Parltitz, U. Lohse, E. Schreier, R. Fricke, *Appl. Catal. A-Gen.* **1998**, 166, 351-361.
- [36] G. Muller, J. Bodis, G. EderMirth, J. Kornatowski, J. A. Lercher, *J. Mol. Struct.* **1997**, 410, 173-178.
- [37] N. N. Tušar, V. Kaučič, S. Geremia, G. Vlaic, *Zeolites* **1995**, 15, 708-713.
- [38] M. Hartmann, L. Kevan, *Res. Chem. Intermed.* **2002**, 28, 625-695.
- [39] M. J. Climent, A. Corma, V. Fornés, R. Guil-Lopez, S. Iborra, *Adv. Synth. Catal.* **2002**, 344, 1090-1096.
- [40] R. Zeidan, M. Davis, *J. Catal.* **2007**, 247, 379-382.
- [41] N. C. Ellebracht, C. W. Jones, *ACS Catal.* **2019**, 9, 3266-3277.
- [42] Q. Deng, J. S. Xu, P. J. Han, L. Pan, L. Wang, X. W. Zhang, J. J. Zou, *Fuel Process. Technol.* **2016**, 148, 361-366.
- [43] R. Xing, A. V. Subrahmanyam, H. Olcay, W. Qi, G. P. van Walsum, H. Pendse, G. W. Huber, *Green Chem.* **2010**, 12, 1933-1946.
- [44] J. Cueto, L. Faba, E. Diaz, S. Ordonez, *Appl. Catal. B-Environ.* **2020**, 263, 118341.
- [45] A. Bohre, M. I. Alam, K. Avasthi, F. Ruiz-Zepeda, B. Likozar, *Appl. Catal. B-Environ.* **2020**, 276, 119069.

- [46] X. Meng, Y. Yang, L. Chen, M. Xu, X. Zhang, M. Wei, *ACS Catal.* **2019**, 9, 4226-4235.
- [47] W. Liu, Y. Yang, L. Chen, E. Xu, J. Xu, S. Hong, X. Zhang, M. Wei, *Appl. Catal. B-Environ.* **2021**, 282, 119569.
- [48] H. Ishikawa, M. Sheng, A. Nakata, K. Nakajima, S. Yamazoe, J. Yamasaki, S. Yamaguchi, T. Mizugaki, T. Mitsudome, *ACS Catal.* **2021**, 11, 750-757.
- [49] R. Osuga, Y. Hiyoshi, T. Yokoi, J. N. Kondo, *Micropor. Mesopor. Mat.* **2019**, 278, 91-98.
- [50] Y. Chai, S. Liu, Z.-J. Zhao, J. Gong, W. Dai, G. Wu, N. Guan, L. Li, *ACS Catal.* **2018**, 8, 8578-8589.
- [51] M. Huang, S. Kaliaguine, A. Auroux, *Stud. Surf. Sci. Catal.* **1995**, 97, 311-318.
- [52] R. A. Schoonheydt, P. Geerlings, E. A. Pidko, R. A. van Santen, *J. Mater. Chem.* **2012**, 22, 18705.

7 Rationalizing the structure-activity relationships in mesoporous CuNiO_x for selective furfural hydrogenation

W. Fang[†], S. Liu[†], A. K. Steffensen, L. Schill, G. Kastlunger, A. Riisager*, ACS *Catalysis* (Under review)



Bimetallic catalysts display outstanding reactivity in valorization of biomass-derived chemicals. In this work, KIT-6-templated mesoporous CuNiO_x catalysts were synthesized and applied for the selective hydrogenation of FF under moderately mild reaction conditions. A combination of experimental characterization and DFT calculations unveiled the critical role of Cu⁺ species for hydrogen activation and corroborated a direct correlation between Cu⁺ concentration and overall hydrogenation activities. Furthermore, a CuNi alloy phase was attributed as the active adsorption site for FF with difference in adsorption configurations being responsible for a shift in product selectivity from FAL towards THFA on Ni-rich phases. The structure-activity relationships established in the work clarify the role of bimetallic CuNi catalysts in this important reaction, and offers rationale for similar catalytic systems involving hydrogenation of C=O and C=C groups.

7.1 Introduction

The reduction of substrates with carbonyl groups and/or unsaturated C=C bonds (e.g. furfural, CO₂, esters, ethers, and carboxylic acids) by hydrogenation is a powerful tool for chemical valorization.¹⁻⁵ Non-noble, cheap Cu-based catalysts are widely used for C=O bond hydrogenations due to their capability to selectively reduce carbonyl groups while leaving C=C bonds unreacted. However, their activities are relatively low compared to many other catalysts.^{6,7} Ni-based catalysts are also attractive in hydrogenation reactions due to their low cost and high ability for adsorption and activation of H₂,⁸ but Ni possesses also strong absorption of both C=O and C=C bonds leading to low product selectivity in such hydrogenation reactions.^{8,9} Nevertheless, a combination of properties in bimetallic CuNi catalysts might possess the advantage of facilitating hydrogenation reactions with high selectivity and good activity.

Several bimetallic CuNi, CuNi/metal oxide (e.g. SiO₂, Al₂O₃, ZrO₂, and TiO₂)¹⁰⁻¹⁵ and CuNi/C^{8,16-18} catalysts have been used in the hydrogenation of FF, which is an important biomass-derived molecule with both C=O and C=C bonds. For instance, alumina-supported mixed copper-nickel oxides (Cu-Ni/ γ -Al₂O₃) obtained 92.6% FF conversion with 93.6% FAL selectivity at 130°C, which is much better than single Cu/ γ -Al₂O₃ (46.6% FAL yield) or Ni/ γ -Al₂O₃ (20.7% FAL yield).¹⁹ CuNi alloy supported on carbon catalyst (Cu_{0.33}Ni/C) achieved 96.7% FF conversion with 93.8% FAL selectivity at 120°C, while Cu/C and Ni/C only yielded 40.2% FF conversion with 10.4% FAL selectivity and 61.2% FF conversion with 82.8% FAL selectivity, respectively.⁸ Hence, in the experimental systems the bimetallic CuNi catalysts showed significant advantages over the monometallic catalysts, which is also supported by a theoretical study showing that Cu-rich CuNi alloy has outstanding activity to hydrogenate FF.²⁰

Structure-activity relationships of bimetallic catalysts are essential to understand in order to elucidate the reaction mechanisms on CuNi systems and clarify possible promotion directions for FF hydrogenation. By using FT-IR and DFT calculations, Tang et al. proposed that Cu₁Ni₃(111) alloy is the active sites of both H₂ activation and FF adsorption *via* a tilted configuration with the C=O group as an adsorptive functional group.⁸ Liu et al. proposed by a combination of FF adsorbed FT-IR and DFT calculation that the addition of Cu⁰ to Ni⁰ catalyst leads to the FF adsorption configuration changing from $\eta^2(\text{C},\text{O})$ to $\eta^1(\text{O})$ mode, greatly inhibiting the hydrogenation of the furan ring, and the addition of Ni⁰ to Cu⁰ catalyst promotes the adsorption of FF.²¹ Besides, Cu-based catalysts with Cu⁺ species was widely used in the hydrogenation of C=O bond for adsorption of C=O group or H₂ dissociation.^{1,22-24} Lee et al. showed that Cu₂O(100) binds FF more strongly than Cu(111) and CuO(100) and also has low migration barrier for

the dissociated H atoms, indicating Cu₂O(100) is the active site for FF hydrogenation.²⁴ However, the respective roles of CuNi alloy and Cu⁺ species have not been scrutinized hindering the mechanistic understanding and further optimization of CuNi catalysts.

In this work, mesoporous CuNiO_x catalysts with various Cu:Ni ratios were synthesized *via* a nanocasting method with KIT-6 and reduced at different temperatures to create various phases (e.g. CuNi alloy, Cu₂O) (Fig. 7.1). The as-synthesized catalysts were applied for FF hydrogenation, which showed that the catalyst with equimolar Cu and Ni reduced at 150 °C (CuNiO_x(1/1)-150) displayed the best performance in terms of FF conversion (100%) and selectivity (≥97%) towards FAL or THFA depending on the reaction conditions. A combination of experiments and DFT calculations indicates that the existence of Cu⁺ species boosts the activation of H₂ and both CuNi alloy and Cu⁺ facilitate the adsorption of FF, and careful investigations of the FF adsorption suggested the origin of the decreased selectivity to FAL on catalysts reduced at higher temperatures.

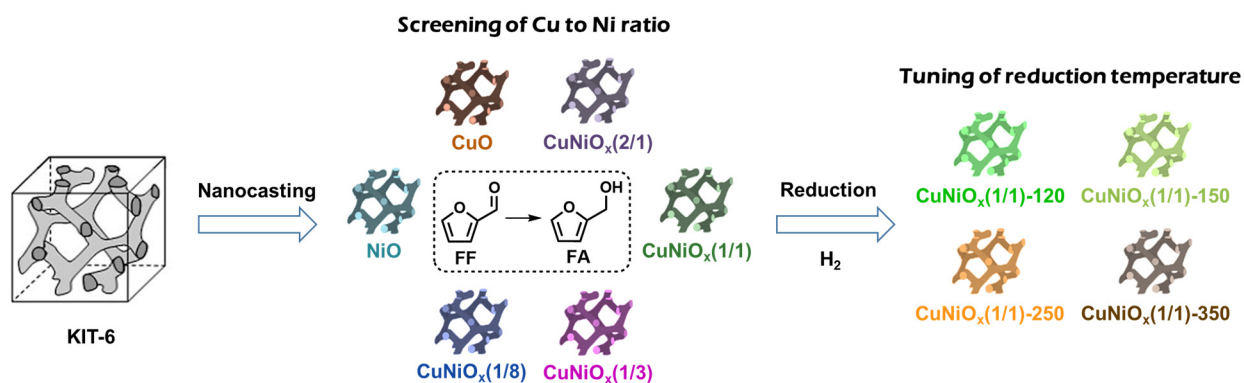


Fig. 7.1 Schematic illustration of the applied synthesis and screening approach of active mesoporous CuNiO_x for FF hydrogenation.

7.2 Results and discussion

7.2.1 Catalytic performance of catalysts

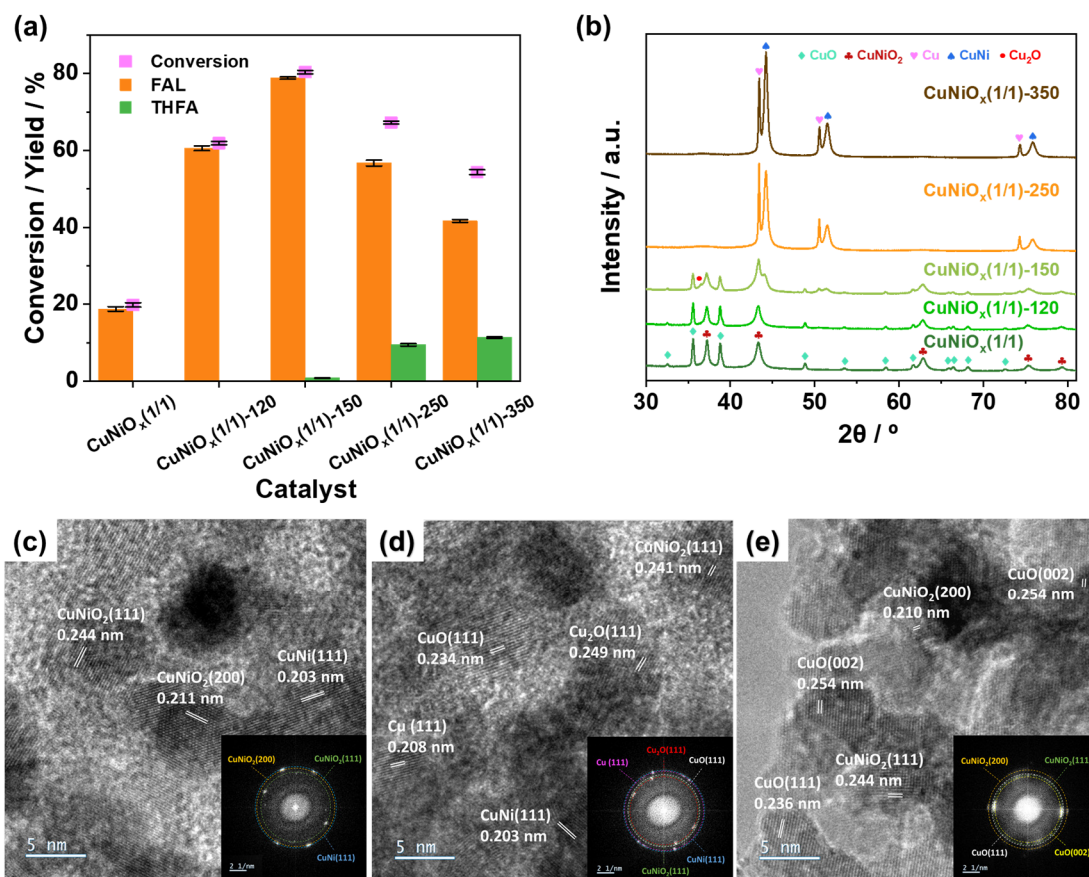


Fig. 7.2 (a) Catalytic performance of as-synthesized and reduced CuNiO_x(1/1) catalysts in the FF hydrogenation. Reaction conditions: FF (96 mg, 1 mmol), catalyst (20 mg), 2-propanol (5 mL), 120°C, 30 bar H₂, 45 min. (b) XRD patterns of the as-synthesized and reduced CuNiO_x(1/1) catalysts. (c)-(e) TEM images of CuNiO_x(1/1)-150 with the corresponding fast Fourier transform patterns.

CuNiO_x catalysts with different Cu/Ni ratios were initially synthesized *via* nanocasting using synthesized KIT-6 support having a three-dimensional pore network²⁵ with mesopores (pore diameter 5.6 nm) (see Figs. S7.3-5 and Table S7.1 for characterization results for KIT-6). Characterization of the as-synthesized (non-reduced) CuNiO_x catalysts, including XRD, N₂ physisorption and Cu and Ni XPS analysis (Figs. S7.6-8 and Table S7.2) showed that they all

contained Cu²⁺ and Ni²⁺ species and had 3.8 nm mesopore size. When the catalysts were subsequently screened for FF hydrogenation (Fig. S7.9), CuNiO_x(1/1) was found to possess the best catalytic performance with highest FF conversion (19.8%) and FAL yield (19.3%). Based on this, CuNiO_x(1/1) was further optimized by reduction at different temperatures (120, 150, 250, or 350°C) which allowed to obtain reduced catalysts with different metal species (Figs. 7.2b). FF hydrogenation with these catalysts (Fig. 7.2a) revealed much better catalytic performance than the as-synthesized CuNiO_x(1/1) with CuNiO_x(1/1)-150 displaying the highest FF conversion and FAL yield.

Interestingly, the CuNiO_x(1/1)-150 catalyst was found to selectively hydrogenate FF to FAL before consecutive hydrogenation resulted in the formation of THFA, thus allowing the two products to be obtained in 98% and 97% yield after 1 h and 6 h of reaction, respectively (Fig. S7.10). The marked reactivity difference of the catalyst was further reflected in the apparent activation energy (E_a) of the hydrogenation of FF to FAL (63.7 kJ/mol) and FAL to THFA (37.0 kJ/mol) calculated *via* numerical regressions (Fig. S7.11) and Arrhenius plots (Fig. S7.12). The CuNiO_x(1/1)-150 catalyst was also prone to direct reuse for FF hydrogenation after isolation without intermediate washing and drying, though a slight activity loss was observed after five recycles (Fig. S7.13). XRD and Cu LMM XAES analyses of the reused catalyst (Figs. S7.14 and 15) suggested this activity loss to be caused by partial reduction of the Cu inventory under the reaction conditions (i.e., 120°C, 30 bar H₂). This was confirmed by blank experiments with 2-propanol only in combination with XRD and Cu and Ni XPS analyses (Figs. S7.16 and 17), where especially CuO species were found to be reduced easier than CuNiO₂ species. Additionally, the catalyst proved also very versatile being able to hydrogenate a broad range of other aliphatic and aromatic

compounds with C=O and C=C in excellent yield of $\geq 95\%$ at 120°C in 1 h (Table S7.3).

7.2.2 Composition, morphology and active phases of catalysts

XRD characterization of the reduced CuNiO_x(1/1) catalysts (Fig. 7.2b) showed bulk compositions corresponding to mixed CuO and CuNiO₂ at lower temperatures,^{26,27} while new phases, such as Cu₂O, Cu, and CuNi alloy, formed after reduction at higher temperatures. The lattice distances obtained by FFT spots in TEM images of CuNiO_x(1/1)-150 (Figs. 7.2c-e) confirmed the presence of CuNiO₂(111), CuNiO₂(200), CuO(111), CuO(002), Cu(111), CuNi(111), and Cu₂O(111), while TEM images (Fig. S7.18) and N₂ physisorption results (Fig. S7.19 and Table S7.4) in general suggested a slight collapse of the porous structure.

Surface analysis by Cu 2p_{3/2} XPS (Fig. S7.20) showed that all reduced catalysts had signatures of Cu²⁺ with binding energies of 934-943 eV and of Cu⁺/Cu⁰ with binding energies around 932.4 eV.²⁸⁻³⁰ The latter species was distinguished by Cu LMM XAES³¹ (Fig. 7.3a) giving deconvoluted peaks at 914.3, 916.5, and 918.2 eV ascribed to Cu⁺, Cu²⁺, and Cu⁰ species, respectively.²⁸ Moreover, Ni 2p_{3/2} XPS (Fig. 7.3b) gave peaks in the range 854-863 eV attributed to Ni²⁺ and peaks at 852.6 assigned to Ni⁰.^{9,32,33} A calculation of the relative amount of Cu and Ni surface species in the catalysts (Figs. 7.3c-d) revealed CuNiO_x(1/1)-120 and CuNiO_x(1/1)-150 to have much more Cu⁺ (51%) than other reduced Cu-based catalysts reported,^{24,34,35} likely due to the stabilization effect of Ni species.^{35,36} Besides, was the reduction of Ni²⁺ slower than that of Cu²⁺ due to different reduction potentials,³⁷ in accordance with H₂-TPR results (Fig. S7.21). Hence, the reduced CuNiO_x(1/1) catalysts were ordered-mesoporous mixed metal oxides

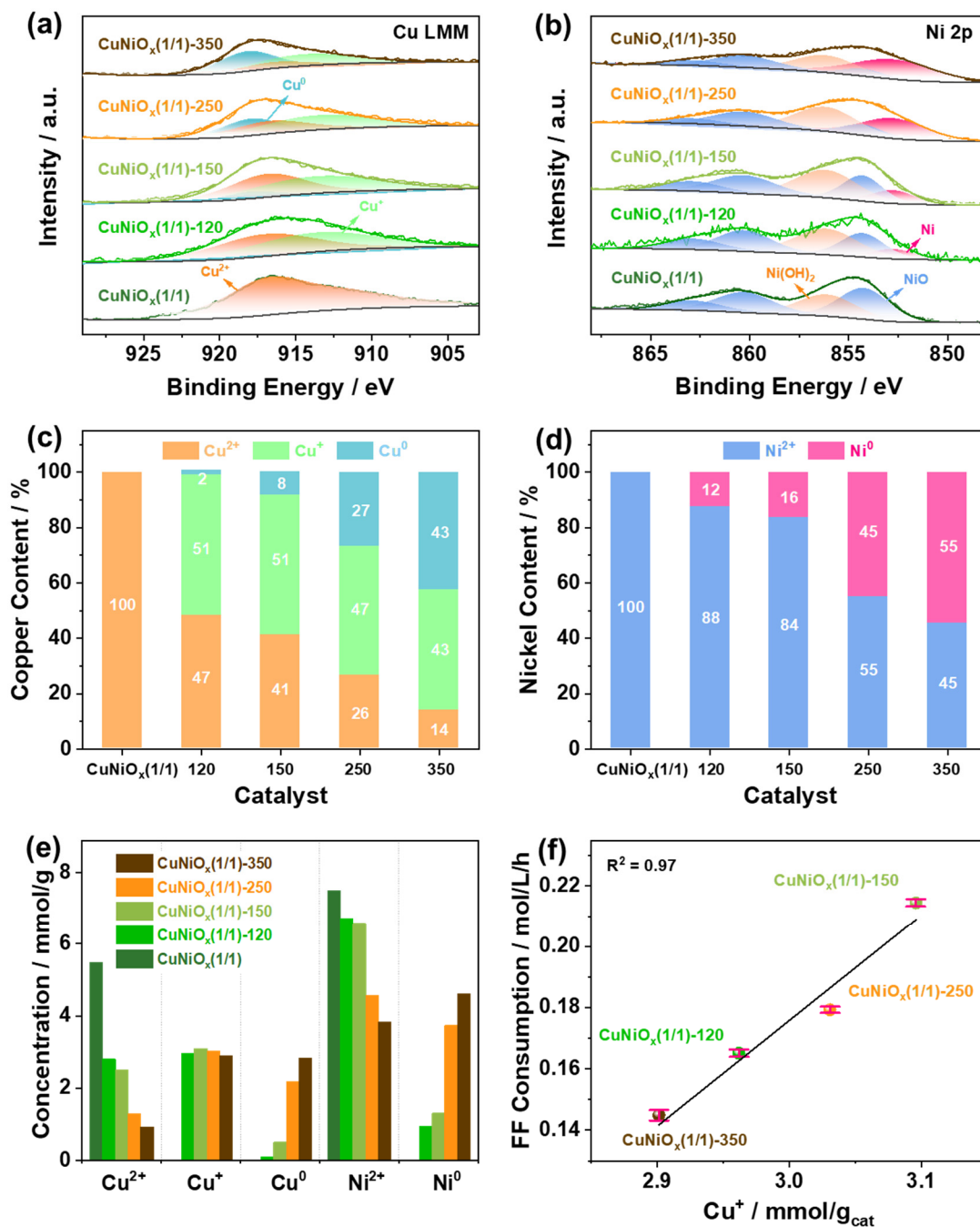


Fig. 7.3 (a) Cu LMM XAES spectra, (b) Ni 2p_{3/2} XPS spectra, (c) content (%) of Cu²⁺, Cu⁺, and Cu⁰, (d) content (%) of Ni²⁺ and Ni⁰, and (e) concentration of Cu²⁺, Cu⁺, Cu⁰, Ni²⁺, and Ni⁰ in the as-synthesized and reduced CuNiO_x(1/1) catalysts. (f) Correlation of FF consumption rate with Cu⁺ concentration during FF hydrogenation for the reduced CuNiO_x(1/1) catalysts. Reaction conditions: FF (96 mg, 1 mmol), catalyst (20 mg), 2-propanol (5 mL), 120°C, 30 bar H₂, 45 min.

with different Cu²⁺, Cu⁺, Cu⁰, Ni²⁺, and Ni⁰ concentrations and various crystal planes, including CuNiO₂(111), CuNiO₂(200), CuO(111), CuO(002), Cu(111), CuNi(111), and Cu₂O(111). Such multicomponent CuNi catalysts could be expected to have more than one active sites for the FF hydrogenation.

To investigate the possible active phases for FF hydrogenation on reduced CuNiO_x catalysts, the concentrations of Cu²⁺, Cu⁺, Cu⁰, Ni²⁺, and Ni⁰ of each catalyst were calculated based on XAES, XPS, and XRF (Fig. 7.3e) and used to build correlations with FF consumption rate. No obvious connection was found for the Cu²⁺, Cu⁰, Ni²⁺, and Ni⁰ species (Fig. S7.22), while a notable linear relationship between the FF consumption rate and Cu⁺ concentration of the catalysts was evident (Fig. 7.3f), i.e., the higher Cu⁺ concentration the higher activity for FF hydrogenation. This result suggested that Cu⁺ species might be potentially determining activity factors during the hydrogenation reaction.

7.2.3 Adsorption sites on catalysts

The activity of the catalysts for the FF hydrogenation could be governed by both H₂ activation and the hydrogenation of FF species on the surface. H₂-TPD of the as-synthesized CuNiO_x(1/1) catalysts (Fig. 7.4a)³⁸ revealed relative low amount of H₂ adsorption, whereas both the amount and strength for the adsorption of H₂ increased after reduction (with the formation of Cu⁺, Cu⁰, and Ni⁰ species), especially for the CuNiO_x(1/1)-150 catalyst. This catalyst also had the highest concentration of Cu⁺ species (see above) strongly suggesting that Cu⁺ species, probably Cu₂O(111) shown in TEM, were the main H₂ adsorptive sites.

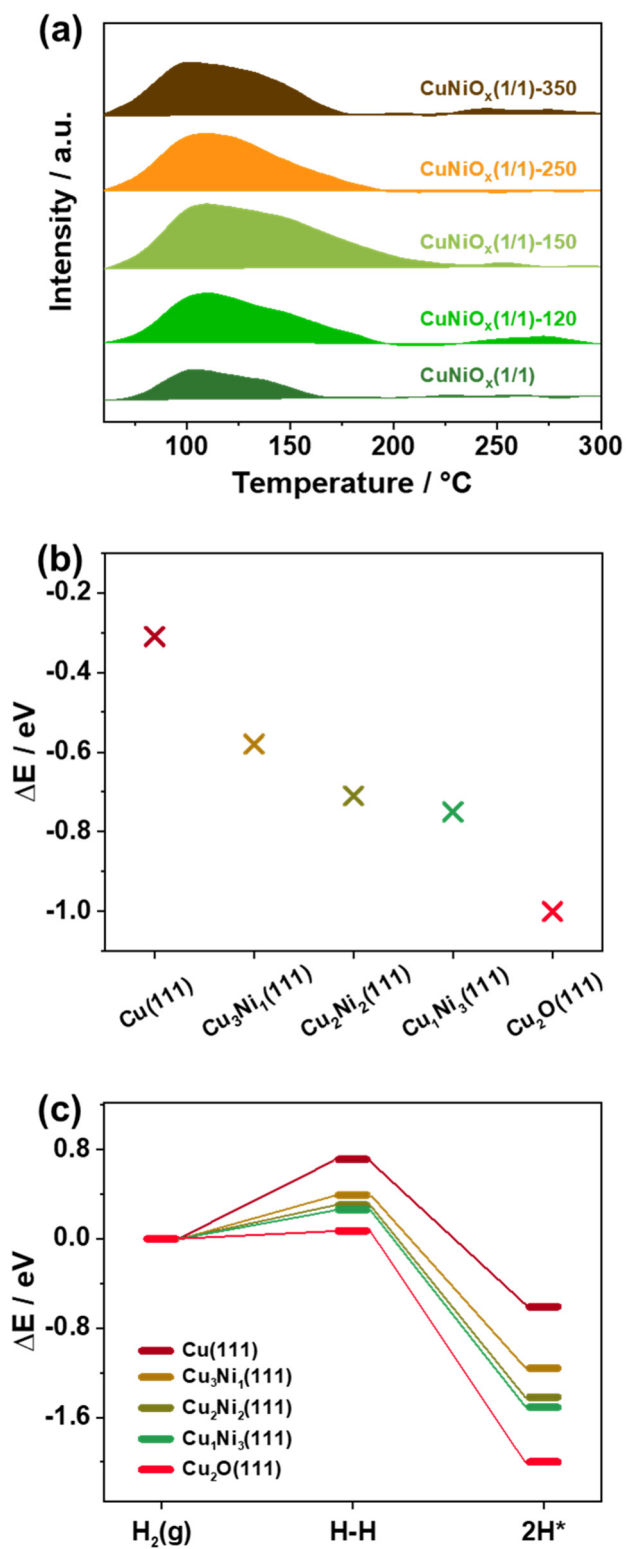


Fig. 7.4 (a) H_2 -TPD of as-synthesized and reduced $\text{CuNiO}_x(1/1)$ catalysts. (b) Calculated adsorption energies of H^* and (c) dissociation energetics of gas-phase H_2 on different Cu- and Ni-based crystal facets.

In order to validate the identified binding trends, the adsorption energies of H* (* denotes an active site on surface models) and dissociation energetics of gas-phase H₂ on Cu(111), Cu₃Ni₁(111), Cu₂Ni₂(111), Cu₁Ni₃(111), and Cu₂O(111) (chosen based on the characterization results of XRD, TEM, XPS, and XRF above) were obtained and compared from DFT calculations (Figs. 7.4b-c). The adsorption energies of H* gave the following order: Cu₂O(111) >> Cu₁Ni₃(111) > Cu₂Ni₂(111) > Cu₃Ni₁(111) >> Cu(111) (Fig. 7.4b). The stronger H* adsorption promoted the H₂ activation by reducing the dissociation barriers displayed in Fig. 7.4c. Thus, Cu₂O(111) had both strongest adsorption energy of H* and lowest dissociation barrier of H₂, further demonstrating Cu₂O(111) planes probably served as the main adsorptive and dissociative sites of H₂ during the FF hydrogenation.

The adsorption of FF on the CuNiO_x(1/1) catalysts was further studied by TGA (Fig. S7.23),³⁹ which revealed a relative low FF desorption temperature range (73-163°C) similar to previously reported work.^{40,41} For the reduced CuNiO_x(1/1) catalysts (Fig. 7.5a) the amount of adsorbed FF increased with reduction temperature, implying that the formed Cu⁺, Cu⁰, and Ni⁰ species favored the adsorption of FF. In line with this had all the catalysts intensive $\nu(\text{C}=\text{C})$ (1569 and 1464 cm⁻¹) and $\nu(\text{C}=\text{O})$ (1671 cm⁻¹)^{7,9} bands in the FT-IR spectra (Fig. 7.5b), indicative of only weak FF adsorption^{42,43} with the bands red-shifted for the catalysts reduced at higher temperatures (150-350°C) due to stronger adsorption (most likely parallel adsorption configuration).

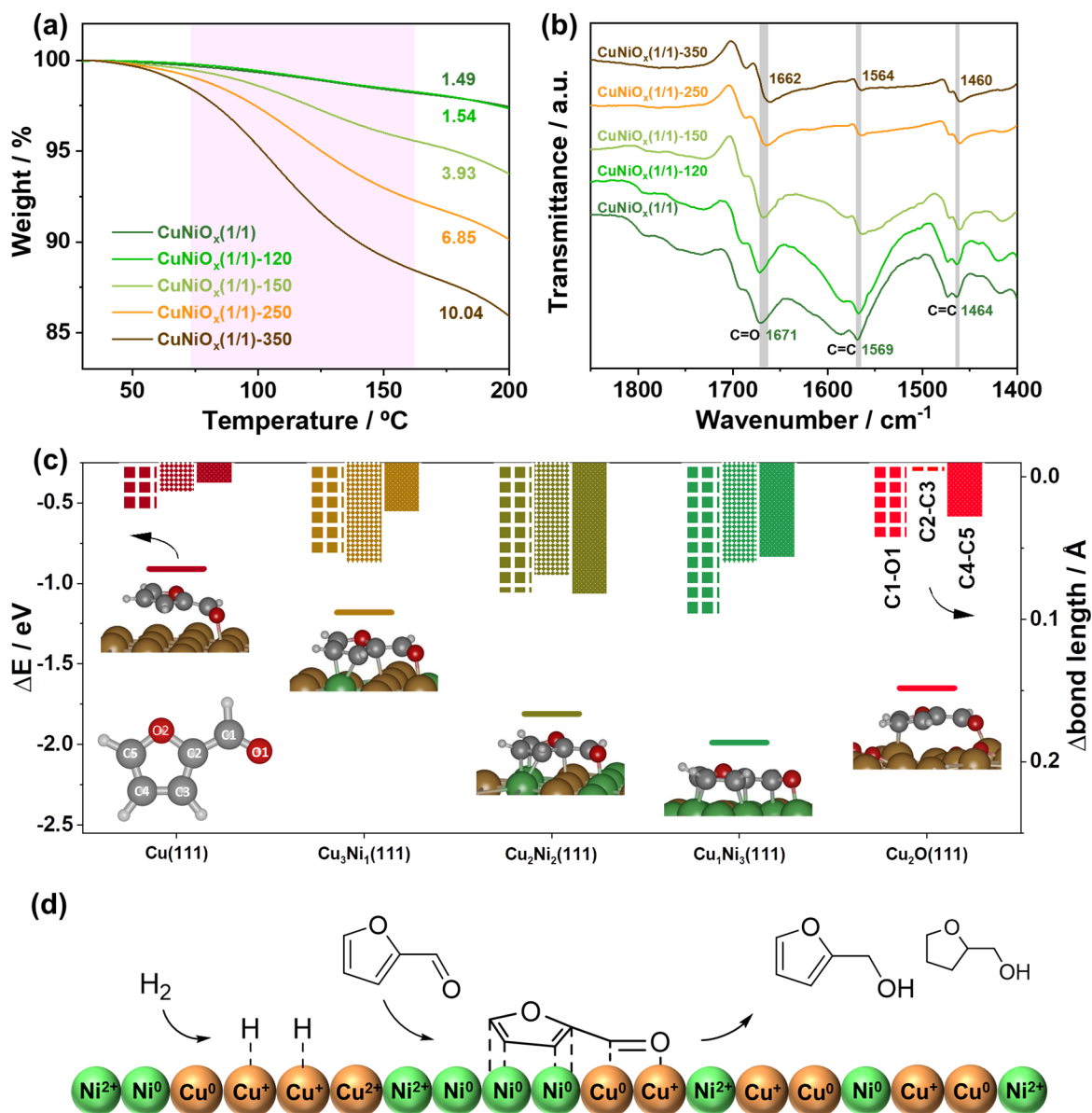


Fig. 7.5 (a) TG profiles and (b) FT-IR spectra of FF-adsorbed as-synthesized and reduced CuNiO_x(1/1) catalysts. (c) Comparison of increased bond lengths (Å) of FF in gas phase and adsorbed on Cu(111), Cu₂O(111), Cu₁Ni₃(111), Cu₂Ni₂(111), and Cu₃Ni₁(111) surfaces and optimized structures of FF adsorbed on different planes accompanying side view with a planar configuration. (d) Schematic illustration of a possible FF hydrogenation mechanism on reduced CuNiO_x(1/1) catalysts.

To provide an atomistic understanding of the FF adsorption on the catalysts were representative surface models calculated by DFT and compared (Fig. 7.5c). Consistent with previous reports^{44,45} was the adsorption of FF on Cu(111) found

to be relatively weak (-0.91 eV) and to occur only in the $\eta^1(\text{O})$ -aldehyde configuration *via* the carbonyl O atom due to the repulsion derived from the overlap of the 3d band of Cu and the furan ring. The addition of Ni to Cu in CuNi alloys led to a marked increase in the FF adsorption energy (i.e. -1.18 to -1.99 eV), but Cu₂O(111) adsorbed FF strongest with an adsorption energy of -1.65 eV. However, the furan ring of FF interacted more strongly with the CuNi alloy surfaces than with Cu(111) and Cu₂O(111) in the optimized adsorption geometries (Fig. 7.5c).^{43,46} Together with increased bond lengths in the adsorbed FF (Fig. 7.5c) and shorter distances between surfaces and carbonyl O atoms as well as furan C2 carbons (Fig. S7.24 and Table S7.5), this suggested that preferential adsorption on CuNi alloys occurred due to stabilization by both the carbonyl group and the C=C in the furan ring.⁴⁴ Hence, overall the DFT and the experimental results corroborated that Cu₁Ni₃(111) likely was the main adsorption site of FF which was further hydrogenated by H* species activated on Cu⁺ sites, as shown in the schematic mechanism in Fig. 7.5d.

7.3 Summary

Mesoporous CuNiO_x catalyst reduced at 150°C was discovered to display excellent activity and selectivity for the hydrogenation of FF to FAL under moderate reaction conditions compared to catalysts reduced at alternative temperatures. Supported by detailed experimental characterization and DFT calculations was Cu⁺ species proposed to dominate the activity by having critical roles for H₂ activation, and CuNi alloy indicated to be the predominant active adsorption sites of FF during reaction activating both the C=O group and the furan ring, with the latter being more difficult to hydrogenate. In perspective, the structure-performance relationships established in this work may provide

important mechanistic understanding and rational design of similar catalysts for other valorization reactions of biomass-derived chemicals.

7.4 References

- [1] J. Gong, H. Yue, Y. Zhao, S. Zhao, L. Zhao, J. Lv, S. Wang, X. Ma, *J. Am. Chem. Soc.* **2012**, *134*, 13922-13925.
- [2] G. A. Filonenko, M. J. Aguila, E. N. Schulpen, R. van Putten, J. Wiecko, C. Muller, L. Lefort, E. J. Hensen, E. A. Pidko, *J. Am. Chem. Soc.* **2015**, *137*, 7620-7623.
- [3] K. Chen, J.-L. Ling, C.-D. Wu, *Angew. Chem. Int. Ed.* **2020**, *59*, 1925-1931.
- [4] Y. Zhu, X. Kong, X. Li, G. Ding, Y. Zhu, Y.-W. Li, *ACS Catal.* **2014**, *4*, 3612-3620.
- [5] H. Kreissl, J. Jin, S.-H. Lin, D. Schüette, S. Störtte, N. Levin, B. Chaudret, A. J. Vorholt, A. Bordet, W. Leitner, *Angew. Chem. Int. Ed.* **2021**, *60*, 26639-26646.
- [6] R. Rao, A. Dandekar, R. T. K. Baker, M. A. Vannice, *J. Catal.* **1997**, *171*, 406-419.
- [7] Q. Wang, J. Feng, L. Zheng, B. Wang, R. Bi, Y. He, H. Liu, D. Li, *ACS Catal.* **2019**, *10*, 1353-1365.
- [8] F. Tang, L. Wang, M. Dessie Walle, A. Mustapha, Y.-N. Liu, *J. Catal.* **2020**, *383*, 172-180.
- [9] W. Liu, Y. Yang, L. Chen, E. Xu, J. Xu, S. Hong, X. Zhang, M. Wei, *Appl. Catal., B* **2021**, *282*, 119569.
- [10] B. Seemala, C. M. Cai, C. E. Wyman, P. Christopher, *ACS Catal.* **2017**, *7*, 4070-4082.
- [11] P. Weerachawanasak, P. Krawmanee, W. Inkamhaeng, F. J. Cadete Santos Aires, T. Sooknoi, J. Panpranot, *Catal. Commun.* **2021**, *149*, 106221.
- [12] A. A. Smirnov, I. N. Shilov, M. V. Alekseeva, S. A. Selishcheva, V. A. Yakovlev, *Catal. Ind.* **2018**, *10*, 228-236.
- [13] A. Aldureid, F. Medina, G. S. Patience, D. Montané, *Catalysts* **2022**, *12*, 390.
- [14] M. E. Şebin, S. Akmaz, S. N. Koc, *J. Chem. Sci.* **2020**, *132*.
- [15] X. Chen, W. Liu, J. Luo, H. Niu, R. Li, C. Liang, *Ind. Eng. Chem. Res.* **2022**.
- [16] S. K. Jaatinen, R. S. Karinen, J. S. Lehtonen, *ChemistrySelect* **2017**, *2*, 51-60.
- [17] S. Jaatinen, M. Stekrova, R. Karinen, *J. Porous Mat.* **2017**, *25*, 1147-1160.
- [18] L. Liu, H. Lou, M. Chen, *Int. J. Hydrog. Energy* **2016**, *41*, 14721-14731.
- [19] S. Srivastava, G. C. Jadeja, J. Parikh, *J. Mol. Catal. A-Chem.* **2017**, *426*, 244-256.
- [20] S. Liu, N. Govindarajan, K. Chan, *ACS Catal.* **2022**, *12*, 12902-12910.
- [21] M. Liu, L. Yuan, G. Fan, L. Zheng, L. Yang, F. Li, *ACS Appl. Nano Mater.* **2020**, *3*, 9226-9237.
- [22] H. Wang, W. Zhao, M. U. Rehman, W. Liu, Y. Xu, H. Huang, S. Wang, Y. Zhao, D. Mei, X. Ma, *ACS Catal.* **2022**, 4724-4736.
- [23] A. Yin, X. Guo, W.-L. Dai, K. Fan, *J. Phys. Chem. C* **2009**, *113*, 11003-11013.
- [24] J. Lee, J. H. Seo, C. Nguyen-Huy, E. Yang, J. G. Lee, H. Lee, E. J. Jang, J. H. Kwak, J. H. Lee, H. Lee, K. An, *Appl. Catal., B* **2021**, *282*, 119576.

- [25] F. Kleitz, F. Bérubé, R. Guillet-Nicolas, C.-M. Yang, M. Thommes, *J. Phys. Chem. C* **2010**, *114*, 9344-9355.
- [26] Q. Hu, W. Li, D. I. Abouelamaiem, C. Xu, H. Jiang, W. Han, G. He, *RSC Adv.* **2019**, *9*, 20963-20967.
- [27] X. H. Deng, K. Chen, H. Tuysuz, *Chem. Mater.* **2017**, *29*, 40-52.
- [28] Y. Ren, Y. Yang, L. Chen, L. Wang, Y. Shi, P. Yin, W. Wang, M. Shao, X. Zhang, M. Wei, *Appl. Catal., B* **2022**, *314*, 121515.
- [29] R. P. Vasquez, *Surf. Sci. Spectra* **1998**, *5*, 262-266.
- [30] J. Yu, J. Ran, *Energ. Environ. Sci.* **2011**, *4*, 1364.
- [31] J. P. Espinós, J. Morales, A. Barranco, A. Caballero, J. P. Holgado, A. R. González-Elipe, *J. Phys. Chem. B* **2002**, *106*, 6921-6929.
- [32] A. N. Mansour, *Surf. Sci. Spectra* **1994**, *3*, 231-238.
- [33] A. N. Mansour, C. A. Melendres, *Surf. Sci. Spectra* **1994**, *3*, 247-254.
- [34] J. Y. Kim, J. A. Rodriguez, J. C. Hanson, A. I. Frenkel, P. L. Lee, *J. Am. Chem. Soc.* **2003**, *125*, 10684-10692.
- [35] A. Kitla, O. V. Safonova, K. Föttinger, *Catal. Letters* **2013**, *143*, 517-530.
- [36] J. Zhu, Y. Tang, K. Tang, *RSC Adv.* **2016**, *6*, 87294-87298.
- [37] S. D. Robertson, B. D. McNicol, J. H. De Baas, S. C. Kloet, J. W. Jenkins, *J. Catal.* **1975**, *37*, 424-431.
- [38] M. B. Fichtl, O. Hinrichsen, *Catal. Letters* **2014**, *144*, 2114-2120.
- [39] G. L. Dimas-Rivera, J. R. de la Rosa, C. J. Lucio-Ortiz, J. A. De Los Reyes Heredia, V. G. Gonzalez, T. Hernandez, *Materials* **2014**, *7*, 527-541.
- [40] S. H. Pang, J. W. Medlin, *ACS Catal.* **2011**, *1*, 1272-1283.
- [41] W. Zhang, Y. Zhu, S. Niu, Y. Li, *J. Mol. Catal. A-Chem.* **2011**, *335*, 71-81.
- [42] X. Meng, Y. Yang, L. Chen, M. Xu, X. Zhang, M. Wei, *ACS Catal.* **2019**, *9*, 4226-4235.
- [43] W. Yu, K. Xiong, N. Ji, M. D. Porosoff, J. G. Chen, *J. Catal.* **2014**, *317*, 253-262.
- [44] S. Sitthisa, W. An, D. E. Resasco, *J. Catal.* **2011**, *284*, 90-101.
- [45] Y. Shi, Y. Zhu, Y. Yang, Y.-W. Li, H. Jiao, *ACS Catal.* **2015**, *5*, 4020-4032.
- [46] X. Meng, L. Wang, L. Chen, M. Xu, N. Liu, J. Zhang, Y. Yang, M. Wei, *J. Catal.* **2020**, *392*, 69-79.

8 Main conclusions and perspectives

This PhD thesis contains five parts focused on various catalytic reactions with FF over heterogeneous catalysts, including acetalization, hydrogenation, reductive etherification, and aldol condensation.

In the first four parts of the thesis (Chapters 3-6), APO-5s and metal-modified APO-5s exhibited excellent catalytic performance in the corresponding reactions (APO-5(1.5) in the acetalization, Ca-loaded APO-5(1.5) in the CTH, Pd-loaded APO-5(1.5) in the reductive etherification, and Zr-APO-5 in the aldol condensation). FT-IR experiments with adsorbed FF showed specific adsorption of FF *via* the carbonyl group of the molecule, which promoted selective conversion of the aldehyde group instead of other competing reactions. Furthermore, the correlation between reaction rate and acidity/basicity or/and poisoning reactions proved that a suitable acidity/basicity contributed mainly to the desired reactions. Importantly, the catalysts also showed general applicability in the conversion of other furanic carbonyl compounds and good reusability. Combined, the work demonstrates simple approaches to design heterogeneous APO-5 catalyst systems for the synthesis of potential biofuels and value-added chemicals, which presents efficient approaches to convert biomass-derived feedstocks. Future work should focus on product separation including the purification of products, recycling of catalysts, and removal of contaminants, and evaluate the potential for industrial implementation, e.g. engine performance test of synthesized biofuels.

In the fifth part of the thesis (Chapter 7), reduced mesoporous CuNiO_x catalyst displayed prominent performance and selectivity for the hydrogenation of FF to FAL under moderate reaction conditions. Based on the detailed experimental

characterization and DFT calculations, Cu^+ species were proposed to have a critical role for H_2 activation, and CuNi alloy phases were indicated to be the predominant active adsorption sites of FF. In perspective, the structure-performance relationships established here provide a mechanistic understanding and rational design of commercial Cu- and/or Ni-based catalysts for other hydrogenation reactions (e.g. CO_2 hydrogenation) in the industry.

Appendices A – Support information for Chapter 3

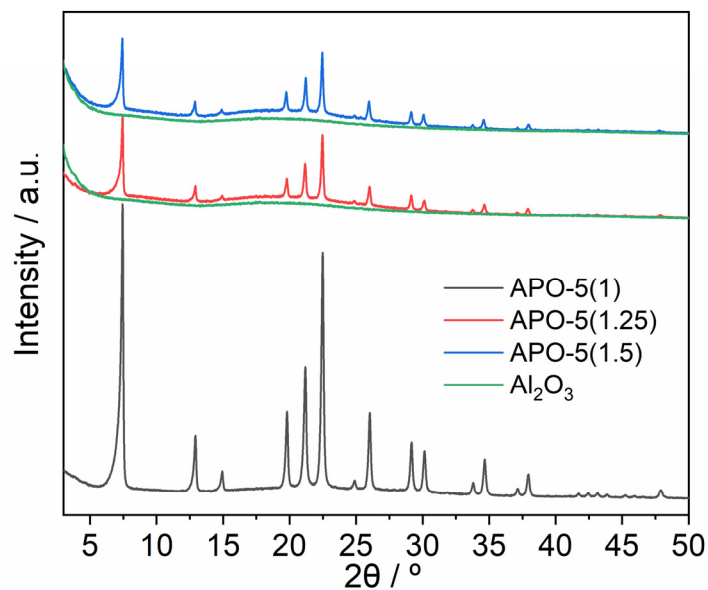


Fig. S3.1 XRD patterns of APO-5 catalysts and Al_2O_3 .

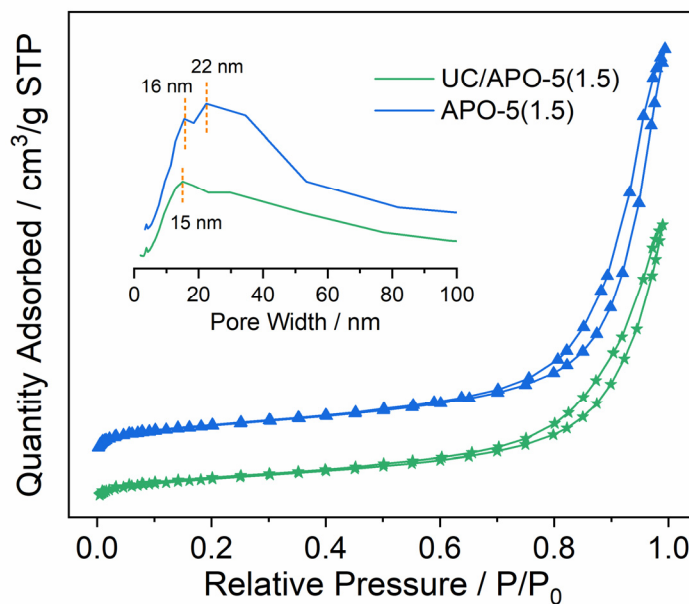


Fig. S3.2 N_2 adsorption-desorption isotherms (inset: BJH mesopore size distribution) of APO-5(1.5) catalyst before and after calcination.

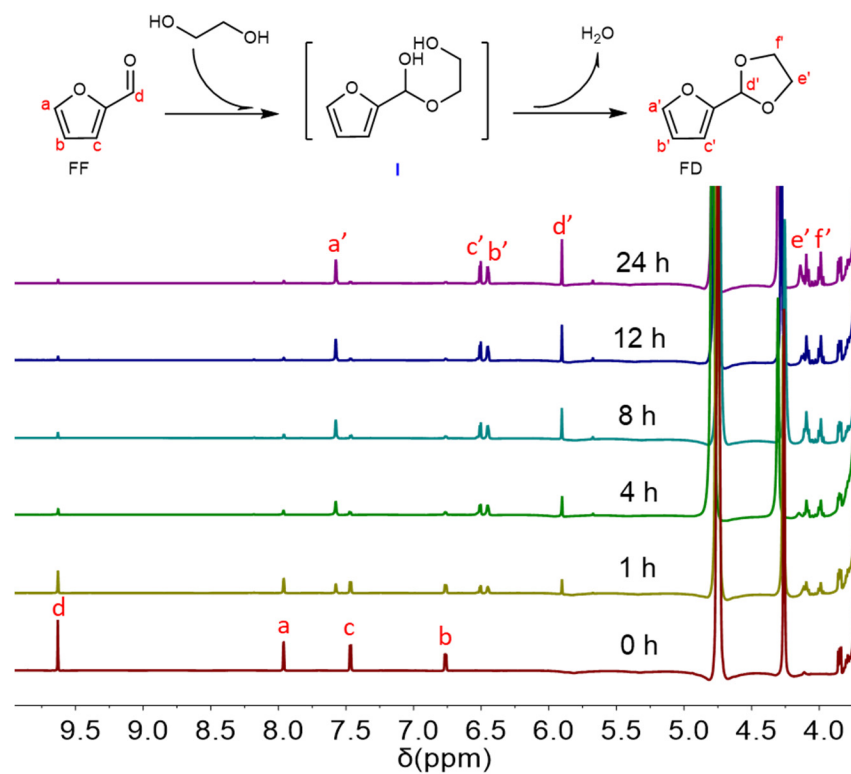


Fig. S3.3 ^1H NMR spectra of the reaction mixtures at different reaction times. Reaction conditions: FF (96 mg, 1 mmol), APO-5(1) (100 mg), EG (2 mL), 1,4-dioxane (3 mL), 150°C.

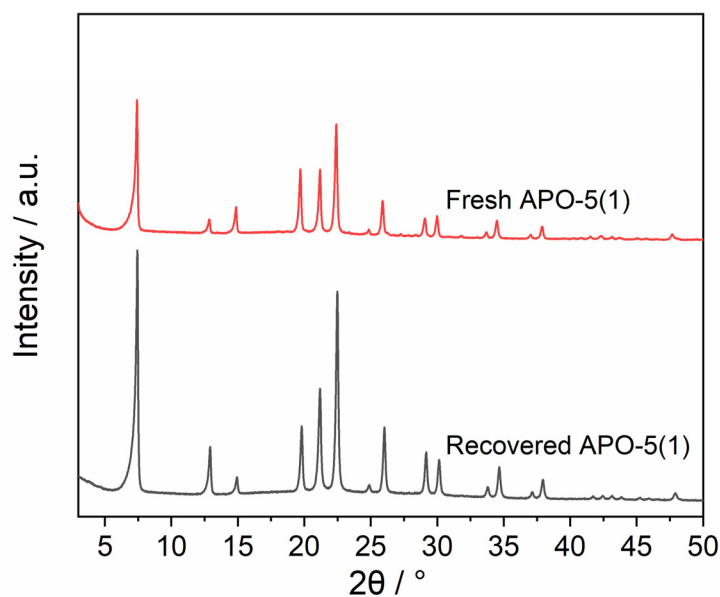


Fig. S3.4 XRD patterns of fresh and recovered (after five cycles) APO-5(1) catalyst.

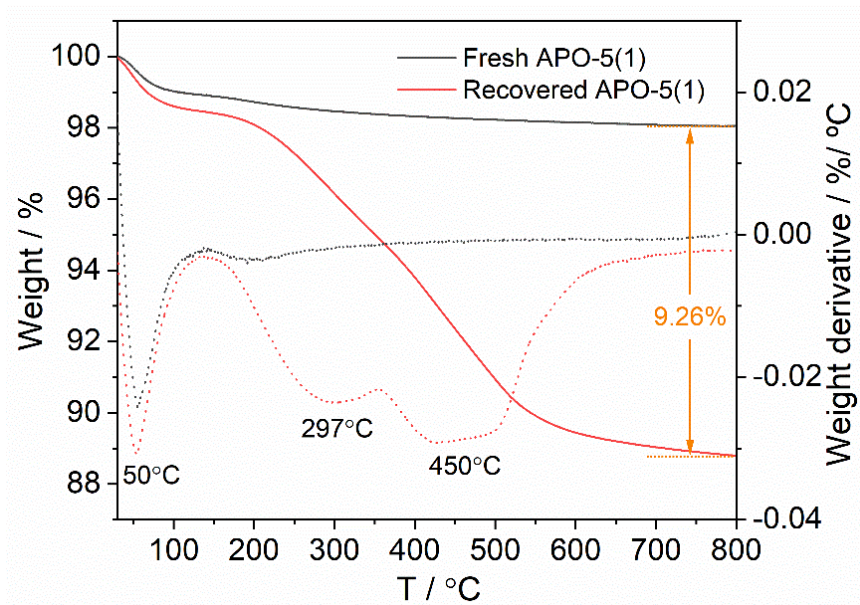


Fig. S3.5 TG curves of fresh and recovered APO-5(1) after 5 recycles.

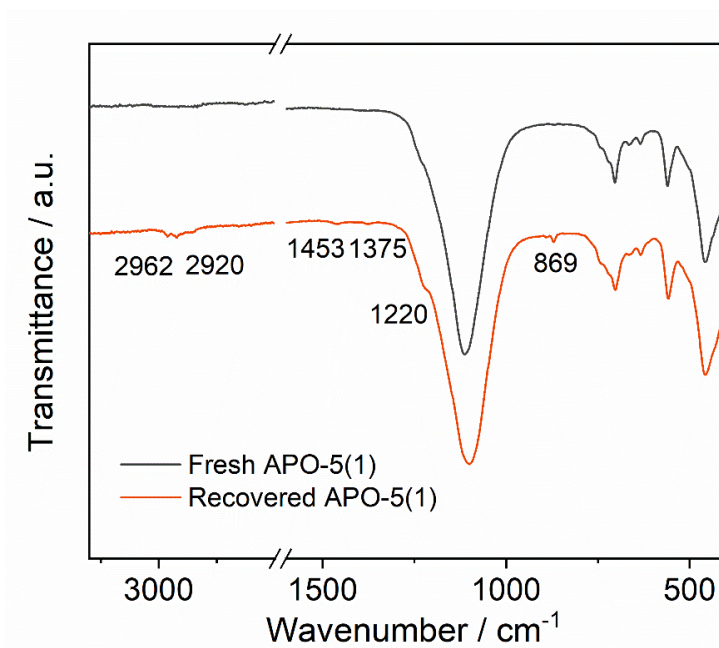


Fig. S3.6 FT-IR spectra of fresh and recovered (after five cycles) APO-5(1) catalyst.

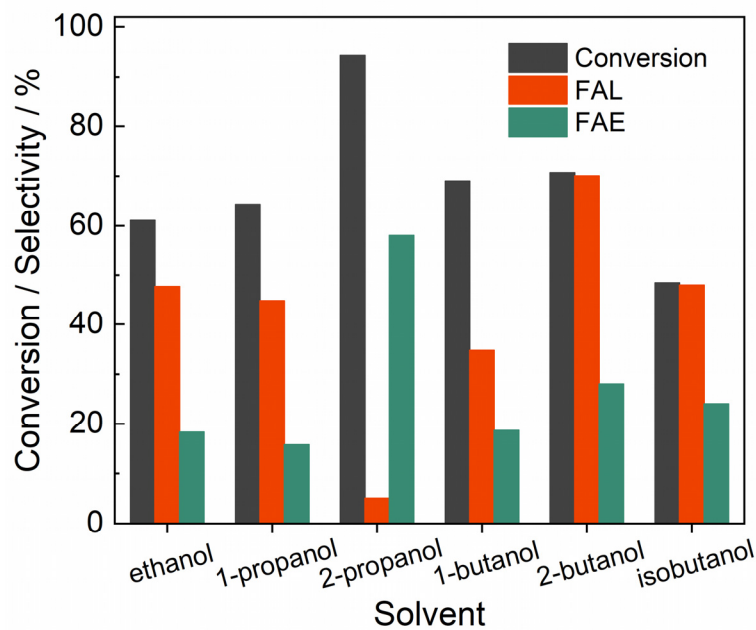


Fig. S3.7 The influence of hydrogen donor on reductive etherification of FF catalyzed by APO-5(1.5). Reaction conditions: FF (96 mg, 1 mmol), APO-5(1.5) (100 mg), solvent (3 mL), 1,4-dioxane (2 mL), 140°C, 24 h.

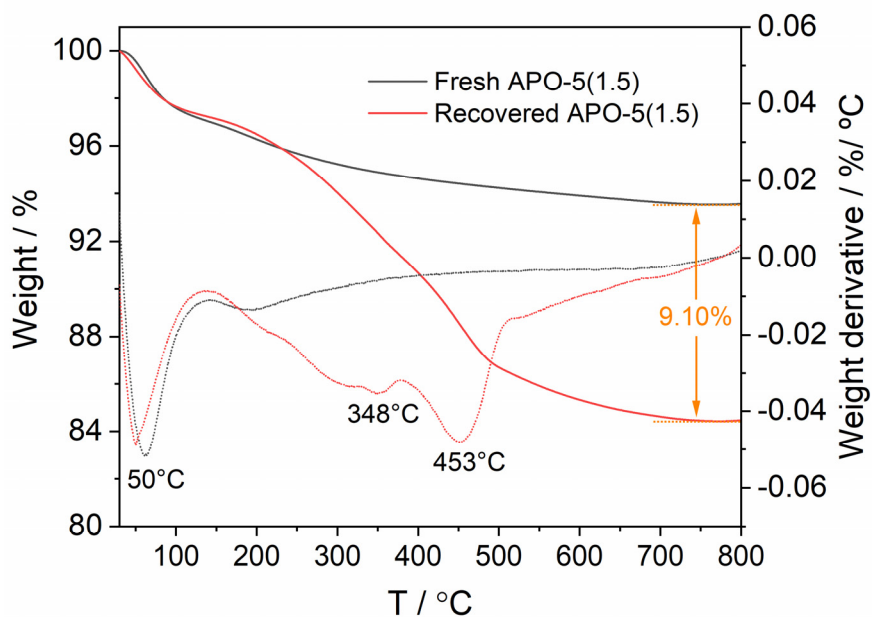


Fig. S3.8. TG curves of fresh and recovered APO-5(1.5) after one reuse.

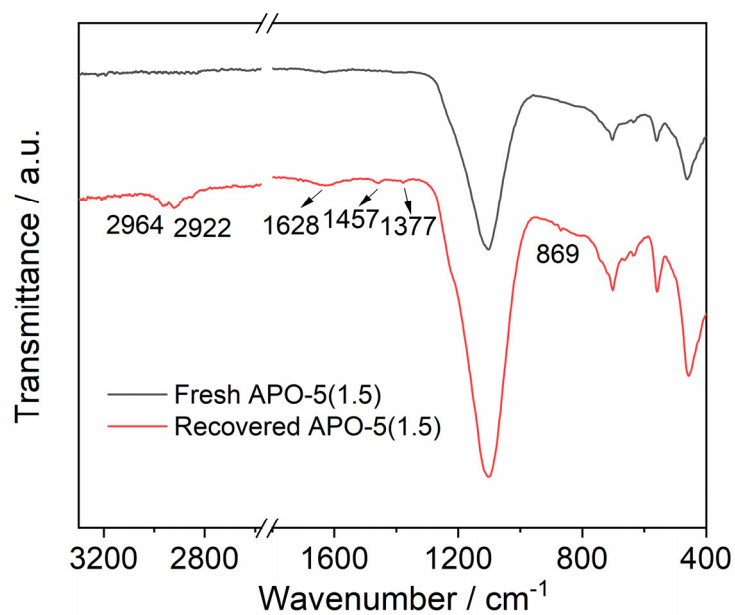


Fig. S3.9 FT-IR spectra of fresh and recovered (after one cycle) APO-5(1.5) catalyst.

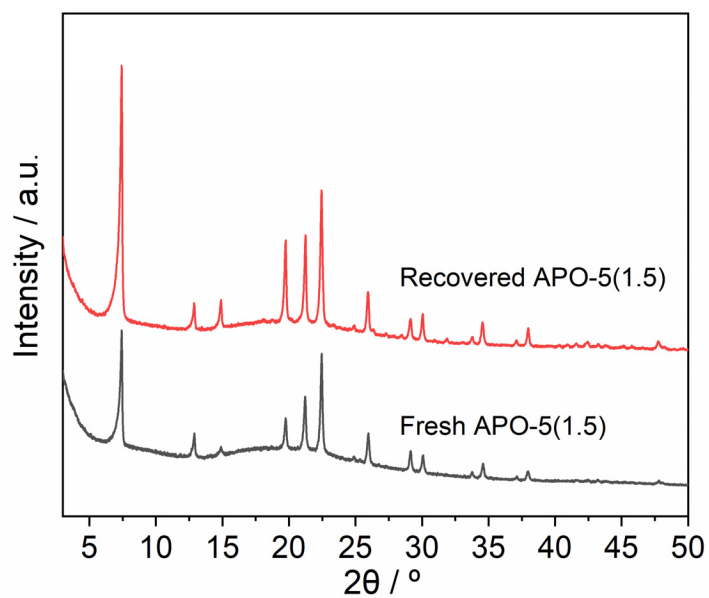


Fig. S3.10 XRD patterns of fresh and recovered (after five cycles) APO-5(1.5) catalyst.

Table S3.1 The physical properties and compositions of the samples.

Sample	S_{BET} (m^2/g) ^a	V_{total} (cm^3/g) ^b	V_{micro} (cm^3/g) ^c	V_{meso} (cm^3/g) ^d
UC/APO-5(1.5)	177	0.37	0.02	0.35
Recovered APO-5(1) ^e	29	0.08	0.00	0.08
Recovered APO-5(1.5) ^f	104	0.30	0.00	0.30

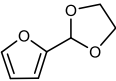
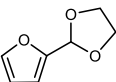
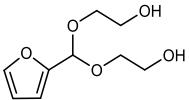
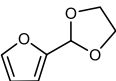
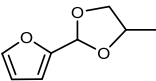
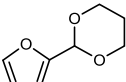
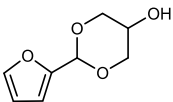
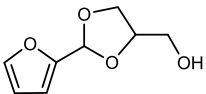
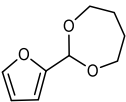
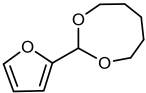
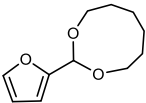
^a Calculated by Brunauer-Emmett-Teller (BET) method. ^b Calculated by single point adsorption at $P/P_0 = 0.95$. ^c Estimated by the t-plot method. ^d Calculated by subtraction of the micro pore volume from the total volume. ^e Recovered APO-5(1) catalyst after five recycles. ^f Recovered APO-5(1.5) catalyst after one recycle.

Table S3.2 Acid characteristics of APO-5 catalysts.^a

Sample	Weak sites		Medium sites		Strong sites		Total acidity (mmol/g)
	T_{max} (°C)	Acidity (mmol/g)	T_{max} (°C)	Acidity (mmol/g)	T_{max} (°C)	Acidity (mmol/g)	
APO-5(1)	164	0.0012	-	-	-	-	0.0012
APO-5(1.25)	169	0.08	239	0.11	335	0.10	0.29
APO-5(1.5)	171	0.12	244	0.16	338	0.12	0.40

^a Determined by NH_3 -TPD.

Table S3.3 Acetalization of FF in different diol solvents using APO-5(1) catalyst.^a

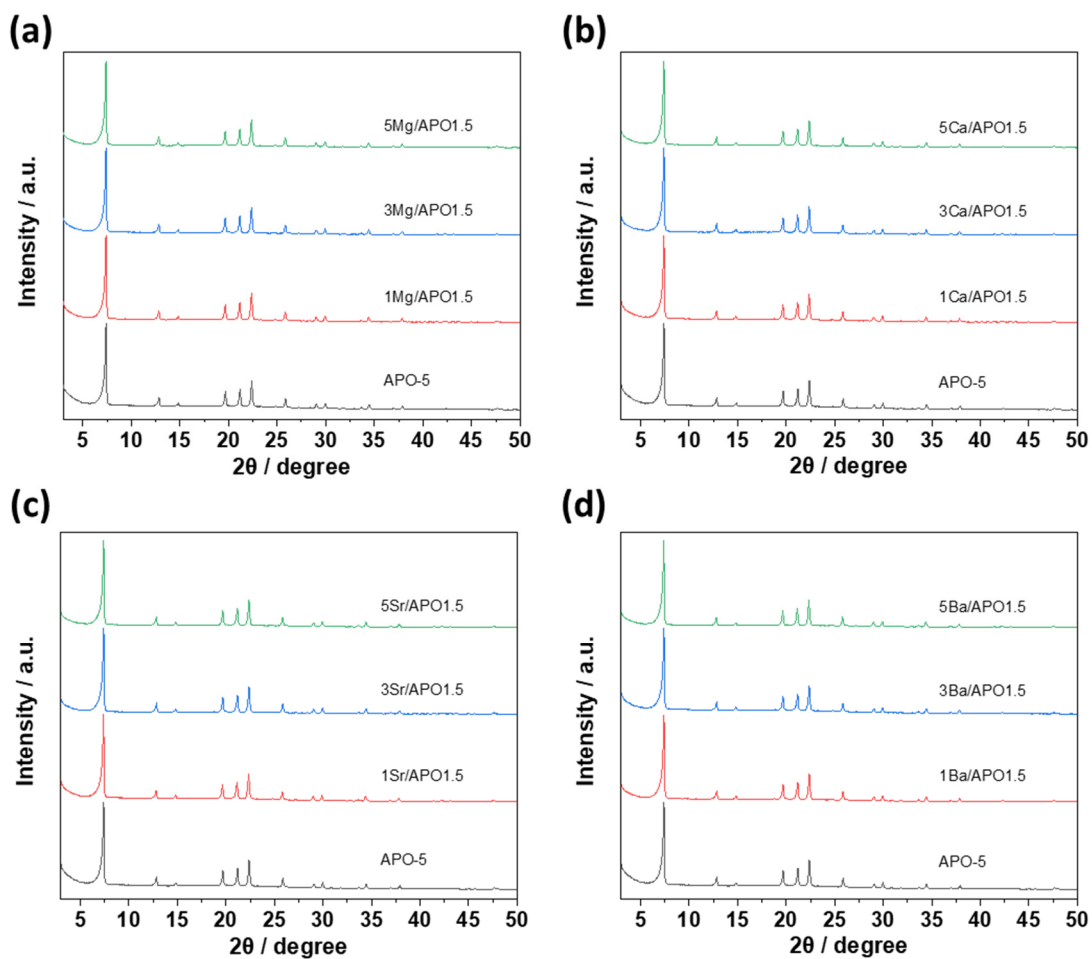
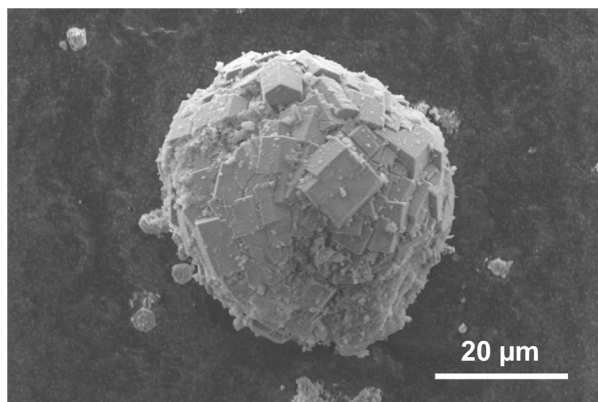
Entry	Solvent	Conv. (%) ^b		Yield (%) ^b		Yield (%) ^b
1	ethylene glycol	97.2		95.7	-	-
2 ^c	ethylene glycol	82.4		52.9		21.5
3 ^d	ethylene glycol	51.4		48.0	-	-
4	1,2-propanediol	89.4		88.4	-	-
5	1,3-propanediol	90.1		89.0	-	-
6	glycerol	84.0		36.4		35.8
7	1,4-butanediol	55.0		37.8	-	-
8	1,5-pentanediol	40.6		24.3	-	-
9	1,6-hexanediol	33.1		20.6	-	-

^a Reaction conditions: FF (96 mg, 1 mmol), APO-5(1) (100 mg), solvent (2 mL), 1,4-dioxane (3 mL), 150°C, 24 h. ^b Conversion and yield were quantified by ¹H NMR. ^c Reaction conditions: FF (96 mg, 1 mmol), APO-5(1) (100 mg), EG (5 mL), 150°C, 24 h. ^d Reaction conditions: FF (0.96 g, 10 mmol), APO-5(1) (100 mg), solvent (2 mL), 1,4-dioxane (3 mL), 150°C, 24 h.

Table S3.4 The effect of co-solvents on the catalytic activity of APO-5(1.5) catalyst.^a

Entry	Substrate	2-Propanol (mL)	1,4-Dioxane (mL)	Conv. (%) ^b	Product Yield (%) ^b		
					FAL	IPF	IPL
1	FAL	5	-	41.2	-	26.6	5.3
2	FAL	3	2	48.4	-	32.9	5.7
3 ^c	FF	5	-	94.3	5.1	54.7	12.7
4 ^c	FF	3	2	85.1	26.7	37.3	4.1

^a Reaction conditions: Substrate (1 mmol), APO-5(1.5) (100 mg), solvent (5 mL), 140°C, 6 h. ^b Conversion and yields were quantified using GC. ^c 18 μ L added H₂O. FAL: furfuryl alcohol; IPF: 2-(isopropoxymethyl)furan; IPL: isopropyl levulinate.

Appendices B – Support information for Chapter 4**Fig. S4.1** XRD patterns of AEM-loaded APO-5 catalysts.**Fig. S4.2** SEM image of APO-5 catalyst.

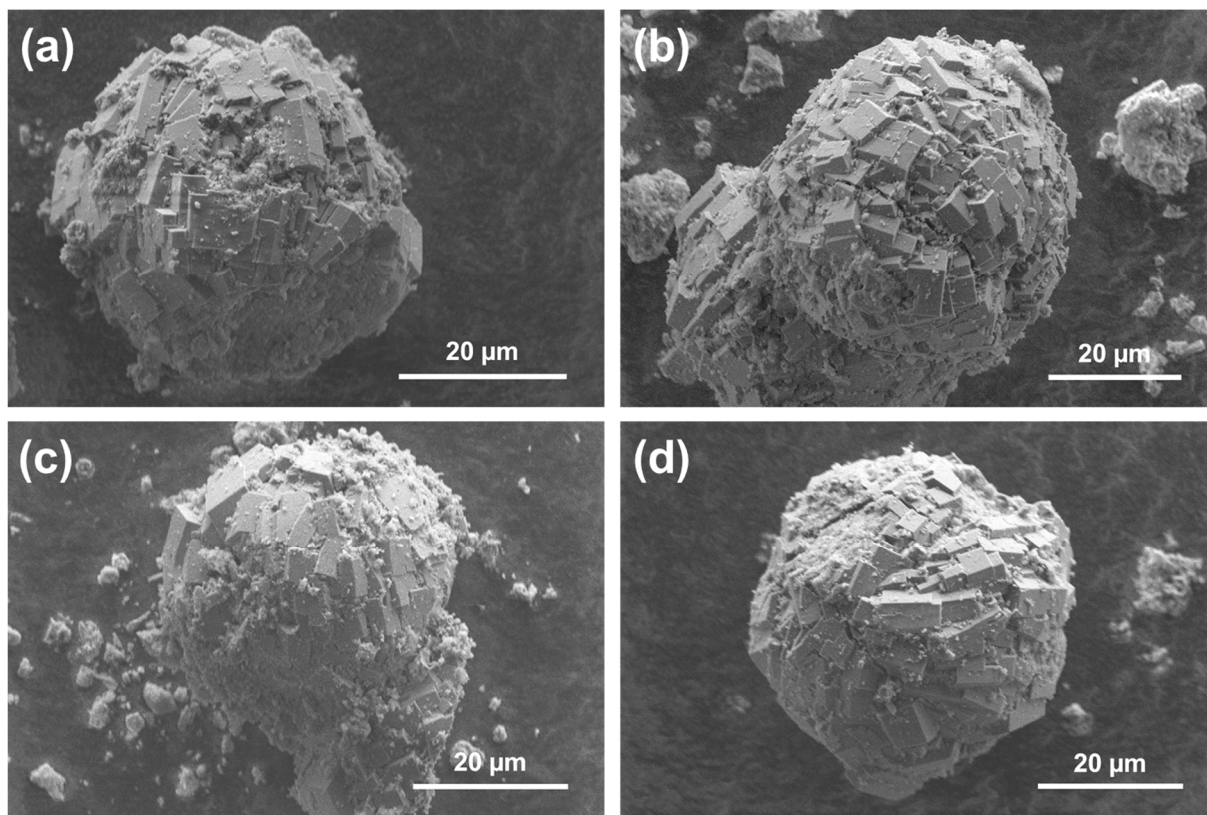


Fig. S4.3 SEM images of (a) 5Mg/APO1.5, (b) 5Ca/APO1.5, (c) 5Sr/APO1.5, and (d) 5Ba/APO1.5 catalysts.

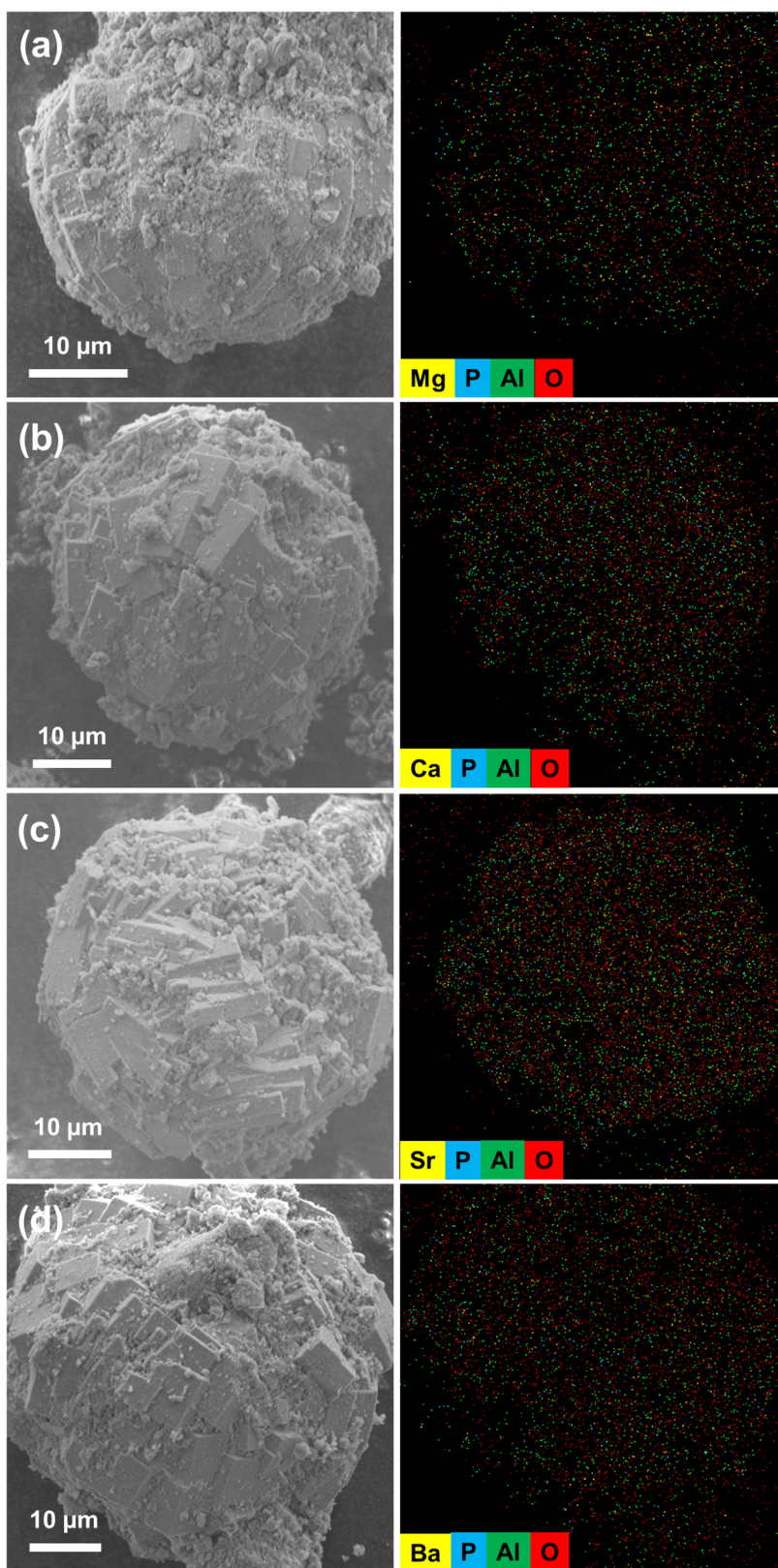


Fig. S4.4 EDS mapping of (a) 5Mg/APO1.5, (b) 5Ca/APO1.5, (c) 5Sr/APO1.5, and (d) 5Ba/APO1.5 catalysts.

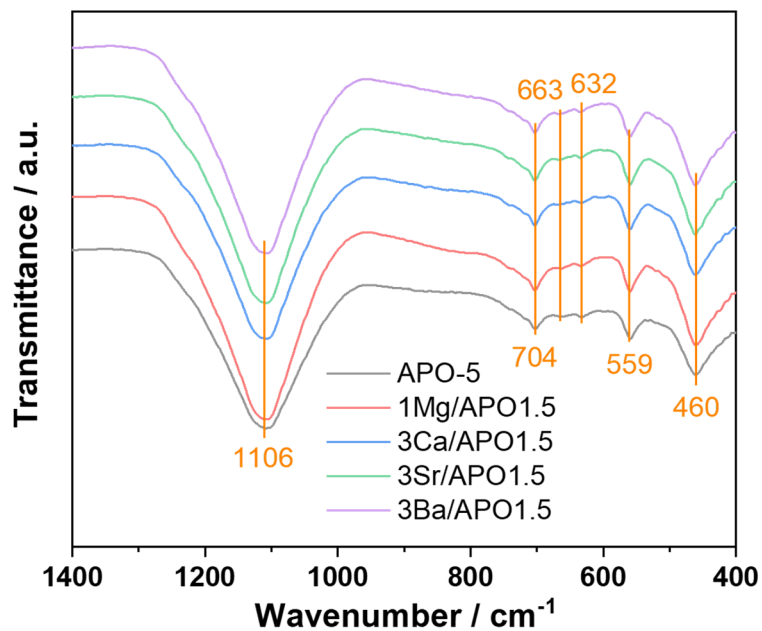


Fig. S4.5 FT-IR spectra of APO-5 and AEM-loaded APO-5 catalysts.

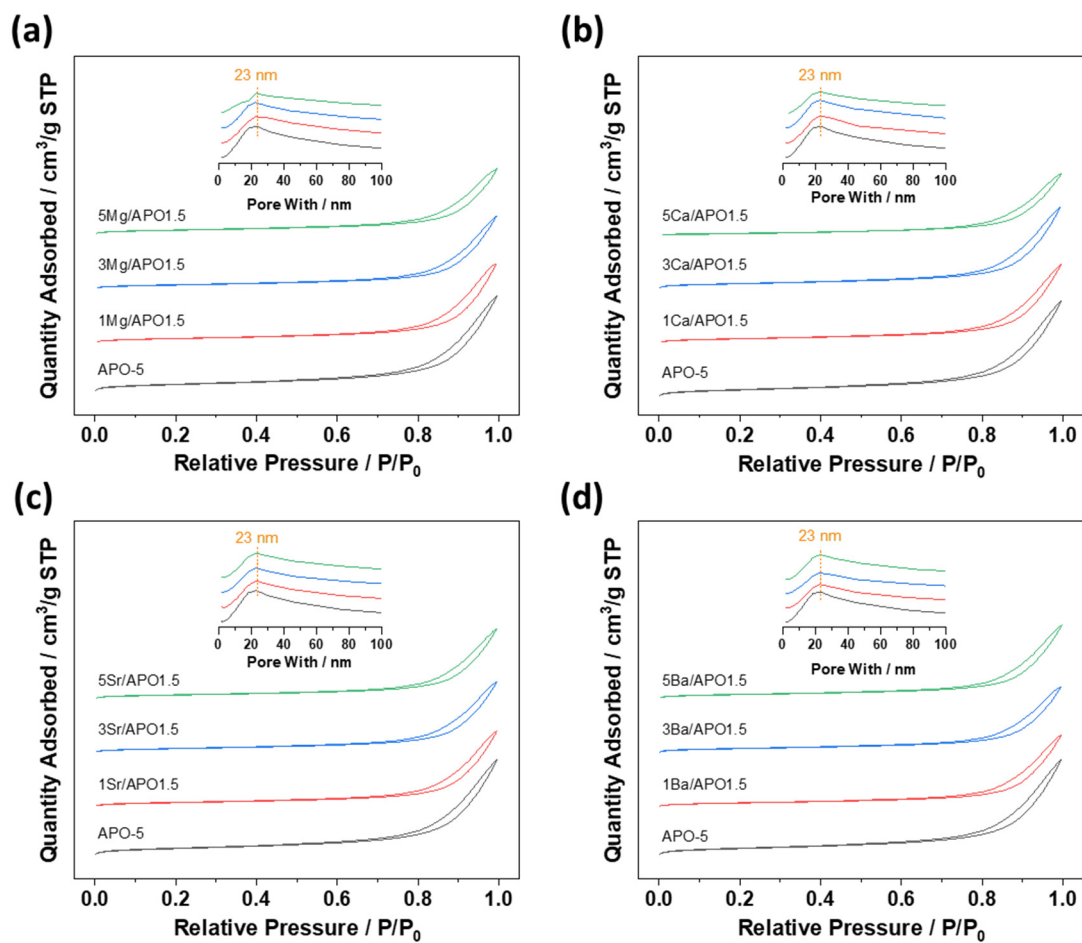


Fig. S4.6 N_2 adsorption-desorption isotherms (inset: BJH mesopore size distribution) of APO-5 and AEM-loaded APO-5 catalysts.

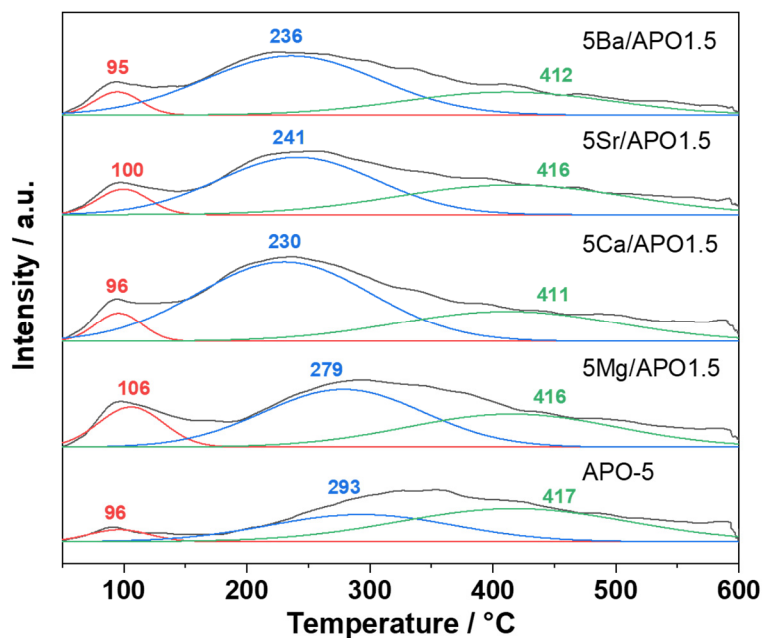


Fig. S4.7 CO₂-TPD profiles of APO-5, 5Mg/APO1.5, 5Ca/APO1.5, 5Sr/APO1.5 and 5Ba/APO1.5 catalysts.

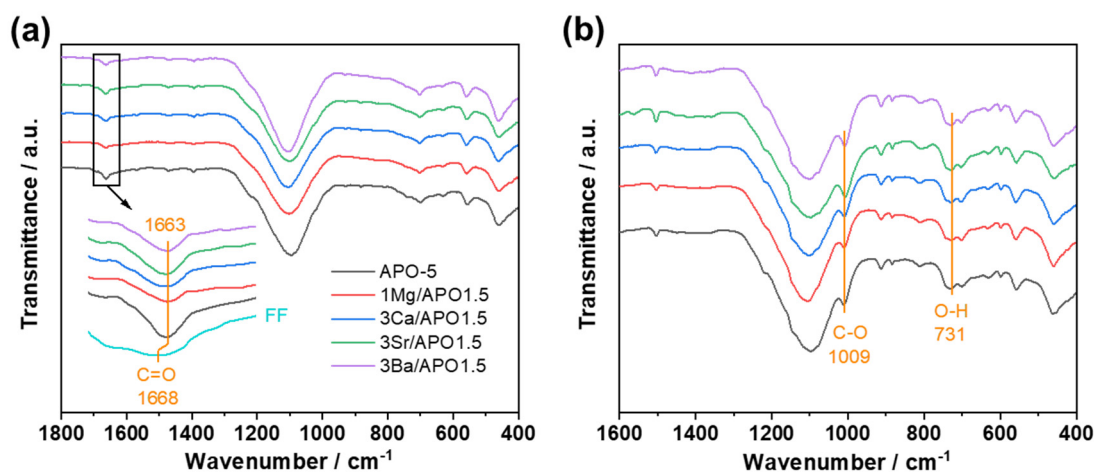


Fig. S4.8 FT-IR spectra of APO-5 and AEM-loaded APO-5 catalysts with pre-adsorbed (a) FF and (b) FAL.

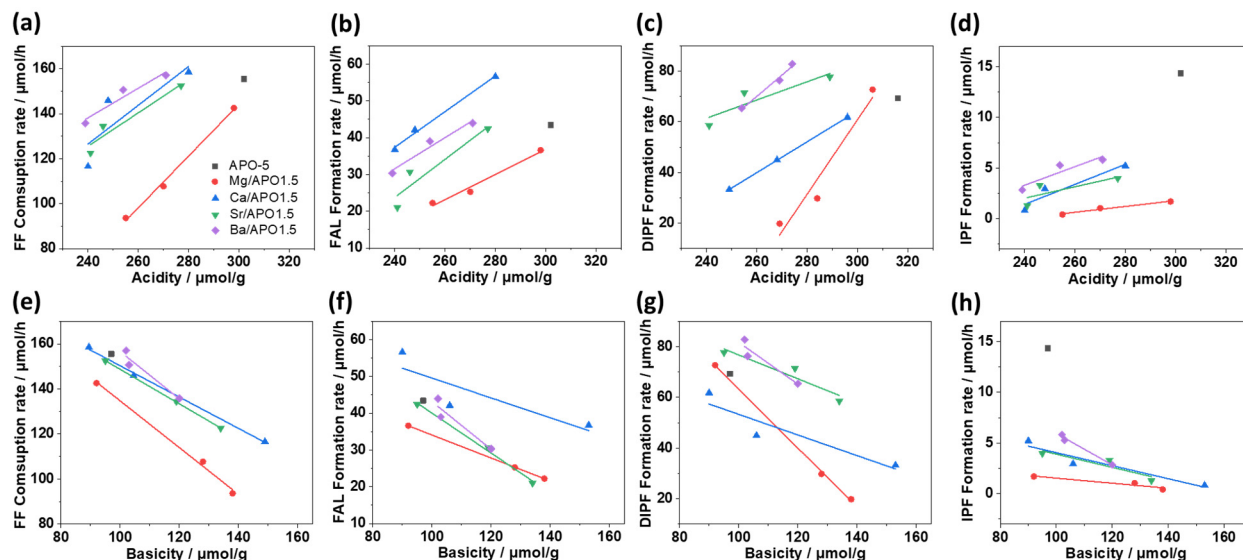


Fig. S4.9 Correlations between acidity/basicity, FF consumption rate and FAL/DIPF/IPF formation rate of the APO-5 and AEM-loaded APO-5 catalysts. Reaction conditions: (a)-(c) and (e)-(g) FF (96 mg, 1 mmol), catalyst (50 mg), 2-propanol (5 mL), 140°C, 2 h; (d) and (h) FAL (98 mg, 1 mmol), catalyst (50 mg), 2-propanol (5 mL), 140°C, 6 h.

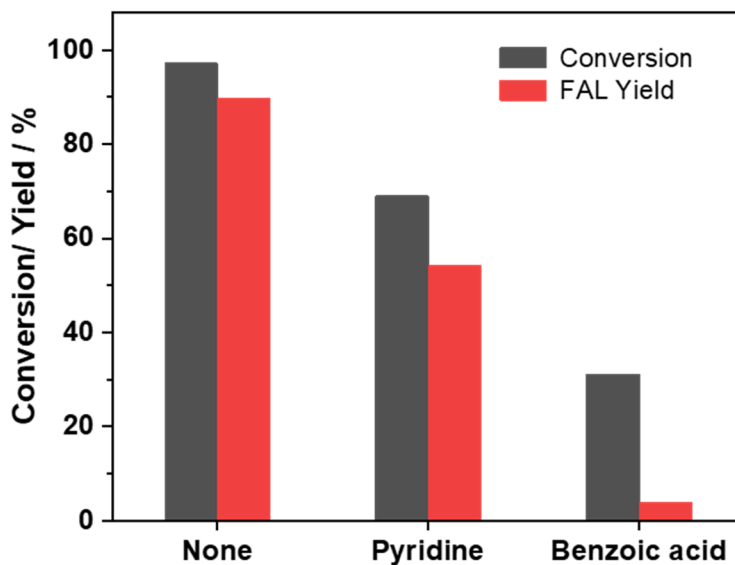


Fig. S4.10 CTH of FF to FAL with 3Ca/APO1.5 catalyst. Reaction conditions: FF (96 mg, 1 mmol), 3Ca/APO1.5 (50 mg), additive (100 mg), 2-propanol (5 mL), 140°C, 48 h.

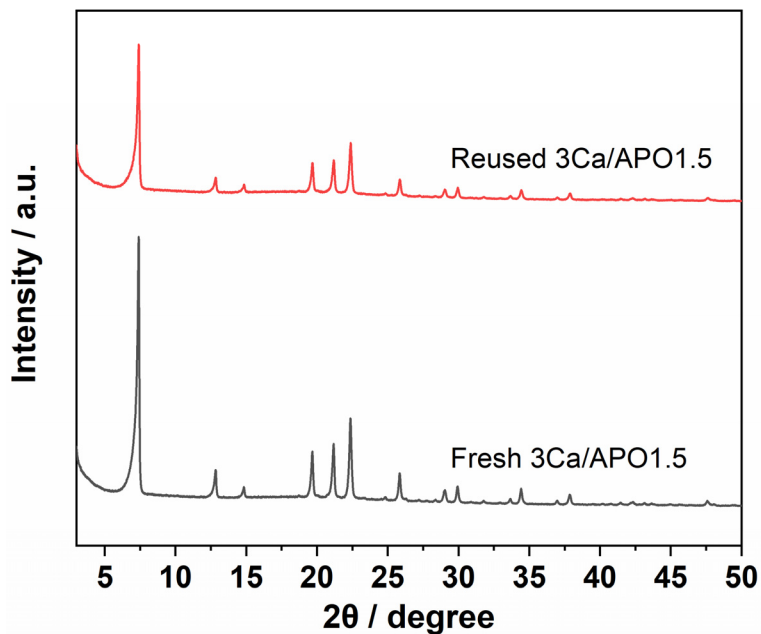


Fig. S4.11 XRD patterns of fresh and reused (after four reaction cycles) 3Ca/APO1.5 catalyst.

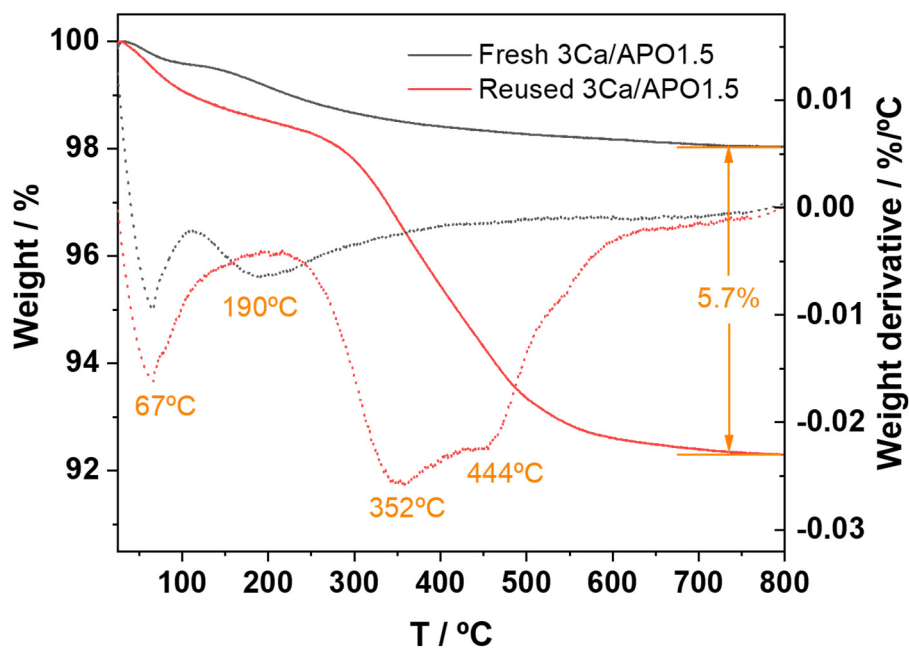


Fig. S4.12 TG curves of fresh and reused (after four reaction cycles) 3Ca/APO1.5 catalyst.

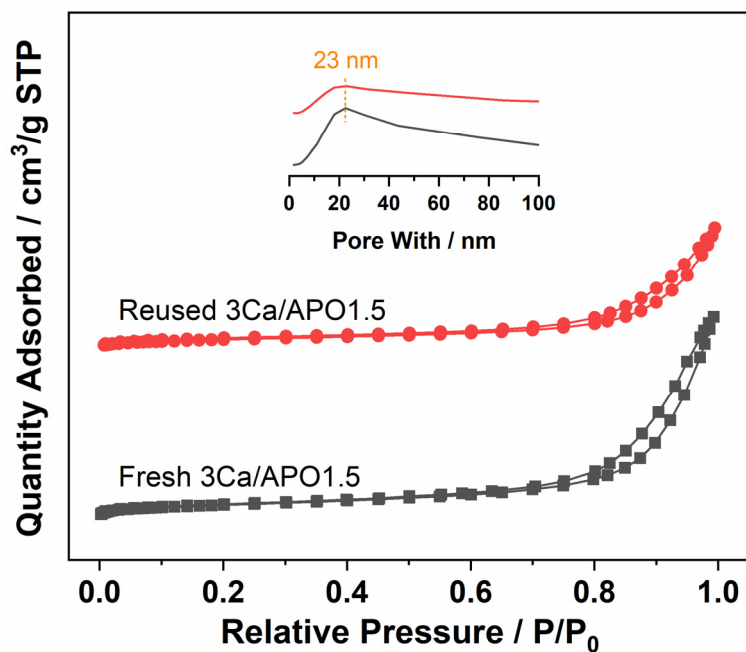


Fig. S4.13 N_2 adsorption-desorption isotherms (inset: BJH mesopore size distribution) of fresh and reused (after four reaction cycles) 3Ca/APO1.5 catalyst.

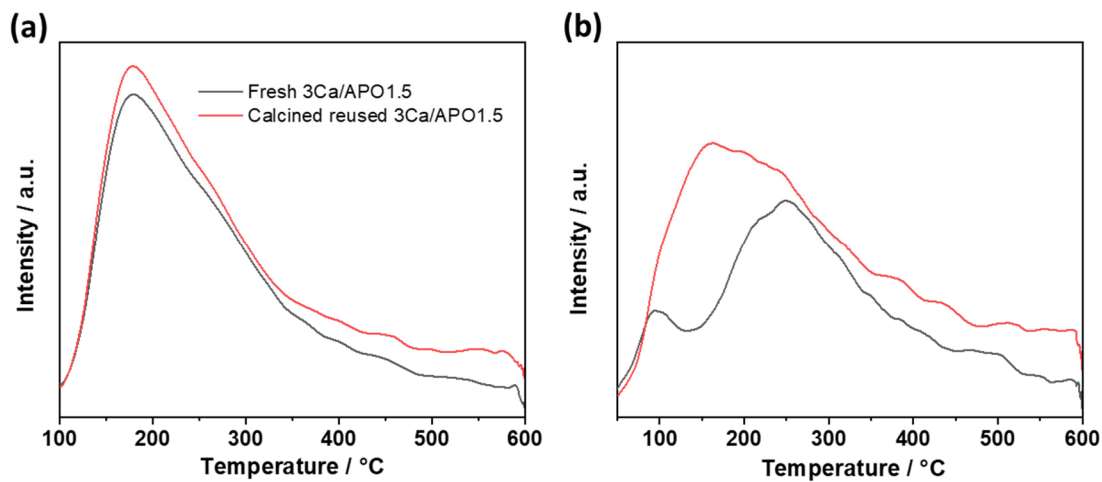


Fig. S4.14 NH_3 -TPD and CO_2 -TPD profiles of calcined 3Ca/APO1.5 catalyst (after four reaction cycles).

Table S4.1 Crystalline size and unit cell size of APO-5 and AEM-loaded APO-5 catalysts.

Catalyst	Unit cell parameter		
	a (Å)	c (Å)	V (Å ³)
APO-5	13.78	8.38	1378.08
1Mg/APO1.5	13.78	8.38	1378.08
3Mg/APO1.5	13.78	8.38	1378.08
5Mg/APO1.5	13.79	8.39	1381.72
1Ca/APO1.5	13.78	8.38	1378.08
3Ca/APO1.5	13.78	8.38	1378.08
5Ca/APO1.5	13.78	8.38	1378.08
1Sr/APO1.5	13.80	8.39	1383.73
3Sr/APO1.5	13.78	8.38	1378.08
5Sr/APO1.5	13.78	8.38	1378.08
1Ba/APO1.5	13.78	8.38	1378.08
3Ba/APO1.5	13.78	8.39	1379.72
5Ba/APO1.5	13.80	8.39	1383.73

Table S4.2 The conversion of FF using 2-propanol as H-donor over APO-5 catalysts.

Catalyst	Conv. (%) ^b	Product yield (%) ^b			
		FAL	DIPF	IPF	IPL
APO-5+CaO	58.3	27.1	5.8	6.0	0

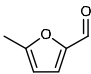
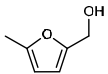
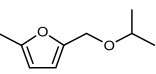
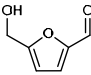
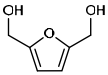
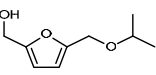
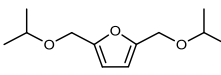
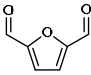
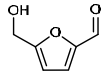
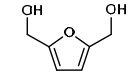
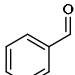
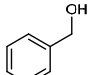
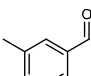
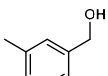
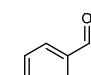
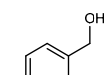
^a Reaction conditions: FF (96 mg, 1 mmol), catalyst (50 mg), 2-propanol (5 mL), 140°C, 24 h. ^b Conversion and yield were quantified using GC.

Table S4.3 The physical properties and compositions of the samples.

Catalyst	Ca content (wt.%) ^a	S _{BET} (m ² /g) ^b	V _{total} (cm ³ /g) ^c	V _{micro} (cm ³ /g) ^d	V _{meso} (cm ³ /g) ^e	Acidity (μmol/g) ^f	Basicity (μmol/g) ^g
3Ca/APO1.5	2.9	106	0.30	0.01	0.29	248	106
3Ca/APO1.5 (reused) ^h	2.2 ⁱ	49	0.17	0.00	0.17	264 ⁱ	198 ⁱ

^a Determined by XRF. ^b Calculated by Brunauer-Emmett-Teller (BET) method. ^c Calculated by single point adsorption at P/P₀ = 0.95. ^d Estimated by the t-plot method. ^e Calculated by subtraction of the micro pore volume from the total volume. ^f Determined by NH₃-TPD. ^g Determined by CO₂-TPD. ^h 3Ca/APO1.5 catalyst after four reaction cycles. ⁱ Calcined 3Ca/APO1.5 catalyst (after four reaction cycles).

Table S4.4 CTH of various carbonyl molecules with 3Ca/APO1.5 catalyst.^a

En try	Substrate	Product	Conv. (%) ^b	Yield (%) ^b	Product	Yield (%) ^b	Product	Yield (%) ^b
1			93.2	90.6		1.9		
2			81.8	76.4		2.6		2.2
3			94.4	48.1		46.3		
4			91.9	91.0				
5			90.5	90.0				
6			91.8	91.0				

^a Reaction conditions: substrate (1 mmol), catalyst (50 mg), 2-propanol (5 mL), 140°C, 48 h. ^b Conversion and yield were quantified using ¹H NMR and GC-MS.

Appendices C – Support information for Chapter 5

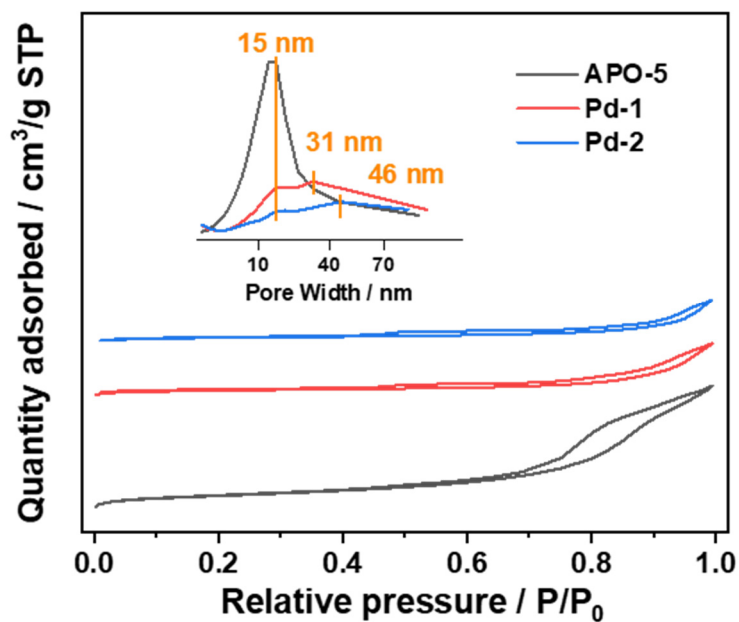


Fig. S5.1 N₂ adsorption-desorption isotherms (inset: BJH mesopore size distribution) of APO-5, Pd-1, and Pd-2.

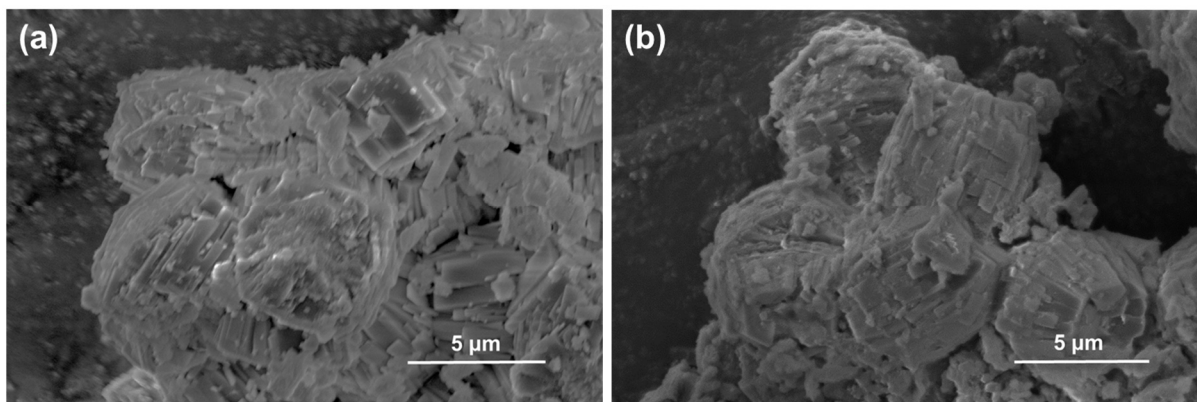


Fig. S5.2 SEM images of APO-5 and Pd-2.

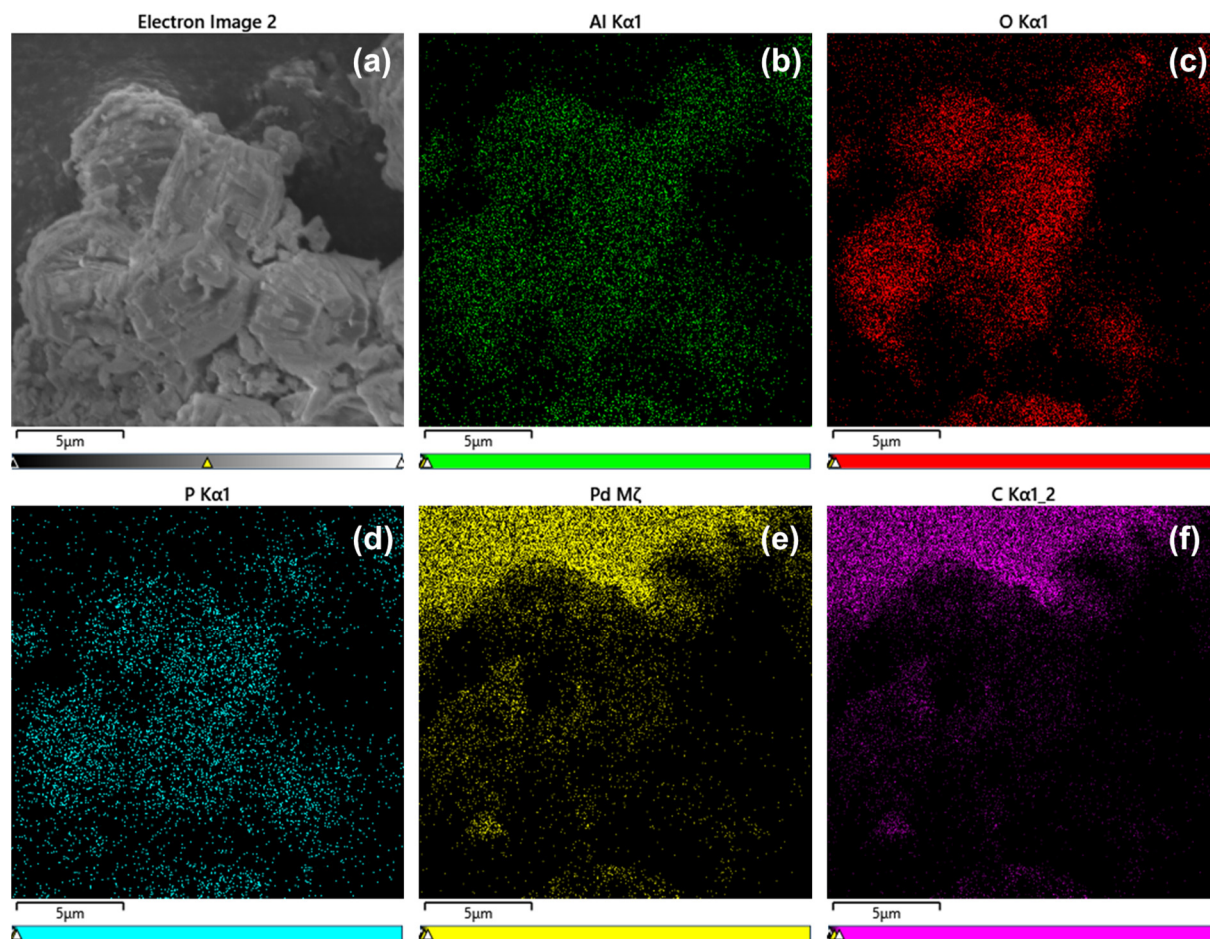


Fig. S5.3 EDS mapping of Pd-2.

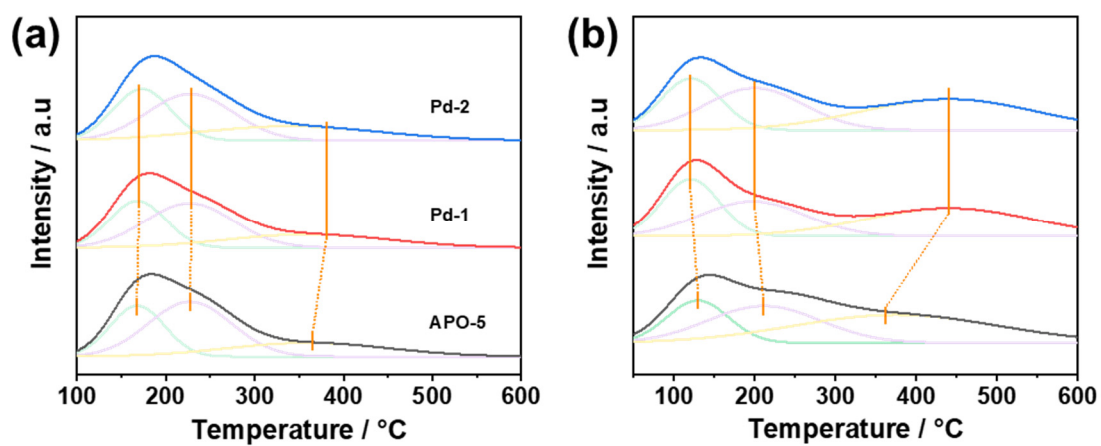


Fig. S5.4 (a) NH₃-TPD and (b) CO₂-TPD profiles of APO-5, Pd-1, and Pd-2.

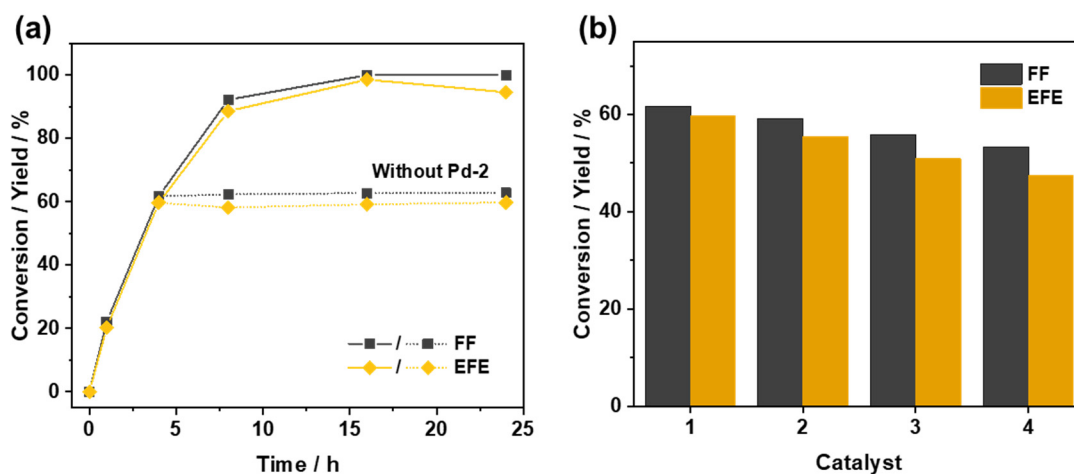


Fig. S5.5 (a) Leaching study with the Pd-2 catalyst. Reaction conditions: FF (96 mg, 1 mmol), Pd-2 (50 mg), FA (0.38 mL, 10 mmol), ethanol (4.62 mL), 140°C. (b) Recycling study with the Pd-2 catalyst. Reaction conditions: FF (96 mg, 1 mmol), Pd-2 (50 mg), FA (0.38 mL, 10 mmol), ethanol (4.62 mL), 140°C, 4 h.

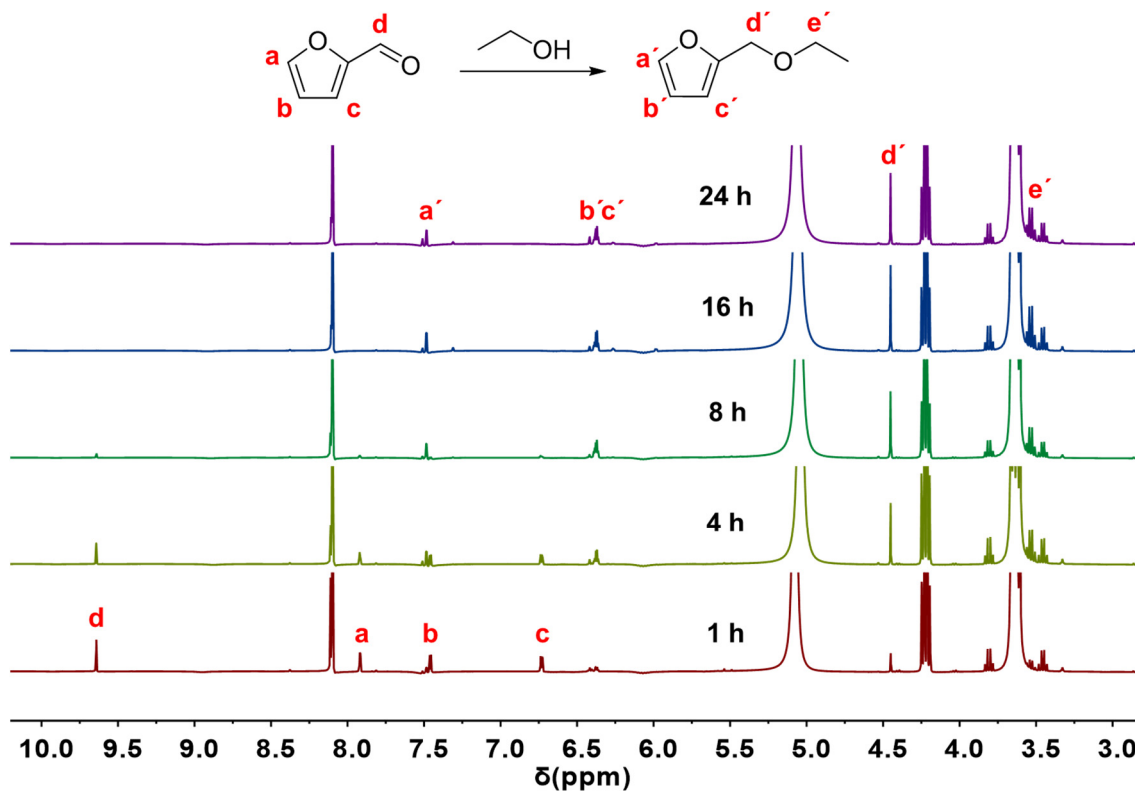


Fig. S5.6 ¹H NMR spectra of the reaction mixtures at different reaction times. Reaction conditions: FF (96 mg, 1 mmol), Pd-2 (50 mg), FA (0.38 mL, 10 mmol), EtOH (4.62 mL), 140°C.

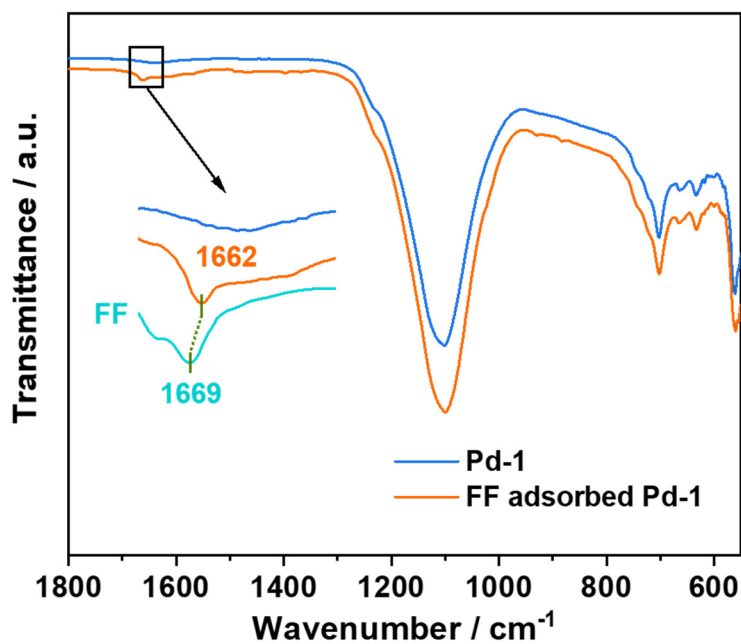
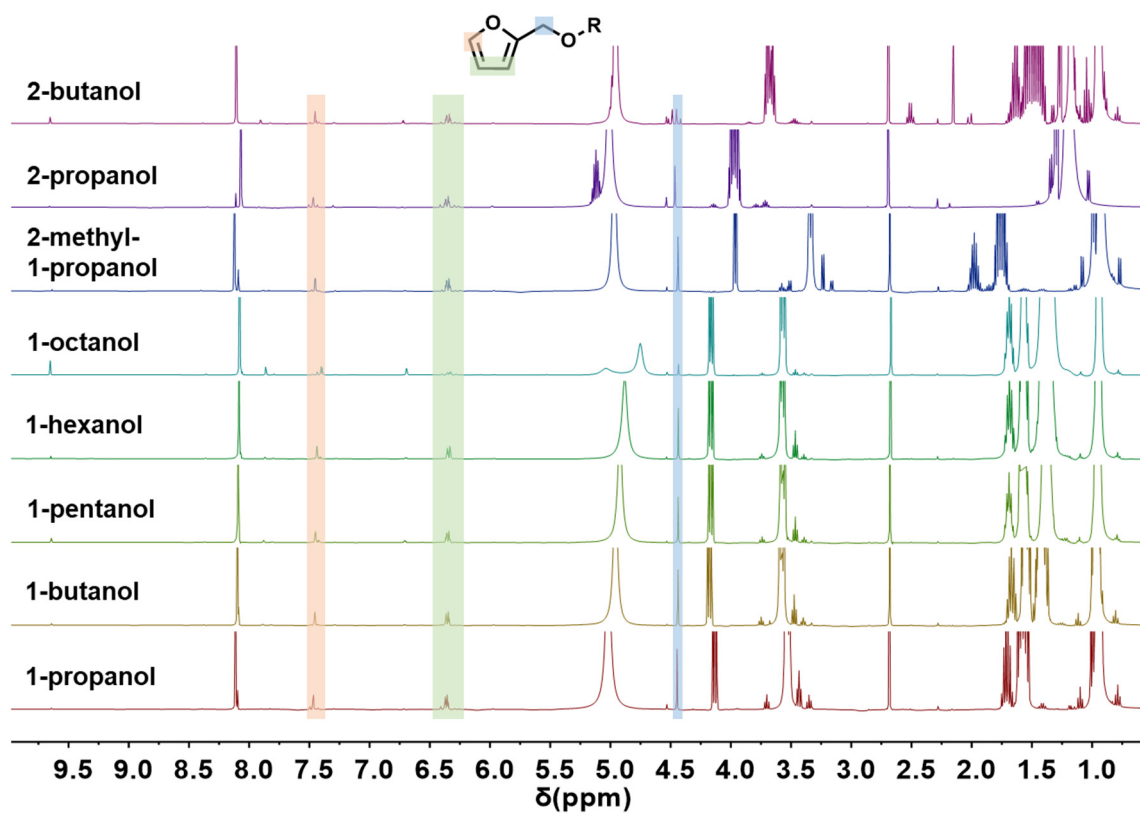
**Fig. S5.7** FT-IR spectra of fresh and FF pre-adsorbed Pd-2.**Fig. S5.8** ^1H NMR spectra of the products in Table 5.1.

Table S5.1 Textural properties of APO-5 and Pd-loaded APO-5.

Sample	Pd-loading (wt.%) ^a	S _{total} (m ² /g) ^b	V _{micro} (cm ³ /g) ^c	V _{meso} (cm ³ /g) ^d	Acidity (mmol/g) ^e	Basicity (mmol/g) ^f
APO-5	-	192	0.05	0.25	0.29	0.24
Pd-1	1.72	163	0.06	0.10	0.20	0.24
Pd-2	2.45	129	0.05	0.05	0.21	0.24

^a Determined by XRF. ^b Calculated by the BET method. ^c Estimated by t-plot method. ^d Calculated by subtracting the micropore volume from the total pore volume. ^e Determined by NH₃-TPD. ^f Determined by CO₂-TPD.

Table S5.2 Acidic characteristics of APO-5 and Pd-loaded APO-5.^a

Sample	Weak sites		Medium sites		Strong sites		Total acidity (mmol/g)
	T _{max} (°C)	Acidity (mmol/g)	T _{max} (°C)	Acidity (mmol/g)	T _{max} (°C)	Acidity (mmol/g)	
APO-5	173	0.09	239	0.13	371	0.07	0.29
Pd-1	168	0.06	227	0.09	360	0.05	0.20
Pd-2	168	0.06	227	0.10	360	0.05	0.21

^a Determined by NH₃-TPD.

Table S5.3 Basic characteristics of APO-5 and Pd-loaded APO-5.^a

Sample	Weak sites		Medium sites		Strong sites		Total basicity (mmol/g)
	T _{max} (°C)	Basicity (mmol/g)	T _{max} (°C)	Basicity (mmol/g)	T _{max} (°C)	Basicity (mmol/g)	
APO-5	129	0.05	211	0.08	375	0.11	0.24
Pd-1	121	0.07	197	0.08	441	0.09	0.24
Pd-2	121	0.06	200	0.08	440	0.10	0.24

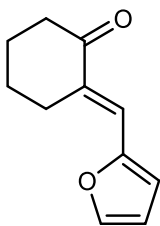
^a Determined by CO₂-TPD.

Table S5.4 Catalytic performances.^a

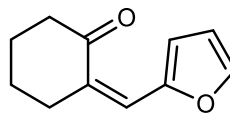
Substrate	Catalyst	Conv. (%) ^b	Yield (%) ^b				Carbon loss (%)
			FAL	DEF	MF	EFE	
FAL	APO-5	41	-	0	0	15	26
FF	Pd/C ^c	18	1	4	0	3	10

^a Reaction conditions: Substrate (1 mmol), catalyst (50 mg), FA (0.38 mL, 10 mmol), ethanol (4.62 mL), 140°C, 4 h. ^b Quantified using ¹H NMR. ^c 5 wt.% Pd/C (20 mg).

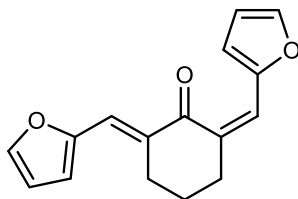
Appendices D – Support information for Chapter 6



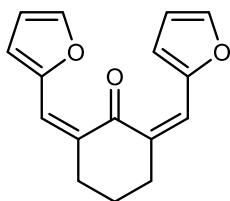
(E)-2-(furan-2-ylmethylene)cyclohexan-1-one



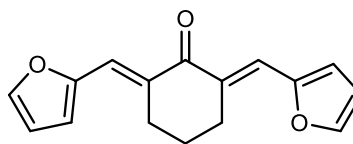
(Z)-2-(furan-2-ylmethylene)cyclohexan-1-one



(2Z,6E)-2,6-bis(furan-2-ylmethylene)cyclohexan-1-one / (2E,6Z)-2,6-bis(furan-2-ylmethylene)cyclohexan-1-one



(2Z,6Z)-2,6-bis(furan-2-ylmethylene)cyclohexan-1-one



(2E,6E)-2,6-bis(furan-2-ylmethylene)cyclohexan-1-one

Fig. S6.1 The structures of the *cis* and *trans* isomers of C₁₁ and C₁₆.

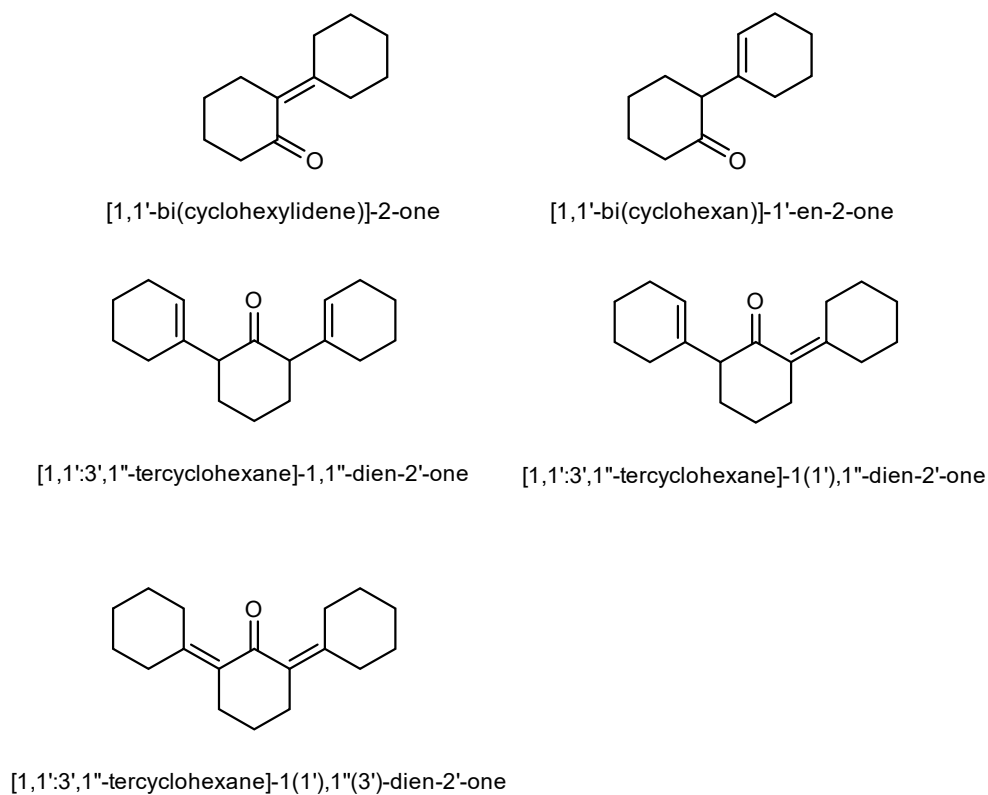


Fig. S6.2 The structures of the stereoisomers of C₁₂ and C₁₈.

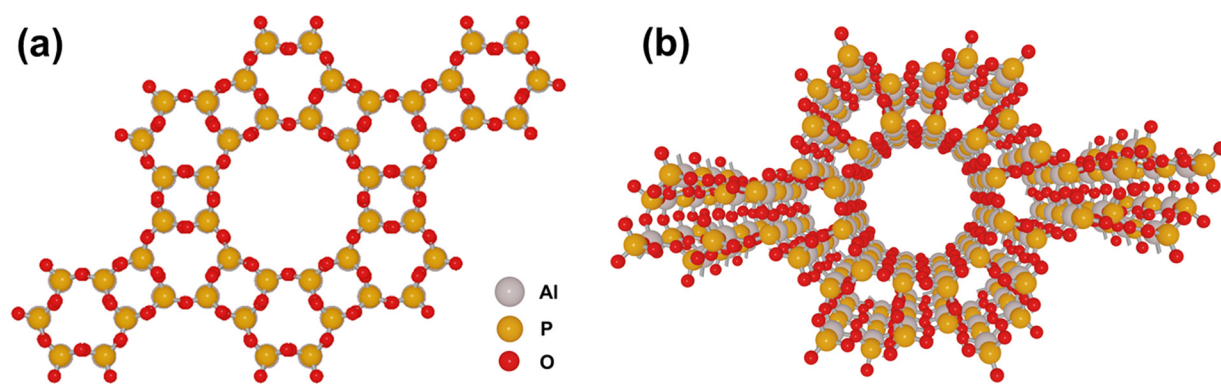


Fig. S6.3 Computational model of APO-5.

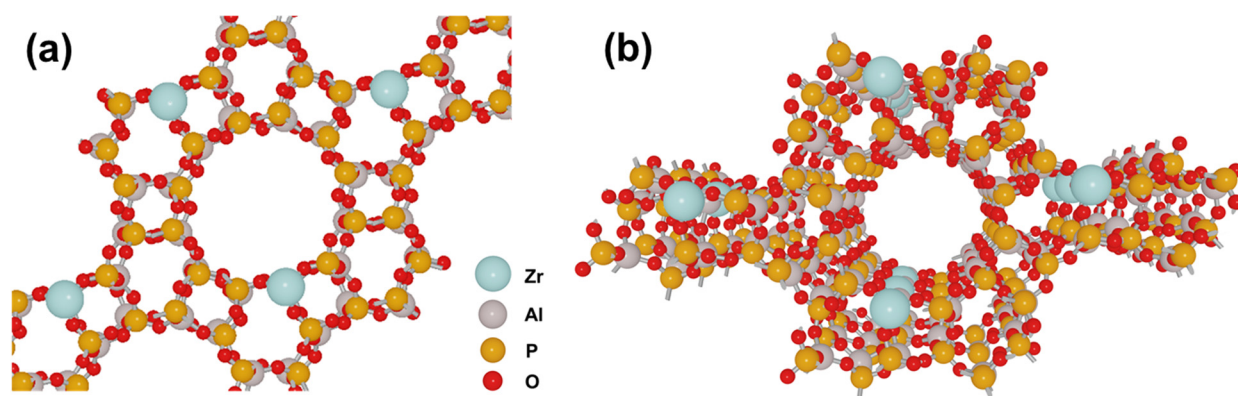


Fig. S6.4 Computational model of ZrAPO-5.

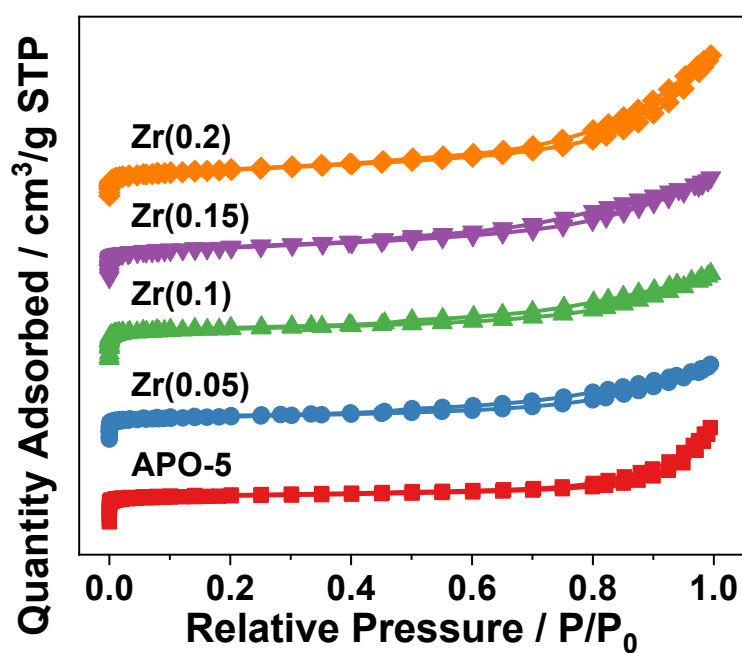


Fig. S6.5 N_2 adsorption-desorption isotherms of APO-5 and ZrAPO-5 catalysts.

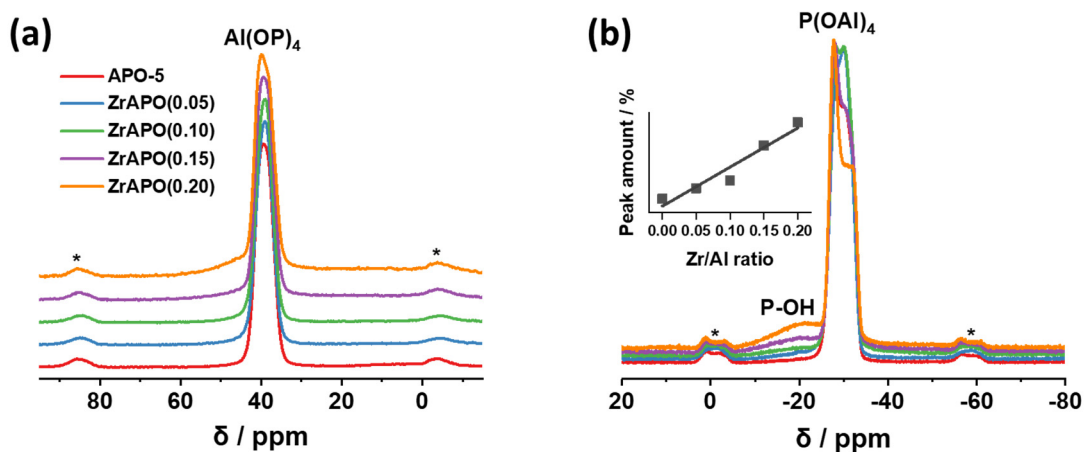


Fig. S6.6 (a) ^{27}Al MAS and (b) ^{31}P MAS NMR spectra of APO-5 and ZrAPO-5 catalysts (* corresponds to spinning side bands; inset: relationship between peak amount and Zr/Al ratio).

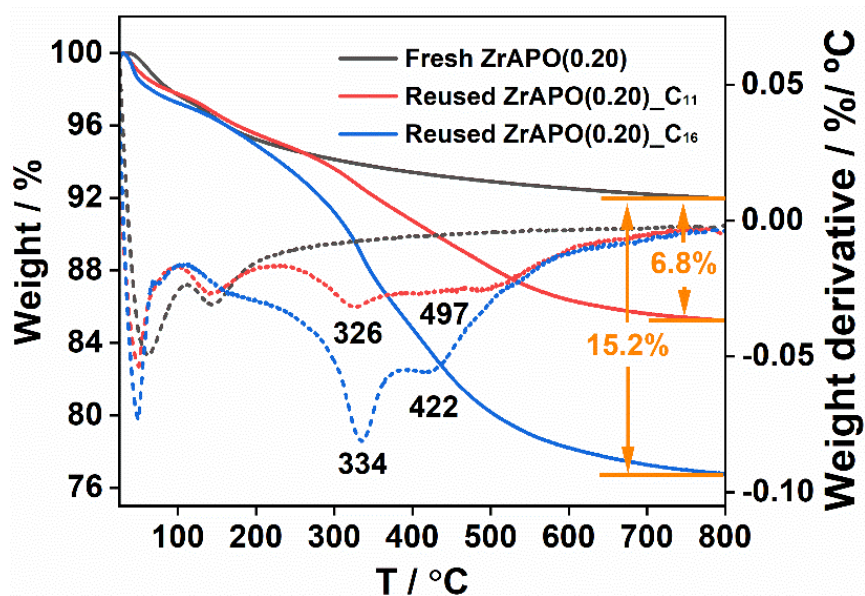


Fig. S6.7 TG analysis of fresh and used ZrAPO(0.20) catalyst after the second reaction run under neat reaction conditions (ZrAPO(0.20)_{C11}) and after the first reaction run in toluene solution (ZrAPO(0.20)_{C16}).

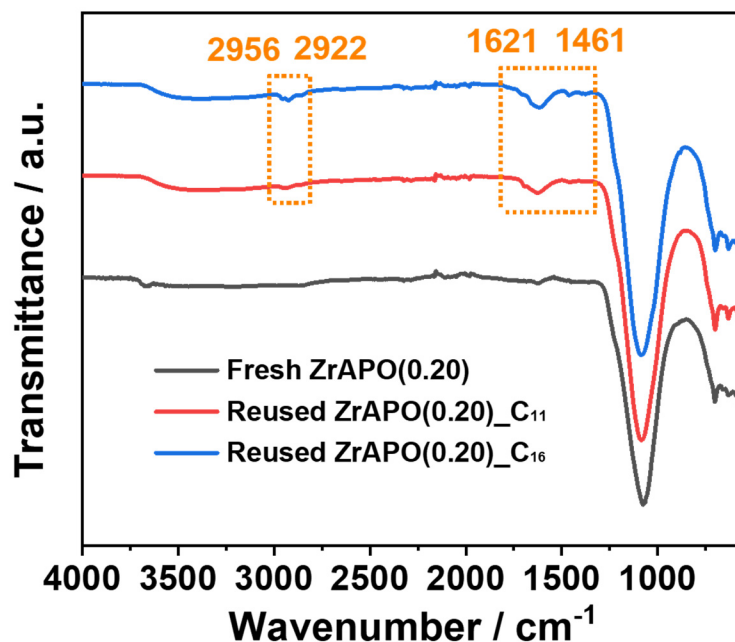


Fig. S6.8 FT-IR spectra of fresh and used ZrAPO(0.20) catalyst after the second reaction run under neat reaction conditions (ZrAPO(0.20)_C₁₁) and after the first reaction run in toluene solution (ZrAPO(0.20)_C₁₆).

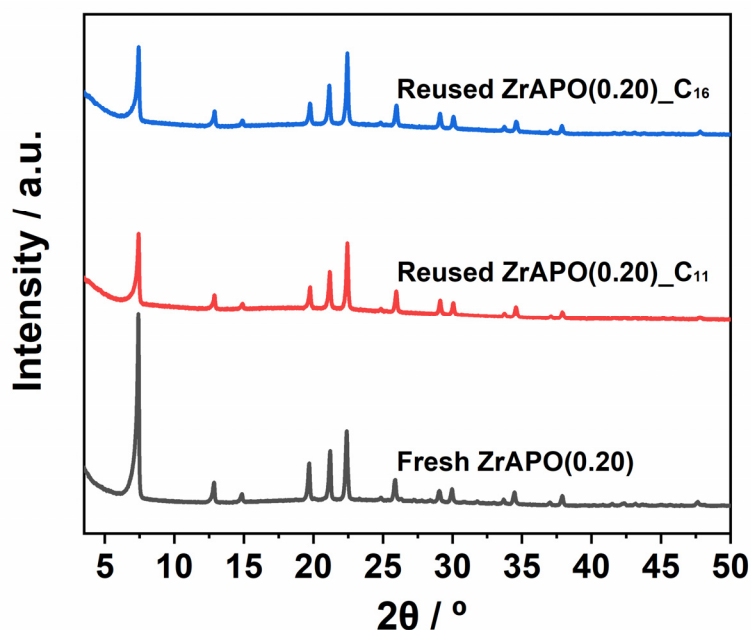
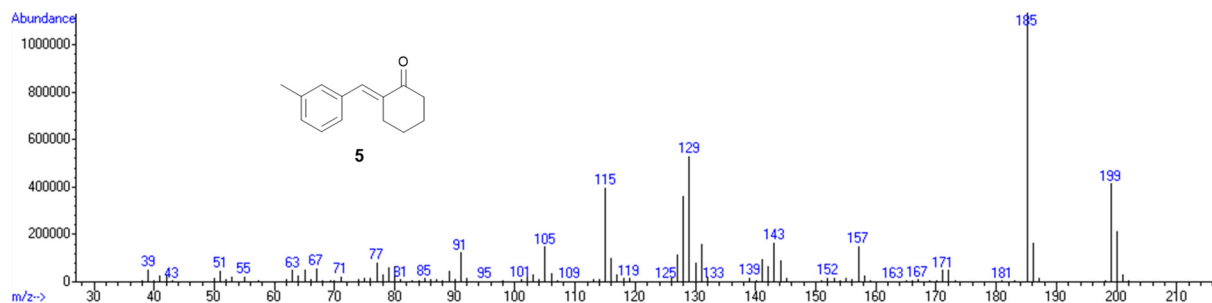
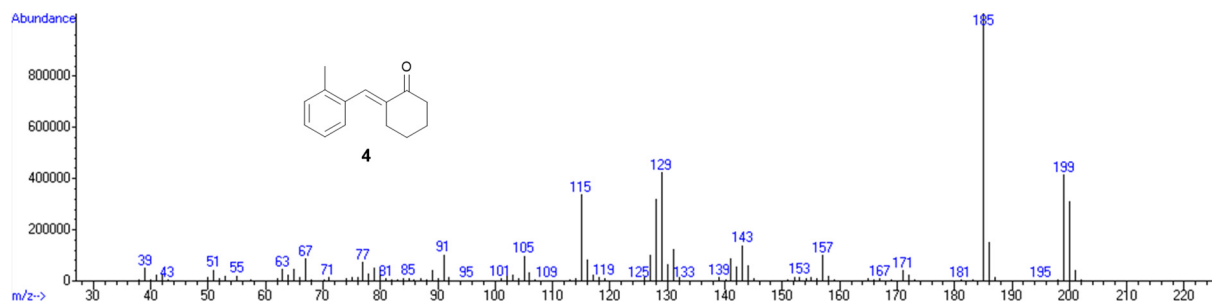
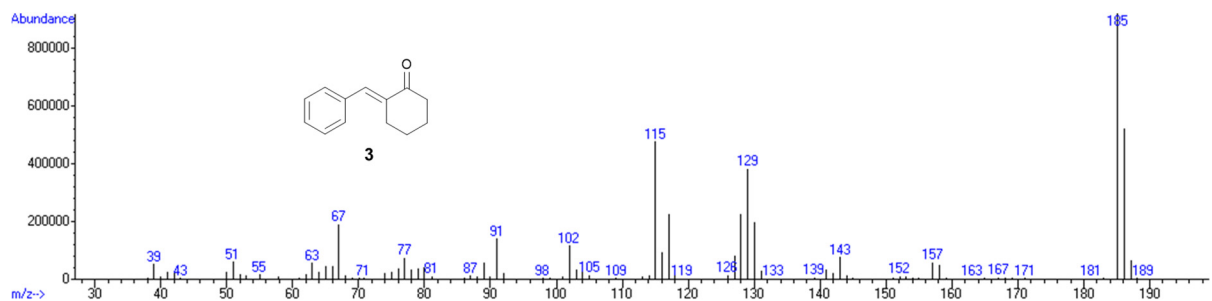
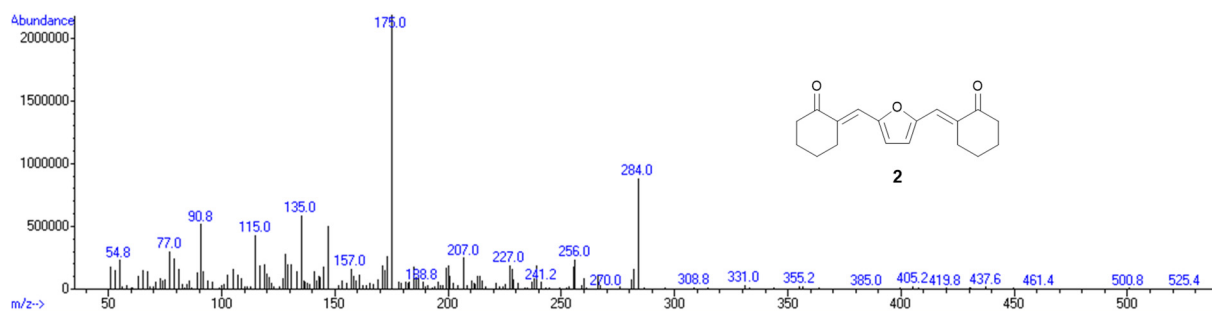
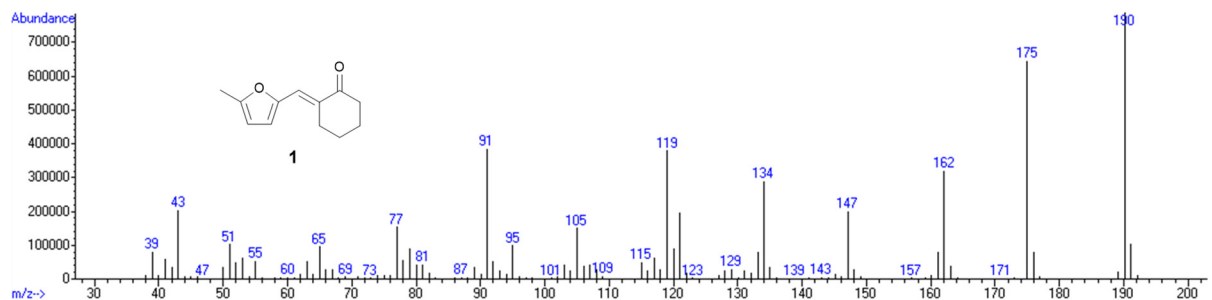
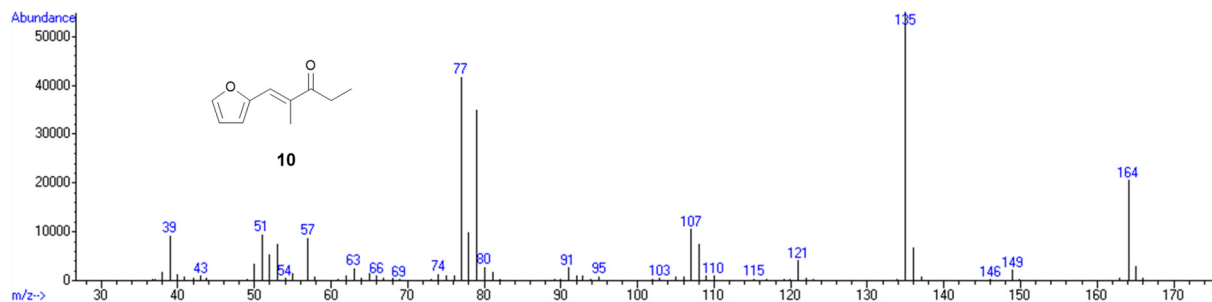
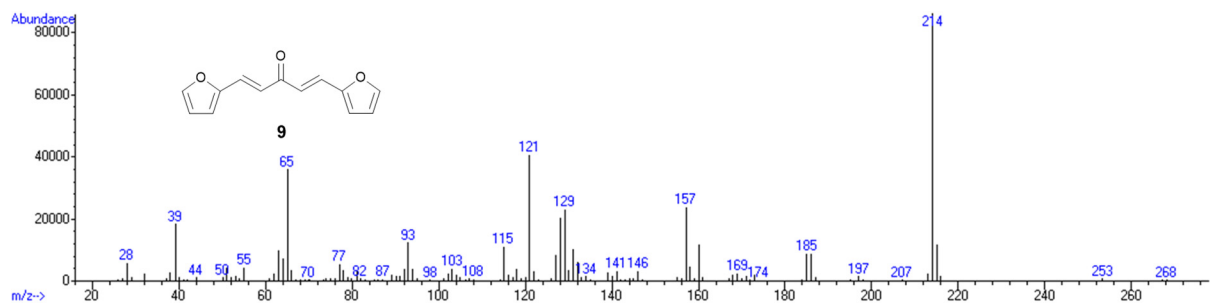
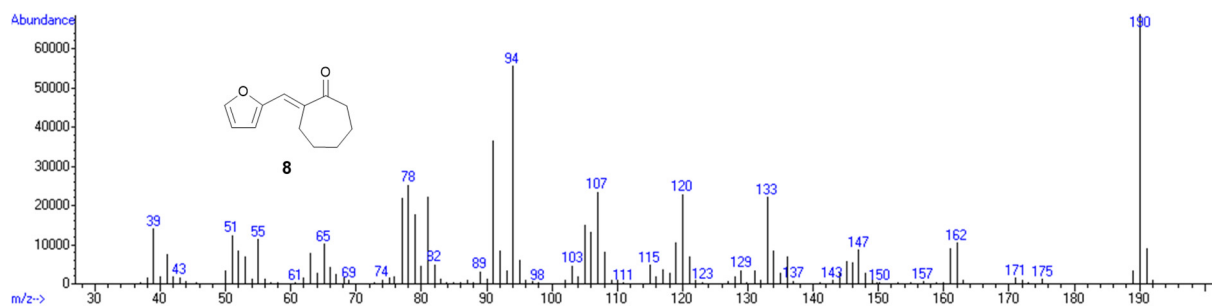
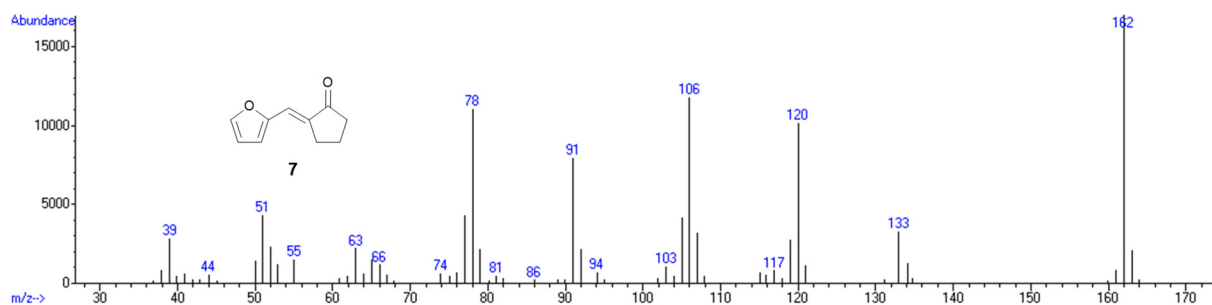
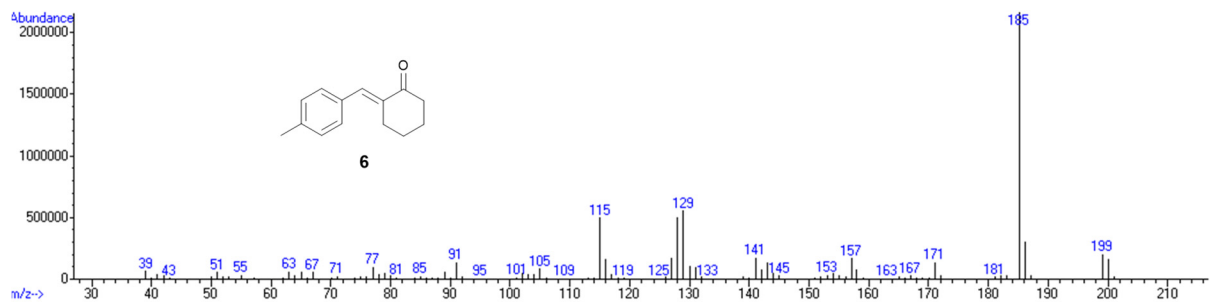


Fig. S6.9 XRD patterns of fresh and used ZrAPO(0.20) catalyst after five reaction runs under neat reaction conditions (ZrAPO(0.20)_C₁₁) and in toluene solution (ZrAPO(0.20)_C₁₆), respectively.





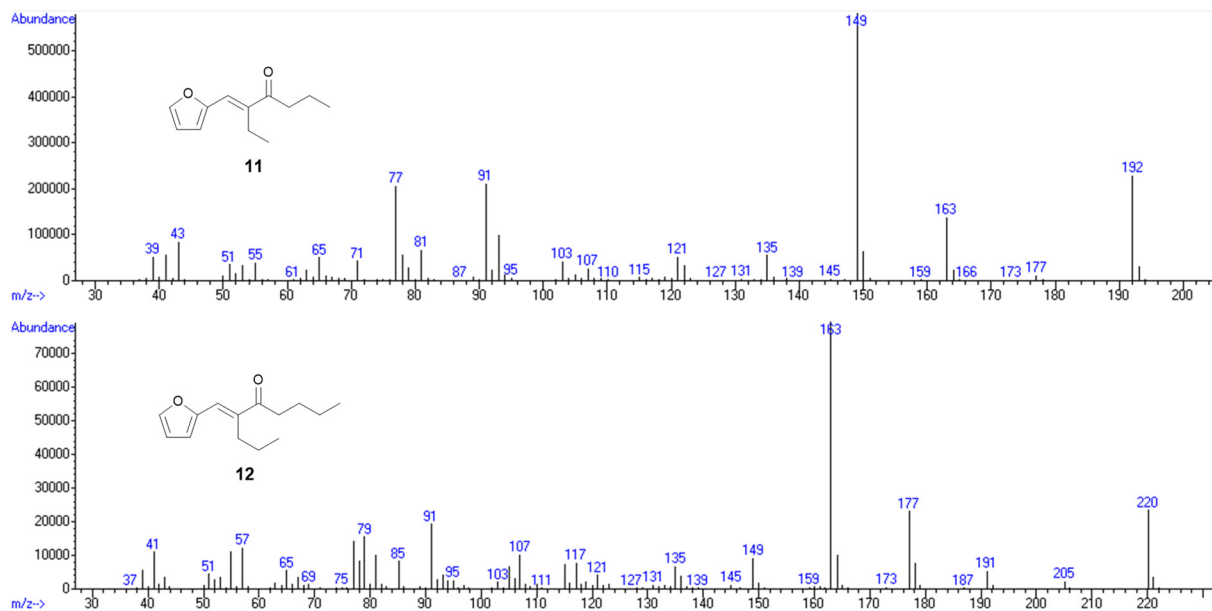
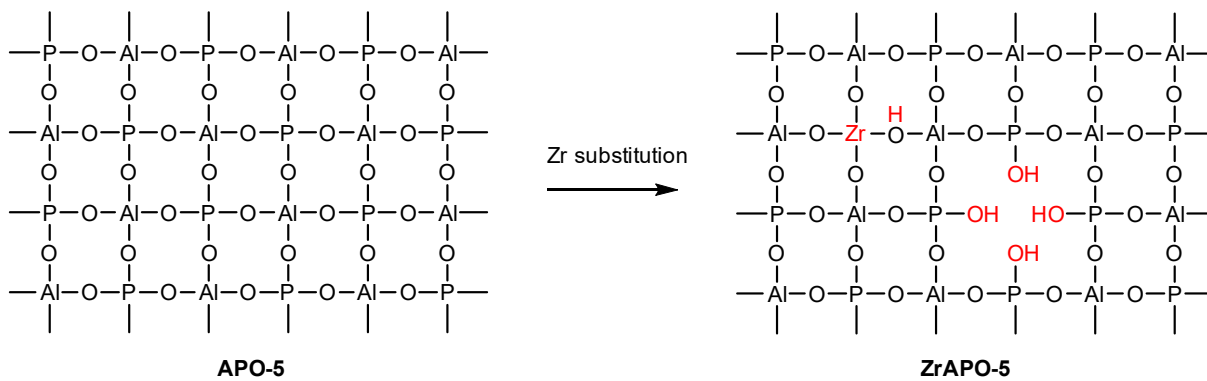


Fig. S6.10 GC-MS spectra of the products in Fig.6.6.



Scheme S6.1 A possible structure of ZrAPO-5.

Table S6.1 Lattice parameters of APO-5 and ZrAPO-5s catalysts obtained from Rietveld refinement analysis of powder X-ray diffraction data using FullProf.^{1,2}

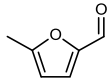
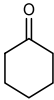
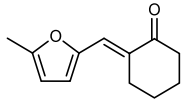
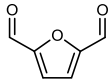
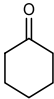
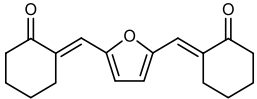
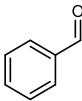
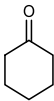
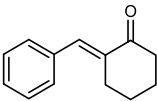
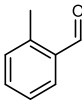
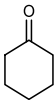
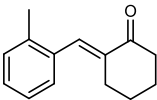
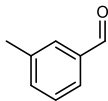
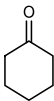
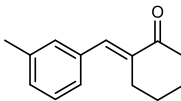
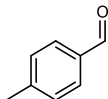
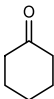
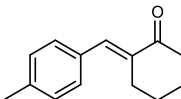
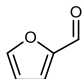
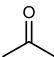
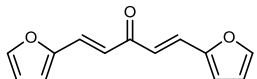
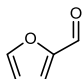
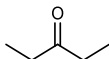
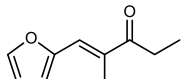
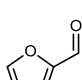
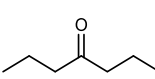
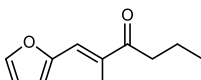
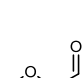
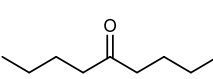
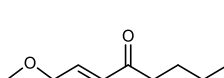
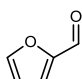
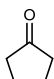
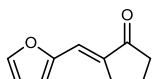
Sample	Unit cell parameter		
	$a = b$ (Å)	c (Å)	V (Å ³)
APO-5	13.7079(5)	8.3484(4)	1358.56(9)
ZrAPO(0.05)	13.7210(9)	8.3873(8)	1367.5(2)
ZrAPO(0.10)	13.743(1)	8.4181(9)	1376.9(2)
ZrAPO(0.15)	13.783(1)	8.4137(9)	1384.2(2)
ZrAPO(0.20)	13.818(1)	8.427(1)	1393.6(3)

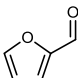
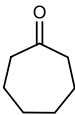
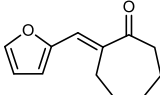
Table S6.2 Textural properties of fresh and used ZrAPO(0.20) catalysts.

Sample	S_{total} (m ² /g) ^a	V_{micro} (cm ³ /g) ^b	V_{meso} (cm ³ /g) ^c
Fresh ZrAPO(0.20)	203	0.03	0.29
Used ZrAPO(0.20)_C ₁₁ ^d	72	0.00	0.16
Used ZrAPO(0.20)_C ₁₆ ^e	74	0.00	0.15

^a Calculated by the BET method. ^b Estimated by the t-plot method. ^c Calculated by subtraction of the micropore volume from the total pore volume. ^d Used ZrAPO(0.20)_C₁₁: used ZrAPO(0.20) catalyst after the second reaction run under neat reaction conditions. ^e Used ZrAPO(0.20)_C₁₆: used ZrAPO(0.20) catalyst after the first reaction run in toluene solution.

Table S6.3 Reaction conditions for the cross-aldol condensation of various carbonyl compounds using ZrAPO(0.20) catalyst in Fig. 6.6.^a

Entry	Aldehyde	Ketone	Product	T (°C)	t (h)
1				120	3
2				120	3
3				120	24
4				120	24
5				120	24
6				120	24
7				120	16
8				120	24
9				120	48
10				120	48
11				120	12

12				120	16
----	---	---	--	-----	----

^a Reaction conditions: Aldehyde (2 mmol), catalyst (50 mg), ketone (20 mmol).

Table S6.4 Acidic characteristics of APO-5 and ZrAPO-5 catalysts.^a

Sample	Weak sites		Medium sites		Strong sites		Total acidity (mmol/g)
	T _{max} (°C)	Acidity (mmol/g)	T _{max} (°C)	Acidity (mmol/g)	T _{max} (°C)	Acidity (mmol/g)	
APO-5	164	0.0012	-	-	-	-	0.0012
ZrAPO(0.05)	167	0.07	221	0.11	321	0.06	0.24
ZrAPO(0.10)	172	0.07	233	0.15	325	0.09	0.31
ZrAPO(0.15)	176	0.10	238	0.22	340	0.10	0.42
ZrAPO(0.20)	181	0.12	246	0.27	377	0.13	0.52

^a Determined by NH₃-TPD.

Table S6.5 Basic characteristics of APO-5 and ZrAPO-5 catalysts.^a

Sample	Weak sites		Medium sites		Strong sites		Total basicity (mmol/g)
	T _{max} (°C)	Basicity (mmol/g)	T _{max} (°C)	Basicity (mmol/g)	T _{max} (°C)	Basicity (mmol/g)	
APO-5	106	0.01	150	0.01	262	0.02	0.04
ZrAPO(0.05)	114	0.02	195	0.10	319	0.05	0.17
ZrAPO(0.10)	121	0.04	212	0.11	335	0.06	0.21
ZrAPO(0.15)	130	0.05	215	0.14	336	0.09	0.28
ZrAPO(0.20)	137	0.08	218	0.16	335	0.10	0.34

^a Determined by CO₂-TPD.

Table S6.6 Zr concentration in catalysts.^a

Sample	Zr concentration (mmol/g _{cat})
APO-5	-
ZrAPO(0.05)	0.28
ZrAPO(0.10)	0.55
ZrAPO(0.15)	0.92
ZrAPO(0.20)	1.13

^a Determined by XRF.

Table S6.7 Catalytic performance of different catalyst systems about FF and CH cross-aldol condensation.

Entry	Catalyst	T (°C)	Conv. (%)	C11 Yield (%)	C11-OH Yield (%)	C16 Yield (%)	Ref.
1	NaOH	30	95			95	3
2	NaOH	40				92	4
3	Mg/Al mixed oxides	80	100	68		10	5
4	Mg-Al mixed oxide	90	97	68	12	14	6
5	Mg-Al mixed oxide	60	88	18	46	22	7
6	ZrAPO(0.20)	120	99	79		16	This work
7	ZrAPO(0.20)	120	100	14		81	This work

References

- [1] T. Roisnel, J. Rodriguez-Carvajal, *Mater. Sci. Forum* **2001**, 378-381, 118-123.
- [2] J. Rodriguez-Carvajal, *Physica B* **1993**, 192, 55-69.
- [3] Q. Deng, J. S. Xu, P. J. Han, L. Pan, L. Wang, X. W. Zhang, J. J. Zou, *Fuel Process. Technol.* **2016**, 148, 361-366.
- [4] Q. Y. Liu, C. H. Zhang, N. Shi, X. H. Zhang, C. G. Wang, L. L. Ma, *RSC Adv.* **2018**, 8, 13686-13696.
- [5] Z. Tisler, P. Vondrova, K. Hrachovcova, K. Stepanek, R. Velvarska, J. Kocik, E. Svobodova, *Catalysts* **2019**, 9.
- [6] O. Kikhtyanin, D. Kadlec, R. Velvarska, D. Kubicka, *ChemCatChem* **2018**, 10, 1464-1475.
- [7] D. Kadlec, Z. Tisler, R. Velvarska, L. Peliskova, U. Akhmetzyanova, *React. Kinet. Mech. Catal.* **2019**, 126, 219-235.

Appendices E – Support information for Chapter 7

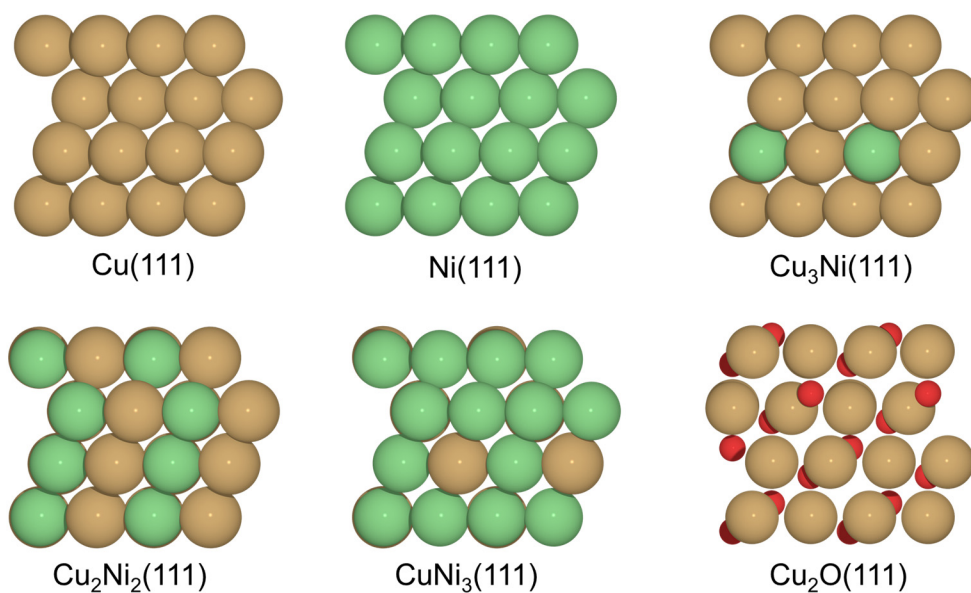


Fig. S7.1 The applied surface models of Cu, Ni, and CuNi alloys (side view).

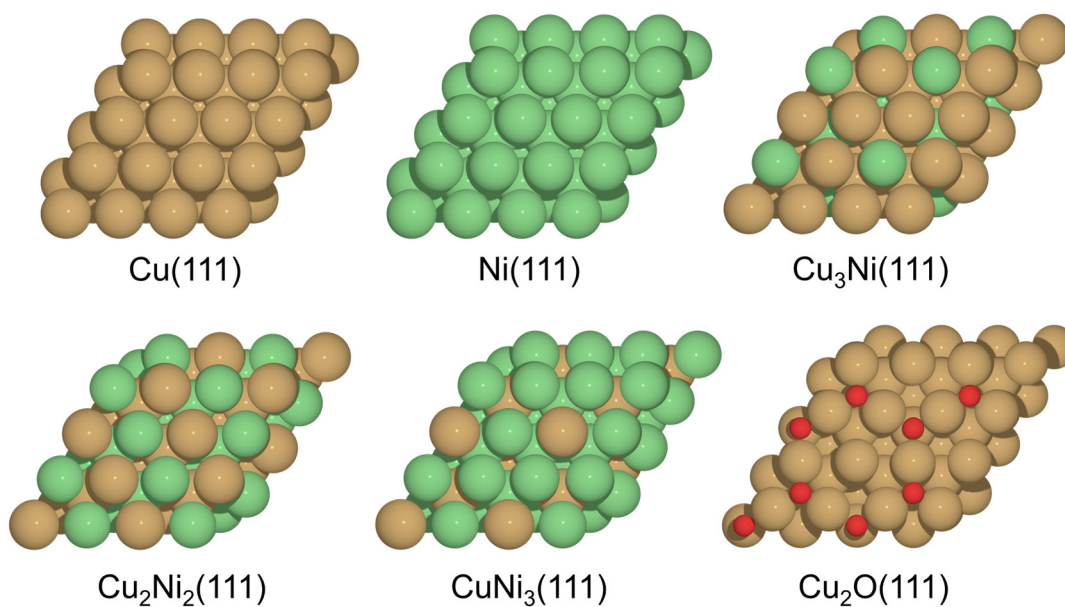


Fig. S7.2 The applied surface models of Cu, Ni, and CuNi alloys (top view).

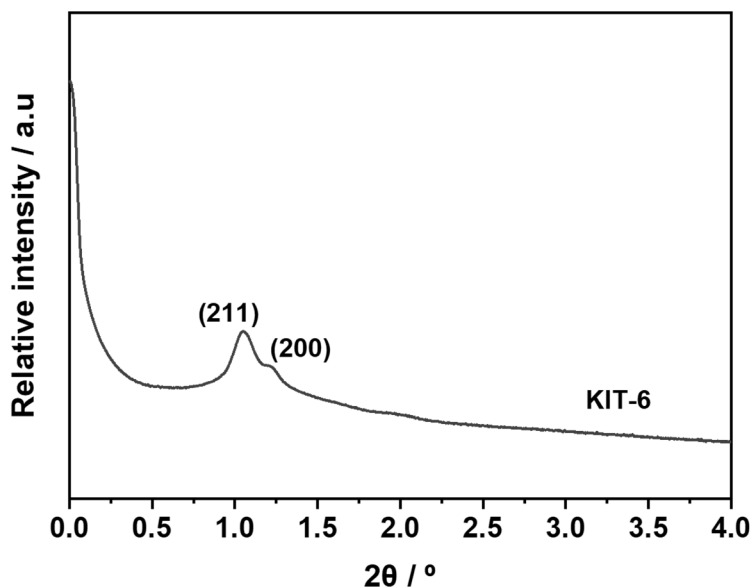


Fig. S7.3 SAXS pattern of synthesized mesoporous KIT-6.

The SAXS of KIT-6 had an intense peak at $2\theta = 1.05^\circ$ with a shoulder peak at 1.22° as well as a weak peak at $2\theta = 1.98^\circ$ corresponding to the (211) and (200) reflections of the cubic bicontinuous $Ia\bar{3}d$ structure.^{1,2} The unit cell parameter of synthesized KIT-6 was 20.6 nm, which is consistent with other reported values.³

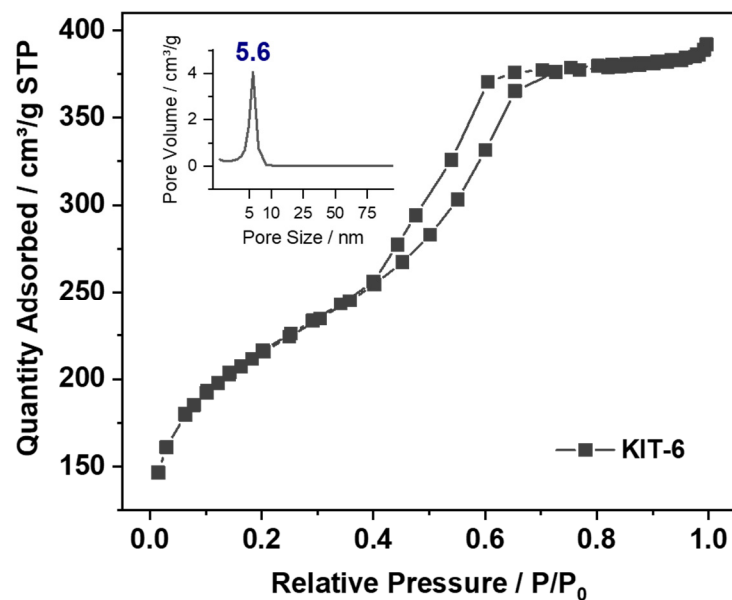


Fig. S7.4 N₂ adsorption-desorption isotherms of the synthesized KIT-6 (inset: Pore size distribution).

KIT-6 showed type IV isotherms with a H1 hysteresis loop at relative P/P₀ pressures of 0.4-0.9 characteristic of a ordered mesoporous material with a narrow range of uniform pores.⁴ The surface area of KIT-6 was 751 m²/g and the pore size was 5.6 nm (Table S7.1).

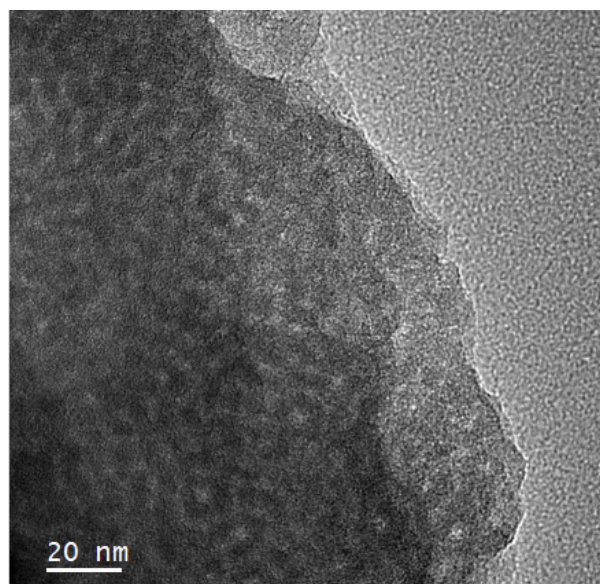


Fig. S7.5 TEM image of the synthesized KIT-6.

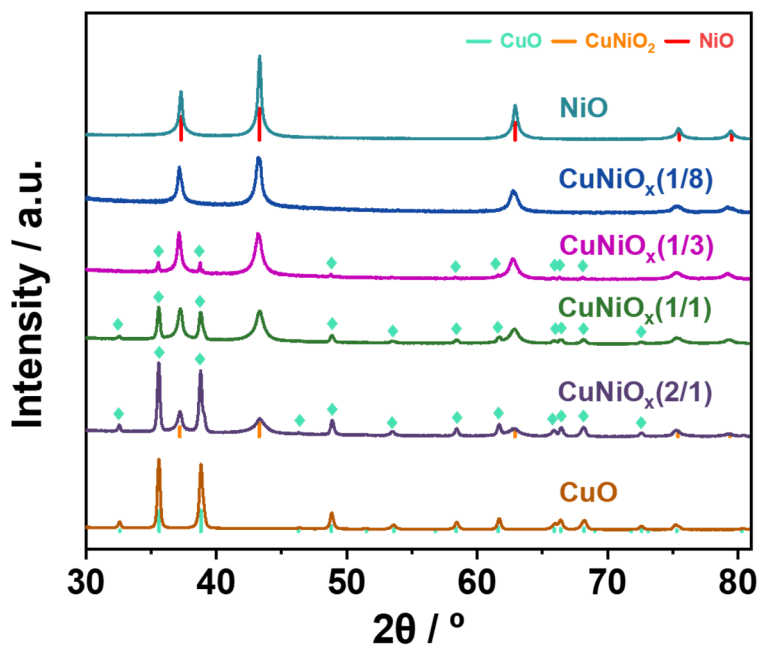


Fig. S7.6 XRD patterns of CuO, NiO, and the as-synthesized CuNiO_x catalysts.

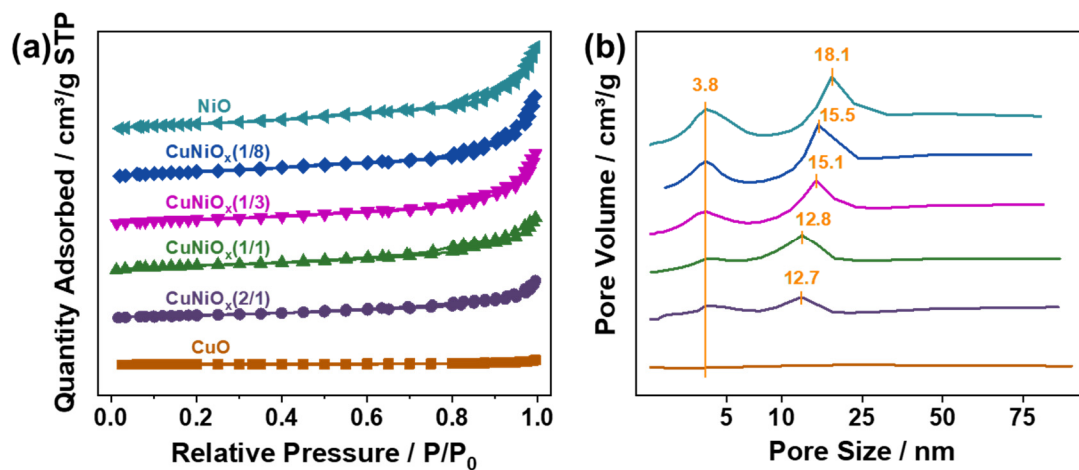


Fig. S7.7 (a) N₂ adsorption-desorption isotherms and (b) pore size distributions of CuO, NiO, and the as-synthesized CuNiO_x catalysts.

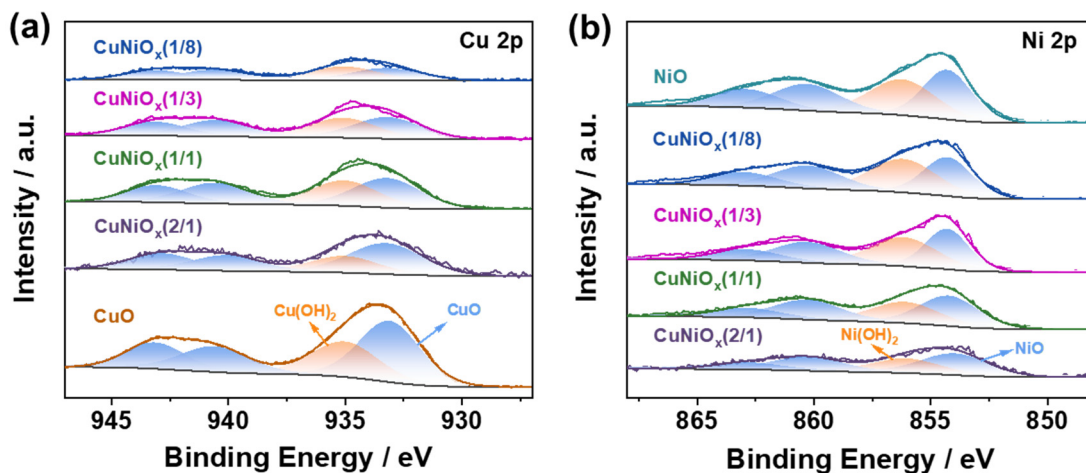


Fig. S7.8 (a) Cu 2p_{3/2} and (b) Ni 2p_{3/2} XPS spectra of CuO, NiO, and the as-synthesized CuNiO_x catalysts.

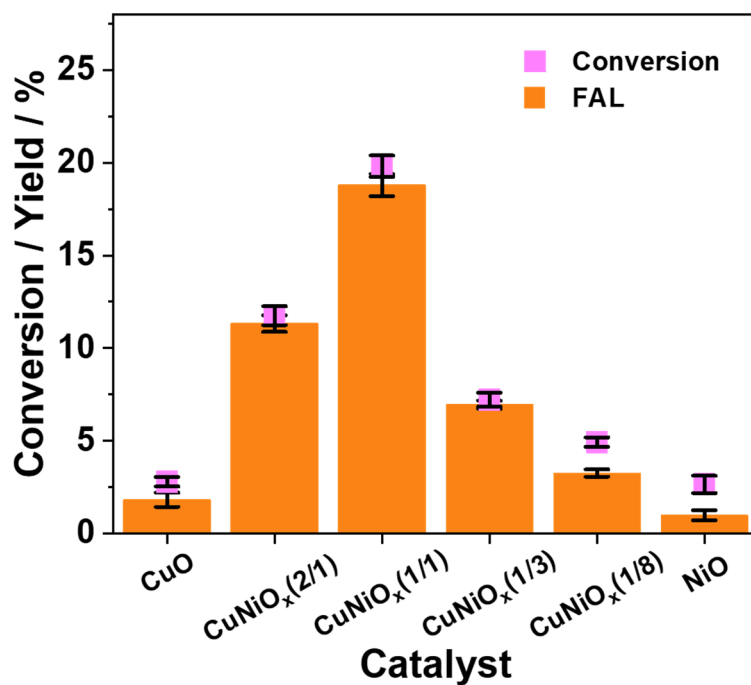


Fig. S7.9 Catalytic performance of CuO, NiO, and the as-synthesized CuNiO_x catalysts in FF hydrogenation. Reaction conditions: FF (96 mg, 1 mmol), catalyst (20 mg), 2-propanol (5 mL), 120°C, 30 bar H₂, 45 min.

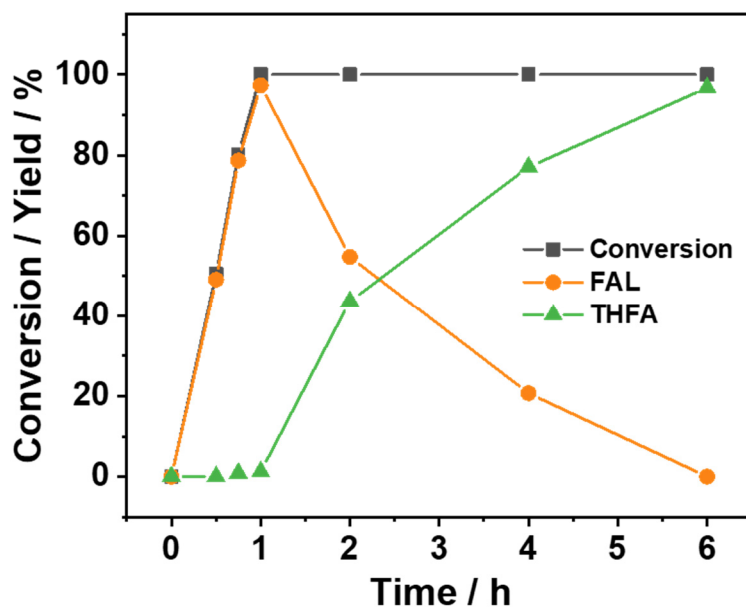


Fig. S7.10 Time course study of FF hydrogenation with CuNiO_x(1/1)-150. Reaction conditions: FF (96 mg, 1 mmol), CuNiO_x(1/1)-150 (20 mg), 2-propanol (5 mL), 120°C, 30 bar H₂.

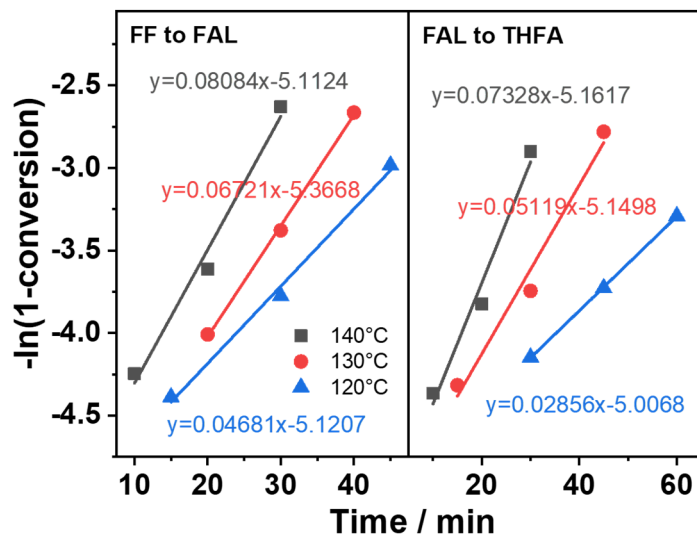


Fig. S7.11 Plots of $-\ln(1-\text{conversion})$ vs. time (min) at different reaction temperatures for FF hydrogenation to FAL and THFA with $\text{CuNiO}_x(1/1)\text{-150}$. Reaction conditions: FF (96 mg, 1 mmol), $\text{CuNiO}_x(1/1)\text{-150}$ (20 mg), 2-propanol (5 mL), 120°C, 30 bar H_2 .

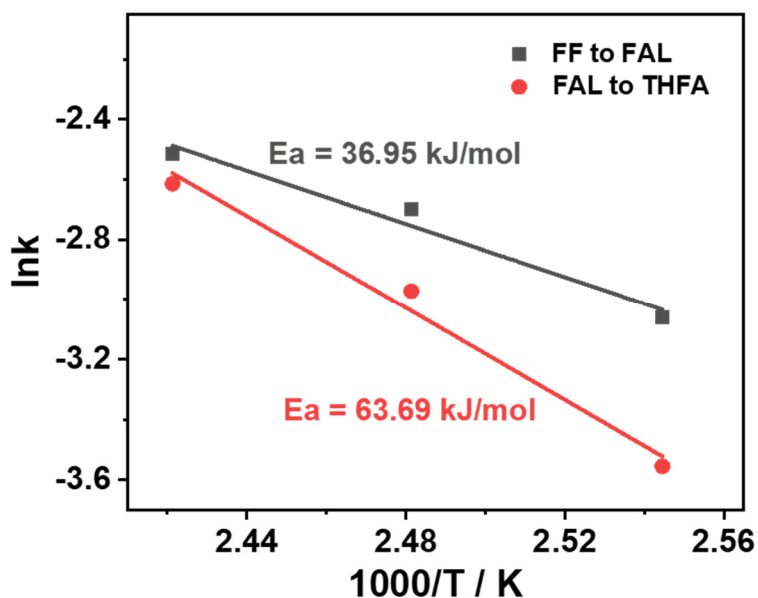


Fig. S7.12 Arrhenius plots for FF hydrogenation to FAL and THFA with $\text{CuNiO}_x(1/1)\text{-150}$. Reaction conditions: FF (96 mg, 1 mmol), $\text{CuNiO}_x(1/1)\text{-150}$ (20 mg), 2-propanol (5 mL), 120°C, 30 bar H_2 .

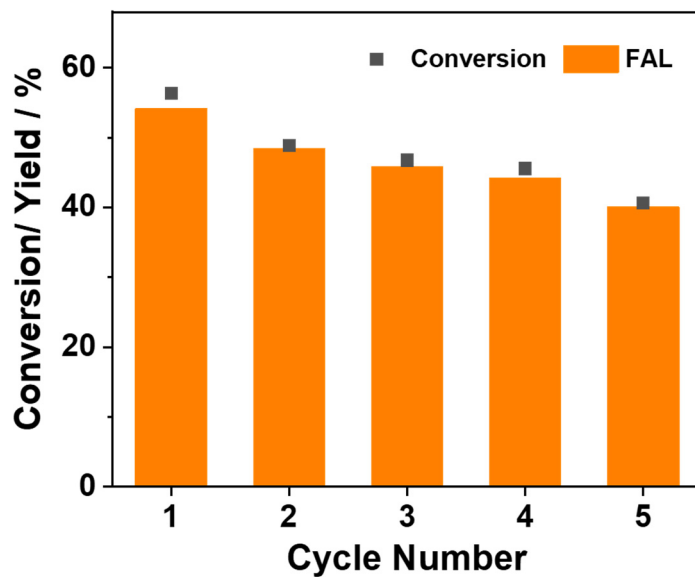


Fig. S7.13 Reusability of $\text{CuNiO}_x(1/1)$ -150 in the FF hydrogenation. Reaction conditions: FF (96 mg, 1 mmol), $\text{CuNiO}_x(1/1)$ -150 (20 mg), 2-propanol (5 mL), 30 bar H_2 , 30 min.

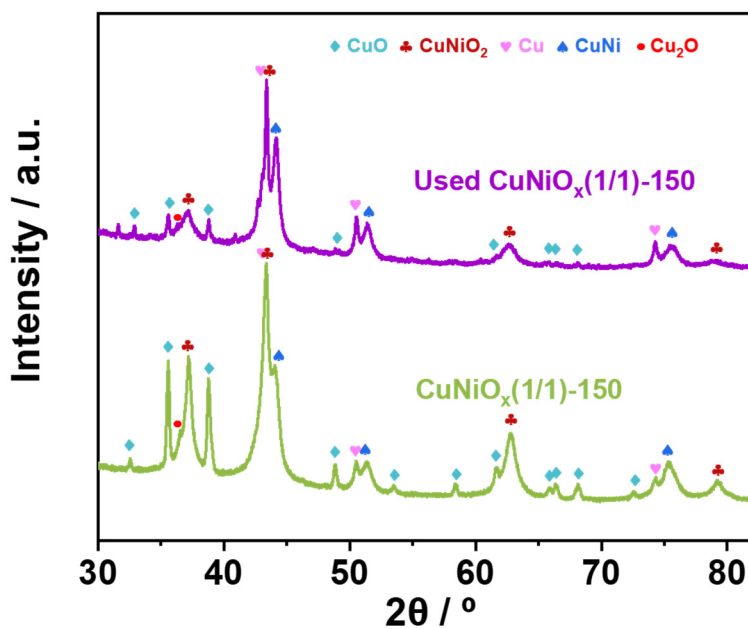


Fig. S7.14 XRD patterns of fresh and reused (five reaction runs) $\text{CuNiO}_x(1/1)$ -150 catalyst after used for FF hydrogenation.

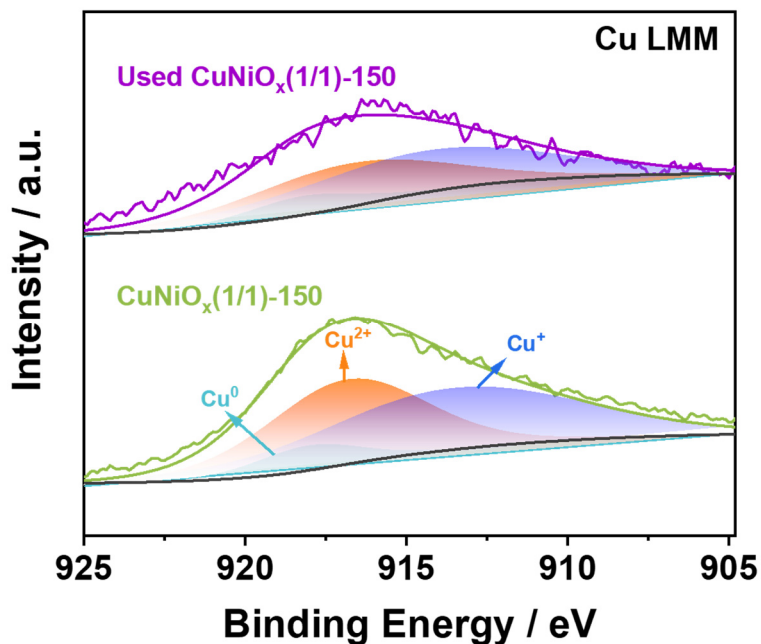


Fig. S7.15 Cu LMM XAES spectra of fresh and recycled (five reaction runs) CuNiO_x(1/1)-150 catalyst after used for FF hydrogenation.

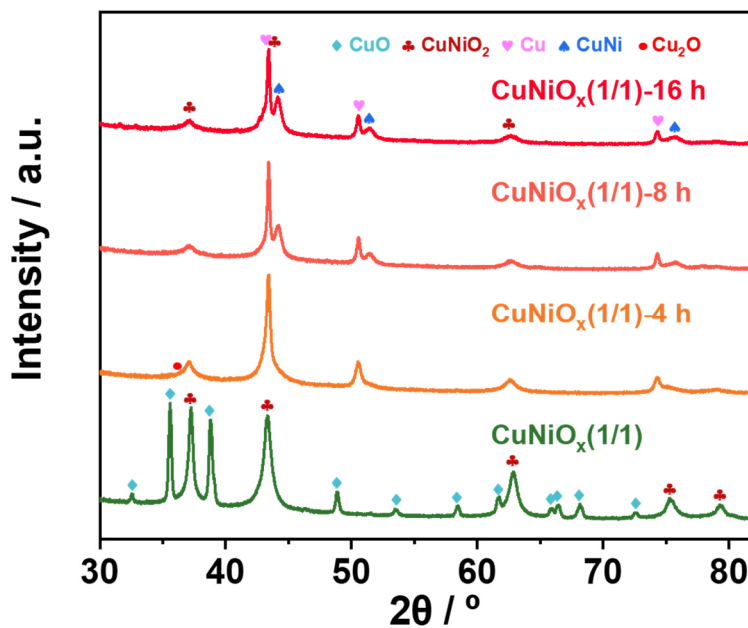


Fig. S7.16 XRD patterns of CuNiO_x(1/1) catalyst after isolation from blank experiments ran at different reaction times with only 2-propanol. Reaction conditions: CuNiO_x(1/1) (20 mg), 2-propanol (5 mL), 30 bar H₂.

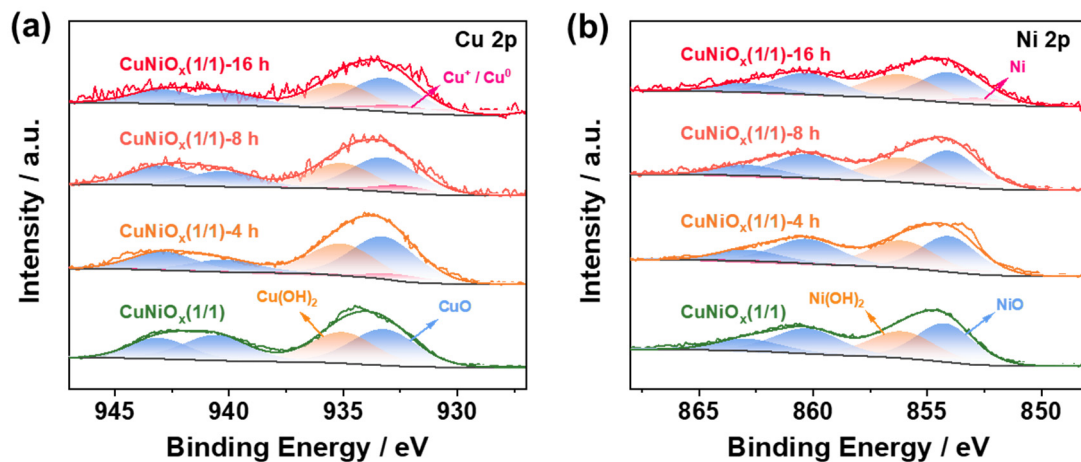


Fig. S7.17 (a) Cu 2p_{3/2} and (b) Ni 2p_{3/2} XPS spectra of the CuNiO_x(1/1) catalyst after isolation from blank experiments run at different reaction times with only 2-propanol. Reaction conditions: CuNiO_x(1/1) (20 mg), 2-propanol (5 mL), 30 bar H₂.

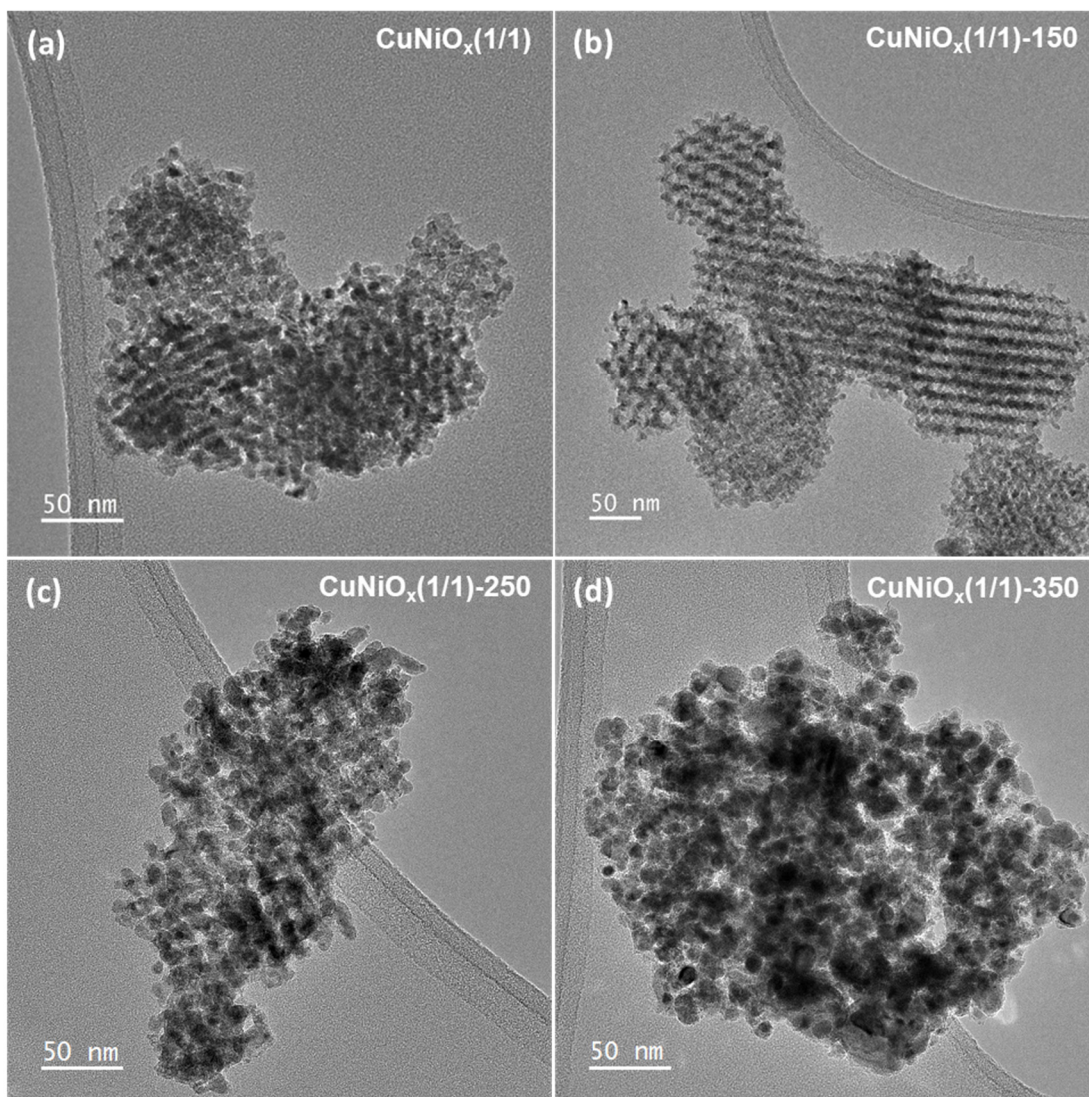


Fig. S7.18 TEM images of (a) as-synthesized $\text{CuNiO}_x(1/1)$ catalyst and $\text{CuNiO}_x(1/1)$ catalysts reduced at (b) 150°C, (c) 250°C, and (d) 350°C.

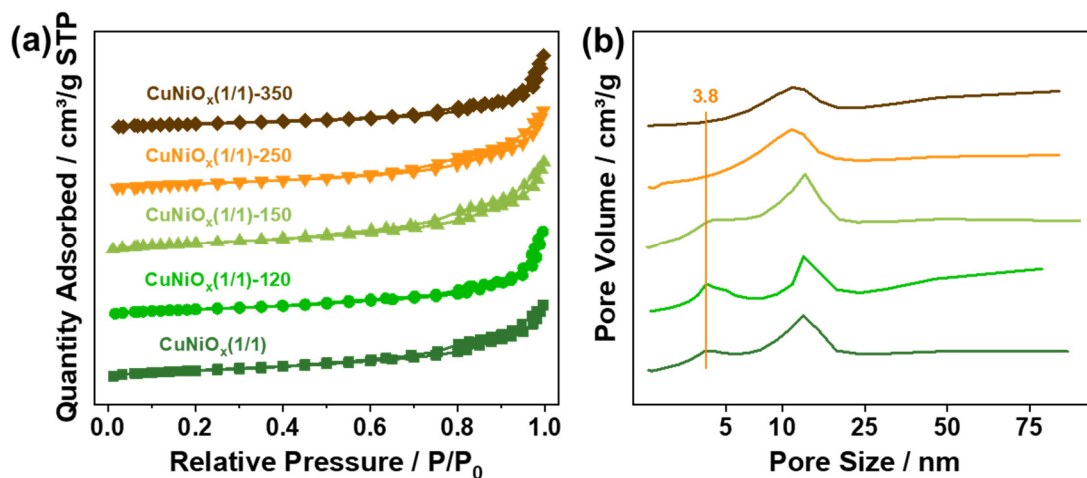


Fig. S7.19 (a) N₂ adsorption-desorption isotherms and (b) pore size distributions of the as-synthesized and reduced CuNiO_x catalysts.

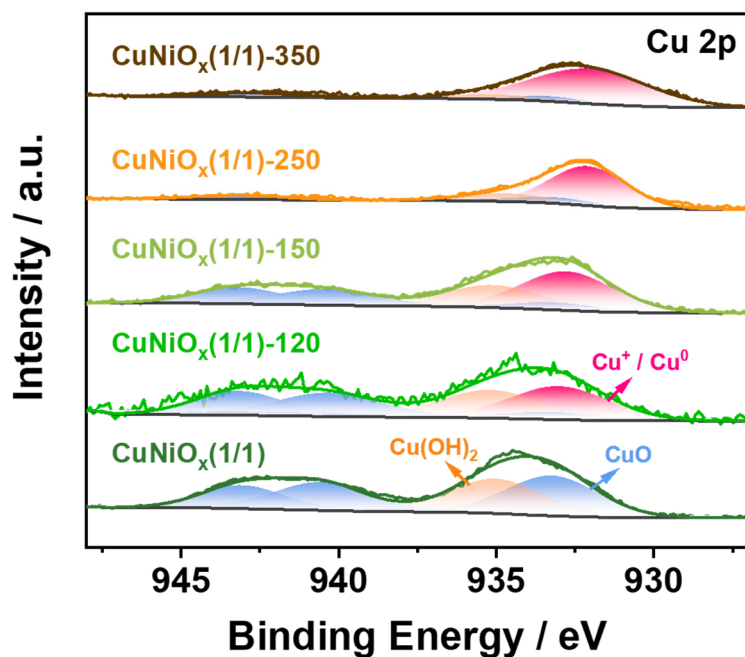


Fig. S7.20 Cu 2p_{3/2} XPS spectra of the reduced CuNiO_x(1/1) catalysts.

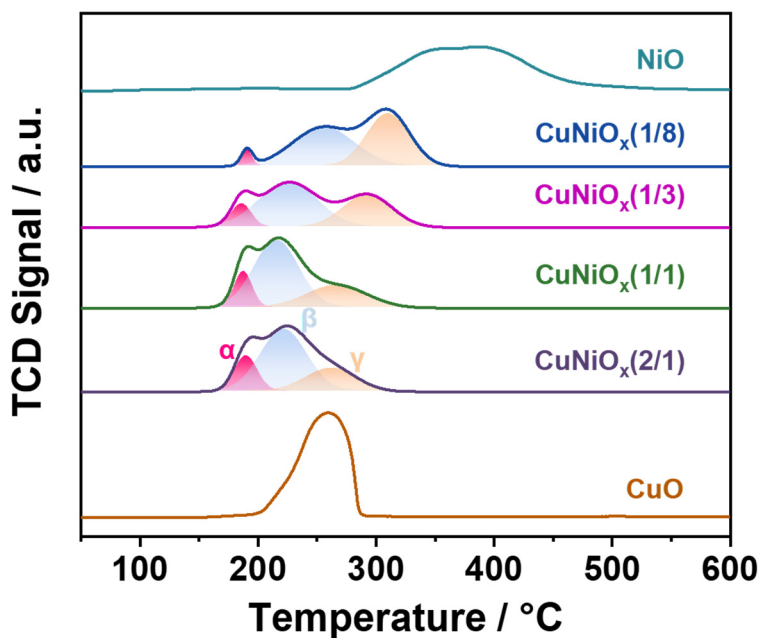


Fig. S7.21 H₂-TPR profiles of CuO, NiO, and the CuNiO_x catalysts.

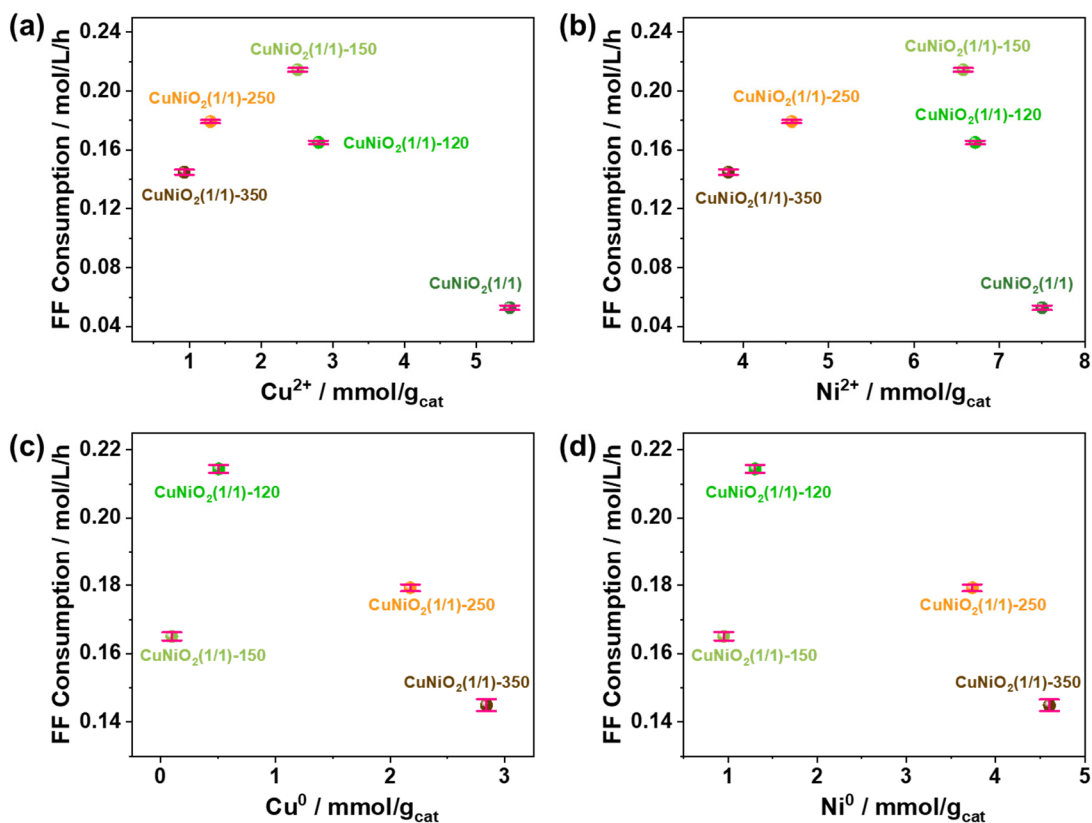


Fig. S7.22 Correlations of FF consumption rate with (a) Cu²⁺, (b) Ni²⁺, (c) Cu⁰, and (d) Ni⁰ concentration on CuNiO_x(1/1) catalysts.

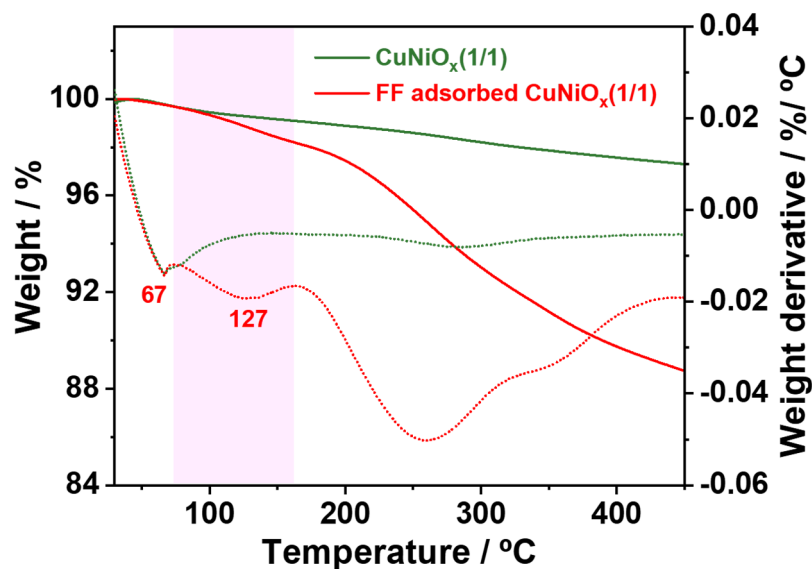


Fig. S7.23 TG curves of pristine and FF-adsorbed as-synthesized $\text{CuNiO}_x(1/1)$ catalyst.

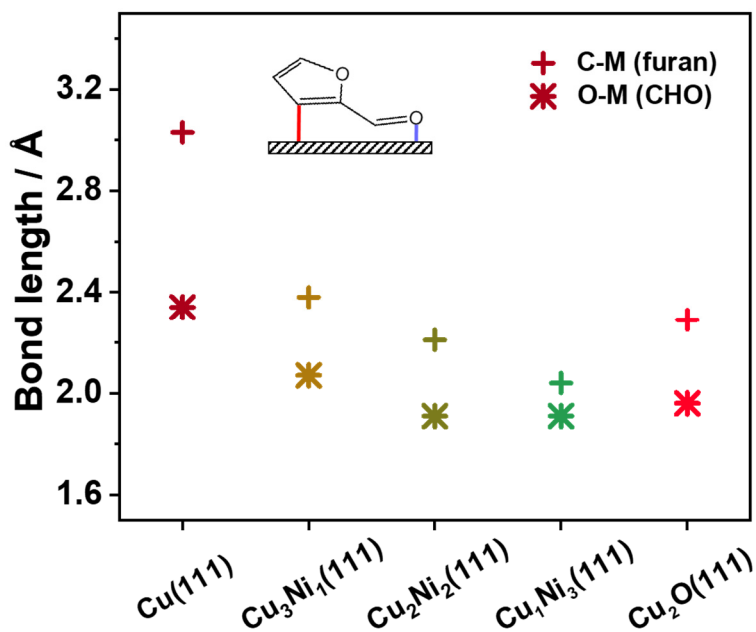


Fig. S7.24 Calculated distances between different surfaces and carbonyl O atoms and C2 carbons in FF.

Table S7.1 Textural properties of synthesized KIT-6.

Sample	S_{BET} (m^2/g)	V_{total} (cm^3/g)	V_{micro} (cm^3/g)	Pore size (nm)
KIT-6	751	0.69	0.12	5.6

Table S7.2 Textural properties of CuO, NiO and the as-synthesized CuNiO_x catalysts.

Sample	Cu/Ni ratio ^a	S_{BET} ($\text{m}^2/\text{g}^{\text{b}}$)	V_{total} ($\text{cm}^3/\text{g}^{\text{c}}$)	V_{micro} ($\text{cm}^3/\text{g}^{\text{d}}$)	Pore size (nm^{e})	H ₂ cons. ($\text{mmol}/\text{g}^{\text{f}}$)
CuO	-	5	0.01	0	-	0.139
CuNiO _x (2/1)	1.76	66	0.09	0	3.8	0.128
CuNiO _x (1/1)	0.70	82	0.13	0	3.8	0.131
CuNiO _x (1/3)	0.25	79	0.14	0	3.8	0.141
CuNiO _x (1/8)	0.09	106	0.17	0.01	3.8	0.137
NiO	-	107	0.18	0.01	3.8	0.136

^a Determined by XRF. ^b Calculated by the BET method. ^c Determined by single point adsorption at $P/P_0 = 0.95$. ^d Estimated by the t-plot method. ^e Determined from the BJH adsorption branch.

^f Determined by H₂-TPR.

Table S7.3 Substrate scope for hydrogenation with CuNiO_x(1/1)-150 catalyst.^a

Entry	Substrate	Product	Conv. (%)	Yield (%)
1			100	96.8
2			100	98.9
3			100	99.1
4			100	97.5
5			100	94.6
6			100	96.4
7			100	97.0
8			100	97.9
9			100	95.0

^a Reaction conditions: Substrate (1 mmol), CuNiO_x(1/1)-150 (20 mg), 2-propanol (5 mL), 120°C, 1 h.

Table S7.4 Properties of the reduced CuNiO_x(1/1) catalysts.

Sample	Cu/Ni ratio ^a	S _{BET} (m ² /g ^b)	V _{total} (cm ³ /g ^c)	V _{micro} (cm ³ /g ^d)	Pore size (nm ^e)	C _{Cu} (mmol /g _{cat} ^a)	C _{Ni} (mmol /g _{cat} ^a)
CuNiO _x (1/1)	0.73	82	0.13	0	3.8	5.47	7.50
CuNiO _x (1/1)-120	0.76	79	0.13	0	3.8	5.82	7.67
CuNiO _x (1/1)-150	0.78	88	0.15	0	3.8	6.11	7.88
CuNiO _x (1/1)-250	0.78	69	0.13	0	-	6.50	8.31
CuNiO _x (1/1)-350	0.79	49	0.09	0	-	6.67	8.43

^a Determined by XRF. ^b Calculated by the BET method. ^c Determined by single point adsorption at P/P₀ = 0.95. ^d Estimated by the t-plot method. ^e Determined from the BJH adsorption branch.

Table S7.5 Comparison of bond lengths (Å) of FF in gas phase and adsorbed on Cu(111), Cu₂O(111), Cu₁Ni₃(111), Cu₂Ni₂(111), and Cu₃Ni₁(111) surfaces.

d	Gas phase	Cu(111)	Cu ₂ O(111)	Cu ₁ Ni ₃ (111)	Cu ₂ Ni ₂ (111)	Cu ₃ Ni ₁ (111)
C1-O1	1.230	1.253	1.273	1.327	1.312	1.287
C1-C2	1.452	1.435	1.447	1.445	1.428	1.417
C2-O2	1.385	1.387	1.387	1.398	1.379	1.398
C2-C3	1.379	1.390	1.376	1.440	1.449	1.440
C3-C4	1.419	1.417	1.440	1.466	1.441	1.447
C4-C5	1.374	1.379	1.403	1.431	1.457	1.399
C5-O2	1.357	1.356	1.374	1.418	1.429	1.357

References

- [1] K. Soni, B. S. Rana, A. K. Sinha, A. Bhaumik, M. Nandi, M. Kumar, G. M. Dhar, *Appl. Catal., B* **2009**, *90*, 55-63.
- [2] W. Wang, R. Qi, W. Shan, X. Wang, Q. Jia, J. Zhao, C. Zhang, H. Ru, *Microporous Mesoporous Mater.* **2014**, *194*, 167-173.
- [3] F. Kleitz, F. Bérubé, R. Guillet-Nicolas, C.-M. Yang, M. Thommes, *J. Phys. Chem. C* **2010**, *114*, 9344-9355.
- [4] M. Thommes, K. Kaneko, A. V. Neimark, J. P. Olivier, F. Rodriguez-Reinoso, J. Rouquerol, K. S. W. Sing, *Pure Appl. Chem.* **2015**, *87*, 1051-1069.

Appendices F – First page of published articles

Green Chemistry



TUTORIAL REVIEW

View Article Online
View Journal | View Issue



Cite this: *Green Chem.*, 2021, **23**, 670

Recent advances in heterogeneous catalytic transfer hydrogenation/hydrogenolysis for valorization of biomass-derived furanic compounds

Wenting Fang and Anders Riisager *

Catalytic transfer hydrogenation/hydrogenolysis is economically and environmentally benign synthetic strategies to valorize renewable compounds derived from biomass. Simple and easily accessible organic molecules such as, e.g. alcohols, formic acid/formate salts and hydrosilane can provide the hydrogen for the reaction thereby avoiding the use of hazardous gaseous hydrogen. This review provides the status and insight into the recent progress made in catalytic transfer hydrogenation/hydrogenolysis on two important carbohydrate-derived furanic platform chemicals, furfural and 5-hydroxymethylfurfural, with focus on catalyst developments and mechanism explanations. Many of the devised metal and catalyst reactivity features are generally applicable for alternative renewable compounds, and a detailed understanding of these features may therefore guide the selection of suitable catalysts for a specific transformation and improve the selectivity and yield of the products.

Received 19th November 2020,
Accepted 18th December 2020
DOI: 10.1039/d0gc03931d
rsc.li/greenchem

1 Introduction

The awareness of global warming and rapid depletion of non-renewable fossil reserves have promoted significantly the

development of sustainable viable synthetic routes for producing chemicals and fuels from various renewable resources like lignocellulosic biomass.^{1,2} Lignocellulosic biomass is the most abundant and available renewable resource in Nature,^{3,4} and furfural (FF) and 5-hydroxymethylfurfural (HMF) formed from lignocellulosic biomass are on the list of the “Top 10” biomass-derived platform compounds endorsed by the U.S. Department of Energy.^{5–7} Due to the molecular content of

Centre for Catalysis and Sustainable Chemistry, Department of Chemistry, Technical University of Denmark, DK-2800 Kgs. Lyngby, Denmark. E-mail: ar@kemi.dtu.dk; Tel: (+45) 45252233



Wenting Fang

Wenting Fang is pursuing her PhD degree in Prof. Anders Riisager's group at the Department of Chemistry, Technical University of Denmark. Her research dissertation is focused on selective catalytic conversion of renewables to chemicals with heterogeneous catalysis. She started her research on biomass conversion with zeolites during her Master's project in Ningbo Institute of Materials Technology & Engineering, Chinese Academy of Sciences.



Anders Riisager

Anders Riisager is Professor at the Department of Chemistry, Technical University of Denmark (DTU). Before being appointed to the current position, he was Associate Professor at DTU and completed four years of postdoctoral research at RWTH-Aachen/University of Erlangen-Nuremberg, Germany. His major scientific focus is on the development of sustainable chemistry with catalysis and renewables as well as chemical technology with ionic liquids. Several of the developed technologies are commercialized to industry and he is also co-founder of two companies focusing on biomass valorization technology.



Contents lists available at ScienceDirect

Applied Catalysis B: Environmental

journal homepage: www.elsevier.com/locate/apcatb


Efficient valorization of biomass-derived furfural to fuel bio-additive over aluminum phosphate

Wenting Fang, Anders Riisager*

Centre for Catalysis and Sustainable Chemistry, Department of Chemistry, Technical University of Denmark, DK-2800, Kgs. Lyngby, Denmark

ARTICLE INFO

Keywords:

Aluminum phosphate
Acetalization
Reductive etherification
Biomass valorization
Fuel bio-additive

ABSTRACT

Aluminum phosphates (APO-5s) were synthesized and evaluated as heterogeneous catalysts for the valorization of furfural to furfuryl acetals (FAs) and furfuryl alcohol ethers (FAEs). Weakly acidic APO-5 (Al/P = 1) exhibited excellent catalytic performance with 96 % FA yield in ethylene glycol, and analysis of the acetalization reaction supported that adsorption and acidic catalyst sites co-catalyzed the reaction. In addition, the catalyst was stable and reusable though with some deactivation after five recycles. Oppositely, more acidic APO-5 (Al/P = 1.5) catalyzed the one-pot synthesis of FAE with 55 % yield in 2-propanol with unchanged performance in three successive reactions after intermediate calcination. The reaction pathway for the direct hydrogenolysis of acetal into ether by catalytic transfer hydrogenation and etherification was promoted by the co-solvent 1,4-dioxane, possibly by hydrogen bonding. The study demonstrates a simple approach to design APO catalyst systems allowing very efficient and highly selective valorization of furfural to fuel bio-additives.

1. Introduction

In the last century, the World's energy demand has predominantly been covered by nonrenewable carbon-based fossil fuels, which are gradually becoming exhausted. This has led to severe environmental problems such as global warming, and uncertainty about future supply safety. Accordingly, great efforts have been undertaken to develop potential substitutes to fossil fuels. Biofuels, which are obtained from biomass, are renewable and environmental friendly alternatives to fossil fuels [1]. Biofuels can either be used directly or mixed in fossil fuels as bio-additives to improve the cetane number, density, cloud point, flash point or other fuel properties [2–4].

Furfural (FF) has been emphasized as one of the top value-added chemicals derived from biomass and can be widely used to produce different other chemicals [5]. Especially bio-additives derived from FF by acetalization (furfuryl acetals, FAs) and reductive etherification (furfuryl alcohol ethers, FAEs) have attracted attention due to their potential as blending high-octane gasoline components [6–10]. Formation of cyclic FAs from FF and diols can be obtained using various heterogeneous acid catalysts, where the pore structure and nature of the acid sites can be important [11,12]. Hence, ZSM-5 zeolite converted 35 % of FF with 100 % selectivity to FA in 1,2-propanediol [13], whereas sulfated-SnO₂ allowed to obtain a total yield of 82 % of 1,3-dioxolane

and 1,3-dioxane isomers in glycerol [14]. Moreover, Zr-Montmorillonite catalyzed the conversion of FF in different C₂-C₆ diols to the corresponding cyclic FAs with yields above 75 %, and particularly the products with ethylene glycol (EG) and 1,5-pentanediol were shown to exhibit high miscible in commercial diesel obtaining improved density, cloud point and flash point [15]. Similarly, FAEs are typically synthesized from acid-catalyzed direct etherification of furfuryl alcohol (FAL) [8,16,17], and furfuryl ethyl ether (EMF) have been noted for its excellent property to curb soot emissions and shows superior anti-knocking properties compared to the reference Euro 95 gasoline [18,19]. Recently, Sn-beta and Zr-TUD-1 zeotype catalysts were applied for one-pot formation of furfuryl butyl ether (BMF) from FF allowing to obtain 58 % BMF yield with 95 % FF conversion and 25 % BMF yield with 87 % FF conversion, respectively [20,21].

In this work, aluminum phosphate (APO-5) catalysts with different Al/P ratios were synthesized by hydrothermal method, characterized by multiple techniques and applied for acetalization and reductive etherification of FF. Weakly acidic APO-5(1) showed excellent catalytic performance and high stability for FF acetalization with EG. The active sites of the catalyst were investigated, and the reaction evaluated with respect to substrate and solvent scope. More acidic APO-5(1.5) exhibited high activity for the one-pot synthesis of FAE from FF in 2-propanol, and isotopic tracing study provided insight to the reaction pathway. The

* Corresponding author.

E-mail address: ar@kemi.dtu.dk (A. Riisager).

<https://doi.org/10.1016/j.apcatb.2021.120575>

Received 15 April 2021; Received in revised form 26 July 2021; Accepted 28 July 2021

Available online 31 July 2021

0926-3373/© 2021 The Author(s). Published by Elsevier B.V. This is an open access article under the CC BY license (<http://creativecommons.org/licenses/by/4.0/>).

Improved Catalytic Transfer Hydrogenation of Biomass-Derived Aldehydes with Metal-Loaded Aluminum Phosphate

Wenting Fang and Anders Riisager*

Cite This: *ACS Sustainable Chem. Eng.* 2022, 10, 1536–1543

Read Online

ACCESS |

Metrics & More

Article Recommendations

Supporting Information

ABSTRACT: Catalytic transfer hydrogenation (CTH) is a benign and effective process for the conversion of biomass-derived platforms into fuels and chemicals. Here, aluminum phosphate (Al/P ratio = 1.5) (APO1.5) and alkali earth metal (AEM)-loaded APO1.5s were synthesized by impregnation and applied in the CTH of furfural (FF) into furfuryl alcohol (FA). The introduction of AEM created weak and medium basic sites instead of weak acidic and strong basic sites in the pristine APO1.5, allowing co-catalysis of the AEM oxide species (basic sites) and the APO1.5 (acidic sites) to facilitate hydrogenation instead of etherification and acetalization. For 3 wt % Ca/APO1.5, this tuning of acidity and basicity improved the FA yield significantly from 54 to 90% (140 °C, 48 h), and the catalyst remained stable as well as reusable for at least four consecutive reactions with only slight deactivation. Notably, 3 wt % Ca/APO1.5 catalyst also showed high catalytic activity for CTH of other bio-derived aldehydes, thus demonstrating its versatile use for valorization of platforms generated during biomass refining.

KEYWORDS: aluminum phosphate, biomass conversion, catalytic transfer hydrogenation, furfural, furfuryl alcohol, sustainable chemistry

1. INTRODUCTION

The steady increase of the world's population and associated demand for energy will gradually result in a future exhausting of traditional fossil resources, that is, coal, oil, and natural gas. Accordingly, the development of renewable energy from consistent alternative resources like biomass has attracted significant attention.^{1–3} Furfural (FF) is a lignocellulosic biomass-derived platform molecule, which can be used directly as an energy source or indirectly via its conversion into value-added chemicals.⁴ The FF molecule is prone to many chemical transformations at both its aldehyde group and its furan ring, such as hydrogenation, oxidation, acetalization, acylation, aldol condensation, and reductive amination.⁵ Furfuryl alcohol (FA), one of the most common hydrogenation products, has been widely used in the manufacture of lubricants, resins, lysine, and vitamins.^{6–8} Conventionally, hydrogen gas is used as an external hydrogen source for the hydrogenation of FF to FA.^{9,10} However, in the last decades, liquid-phase catalytic transfer hydrogenation (CTH) of FF to FA using different alcohols as hydrogen donors has been investigated as an attractive green alternative.⁷ CTH provides a more benign protocol by avoiding the use of hydrogen gas, thereby rendering the complexity and cost of experimental procedures.¹¹

Previous studies with solid catalysts have confirmed that CTH is both acid- and base-catalyzed,^{12,13} and competing side reactions also catalyzed by acidity or basicity, such as

acetalization, etherification, and aldol condensation,^{14–17} are usually associated when using an alcohol as the hydrogen donor. Zeolites with pore structures and adjustable acidity and basicity have been applied in the CTH reaction.⁷ For example, CTH of FF in ethanol with the zeolite β catalyst loaded with zirconium (Zr- β) afforded a FA selectivity of 81.7% at 49.2% conversion at 140 °C with acetalization and aldol condensation reducing the FA selectivity.¹⁶ Gao et al. also used Zr-substituted β (Zr-Al- β) as the catalyst in the CTH of FF in 2-propanol and obtained 32.7% FF conversion at 120 °C with a selectivity of 90.2% of 2-(isopropoxymethyl)furan (IPF) formed by the etherification of FA. However, after the modification of the Zr-Al- β catalyst with alkalimetal ions (Li⁺, Na⁺ or K⁺) using a post-synthetic reflux method, etherification was significantly suppressed, and Na⁺-Zr-Al- β afforded 97.7% FA selectivity with 99.6% FF conversion at the same reaction conditions.¹⁸ In another study, Wei et al. found that the introduction of basic BaO could inhibit the etherification reaction.¹⁹ Thus, the introduction of alkali metal- or alkali earth metal (AEM) ions into solid catalysts

Received: October 12, 2021

Revised: December 29, 2021

Published: January 14, 2022






Cite this: *Green Chem.*, 2022, **24**, 7346Received 9th June 2022,
Accepted 6th September 2022

DOI: 10.1039/d2gc02190k

rsc.li/greenchem

Reductive etherification of furfural via hydrogenolysis with Pd-modified aluminum phosphate and formic acid†

Wenting Fang,  Jonas Egebo, Leonhard Schill,  Hua Chen and Anders Riisager  *

Practical and versatile one-pot synthesis of alkyl furanic ethers is achieved in 92–99% yield from furfural with Pd nanoparticles supported on aluminum phosphate as catalyst in various primary alcohols (C₂–C₆) using formic acid as a hydrogen donor. The reductive etherification of furfural occurs via acetalization and subsequent hydrogenolysis.

The exploitation of renewable biomass to produce carbon-containing fuels and chemicals is established as an important approach to avoid the overuse of non-renewable fossil resources.^{1,2} Furfural (FF) is an attractive platform compound accessible from lignocellulosic biomass and it finds wide use as a feedstock for other numerous chemicals, especially biofuels.^{3,4} Such biofuels can either be used directly or mixed in fossil fuels as bio-additives to improve the fuel properties,⁵ and in particular furanic ethers have become very promising blending components in high-octane gasoline.^{4,6,7} Two different strategies prevail for the synthesis of furanic ethers from FF with heterogeneous catalysis; a two-step process with FF hydrogenation to furfuryl alcohol (FAL) followed by etherification or a one-pot process relying on direct reductive etherification of FF, respectively. Due to a simpler mode of operation, the latter approach is often preferred even though it requires a bifunctional hydrogenation/acid catalyst system. Examples of such systems includes Pd/C used for the reductive etherification of FF in ethanol with pressurized hydrogen gas, where the formation of acidic PdH species allowed obtaining moderate yield (81%) of furanic ether.⁸ Likewise, Pd-I/Al₂O₃ yielded 76% of furanic ether in 2-propanol with hydrogen gas because the combination of iodine species on the Pd nanoparticles (NPs) with dissociated hydrogen generated “*in situ*” Brønsted acid sites.⁹ Notably, in both systems the use of hydrogen gas also

formed hydrogenation products, which led to the moderate selectivity of ether.^{8,9}

Catalytic transfer hydrogenation (CTH) with alcohols, formic acid (FA) or formate salts as hydrogen donors¹⁰ offers an attractive alternative to the use of pressurized hydrogen gas for reductive etherification of FF in terms of both cost and safety. Recently, Zr/Si mixed oxide and Sn-beta catalysts were shown to give 95% and 58% yield of furanic ether from FF with 2-butanol as a hydrogen donor,^{11,12} while mixed Zr-Mont/ZrO(OH)₂ catalyst gave 67% and 69% furanic ether yields with 2-propanol and 2-butanol as hydrogen donors, respectively.¹³ Noticeably, all catalytic systems failed to offer good yields of furanic ethers of FF in primary alcohols such as, e.g. ethanol and 1-propanol, which possesses limited hydrogen transfer capability.¹⁴ However, the use of FA (also obtainable from biomass)¹⁵ as a hydrogen source instead of alcohols can circumvent this drawback as FA can decompose catalytically into H₂ and CO₂ over metal-based catalysts, especially Pd-based catalysts.^{16–18} According to our previous work, aluminum phosphate (APO-5) has specific adsorption of aldehydes which may promote reductive etherification.^{19,20} Thus in this work are bifunctional Pd-loaded APO-5 catalysts introduced as highly efficient and selective heterogeneous catalysts for the reductive etherification of FF to form alkyl furfuryl ethers with FA in primary alcohols, including ethanol and 1-propanol.

Pd-loaded APO-5 catalysts with different metal content (Pd-1: 1.72 wt% Pd; Pd-2: 2.45 wt% Pd) were synthesized by wet impregnation and characterized. The XRD patterns of the Pd catalysts (Fig. 1a) matched well with the AFI-type structure of APO-5²¹ and confirmed that the structure was retained after metal introduction. Furthermore, the intensity of the peak corresponding to the Pd (111) facet (40.1°)^{22–24} was higher for Pd-2 than for Pd-1 as also expected based on their relative metal content. Porosity analysis by N₂ physisorption (Fig. S1 and Table S1†) revealed that the Pd catalysts had larger mesopores (31–46 nm) than the APO-5 support (15 nm), which was attributed to an expansion of the mesopores by agglomerated Pd NPs.²⁵ This expansion also resulted in altered hysteresis

Centre for Catalysis and Sustainable Chemistry, Department of Chemistry, Technical University of Denmark, DK-2800 Kgs. Lyngby, Denmark.
E-mail: ar@kemi.dtu.dk; Tel: (+45)4525 2233

† Electronic supplementary information (ESI) available. See DOI: <https://doi.org/10.1039/d2gc02190k>



Contents lists available at ScienceDirect

Applied Catalysis B: Environmental

journal homepage: www.elsevier.com/locate/apcatb


On the role of Zr to facilitate the synthesis of diesel and jet fuel range intermediates from biomass-derived carbonyl compounds over aluminum phosphate

Wenting Fang^a, Sihang Liu^b, Leonhard Schill^a, Mariusz Kubus^a, Thomas Bligaard^c, Anders Riisager^{a,*}

^a Centre for Catalysis and Sustainable Chemistry, Department of Chemistry, Technical University of Denmark, DK-2800 Kgs. Lyngby, Denmark

^b Catalysis Theory Center, Department of Physics, Technical University of Denmark, DK-2800 Kgs. Lyngby, Denmark

^c Department of Energy Conversion and Storage, Technical University of Denmark, DK-2800 Kgs. Lyngby, Denmark

ARTICLE INFO

Keywords:

Aldol condensation
Biomass conversion
Zr-modified aluminum phosphate
Cyclohexanone
Furfural

ABSTRACT

Heterogeneous zeolite/zeotype catalysts are attractive for converting renewable biomass-derived chemicals into transportation fuels by aldol condensation reactions, which provide a simple strategy to improve carbon numbers. Herein, Zr-doped aluminum phosphate (ZrAPO-5) were applied for efficient syntheses of diesel and jet fuel range C₁₁, C₁₂ and C₁₆ intermediates from biomass-derived furfural (FF) and cyclohexanone (CH). Incorporation of Zr in the APO-5 framework facilitated the adsorption of the C=O groups of FF and CH and created more and stronger acid and base sites, which co-catalyzed the aldol condensation and facilitated the product yields. ZrAPO-5 (Zr/Al = 0.20) yielded up to 79.3% single aldol condensation product C₁₁ or 80.7% double aldol condensation product C₁₆ in the cross-aldol condensation of FF and CH under appropriate reaction conditions, and also realized 83.3% C₁₂ yield in the self-aldol condensation of CH. In addition, the catalytic system displayed good to excellent yields of other value-added chemicals in aldol condensations of alternative carbonyl compounds.

1. Introduction

Catalytic conversion of renewable biomass to chemicals and potential fuels is a highly relevant topic for dealing with global challenges such as environmental preservation and the future energy demand. [1] Especially the synthesis of diesel and jet fuel range hydrocarbons from lignocellulose-derived platform compounds has drawn tremendous attention, [2,3] and one of the frequently adopted strategies to increase carbon numbers of biomass-derivatives for producing jet fuel (C₉₋₁₄) and diesel (C₁₂₋₂₀) is the aldol condensation of carbonyl compounds. [4] The reaction may occur between two ketones, two aldehydes or an aldehyde and a ketone.

Furfural (FF) and cyclohexanone (CH) are platform chemicals with carbonyl groups which may be derived from xylose and aromatic ethers [5,6] though CH synthesized from the biomass-derived compounds is not widely used. The cross-aldol condensation between FF and CH can generate (E)-2-(furan-2-ylmethylene)cyclohexan-1-one (labelled C₁₁) and (2E,6E)-2,6-bis(furan-2-ylmethylene)cyclohexan-1-one (labelled

C₁₆). [7] The self-aldol condensation of CH forms two isomers, [1,1'-bi(cyclohexylidene)]-2-one and [1,1'-bi(cyclohexan)]-1'-en-2-one (together labelled C₁₂) (Scheme 1). All of the C₁₁, C₁₂ and C₁₆ compounds are fuel precursors with high volumetric energy density and high pour point. [7,8]

In order to generate C-C bonds with carbonyl compounds, bases are typically exploited for the abstraction of α-protons to form the enolate intermediate required for the bond formation. [9] Accordingly, homogeneous basic catalysts (e.g., NaOH and Ca(OH)₂) [10–12] and heterogeneous basic catalysts (e.g., earth alkali oxides, MgZr or MgAl mixed oxides and hydrotalcite) [13–16] have been widely used for the aldol condensation between FF and ketones. Although homogeneous basic catalysts show excellent activity and high selectivity for the desired products, several drawbacks remain during the synthesis, such as catalyst/product separation and equipment corrosion. [9] Heterogeneous basic catalysts could circumvent these issues and are thus preferred, however, they are easily deactivated in the presence of furoic acid which can form as byproduct by base-catalyzed Cannizzaro reaction of FF. [7,

* Corresponding author.

E-mail address: ar@kemi.dtu.dk (A. Riisager).

<https://doi.org/10.1016/j.apcatb.2022.121936>

Received 4 June 2022; Received in revised form 12 August 2022; Accepted 1 September 2022

Available online 5 September 2022

0926-3373/© 2022 The Author(s). Published by Elsevier B.V. This is an open access article under the CC BY license (<http://creativecommons.org/licenses/by/4.0/>).